Advances
in Clinical and Experimental Medicine

Wroclaw
MEDICAL UNIVERSITY

Advances
in Clinical and Experimental Medicine

Editorial Policy

Contents

Laser dentistry in daily practice during the COVID-19 pandemic: Benefits, risks and recommendations for safe treatments

Josep Arnabat-Dominguez[1,A–F], Alessandro Del Vecchio[2,A–F], Carmen Todea[3,A–F],
Kinga Grzech-Leśniak[4,A–F], Paolo Vescovi[5,A–F], Umberto Romeo[2,A–F], Samir Nammour[6,A–F]

[1] Oral and Maxillofacial Surgery Unit, University of Barcelona, Spain

[2] Department of Oral Sciences and Maxillofacial Surgery, Sapienza University of Rome, Italy

[3] School of Dentistry, Victor Babes University of Medicine and Pharmacy, Timișoara, Romania

[4] Laser Laboratory, Department of Oral Surgery, Wroclaw Medical University, Poland

[5] Department of Medicine and Surgery, Oral Medicine and Laser Surgery Unit, Centro Universitario di Odontoiatria, University of Parma, Italy

[6] Department of Dental Sciences, Faculty of Medicine, University of Liege, Belgium

A – research concept and design; B – collection and/or assembly of data; C – data analysis and interpretation;
D – writing the article; E – critical revision of the article; F – final approval of the article

Address for correspondence
Kinga Grzech-Leśniak
E-mail: kgl@periocare.pl

Abstract

Background. The COVID-19 pandemic forced dental professionals to cope with an unexpected challenge and caused an abrupt cessation of conventional care practices. The high degree of contagiousness as well as the diffusion of the virus through the air and droplets via respiratory transmission placed dental professionals at top-level risk of contracting and spreading the disease. General recommendations were announced in different countries, including patient distancing, air ventilation, surface and instrument sanitization, and the wearing of suitable masks and shields. However, many dental treatments are performed using lasers, and some specific precautions must be added to conventional procedures to ensure the advantages of this technology to patients because of the particular tissue–matter interaction effects of laser wavelengths.

Objectives. Based on the literature, the authors evaluated all of using laser wavelengths to analyze the risk and the benefits of using lasers in daily dental practice, and to provide safety recommendations during pandemic.

Material and methods. An unrestricted search of indexed databases was performed. Laser use effects were categorized into: 1) explosive processes that produce tissue ablation and aerosol formation; 2) thermal actions that create vaporization and smoke plume; 3) photobiomodulation of the cells; and 4) enhanced chemical activity.

Results. Knowledge of the device functions and choice of adequate parameters will reduce aerosol and plume formation, and the application of suction systems with high flow volume and good filtration close to the surgical site will avoid virus dissemination during laser use. In the categories that involve low energy, the beneficial effects of lasers are available and sometimes preferable during this pandemic because only conventional precautions are required.

Conclusions. Lasers maintain the potential to add benefits to dental practice even in the COVID-19 era, but it is necessary to know how lasers work to utilize these advantages. The great potential of laser light, with undiscovered limits, may provide a different path to face the severe health challenges of this pandemic.

Key words: safety, dentistry, laser, COVID-19, SARS-CoV-2

Background

Coronaviruses are a large family of viruses that cause illness in animals and humans. Several coronaviruses cause respiratory infections in humans and range from the common cold to more severe diseases, such as Middle East Respiratory Syndrome (MERS) and Severe Acute Respiratory Syndrome (SARS). Acute respiratory diseases caused by the new coronavirus SARS-CoV-2 (formerly known as 2019-nCoV) spread across China by the end of 2019 and gained worldwide attention. On January 30, 2020, the World Health Organization (WHO) officially declared the coronavirus 2019 (COVID-19) outbreak a public health emergency of international concern.[1] The coronavirus pandemic has challenged the activities of health professions around the world in the last 4 months.

The role of dentists in the management of patients and simultaneous prevention of the transmission of CO-VID-19 is crucial. A continuation of normal dental procedures is not adequate because of the social distancing measures introduced by governments in countries affected by this pandemic. Therefore, routine dental care was suspended, and only emergency dental care is provided. However, patients suffering from systemic diseases, such as diabetes and cardiovascular disease, are more sensitive to this viral infection and its life-threatening consequences. Therefore, the return-to-work care for dental professionals is urgent and fundamental for the population.[2,3]

All healthcare professionals have the moral duty to treat patients in the safest manner to avoid the spread of the virus. The use of lasers in medical and dental practices has become widespread in the past decades, and the benefits of lasers in dental practice are universally recognized and have been reported in the literature for more than 30 years. These advantages should be emphasized and discussed in this particular moment because the adaptation of the laser clinical protocols during this pandemic is essential to ensure the best prevention and safety for patients and practitioners.

All dental laser professionals in the affected countries are involved in preventing the spread of CO-VID-19. Many countries are gradually de-confining and renewing their normal activities. The need to restart regular dental care is rising. Consequently, practitioners who use lasers in their daily practices need clear recommendations.

Objectives

This short article focuses on the risks and benefits of using some laser wavelengths and provides safety recommendations for various laser treatments in daily practice during the COVID pandemic.

Characteristics of the wavelengths in dentistry: general considerations

Several laser wavelengths are used in different medical and dental fields. The interaction between laser beams and tissues or matter depends on the wavelength and its absorption parameters. We limit our analysis to the most commonly used lasers on oral hard and soft tissues, such as erbium family lasers (Er:YAG, Er,Cr:YSGG), Nd:YAG (yttrium aluminium garnet) and Nd:YAP (yttrium aluminium perovskite doped with neodymium crystal) lasers, diode lasers or KTP (potassium-titanyl-phosphate) and CO_2 lasers, as well as red and near infrared (NIR) lights used for photobiomodulation.

We divided the main tissue and matter interaction effects of the laser wavelengths into the following categories:

1. Explosive process leading to tissue and matter ablation. The high absorption of some wavelengths produces an explosive process in the target hard and soft tissues, which leads to photothermal and photomechanical ablation. Many lasers are in this category, including Er:YAG, Er,Cr:YSGG, Nd:YAP and Nd:YAG lasers action on dark matter and metals.

2. Heat generation leading to the vaporization of soft tissues and fusion followed by the melting of hard tissues. This group includes CO_2 lasers (10.6 µm), diode lasers (445 nm and 810–980 nm) and Nd:YAP and Nd:YAG lasers action on soft tissues. The vaporization process of soft tissues produces smoke.

3. Biological photobiomodulation in tissues. Low energy red and NIR light irradiation produces a harmless interaction with cells, improves cell viability, and reduces pain and inflammation.

4. Chemical reaction enhancement. The absorption of laser light enhances chemical reactions and causes the release of free radicals (e.g., antimicrobial photodynamic therapy (aPDT), photoactivated disinfection (PAD), photodynamic inactivation (PDI), and teeth bleaching). Visible light wavelengths are primarily included in this category because of its ability to react with electrons.

Based on those 4 simplified categories, we analyzed the benefits and risks during dental treatments and suggested recommendations for safe clinical protocols of the use of lasers in different fields of dentistry.

Photothermal and photomechanical laser ablation

An aerosol is a heterogeneous system that consists of solid or/and liquid particles dispersed and suspended in the air. The particle size is between 0.001 µm and 100 µm, and aerosols can contain dust, industrial dust particles, bacteria, microorganisms, and plant spore dust. For example, atmospheric smog, which contains PM 2.5 dust particles, is a "huge" aerosol compared to a virus. PM 2.5

particulate matter is 2.5 μm or less, and the diameter of the SARS coronavirus particles is about 0.08–0.12 μm. Splatter is a mixture of air, water and/or solid substances that range from 50 μm to several millimeters in diameter. Obviously, viruses with these small dimensions easily float in the air.

SARS-CoV-2 persists in aerosols and splatter for up to 3 h, and it has a relatively long half-life of about 1.1–1.2 h.[4]

Aerosols and droplets generated during speech have been implicated in the person-to-person transmission of viruses, and there is great interest in understanding the mechanisms responsible for the spread of COVID-19 in this manner. Speaking generates different sizes of oral fluid droplets that may contain infectious virus particles. Large droplets quickly fall to the ground, but small droplets dehydrate and linger in the air as "droplet nuclei", where they act as an aerosol and expand the spatial extent of the emitted infectious particles.[5]

The transmission of SARS-CoV-2 in humans occurs through 4 different ways:

1) inhalation of infected droplets;

2) close contact with infected person;

3) contact with contaminated surfaces followed by face contact and dissemination; and

4) aerosol transmission of pathogens in closed spaces.

During the earlier SARS outbreak, emergency dental care was provided with advice on strict personal protection, and protocols were recommended to reduce or avoid the production of droplets and aerosols using high volume and power suction.[6]

Several publications reported that dental professionals were at high risk of COVID-19 infection due to close face-to-face contact.[7] Some studies also suggested that COVID-19 was suspended in the air in aerosols that formed during medical procedures or indirectly through saliva in asymptomatic patients.[8] COVID-19 is about 0.12 μm in diameter, and aerosol particle sizes range from 0.001 μm to 100 μm. Therefore, it is mandatory to consider the risk of viral diffusion in aerosols produced by some laser wavelengths.

The Er:YAG and Er,Cr:YSGG lasers induce bubble dynamics, a fragmentation process and tissue ablation through photothermal and photomechanical/photoacoustical mechanisms.[9] At the beginning of irradiation with erbium lasers, the rapid expansion of the layer of evaporated water leads to an increase in pressure. The fragmentation process occurs with and without plasma formation. In both cases, ablation occurs shortly after the beginning of laser irradiation, and a plume of fine, emulsified material is expelled into the surrounding water.[10]

The ablation process accelerates with increased laser energy, which reduces the thermal side effects. When the energy is increased, the pressure and speed of the ejected material also increases, which creates a larger plasma formation.[11]

The lasers used for oral hard and soft tissue ablation and skin resurfacing are pulsed for short exposures of 1–10 ms (or even less than 1 ms). These fast pulses produce a more explosive effect with greater tissue ablation and, consequently, a greater spread of viral particles.[12] Some authors using erbium lasers demonstrated the dissemination of viable cells, viral genes and infectious viruses using in vitro methods.[13]

Due to the proven potential of COVID-19 transmission, it is even more relevant to maintain safety precautions during dental laser applications, including limiting the use of laser-producing aerosols, except when their use has a strong therapeutic advantage compared with other modalities. The choice of the lowest parameters that allow good clinical effects and a reduction of air-flow is important. An accurate adaptation of the water–air spray during laser ablation to reduce aerosols and viral diffusion must be utilized. The suction system of the dental chair must have a high flow volume. The use of rubber dam isolation is strictly recommended. All laser handpieces and the entire device must be disinfected before and after the treatment. The protection of skin, eyes, mouth, and respiratory tract is essential.

Laser-generated heat leads to vaporization of soft tissues and smoke production

Some lasers offer several advantages during surgery compared to the scalpel. Due to the nature of the pathological tissue and the anatomical district, better results may be obtained by selecting the most suitable laser device. For example, a CO_2 laser (10,600 nm) is optimal for the excision of very hydrated lesions, such as fibrous lesions, while diode lasers (445 nm, 810 nm and 980 nm) and Nd:YAG (1064 nm) lasers, which have a better coagulating action, may be used for very vascularized lesions or tissues that are rich in vessels with a high amount of hemoglobin and risk of hemorrhage.[14,15]

The factor that unites all of these wavelengths is the utilization of the photothermal effect, because the absorbed laser energy is converted to heat. Therefore, considerable amounts of smoke plume are generated, which necessitate constant suction away from the surgical site.[12] Several studies suggested that laser-derived vapors contained infectious particles or viral DNA.[13] Garden et al. detected the presence of human and bovine papilloma virus DNA (HPV and BPV) in laser vapors from warts treated with a CO_2 laser,[16] and Sawchuk et al. showed that laser vapor-derived from the excision of bovine papilloma contained infectious particles.[17] A single case of a laryngeal papillomatosis (HPV type 6 and 11) was detected in a surgeon who previously treated patients with anogenital warts using a Nd:YAG laser.[18] Garden et al.[12] presented the possibility that BPV maintained its vitality and potential to infect tissue in the smoke plume produced by the laser beam. Several CO_2 laser settings were evaluated, and the laser plume at each laser setting was collected and inoculated into animals. Typical BPV lesions containing BPV developed at all laser settings. These viral tumors confirmed

the ability of the laser plume to produce infection. Aside from viable viruses, the laser smoke may also contain partially inactive or incompetent viruses. Virus-infected cells and viral genes as far as 6.3 cm from the point of laser impact and laser debris at distances of up to 100 cm were described.[13] However, the lack of HPV DNA in the smoke plume after warts treatment with an Er:YAG laser was reported in 1998.[19]

The literature confirmed that lasers generating smoke during surgical procedures may have infectious potential and pose a significant risk to healthcare providers. Because the presence of 2019-nCoV on the oral mucosa, tongue and saliva was confirmed, the use of photothermal lasers that produce smoke must be performed with caution, using the same precautions that were adopted for treatments that produce aerosols. The concern for laser surgeons and their assistants to inhale the SARS-CoV-2 virus via the smoke plume produced by thermal lasers is only theoretic, but likely. Considering several advantages of laser technology in oral soft tissue treatment, it is important to continue its use with the adoption of strict safety precautions for practitioners and assistants, including skin protection with gloves and gowns, eye protection, use of masks (FFP2, FFP3 if possible), and the use of a smoke suction system with a high flow volume and good filtration, positioned at the closest distance from the surgical site to avoid nosocomial viral dissemination.[12]

Lasers inducing biological photobiomodulation in tissue

Photobiomodulation (PBM) is the medical way to use red or NIR laser light to achieve a chemical- and thermal-free beneficial interaction with tissues and cells. Many studies support its properties of tissue regeneration, wound healing, anti-inflammation, analgesia, and neuroregeneration.[20–22] Moreover, PBM may also act against microorganisms, such as yeasts, bacteria and viruses. The literature includes several interesting studies about the potential efficiency of PBM directly against microorganisms and indirectly to reinforce the immune response or reduce the damage induced by the inflammatory process.[23]

Tsen et al.[24] demonstrated damage of the viral capsid caused by the Raman resonance induced by the irradiation of a femtosecond 425-nm low level laser. This particular kind of damage modified the protein structure of viral capsid and induced viral aggregation. The damage to the capsid did not prevent the penetration of viruses into the host cells, but it did not allow the viral envelope to dissolve and transmit the viral genetic message to the nucleus. Therefore, the virus was blocked and remained ineffective in the host cell cytoplasm.

Zupin et al.[25] investigated the direct and indirect antiviral actions of PBM and demonstrated the efficiency of 2 different PBM protocols using a 445-nm blue laser and a 970-nm NIR on neurological microglia cells infected with Zika virus (ZIKV). In both cases, the PBM irradiation enhanced the vitality of the infected cells and reduced the viral load.

Great interest should be focused on the interesting potential of the so-called transdermal PBM.[26] This technique displaced the old intravenous laser irradiation and consists of the PBM irradiation of blood via laser application over the surface of the radial artery.[27] The irradiation of blood induces the production of super oxide dismutase (SOD), which is fundamental in the protection of the cells against the toxic overproduction of reactive oxygen species (ROS). The possibility to vehiculate the beneficial effects of this positive and proven action of PBM to all organs, such as the lungs, which are highly damaged by the COVID-19 infection because of the immune system overreaction, could be very helpful and should open a path of research and clinical applications of unexpected potential.

The application of PBM in daily clinical practice is slowly increasing, with great benefits for clinicians and patients.

The PBM protocols involve the use of red and near-infrared lasers emitting in the so-called "therapeutic window" wavelength between 600 nm and 1400 nm.[20] The lasers most frequently used for the PBM are the red visible or NIR diode lasers and the more penetrating Nd:YAG lasers. It is important to emphasize that the PBM protocols do not generate heat, smoke or aerosol droplets, which is different from the traditional high-energy surgical laser applications.

Dental professionals are at high risk for nosocomial infections, and they may become potential carriers of the disease. These risks are attributable to the unique nature of dental interventions, which include aerosol generation, the handling of sharp implements, and the proximity of the practitioner to the patient's oropharyngeal region.[28]

Therefore, in the present pandemic condition, the well-documented and effective anti-inflammatory, regenerative or analgesic applications of PBM may represent an essential tool to face the various emergencies of our patients, although the crucial step of correctly identifying the proper and standardized dosages is not resolved at the moment. However, the wide consensus in the literature concerning its clinical benefits encourages the spread of its use as much as possible in daily clinical practice. The PBM may be used as an adjuvant or alternative therapy in a wide variety of situations, without side effects or drug interactions.[29]

Therefore, practitioners may treat acute diseases, such as recurrent aphthous stomatitis and traumatic ulcers, temporomandibular disorders, recurrent intraoral and labial herpes, oral edema, postoperative pain following periodontal treatments, oral surgery, and endodontic procedures in emergencies using PBM, even in suspected

or confirmed cases of COVID-19 infection. Similarly, endodontists may be called upon for the assessment and management of odontogenic pain, swelling and dental alveolar traumas, and they may find the support of PBM helpful.[28]

All of the aforementioned considerations should lead researchers and clinicians to dedicate increasing efforts in the identification of precise and standardized PBM protocols to test the impact that this proven and biologically safe therapeutic method could have in treatment during the present COVID-19 pandemic.

Lasers enhancing chemical reactions

One of the objectives during this pandemic is to decrease the viral load in our patients during dental treatments. There are antecedents in which the use of photodynamic antimicrobial chemotherapy significantly decreased the viral load in different types of oral viruses.[30–35]

Antimicrobial photodynamic therapy (aPDT) is a form of phototherapy that is performed using nontoxic, light-sensitive compounds with selectively exposed/absorbed laser light, which become toxic to target pathogens. The efficacy of PDT was demonstrated in recent clinical research on periopathogens,[36–38] carious bacteria,[39,40] onychomycosis,[41,42] and paracoccidiodomycosis.[43]

Antiviral therapy using laser light, known as photodynamic inactivation (PDI), is based on the same mechanisms as photodynamic antimicrobial chemotherapy (PACT), i.e., non-thermal viral inactivation. We can differentiate 2 types of virus structural damage caused by light – type I and type II photoreactions. Both mechanisms may be active at the same time, but that depends on the photosensitizer (PS), its concentration and the concentration of oxygen.[44] The PDI can use many compounds with potential photodynamic antiviral activity, ranging from plant extracts (psoralen), eosin, curcumin, and hypericin (St. John's wort), to synthetic compounds.[45]

The sensitivity of viruses to photodynamic therapy was reported for herpes infections,[30,31] HPV infections (papillomatosis),[32–34] cytomegalovirus CMV,[35] and other viruses.[46] Many studies showed that enveloped viruses are significantly more sensitive to photodynamic destruction than non-enveloped ones.[47]

To evaluate the sensitivity of the viral photoinactivation process, molecular quantitative methods, such as nucleic acid amplification, including real time polymerase chain reaction (RT-PCR), are needed. This method is sensitive and fast, but it only detects viral nucleic acid, and it does not determine infectivity. Other methods using bacteriophages as surrogates of mammalian viruses may be useful for the quantification of infectivity.[25,44]

Some studies reported reactivation of viruses, such as herpes simplex virus (HSV), after photodynamic treatment as a side effect of PDT. Photo-inactivated viruses still trigger an immune response that may be unwanted, but the treatment is still useful to generate a competent immune response and vaccination.[45,48] Schikora et al. reported that aPDT mediated by methylene blue and 660-nm red laser light applied to nasal and oral cavities of patients with COVID-19 reduced mortality and comorbidities.[49]

There is no evidence from randomized controlled trials for any specific anti-nCoV treatment. One of the most frequent recommendations during this COVID-19 pandemic is the use of mouth rinses prior to dental treatments with 0.5–1% H_2O_2 or 0.1% sodium hypochlorite for 1 min.[50,51] Other antimicrobial agents, such as 0.02% chlorhexidine digluconate, are less effective.[51]

Different studies showed that the combination of H_2O_2 with a laser produced benefits, especially related to bacterial load.[52,53] This reduction of microbial viability was demonstrated when combined with diode, neodymium or erbium lasers. Some studies demonstrated that the photoactivation of 3% H_2O_2 with a diode laser increased the bactericidal effect due to the acceleration of hydroxyl radical generation.[53,54] Laser light activates H_2O_2 release of free radicals and singlet oxygen. The stabilized H_2O_2 and presence of oxygen allow the reactions of photoactivation and singlet oxygen release, which induce microbial death through the destruction of the bacterial membrane, degradation of the lysosomal membrane, alteration of mitochondrial function, and denaturation of DNA molecules. Caccianiga et al.[55] reported the successful reduction of periopathogens from implant surfaces in a clinical study using high-level laser therapy (HLLT). These studies demonstrated that the combination of different laser wavelengths (405 nm, 940 nm, 980 nm, 1064 nm, and 2940 nm) with the H_2O_2 was much more effective than laser or antioxidant alone.[52–57] Nammour et al.[57] performed a randomized clinical study using 980-nm wavelength and 3% H_2O_2, and showed significant clinical improvement and microbiological reduction in a twelve-month follow-up. Grzech-Leśniak et al.[56] evaluated the effectiveness of treatments with Nd:YAG laser irradiation and 0.5% NaOCl and 0.5% H_2O_2 solutions as single or combined treatment modalities. The authors demonstrated that combined treatment with the Nd:YAG laser at low level laser settings and a low concentration of H_2O_2 (0.5%) or NaOCl (0.5%) solution effectively reduced the microorganisms. The combination of lasers and H_2O_2 may be helpful for viral reduction. The good efficacy of photodynamic viral inactivation has been well-known since its early application in 1973 for the treatment of HSV infections performed by Felber.[58] The development of medicine increased the treatment options used in dental practice, which now include a wide range of antiviral application portfolios.

Future research on the possibility of destroying SARS COVID-19 using PDI is necessary.

Specific recommendations for laser dentistry in the SARS-CoV-2 pandemic

All universal recommendations for general dentistry must be respected, and practitioners must follow their own national recommendations. Additional specific care must be used for lasers, according to the following guidelines:

1. Choose the lowest laser parameters that permit efficient clinical effects and a reduction of air flow. A correct water spray during laser ablation may reduce the aerosol production and viral spread.

2. Face and eyes protection: wear safety glasses/google for each laser wavelength to avoid eye contamination. It is also necessary to use a face shield for splash protection. Use a face mask (e.g., FFP3) to protect the respiratory tract from droplets and smoke plume.[59]

3. Use a rubber dam to avoid viral contamination from the mouth and saliva.

4. Use a high-volume saliva ejector/volume suction system placed at the closest distance to the treated site.

5. If a smoke plume is produced, use a vacuum system with a high flow volume positioned at the closest distance to the surgical site. The ventilation of the room and disinfection of the dental operating area can effectively limit the transmission of SARS-CoV-2 aerosols.

6. For PBM treatments: The handpieces of the devices are easily protected through the application of transparent removable plastic films to avoid any contact with the skin, mucosa and oral fluids, and permit superficial or deep penetration of the Red/NIR laser beams.

7. Special care must be dedicated to the disinfection of laser devices before and after their use. Handpiece and tips must be autoclaved.

Conclusions

Even during the present pandemic, all lasers retained their well-known advantages and benefits. However, it is mandatory to know the specific functions and properties of lasers in order to utilize their potential and adapt to the present situation using previously adopted safety recommendations. Moreover, laser light may provide a different path to face the severe health challenges of the current COVID-19 pandemic.

ORCID iDs

Josep Arnabat-Dominguez https://orcid.org/0000-0003-1653-8043
Alessandro Del Vecchio https://orcid.org/0000-0002-9278-8872
Carmen Todea https://orcid.org/0000-0002-1654-4067
Kinga Grzech-Leśniak https://orcid.org/0000-0002-5700-4577
Paolo Vescovi https://orcid.org/0000-0002-2223-3716
Umberto Romeo https://orcid.org/0000-0003-2439-2187
Samir Nammour https://orcid.org/0000-0003-0321-9764

References

1. Guo YR, Cao QD, Hong ZS, et al. The origin, transmission and clinical therapies on coronavirus disease 2019 (COVID-19) outbreak: An update on the status. *Mil Med Res*. 2020;7(1):1–10. doi:10.1186/s40779-020-00240-0

2. Dominiak M, Różyło-Kalinowska I, Gedrange T, et al. COVID-19 and professional dental practice. The Polish Dental Association Working Group recommendations for procedures in dental office during an increased epidemiological risk. *J Stomatol*. 2020;73(1):1–10. doi:10.5114/jos.2020.94168

3. Matys J, Grzech-Leśniak K, Dominiak M. Disinfectants and devices for surface and air disinfection in dental offices. *J Stomatol*. 2020; 73(4):200–205. doi:10.5114/jos.2020.98267

4. van Doremalen N, Bushmaker T, Morris D, et al. Aerosol and surface stability of SARS-CoV-2 as compared with SARS-CoV-1. *N Engl J Med*. 2020:382(16):1564–1567. doi:10.1056/NEJMc2004973 %0A

5. Anfinrud P, Stadnytskyi V, Bax CE, Bax A. Visualizing speech-generated oral fluid droplets with laser light scattering. *N Engl J Med*. 2020: 382(21):2061–2063. doi:10.1056/nejmc2007800

6. Li RWK, Leung KWC, Sun FCS, Samaranayake LP. Severe acute respiratory syndrome (SARS) and the GDP. Part II: Implications for GDPs. *Br Dent J*. 2004;197(3):130–134. doi:10.1038/sj.bdj.4811522

7. Hayden C, Bowler JO, Chambers S, et al. Obesity and dental caries in children: A systematic review and meta-analysis. *Commun Dent Oral Epidemiol*. 2013;41(4):289–308. doi:10.1111/cdoe.12014

8. Wax RS, Christian MD. Practical recommendations for critical care and anesthesiology teams caring for novel coronavirus (2019-nCoV) patients. *Can J Anesth*. 2020;67(5):568–576. doi:10.1007/s12630-020-01591

9. Romeo U, Libotte F, Palaia G, Tenore G, Galanakis A, Annibali S. Is erbium:yttrium-aluminum-garnet laser versus conventional rotary osteotomy better in the postoperative period for lower third molar surgery? Randomized split-mouth clinical study. *J Oral Maxillofac Surg*. 2015;73(2):211–218. doi:10.1016/j.joms.2014.08.013

10. Nahen K, Vogel A. Plume dynamics and shielding by the ablation plume during Er:YAG laser ablation. *J Biomed Opt*. 2002;7(2):165. doi:10.1117/1.1463047

11. Van As G. Erbium lasers in dentistry. *Dent Clin North Am*. 2004;48(4): 1017–1059. doi:10.1016/j.cden.2004.06.001

12. Garden JM, Kerry O'Banion M, Bakus AD, Olson C. Viral disease transmitted by laser-generated plume (aerosol). *Arch Dermatol*. 2002; 138(10):1303–1307. doi:10.1001/archderm.138.10.1303

13. Ziegler BL, Thomas CA, Meier T, Müller R, Fliedner TM, Weber L. Generation of infectious retrovirus aerosol through medical laser irradiation. *Lasers Surg Med*. 1998;22(1):37–41. doi:10.1002/(SICI)1096-9101(1998)22:1<37::AID-LSM9>3.0.CO;2-Y

14. Palaia G, Pergolini D, D'Alessandro L, et al. Histological effects of an innovative 445 Nm blue laser during oral soft tissue biopsy. *Int J Environ Res Public Health*. 2020;17(8):2651. doi:10.3390/ijerph17082651

15. Miyazaki H, Ohshiro T, Romeo U, et al. Retrospective study on laser treatment of oral vascular lesions using the "leopard technique": The multiple spot irradiation technique with a single-pulsed wave. *Photomed Laser Surg*. 2018;36(6):320–325. doi:10.1089/pho.2017.4410

16. Garden JM, O'Banion MK, Shelnitz LS, et al. Papillomavirus in the vapor of carbon dioxide laser-treated *Verrucae*. *JAMA*. 1988;259(8); 1199–1202.

17. Sawchuk WS, Weber PJ, Lowy DR, Dzubow LM. Infectious papillomavirus in the vapor of warts treated with carbon dioxide laser or electrocoagulation: Detection and protection. *J Am Acad Dermatol*. 1989; 21(1):41–49. doi:10.1016/s0190-9622(89)70146-8

18. Hallmo P, Naess O. Laryngeal papillomatosis with human papillomavirus DNA contracted by a laser surgeon. *Eur Arch Otorhinolaryngol*. 1991;248(7):425–427. doi:10.1007/BF01463570

19. Hughes PSH, Hughes AP. Absence of human papillomavirus DNA in the plume of erbium: YAG laser-treated warts. *J Am Acad Dermatol*. 1998;38(3):426–428. doi:10.1016/S0190-9622(98)70500-6

20. Hamblin MR. Mechanisms and mitochondrial redox signaling in photobiomodulation. *Photochem Photobiol*. 2018;94(2):199–212. doi:10.1111/php.12864

21. Grzech-Leśniak K, Nowicka J, Pajączkowska M, et al. Effects of Nd:YAG laser irradiation on the growth of *Candida albicans* and *Streptococcus mutans*: In vitro study. *Lasers Med Sci*. 2019;34(1):129–137. doi:10.1007/s10103-018-2622-6

22. Dompe C, Moncrieff L, Matys J, et al. Photobiomodulation-underlying mechanism and clinical applications. *J Clin Med*. 2020;9(6):1724. doi:10.3390/jcm906172421

23. Enwemeka CS, Bumah VV, Masson-Meyers DS. Light as a potential treatment for pandemic coronavirus infections: A perspective. *J Photochem Photobiol B*. 2020;207:111891. doi:10.1016/j.jphotobiol.2020.111891

24. Tsen S, Chapa T, Beatty W, Xu B, Tsen K, Achilefu S. Ultrashort pulsed laser treatment inactivates viruses by inhibiting viral replication and transcription in the host nucleus. *Antiviral Res*. 2014;110:70–76. doi:10.1016/j.antiviral.2014.07.012

25. Zupin L, Caracciolo I, Tricarico PM, Ottaviani G, D'Agaro P, Crovella S. Photobiomodulation therapy reduces viral load and cell death in ZIKV-infected glioblastoma cell line. *Lasers Med Sci*. 2018;33(9):2011–2013. doi:10.1007/s10103-018-2568-8

26. Domínguez A, Velásquez SA, David MA. Can transdermal photobiomodulation help us at the time of COVID-19? *Photobiomodul Photomed Laser Surg*. 2020;38(5):258–259. doi:10.1089/photob.2020.4870

27. Szymczyszyn A, Doroszko A, Szahidewicz-Krupska E, et al. Effect of the transdermal low-level laser therapy on endothelial function. *Lasers Med Sci*. 2016;31(7):1301–1307. doi:10.1007/s10103-016-1971-2

28. Ather A, Patel B, Ruparel NB, Diogenes A, Hargreaves KM. Coronavirus disease 19 (COVID-19): Implications for clinical dental care. *J Endod*. 2020;46(5):584–595. doi:10.1016/j.joen.2020.03.008

29. Fekrazad R. Photobiomodulation and antiviral photodynamic therapy as a possible novel approach in COVID-19 management. *Photobiomodul Photomed Laser Surg*. 2020;38(5):255–257. doi:10.1089/photob.2020.4868

30. Namvar MA, Vahedi M, Abdolsamadi H, Mirzaei A, Mohammadi Y, Azizi Jalilian F. Effect of photodynamic therapy by 810 and 940 nm diode laser on Herpes Simplex Virus 1: An in vitro study. *Photodiagnosis Photodyn Ther*. 2019;25:87–91. doi:10.1016/j.pdpdt.2018.11.011

31. La Selva A, Negreiros RM, Bezerra DT, et al. Treatment of herpes labialis by photodynamic therapy. *Medicine (Baltimore)*. 2020;99(12):e19500. doi:10.1097/md.0000000000019500

32. Zhang W, Zhang A, Sun W, Yue Y, Li H. Efficacy and safety of photodynamic therapy for cervical intraepithelial neoplasia and human papilloma virus infection: A systematic review and meta-analysis of randomized clinical trials. *Medicine (Baltimore)*. 2018;97(21):e10864. doi:10.1097/MD.0000000000010864

33. Shikowitz MJ, Abramson AL, Freeman K, Steinberg BM, Nouri M. Efficacy of DHE photodynamic therapy for respiratory papillomatosis: Immediate and long-term results. *Laryngoscope*. 1998;108(7):962–967. doi:10.1097/00005537-199807000-00002

34. Abramson AL, Shikowitz MJ, Mullooly VM, Steinberg BM, Amella CA, Rothstein HR. Clinical effects of photodynamic therapy on recurrent laryngeal papillomas. *Arch Otolaryngol Neck Surg*. 1992;118(1):25–29. doi:10.1001/archotol.1992.01880010029011

35. Belousova IM, Kislyakov IM, Muraviova TD, et al. Photodynamic inactivation of enveloped virus in protein plasma preparations by solid-phase fullerene-based photosensitizer. *Photodiagnosis Photodyn Ther*. 2014;11(2):165–170. doi:10.1016/j.pdpdt.2014.02.009

36. Grzech-Leśniak K, Gaspirc B, Sculean A. Clinical and microbiological effects of multiple applications of antibacterial photodynamic therapy in periodontal maintenance patients: A randomized controlled clinical study. *Photodiagnosis Photodyn Ther*. 2019;27(5):44–50. doi:10.1016/j.pdpdt.2019.05.028

37. Grzech-Leśniak K, Matys J, Dominiak M. Comparison of the clinical and microbiological effects of antibiotic therapy in periodontal pockets following laser treatment: An in vivo study. *Adv Clin Exp Med*. 2018;27(9):1263–1270. doi:10.17219/acem/70413

38. Świder K, Dominiak M, Grzech-Leśniak K, Matys J. Effect of different laser wavelengths on periodontopathogens in peri-implantitis: A review of in vivo studies. *Microorganisms*. 2019;7(7):189. doi:10.3390/microorganisms7070189

39. Alves LVGL, Curylofo-Zotti FA, Borsatto MC, et al. Influence of antimicrobial photodynamic therapy in carious lesion: Randomized split-mouth clinical trial in primary molars. *Photodiagnosis Photodyn Ther*. 2019;26(11):124–130. doi:10.1016/j.pdpdt.2019.02.018

40. Bargrizan M, Fekrazad R, Goudarzi N, Goudarzi N. Effects of antibacterial photodynamic therapy on salivary mutans streptococci in 5- to 6-year-olds with severe early childhood caries. *Lasers Med Sci*. 2019;34(3):433–440. doi:10.1007/s10103-018-2650-2

41. Alberdi E, Gómez C. Efficiency of methylene blue-mediated photodynamic therapy vs intense pulsed light in the treatment of onychomycosis in the toenails. *Photodermatol Photoimmunol Photomed*. 2019;35(2):69–77. doi:10.1111/phpp.12420

42. Koren A, Salameh F, Sprecher E, Artzi O. Laser-assisted photodynamic therapy or laser-assisted amorolfine lacquer delivery for treatment of toenail onychomycosis: An open-label comparative study. *Acta Derm Venereol*. 2018;98(4):467–468. doi:10.2340/00015555-2874

43. dos Santos LFM, Melo NB, de Carli ML, et al. Photodynamic inactivation of *Paracoccidioides brasiliensis* helps the outcome of oral paracoccidiodomycosis. *Lasers Med Sci*. 2017;32(4):921–930. doi:10.1007/s10103-017-2193-y

44. Costa L, Faustino MAF, Tomé JPC, et al. Involvement of type I and type II mechanisms on the photoinactivation of non-enveloped DNA and RNA bacteriophages. *J Photochem Photobiol B*. 2013;120:10–16. doi:10.1016/j.jphotobiol.2013.01.005

45. Wiehe A, O'Brien JM, Senge MO. Trends and targets in antiviral phototherapy. *Photochem Photobiol Sci*. 2019;18(11):2565–2612. doi:10.1039/c9pp00211a

46. Tsen SWD, Kingsley DH, Poweleit C, et al. Studies of inactivation mechanism of non-enveloped icosahedral virus by a visible ultrashort pulsed laser. *Virol J*. 2014;11(1):1–9. doi:10.1186/1743-422X-11-20

47. Costa L, Faustino MAF, Neves MGPMS, Cunha Â, Almeida A. Photodynamic inactivation of mammalian viruses and bacteriophages. *Viruses*. 2012;4(7):1034–1074. doi:10.3390/v4071034

48. Schneider K, Wronka-Edwards L, Leggett-Embrey M, et al. Psoralen inactivation of viruses: A process for the safe manipulation of viral antigen and nucleic acid. *Viruses*. 2015;7(11):5875–5888. doi:10.3390/v7112912

49. Schikora J, Hepburn J, Plavin SR. Reduction of the viral load by non-invasive photodynamic therapy in early stages of COVID-19 infection. *Am J Vir Dis*. 2020; 2(1):01–05.

50. Kampf G. Potential role of inanimate surfaces for the spread of coronaviruses and their inactivation with disinfectant agents. *Infect Prev Pract*. 2020;2(2):100044. doi:10.1016/j.infpip.2020.100044

51. Pratelli A. Action of disinfectants on canine coronavirus replication in vitro. *Zoonoses Public Health*. 2007;54(9–10):383–386. doi:10.1111/j.1863-2378.2007.01079.x

52. Deeb JG, Smith J, Belvin BR, Grzech-Leśniak K, Lewis J. Er:YAG laser irradiation reduces microbial viability when used in combination with irrigation with sodium hypochlorite, chlorhexidine, and hydrogen peroxide. *Microorganisms*. 2019;7(12):612. doi:10.3390/microorganisms7120612

53. Odor AA, Bechir ES, Violant D, Badea V. Antimicrobial effect of 940 nm diode laser based on photolysis of hydrogen peroxide in the treatment of periodontal disease. *Rev Chim*. 2018;69(8):2081–2088. doi:10.37358/rc.18.8.6478

54. Kanno T, Nakamura K, Ishiyama K, et al. Adjunctive antimicrobial chemotherapy based on hydrogen peroxide photolysis for non-surgical treatment of moderate to severe periodontitis: A randomized controlled trial. *Sci Rep*. 2017;7(1):12247. doi:10.1038/s41598-017-12514-0

55. Caccianiga G, Rey G, Baldoni M, Paiusco A. Clinical, radiographic and microbiological evaluation of high level laser therapy, a new photodynamic therapy protocol, in peri-implantitis treatment: A pilot experience. *Biomed Res Int*. 2016;2016:6321906. doi:10.1155/2016/6321906

56. Grzech-Leśniak K, Belvin BR, Lewis PJ, Golob Deeb J. Treatment with Nd:YAG laser irradiation combined with sodium hypochlorite or hydrogen peroxide irrigation on periodontal pathogens: An in vitro study. *Photobiomodul Photomed Laser Surg*. 2021;39(1):46–52. doi:10.1089/pho.2019.4775

57. Nammour S, El Mobadder M, Maalouf E, et al. Clinical evaluation of diode (980 nm) laser-assisted nonsurgical periodontal pocket therapy: A randomized comparative clinical trial and bacteriological study. *Photobiomodul Photomed Laser Surg*. 2021;39(1):10–22. doi:10.1089/photob.2020.4818

58. Wainwright M. Local treatment of viral disease using photodynamic therapy. *Int J Antimicrob Agents*. 2003;21(6):510–520. doi:10.1016/S0924-8579(03)00035-9

59. Ramanathan K, Antognini D, Combes A, Douthwaite S, Goldenberg SD, Weber DJ. Transmission of SARS and MERS coronaviruses and influenza virus in healthcare settings: The possible role of dry surface contamination. *J Hosp Infect*. 2020;92(3):235–250.

Diagnosis of type 1 diabetes during the SARS-CoV-2 pandemic: Does lockdown affect the incidence and clinical status of patients?

Agnieszka Zubkiewicz-Kucharska[A–F], Monika Seifert[B–F], Michał Stępkowski[B–F], Anna Noczyńska[A–F]

Department of Endocrinology and Diabetology for Children and Adolescents, Wroclaw Medical University, Poland

A – research concept and design; B – collection and/or assembly of data; C – data analysis and interpretation;
D – writing the article; E – critical revision of the article; F – final approval of the article

Address for correspondence
Agnieszka Zubkiewicz-Kucharska
E-mail: agnieszka.zubkiewicz-kucharska@umed.wroc.pl

Abstract

Background. Currently, the only effective method to control the spread of the COVID-19 pandemic is social distancing. The lockdown measures during the epidemic may have an impact on the presentation of diabetes and may disturb metabolic control.

Objectives. In order to address the hypothesis that the COVID-19 lockdown affected the incidence rate (IR) of type 1 diabetes (T1D) in the pediatric population of Lower Silesia and the patients' clinical status, the incidence of T1D during the COVID-19 pandemic was analyzed.

Material and methods. Incidence estimates were obtained from the T1D pediatric registry for Lower Silesia which has been maintained since January 1, 2000. The observation was completed on April 30, 2020.

Results. A total of 1961 cases were diagnosed (1054 boys, 53.72%). An increase in the T1D IR was observed, from 10.43/100,000/year in 2000 to 22.06/100,000/year in 2019. The seasonality of T1D incidence was also observed, with the highest IR appearing in January and February. There were half as many cases of T1D in March and April 2020 as in the same months in 2019 (p > 0.05). Diabetic ketoacidosis (DKA) occurred in 31.75% of patients in years 2000-2019, comparably (p > 0.05) to 2020 (36.67% patients), including March and April (50% of patients). The duration of hyperglycemia symptoms was 20.2 ±25.4 days, which was comparable to 2020 (13.1 ±10.96 days; p = 0.1675) and March and April of 2020 (9.67 ±5.63 days; p = 0.0831). Glycated hemoglobin (HbA1c) level was 11.79 ±2.63%, which was comparable to March and April 2020 (13.06 ±2.35%; p = 0.1171), while in all of 2020 it was 13.41 ±2.50% (p = 0.0003).

Conclusions. The IR of T1D in Lower Silesian children in the months of the COVID-19 pandemic was comparable to previous years, while their clinical condition at the time of diagnosis was worse than in previous years.

Key words: type 1 diabetes, COVID-19 pandemic, incidence rate

Background

Spread by droplet transmission, severe acute respiratory syndrome coronavirus 2 (SARS-CoV-2) causes respiratory coronavirus disease (COVID-19). The first reports of SARS-CoV-2 viral infections in the Chinese province of Hubei appeared in the last months of 2019. The high infectivity of this pathogen caused a rapid spread of the COVID-19 disease and an unprecedented outbreak, first in many cities of China and then globally. On January 30, 2020, the World Health Organization (WHO) announced a global health emergency; on March 11, 2020 it was declared a pandemic.

The classic clinical symptoms of COVID-19, in addition to high fever and flu-like symptoms (including muscle pain), relate to the respiratory tract and include fatigue, dry cough, severe interstitial pneumonia, and acute respiratory distress syndrome (ARDS), often requiring the use of respiratory support with mechanical ventilation. Disorders of smell and taste, gastrointestinal symptoms (diarrhea) and neurological symptoms (headache, disturbance of consciousness, and confusion) have also been reported. In severe cases, SARS-CoV-2 infection can cause complications such as renal and circulatory failure. On the other hand, asymptomatic infections seem to be quite common (up to 80% of cases).[1] The risk of a serious course of the disease applies primarily to the elderly and to those with comorbidities, including diabetes.

Because SARS-CoV-2 is a new virus for humanity, only those who have suffered COVID-19 now have adaptive immunity against this coronavirus. It can therefore be concluded that all humanity is susceptible to infection. Since it is a new pathogen, vaccination against it is still unavailable. Unfortunately, there is also no causal treatment.

The reproduction ratio (R0) of this virus is estimated to be between 2 and 3, which means that every patient with COVID-19 infects 2 to 3 people on average, and that the number of affected people therefore doubles every week.[2] Currently, the only effective method of controlling the spread of the COVID-19 epidemic is social distancing. Therefore, governments of many countries, including Poland, decided to close borders, limit travel and introduce quarantine for people returning from abroad. Large gatherings – cultural, sport and religious events – were cancelled. Schools and universities were closed, which affected more than 90% of students globally.[3]

Medical facilities proved to be critical places for the development of the epidemic, and the protection of medical personnel against infection is a priority. Access to medical care has become limited, not only because of the cancellation of planned services, but also because of the closure of health centers due to diagnoses of COVID-19 among staff and/or patients of wards beyond those dedicated to treating the infection. In addition, even in urgent situations, patients delay contacting healthcare providers, as they are afraid of being infected with SARS-CoV-2.

Objectives

With this in mind, the aim of the research was to determine whether the restrictions introduced due to the SARS-CoV-2 epidemic have affected the incidence of type 1 diabetes (T1D) in the pediatric population of Lower Silesia (a region in southwest Poland) or the clinical status of children and adolescents hospitalized because of newly diagnosed T1D.

Material and methods

The incidence of T1D and the clinical status of children and adolescents with T1D diagnosed in the first 4 months of 2020 were compared to historical data. The analysis covered a reference period from January 1, 2000 to December 31, 2019, and an examined period from January 1, 2020 to April 30, 2020. All new cases of T1D in children aged 0–18 years were recorded. All patients were treated in the same reference Center for Pediatric Endocrinology and Diabetology for Lower Silesia. The diagnoses of diabetes were made based on the WHO criteria, with the date of onset defined as the day of the first insulin administration.[4] The incidence rate (IR) was expressed as the number of new cases of T1D per 100,000 people in the general population of a given age group per year. The demographic data was obtained from the Statistical Yearbooks of the Lower Silesian Voivodeship. For the years 2019 and 2020, demographic data from 2018 was used because the statistical data had not been updated yet. The IR was assessed for each year and for individual months of the year.

In addition, the clinical status of children with T1D at the time of diagnosis was analyzed by assessing the presence of diabetic ketoacidosis (DKA) and pH at presentation, the duration of hyperglycemia symptoms before the diagnosis of diabetes, and the glycated hemoglobin (HbA1c) level. Diabetic ketoacidosis was diagnosed according to International Society for Pediatric and Adolescent Diabetes (ISPAD) recommendations.[5]

The statistical measures presented herein are the arithmetic mean (M) and standard deviation (SD). The distribution of the quantitative variables in the analyzed sample was compared with the normal distribution using the Shapiro–Wilk test. When the distribution of the compared samples did not differ significantly from the normal distribution with statistically equal variance, Student's t-test was used to assess the differences. When the assumptions required for Student's t-test were not met, the Mann–Whitney U test was used. A comparison of the frequencies between groups was performed using the χ^2 test. In the case of small sample sizes (i.e., a total <20 or a total <40 and the smallest sample <5), Yates's correction or Fisher's exact test were applied. In all statistical tests, a significance level of $\alpha = 0.05$ was assumed.

Results

In the period 2000–2019 in Lower Silesia, T1D was diagnosed in 1961 children and adolescents, including 1054 boys (53.72%). The overall IR in the study period was 17.51/100,000/year. An increase in the IR was observed – from 10.43/100,000/year in 2000 to 22.06/100,000/year in 2019, with a peak in 2017 (27.10/100,000/year) (Table 1, Fig. 1).

Due to the lack of statistically significant differences between IRs in five-year intervals (Table 1), further analyses were carried out jointly for individual intervals (period I – 2000–2004, period II – 2005–2009, period III – 2010–2014, and period IV – 2015–2019). It should be noted that the IR for T1D in from 2015 to 2019 was twice as high as from 2000 to 2005. The forecast of the IR for T1D in 2020, based on the IR in the first 4 months, is 17.27/100,000/year, which is significantly lower (p = 0.0016) than the IR in the previous period (2014–2019), but comparable to the IR in 2019 (p = 0.0808).

From 2000 to 2019, the IR of T1D among boys (M) was higher than among girls (F) (M: 18.60/100,000/year, F: 16.40/100,000/year; p = 0.0053); however, this result was influenced by the significant difference in the IRs for the period 2010–2014 (M: 21.26/100,000/year; F: 16.27/100,000/year; p = 0.0031), because in the remaining period, the IR for both sexes was comparable. Also, in 2020, the T1D IR was comparable for both sexes (p = 0.5506).

A degree of seasonality in T1D incidence was observed in the study period. Most often, T1D was diagnosed from September to February, with the highest IR being observed
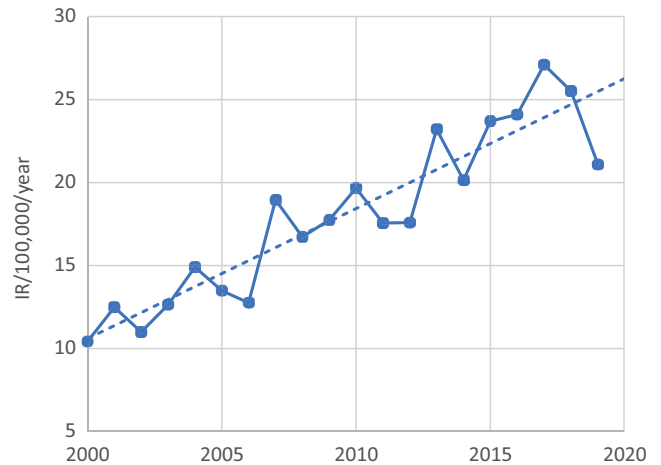
Fig. 1. Incidence rate of type 1 diabetes in Lower Silesia in the period 2000–2019

in January and February. Starting in March, the T1D IR decreased, with the minimum being observed in June and July, followed by an increase in the autumn. Detailed data is presented in Table 2 and Fig. 2. There were half as many cases of T1D in Lower Silesian children in March and April 2020 than in the same months in 2019, but the difference between the IRs was not statistically significant; this was also true when compared with the whole study period (for March p = 0.2788; for April p = 0.8843), as well as for period IV (p = 0.1059 and p = 0.3741 for March and April, respectively). Surprisingly, T1D IRs in March and April 2020 were also comparable to those calculated for January and February this year (p > 0.05).

Table 1A. Incidence rate (IR) of type 1 diabetes in Lower Silesia in the period 2000–2019

Year	2000–2004	2000	2001	2002	2003	2004	p-value
IR/100,000/year	12.22	10.43	12.49	11.0	12.64	14.91	p = 0.1878 p = 0.0358 p = 0.0675
Year	2005–2009	2005	2006	2007	2008	2009	
IR/100,000/year	15.91	13.49	12.76	18.96	16.73	17.75	p = 0.0358
		p = 0.0003					
		p = 0.0087					
Year	2010–2014	2010	2011	2012	2013	2014	
IR/100,000/year	18.77	19.57	17.56	17.59	23.21	20.15	p = 0.0675
Year	2015–2019	2015	2016	2017	2018	2019	
IR/100,000/year	24.46	23.51	24.10	27.10	25.52	22.06	p = 0.5322
	p < 0.0001						

Table 1B. Level of significance of the differences between IRs from different study periods

Years	2000–2004	2005–2009	2010–2014	2015–2019
2000–2004	–	p = 0.0001	p < 0.0001	p < 0.0001
2005–2009	p = 0.0001	–	p = 0.0113	p < 0.0001
2010–2014	p < 0.0001	p = 0.0113	–	p < 0.0001
2015–2019	p < 0.0001	p < 0.0001	p < 0.0001	–

Table 2A. Incidence rate (IR) of type 1 diabetes in Lower Silesia by month

Month	IR/100,000/year						
	2000–2004	2005–2009	2010–2014	2015–2019	2000–2019	2019	2020
January	14.70	23.92	28.58	33.57	23.32	36.84	16.12
February	15.08	21.74	26.29	36.46	23.64	34.53	25.33
March	13.20	20.65	22.86	24.31	18.79	23.02	11.51
April	10.18	13.05	17.15	23.15	15.22	23.02	16.12
May	12.82	10.87	18.29	19.10	15.06	23.02	–
June	6.03	8.70	11.43	19.10	10.85	20.72	–
July	6.41	13.05	17.15	20.83	12.96	18.42	–
August	12.44	10.87	12.57	24.31	15.55	27.63	–
September	10.93	22.83	21.72	20.26	16.84	9.21	–
October	14.70	16.31	22.86	20.26	17.65	11.51	–
November	16.97	13.05	22.86	28.36	20.41	18.42	–
December	13.20	11.96	22.86	27.20	18.30	18.42	–

Table 2B. Statistical significance of the differences in Lower Silesia by month

Month	January	February	March	April	May	June	July	August	September	October	November	December
	p-value											
January	–	0.9065	0.0825	**0.0012**	**0.0009**	**<0.0001**	**<0.0001**	**0.0019**	**0.0111**	**0.0278**	0.2733	0.0531
February	0.9065	–	0.0638	**0.0008**	**0.0006**	**<0.0001**	**<0.0001**	**0.0013**	**0.0079**	**0.0205**	0.2253	**0.0403**
March	0.0825	0.0638	–	0.1290	0.1116	**0.0003**	**0.0101**	0.1696	0.4185	0.6407	0.5203	0.8429
April	**0.0012**	**0.0008**	0.1290	–	0.9417	**0.0333**	0.2885	0.8846	0.4773	0.2924	**0.0310**	0.1866
May	**0.0009**	**0.0006**	0.1116	0.9417	–	**0.0398**	0.3230	0.8273	0.4332	0.2603	**0.0258**	0.1635
June	**<0.0001**	**<0.0001**	**0.0003**	**0.0333**	**0.0398**	–	0.2836	**0.0231**	**0.0047**	**0.0015**	**<0.0001**	**0.0006**
July	**<0.0001**	**<0.0001**	**0.0101**	0.2885	0.3230	0.2836	–	0.2278	**0.0768**	**0.0349**	**0.0014**	**0.0175**
August	**0.0019**	**0.0013**	0.1696	0.8846	0.8273	**0.0231**	0.2278	–	0.5716	0.3639	**0.0441**	0.2396
September	**0.0111**	**0.0079**	0.4185	0.4773	0.4332	**0.0047**	0.0768	0.5716	–	0.7319	0.1469	0.5412
October	**0.0278**	**0.0205**	0.6407	0.2924	0.2603	**0.0015**	**0.0349**	0.3639	0.7319	–	0.2675	0.7883
November	0.2733	0.2253	0.5203	**0.0310**	**0.0258**	**<0.0001**	**0.0014**	**0.0441**	0.1469	0.2675	–	0.4004
December	0.0531	**0.0403**	0.8429	0.1866	0.1635	**0.0006**	**0.0175**	0.2396	0.5412	0.7883	0.4004	–

Values in bold denote statistical significance at the p < 0.05 level.

The clinical status of children was evaluated in five-year clusters: 2000–2004, 2005–2009, 2010–2014, and 2015–2019. In addition, the clinical condition of children diagnosed with T1D in 2019 and 2020 was compared, with a separate group for children diagnosed with T1D in March and April of 2020.

Over the entire study period, DKA occurred in 31.75% of patients with newly diagnosed T1D, statistically significantly less often (p = 0.0210) in period I (23.65%), while in subsequent years, there was a comparable percentage of children (34.23% in period II, 35.59% in period III and 36.71% in period IV; p = 0.9298). In the first 4 months of 2020, DKA was associated with the diagnosis of diabetes in 36.67% of patients, similarly to previous years (p = 0.6874), including 2019 (p = 0.9396). Diabetic ketoacidosis was present in 50% of patients diagnosed with T1D in March and April 2020; nevertheless, its incidence was comparable to previous years (p = 0.3635), including 2019 (p = 0.7450).

The mean pH upon admission to the Department was 7.34 ±0.11. This differed significantly over the study period: from 2015 to 2019, the mean pH was 7.31 ±0.14, significantly lower than in other years (Fig. 3); in period I, the pH was 7.36 ±0.09; in period II, it was 7.36 ±0.11; and in period III, it was 7.33 ±0.10. Metabolic disorders in children diagnosed with T1D in 2020 were even more severe, as the mean pH was 7.26 ±0.19 (p = 0.0169). Moreover, the mean pH in children hospitalized in March and April 2020 (7.19 ±0.24) was lower than in previous years (p = 0.0199).

The mean duration of symptoms of hyperglycemia, as declared by the patient or legal guardian, was 20.2 ±25.4 days throughout the whole study period. It was the longest in period I (25.5 ±30.6 days) and the shortest in period IV (15.1 ±14.5 days) (p < 0.0001). In period II, it was 24.7 ±33.3 days and in period III – 16.9 ±22.2 days (Fig. 4). In 2020, the mean declared duration of symptoms was 13.1 ±10.96 days, which was similar to that observed
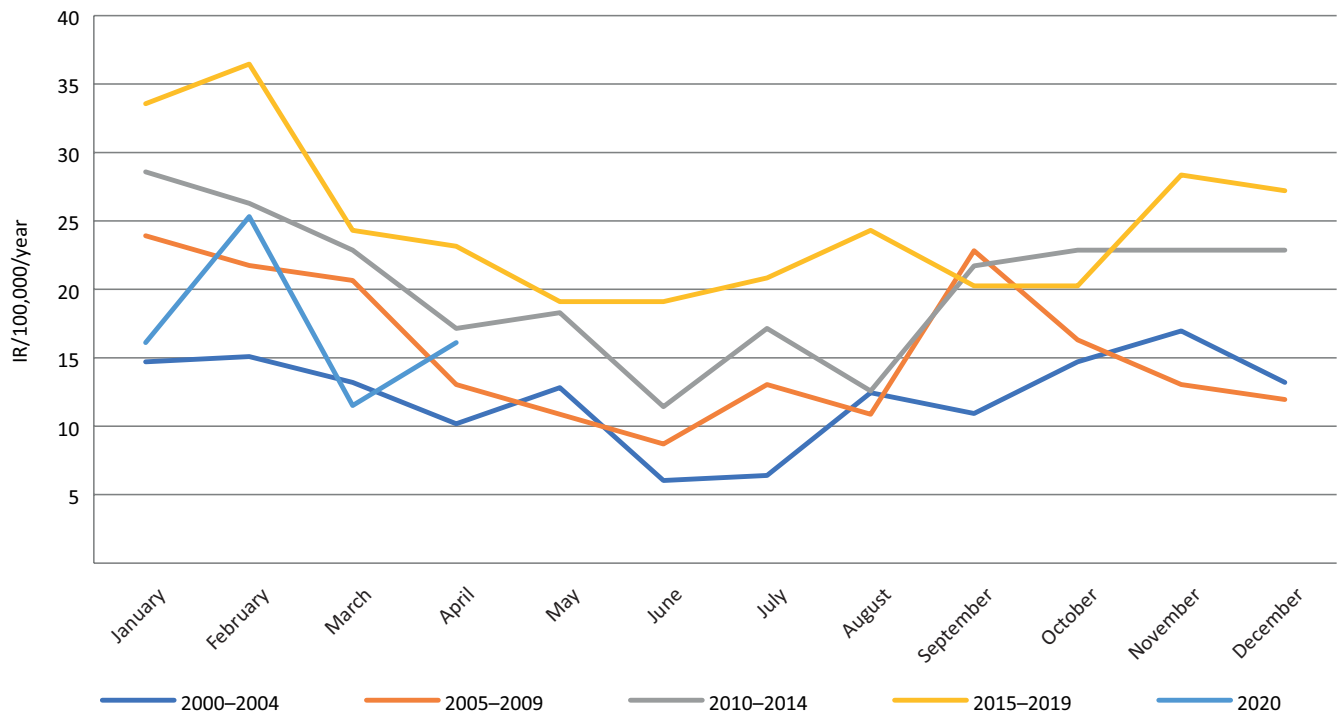
Fig. 2. Incidence rate of type 1 diabetes each month
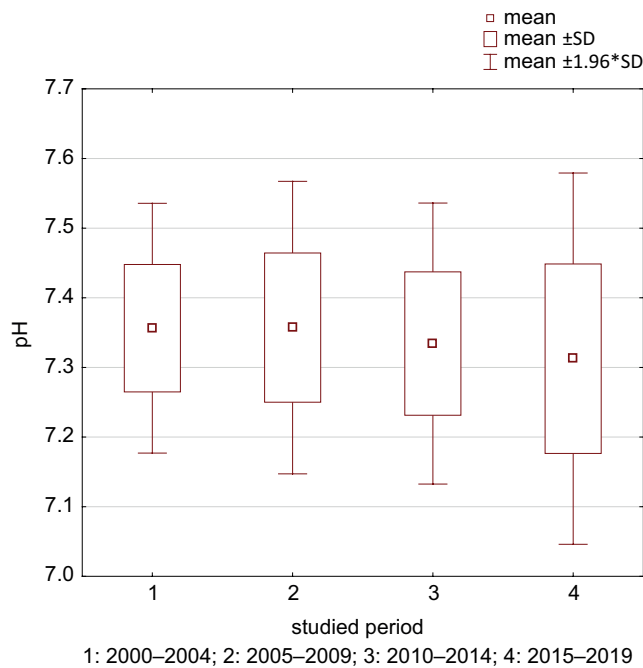
Fig. 3. Mean pH at the presentation of type 1 diabetes in the study periods
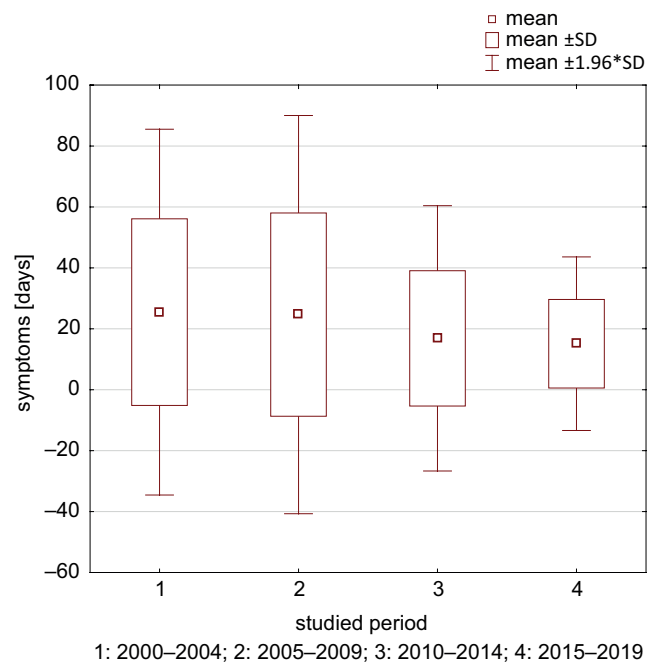
Fig. 4. Mean declared time of hyperglycemia symptoms before type 1 diabetes diagnosis in the study periods

in previous years (p = 0.1675). It should be emphasized that the mean duration of symptoms in patients hospitalized in March and April of 2020 was 9.67 ±5.63 days, though it was comparable both to the previous years (p = 0.0831), to the year 2019 (p = 0.8031), and to January and February of 2020 (p = 0.6149).

The mean HbA1c level in the study group was 11.79 ±2.63%. The highest percentage of HBA1c was

found in children with T1D diagnosed between 2015 and 2019 (12.08 ±2.83%), while the lowest in patients hospitalized from 2010 to 2014 (11.37 ±2.11%) (p = 0.0013). In patients with T1D diagnosed in period I, HbA1c level was 11.59 ±2.72%, while for those diagnosed in period II, it was 11.99 ±2.30% (p = 0.0391). The mean HbA1c levels between periods I and III, as well as between periods II and IV were comparable (p > 0.05), while the mean HbA1c
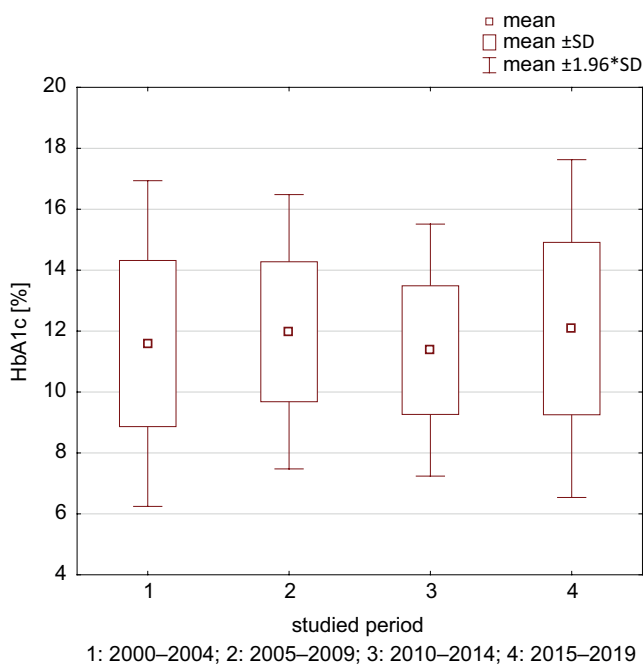
Fig. 5. Mean HbA1c at type 1 diabetes presentation in the study periods

level between periods II and III and between periods I and IV differed significantly (p = 0.0125 and p = 0.0032, respectively) (Fig. 5). The mean HbA1c level in patients diagnosed with T1D in 2020 was 13.41 ±2.50%, which was higher than in previous years (p = 0.0003), including the HbA1c level of patients diagnosed in 2019 (12.17 ±3.0%; p = 0.0234). On the other hand, the HbA1c level in patients in whom T1D was confirmed in March and April of 2020 was 13.06 ±2.35% and did not differ from the mean HbA1c in patients diagnosed in previous years (p = 0.1171), including 2019 (p = 0.3620) and the period of 2020 before the COVID-19 pandemic was announced (p = 0.2915).

Discussion

Numerous studies have indicated an increase in the incidence of T1D at a rate of about 3% per year.[6] Epidemiological studies carried out in Poland have also confirmed this trend, with the T1D IRs for some regions of the country being comparable to data from Western Europe and North America.[7,8] Also, the current study found a two-fold increase in the IR of T1D in children and adolescents in Lower Silesia over the last 20 years. It is noteworthy, however, that in the last 2 years, the IR has decreased: in 2019, it was the lowest in the last 5 years, and the forecast for 2020 is also lower than in previous years. The trend towards stabilization or even a slowdown in the growth of new cases of T1D has been observed in recent years in other countries, not only European ones. Recent reports have also indicated a certain cyclical incidence of diabetes and a periodic decrease in the IR.[6,8] It is therefore possible

that the current decrease in the incidence of T1D among Lower Silesian children, especially the lower IR in the current year, may be due to cyclical fluctuations, as previously described by Chobot et al.[9] On the other hand, the "silence" observed at our center regarding the diagnosis of new cases of T1D in children may be the result of avoiding contact with healthcare providers out of fear of being infected with the new coronavirus, together with the seasonality of the incidence of T1D.

The role of environmental factors in the pathogenesis of diabetes is indisputable and has been confirmed by the fact that the incidence of T1D – especially among older children – changes seasonally, decreasing significantly in the summer months.[10] The seasonality of the presentation of new cases of T1D was previously observed in the Lower Silesian population.[11] Data from 20 years of observation confirms this trend. In the winter months, there are significantly more new cases of T1D in children and adolescents than in summer, and the IR in January and February covered, on average, 1/5 of all new diagnoses in a given year. In absolute numbers, the number of new cases of T1D in our center has been steadily decreasing since March; however, the IR for March was comparable to the IR for January and February, while the IR for April was significantly lower. A similar relationship can be observed this year, although the IR for March 2020 is half that of the previous months and the lowest value for the month of March in the last 20 years.

On March 4, 2020 the first case of SARS-CoV-2 infection in Poland was diagnosed in a man travelling from Germany. On March 20, 2020, an epidemic was announced in the country; however, some restrictions were introduced a few days earlier, including the cancellation of mass events, the closure of national borders and obligatory quarantines for returnees. International rail and air transportation was suspended, domestic transportation was restricted, and schools, colleges, preschools, and nurseries were closed. On March 24, 2020, significant restrictions on movement were introduced: only trips to work, to grocery stores or pharmacies, or to help others were allowed. Children and adolescents up to 18 years of age could only leave home under adult supervision. We were constantly reminded of the need for social distancing.

At the same time, access to the healthcare system was limited, as all planned hospital admissions and surgical procedures were cancelled, and the activities of specialist outpatient clinics were limited to telemedicine consultations. Primary healthcare providers also carried out telemedicine consultations whenever possible. All of these measures were aimed not only at limiting gatherings of people, but also at protecting healthcare workers and securing hospitalization in the situation of an uncontrolled outbreak.

Social distancing is the most important intervention in the case of an epidemic of a disease for which there is no cure or vaccination, as it aims to reduce the possibility

of infection. It seems that – at least so far – the actions taken have had the intended effect, because in Poland there was no rapid increase in infections comparable to that seen in Italy, Spain or Great Britain.[12] On the other hand, public opinion is that contact with the healthcare system has become associated with a high risk of infection, and as such, is limited and delayed.

However, the appearance of T1D in children usually takes a rapid course and has symptoms that are difficult to overlook, which (in a way) forces families to seek help from the healthcare system. Therefore, it was expected that the incidence of T1D in children in 2020 would be comparable to that in previous years. According to the statistical comparison of IRs, this is indeed the case.

On the other hand, if parents and caregivers have deferred contact with the healthcare system for fear of infection with the new virus, the effect should be a deterioration of the children's condition at presentation (e.g., DKA) and a longer duration of hyperglycemia symptoms and higher HbA1c levels. Our study found that DKA was present in half of the children diagnosed with T1D during the pandemic. The pH of these children was significantly lower than that of children diagnosed in previous years and in the months preceding the COVID-19 pandemic. One of the children was in a diabetic coma, which had not been seen in our center since 2000. However, the declared duration of symptoms was shorter and the level of HbA1c lower than in previous years, which would contradict the thesis that parents are postponing contact with healthcare providers and, consequently, delaying diagnosis and treatment; it would rather indicate a more rapid course of the disease.

As with Middle East Respiratory Syndrome (MERS) infection, diabetes is one of the factors determining a severe course and increased mortality in COVID-19. Data from the Centers for Disease Control and Prevention (CDC) registers indicate that patients with diabetes have a 50% higher risk of dying from SARS-CoV-2 infection than those without carbohydrate disorders.[13] This is due to the fact that hyperglycemia alters the immune response, phagocytosis, neutrophil chemotaxis, and cell-mediated immunity. Angiotensin 2 converting enzyme (ACE2) has been identified as the receptor for the main protein of SARS-CoV-2 and is necessary for it to enter the host cell. The ACE2 molecule was proven to be anti-inflammatory and to protect against AH5N1 influenza infection. Acute hyperglycemia has been shown to increase ACE2 cell expression, facilitating SARS-CoV-2 infection. However, after the virus enters the cell, ACE2 expression decreases, resulting in increased susceptibility to the development of an excessive immune response and the occurrence of acute respiratory distress syndrome. It should be emphasized that a lower expression of anti-inflammatory ACE2 is also observed because of long-lasting poor metabolic control of diabetes. This may result in an excessive inflammatory response of the body and cell damage. Then, even a mild COVID-19 infection in patients with chronic hyperglycemia may cause excessive secretion of interleukin 6 (IL-6), IL-1b and tumor necrosis factor α (TNF-α), monocyte chemotactic protein 1 (MCP-1), and other cytokines, thus causing cytokine release syndrome, a "cytokine storm" that leads to rapid deterioration of the patient's health.[14–16]

The expression of ACE2 on pancreatic β cells may potentially lead to β cell damage by the virus and result in insulin deficiency.[17,18] In addition, it should be underlined that inflammation itself is a factor which causes a decrease in insulin sensitivity, and thus an increase in insulin demand. Therefore, in insulinopenic conditions, this will result in a deterioration of metabolic control or faster diabetes manifestation, and potentially its more rapid course. Italian studies have indicated a higher incidence of DKA and of the severe form of the disease.[19]

Patients admitted to our center during the ongoing pandemic did not have any infections. This includes COVID-19, though due to the lack (at that time) of reliable serological tests for SARS-CoV-2, we could not determine whether our patients were infected before the presentation of diabetes. This is undoubtedly a limitation of this study. While a shorter duration of symptoms and a lower percentage of HbA1c indicate a worse clinical condition when diagnosing diabetes, the higher rates of DKA and the significantly lower blood pH could indicate a more rapid course of the disease in these patients. Whether it was due to a COVID-19 infection, needs to be determined in the future.

It should also be remembered that a viral infection trigger an autoimmune reaction, leading to the presentation of T1D, as has already been seen with the coincidence of the outbreak of Coxsackie B5 virus in Jefferson County, Alabama in 1983 and an increase in T1D IR.[20] However, to test this hypothesis, an analysis of the IR of T1D in the following months and years needs to be performed.

Conclusions

The IR of T1D in Lower Silesian children in the months of the COVID-19 pandemic was comparable to previous years, while their clinical condition at the time of diagnosis was worse compared to previous years.

ORCID iDs

Agnieszka Zubkiewicz-Kucharska
    https://orcid.org/0000-0002-6641-6776
Monika Seifert   https://orcid.org/0000-0002-8556-0204
Michał Stępkowski   https://orcid.org/0000-0003-0456-9360
Anna Noczyńska   https://orcid.org/0000-0002-6712-2673

References

1. Yuki K, Fujiogi M, Koutsogiannaki S. COVID-19 pathophysiology: A review. *Clin Immunol*. 2020;215:108427. doi:10.1016/j.clim.2020.108427
2. Zhao S, Lin Q, Ran J, et al. Preliminary estimation of the basic reproduction number of novel coronavirus (2019-nCoV) in China, from 2019 to 2020: A data-driven analysis in the early phase of the outbreak. *Int J Infect Dis*. 2020;92:214–217. doi:10.1016/j.ijid.2020.01.050

3. United Nations Educational, Scientific and Cultural Organization (UNESCO). COVID-19 educational disruption and response. Paris, France: UNESCO; 2020. https://en.unesco.org/covid19/educationresponse. Accessed on April 24, 2020.

4. Wolfsdorf JI, Glaser N, Agus M, et al. ISPAD Clinical Practice Consensus Guidelines 2018: Diabetic ketoacidosis and the hyperglycemic hyperosmolar state. *Pediatr Diabetes*. 2018;19(Suppl 27):155–177. doi:10.1111/pedi.12701.

5. Alberti KG, Zimmet PZ. Definition, diagnosis and classification of diabetes mellitus and its complications. Part 1: Diagnosis and classification of diabetes mellitus provisional report of a WHO consultation. *Diabet Med*. 1998;15(7):539–553. doi:10.1002/(SICI)1096-9136(199807)15:7<539::AID-DIA668>3.0.CO;2-S

6. Patterson CC, Harjutsalo V, Rosenbauer J, et al. Trends and cyclical variation in the incidence of childhood type 1 diabetes in 26 European centres in the 25 year period 1989–2013: A multicentre prospective registration study. *Diabetologia*. 2019;62(3):408–417. doi:10.1007/s00125-018-4763-3

7. Fendler W, Borowiec M, Baranowska-Jazwiecka A, et al. Prevalence of monogenic diabetes amongst Polish children after a nationwide genetic screening campaign. *Diabetologia*. 2012;55(10):2631–2635. doi:10.1007/s00125-012-2621-2

8. Patterson CC, Karuranga S, Salpea P, et al. Worldwide estimates of incidence, prevalence and mortality of type 1 diabetes in children and adolescents: Results from the International Diabetes Federation Diabetes Atlas, 9th edition. *Diabetes Res Clin Pract*. 2019;157:107842. doi:10.1016/j.diabres.2019.107842

9. Chobot A, Polanska J, Brandt A, et al. Updated 24-year trend of type 1 diabetes incidence in children in Poland reveals a sinusoidal pattern and sustained increase. *Diabet Med*. 2017;34(9):1252–1258. doi:10.1111/dme.13345

10. Szypowska A, Ramotowska A, Wysocka-Mincewicz M, et al. Seasonal variation in month of diagnosis of Polish children with type 1 diabetes: A multicenter study. *Exp Clin Endocrinol Diabetes*. 2019;127(5):331–335. doi:10.1055/s-0043-125321

11. Zubkiewicz-Kucharska A, Noczyńska A. Epidemiologia cukrzycy typu 1 na Dolnym Śląsku w latach 2000–2005. *Pediatr Endocrinol Diabetes Metab*. 2010;16(1):45–49.

12. COVID-19 Coronavirus Pandemic. https://www.worldometers.info/coronavirus/. Accessed May on 20, 2020.

13. Remuzzi A, Remuzzi G. COVID-19 and Italy: What next? *Lancet*. 2020;395(10231):1225–1228. doi:10.1016/S0140-6736(20)30627-9

14. Hoffmann M, Kleine-Weber H, Schroeder S, et al. SARS-CoV-2 cell entry depends on ACE2 and TMPRSS2 and is blocked by a clinically proven protease inhibitor. *Cell*. 2020;181(2):271–280.e8. doi:10.1016/j.cell.2020.02.052

15. de Lucena TMC, da Silva Santos AF, de Lima BR, de Albuquerque Borborema ME, de Azevêdo Silva J. Mechanism of inflammatory response in associated comorbidities in COVID-19. *Diabetes Metab Syndr*. 2020;14(4):597–600. doi:10.1016/j.dsx.2020.05.025

16. Hirano T, Murakami M. COVID-19: A new virus, but a familiar receptor and cytokine release syndrome. *Immunity*. 2020;52(5):731–733. doi:10.1016/j.immuni.2020.04.003

17. Fu J, Zhou B, Zhang L, et al. Expressions and significances of the angiotensin-converting enzyme 2 gene, the receptor of SARS-CoV-2 for COVID-19. *Mol Biol Rep*. 2020 May 14:1–10. doi:10.1007/s11033-020-05478-4

18. Li MY, Li L, Zhang Y, Wang XS. Expression of the SARS-CoV-2 cell receptor gene ACE2 in a wide variety of human tissues. *Infect Dis Poverty*. 2020;9(1):45. doi:10.1186/s40249-020-00662-x

19. Bornstein SR, Rubino F, Khunti K, et al. Practical recommendations for the management of diabetes in patients with COVID-19. *Lancet Diabetes Endocrinol*. 2020;8(6):546–550. doi:10.1016/S2213-8587(20)30152-2

20. Wagenknecht LE, Roseman JM, Herman WH. Increased incidence of insulin-dependent diabetes mellitus following an epidemic of Coxsackievirus B5. *Am J Epidemiol*. 1991;133(10):1024–1031. doi:10.1093/oxfordjournals.aje.a115811

Unsuspected femoral hernias diagnosed during endoscopic inguinal hernia repair

Jacek Białecki[1,A–D], Przemysław Pyda[1,2,B,D–E], Ryszard Antkowiak[3,E,F], Paweł Domosławski[4,E,F]

[1] Department of General, Minimally Invasive and Trauma Surgery, Franciszek Raszeja Municipal Hospital, Poznań, Poland

[2] Department of General and Endocrine Surgery and Gastroenterological Oncology, Poznań University of Medical Sciences, Poland

[3] Department of General and Multiorgan Surgery, 3rd Provincial Hospital, Rybnik, Poland

[4] Lower Silesian General Surgery Consultant, Department of General, Gastroenterologic and Endocrine Surgery, Wroclaw Medical University, Poland

A – research concept and design; B – collection and/or assembly of data; C – data analysis and interpretation;
D – writing the article; E – critical revision of the article; F – final approval of the article

Abstract

Background. The laparoscopic totally extraperitoneal inguinal hernia repair (TEP), unlike the Lichtenstein tension-free mesh repair, allows for inspecting the femoral canal area for the presence of an occult femoral hernia.

Objectives. To determine the incidence of an unsuspected femoral hernia in patients undergoing TEP repair.

Material and methods. Data was collected prospectively from 180 patients (23 women) who underwent hernia repair, including examination of the femoral canal, between November 2017 and March 2019, and the incidence of a femoral hernia was determined. Correlations between the incidence of a femoral hernia and sex, age and the type of inguinal hernia diagnosed in the patients (indirect, direct, both indirect and direct) were assessed.

Results. Femoral hernias were found in 14 patients (7.77%). None of the hernias had previously been detected clinically. The incidence of a femoral hernia was higher in women (6/23, 26.07%) than in men (8/157, 5.09%). The incidence of a femoral hernia was higher in older patients: the average age of patients with a femoral hernia was 57.86 years (median: 60 years), whereas the average age of patients without a femoral hernia was 49.92 years (median: 49 years). However, the correlation was not statistically significant. No correlation was found between the incidence of a femoral hernia and the type of inguinal hernia diagnosed in the patients (direct, indirect, both indirect and direct).

Conclusions. The TEP repair allows for detecting and repairing an occult femoral hernia.

Key words: unsuspected femoral hernia, occult hernia, laparoscopic totally extraperitoneal inguinal hernia repair

Background

The Lichtenstein tension-free mesh repair and the laparoscopic totally extraperitoneal inguinal hernia repair (TEP) are the 2 most common methods of inguinal hernia repair. Each method has advantages over the other.[1–3] The Lichtenstein method does not require general anesthesia and is associated with a shorter operating time compared with the TEP method of repair; it also involves a lower risk of complications and recurrence. The main advantages of the TEP method over the Lichtenstein method include better cosmetic results, a faster return to usual activities and a lower risk of chronic postoperative pain. One other advantage of the TEP method is that it allows for inspecting the femoral canal area for the presence of an occult femoral hernia. Routine inspection of the femoral canal is particularly crucial given the low clinical and sonographic detection rate of femoral hernias.[4,5] To inspect the femoral canal area, the preperitoneal space needs to be dissected in the area of iliac vessels. If an unsuspected femoral hernia is found, it can be reduced, and the femoral canal can be secured with the same mesh that is used for inguinal hernia repair in the patient concerned.

Objectives

The purpose of the study was to determine the incidence of femoral hernias found during TEP repair, with a particular focus on the femoral canal examination. One additional objective of the study was to verify to what extent age and sex are risk factors for a femoral hernia and to examine the correlation between the incidence of a femoral hernia and the type of an inguinal hernia diagnosed in the patients (indirect, direct, both indirect and direct).

Material and methods

Data was collected prospectively from 180 patients (23 women) who underwent TEP hernia repair, including examination of the femoral canal, between November 2017 and March 2019, and the incidence of a femoral hernia was determined. We used the following definition of 'femoral hernia' (after Old et al.)[6]: "[Femoral hernia is] any tissue protruding through a well-defined myofascial defect". Correlations between the incidence of a femoral hernia and sex, age and the type of inguinal hernia diagnosed in the patients (indirect, direct, both indirect and direct) were assessed. To determine the relationships between variables in a nominal scale, the phi correlation coefficient (Φ) was calculated. The relationship between the 'age' variable (interval scale) and the 'femoral hernia' variable (nominal scale) was determined using the point-biserial the correlation coefficient. The statistical significance of the calculated correlation coefficients was examined – a level of significance of 0.05 was used. All the patients had given their signed consent for the procedure.

As this is a standard procedure performed at our Center, no consent was sought from the relevant ethics committee.

Surgical procedure

During standard TEP repair, once the inguinal hernia was reduced, the surgeon dissected the preperitoneal space in the area of iliac vessels. Once the area was visualized, the surgeon assessed whether the femoral canal was closed or whether there was a femoral hernia emerging through it. If a femoral hernia was detected, the hernia sac was reduced from the femoral canal. In such a case, the mesh intended to prevent the inguinal hernia from recurring was shaped and positioned in such a way as also to secure the femoral canal. Small fat tissue fragments protruding through the femoral canal were not regarded as a hernia. The content of the femoral canal was reduced only if the tissue appeared to be connected with the peritoneum when pulled towards the bladder and the peritoneum with an instrument. Once the tissue was reduced, it was confirmed whether it was preperitoneal fat or a hernia. In other cases, where the tissue filling the femoral canal was not connected with the peritoneum or preperitoneal fat, it was not removed from the opening.

Results

A total of 182 patients underwent TEP repair. Two patients were excluded from the study due to conversion

Table 1. Characteristics of the study group

Variable	Value	%
Patients, n	182	–
Conversion to Lichtenstein repair, n	2	1.1
Patients included in the study, n	180	–
Average age [years]	50.53	–
Men, n	157	87.2
Women, n	23	12.8
Patients diagnosed with a femoral hernia, n	14	7.77
The average age of patients with a femoral hernia [years]	57.86	–
The average age of patients without a femoral hernia [years]	49.92	–
Men diagnosed with a femoral hernia, n	8	5.1
Women diagnosed with a femoral hernia, n	6	26.1
Indirect inguinal hernias (diagnosed with a femoral hernia), n	119 (9)	66.1 (5.0)
Direct inguinal hernias (diagnosed with a femoral hernia), n	38 (4)	21.1 (2.2)
Indirect and direct inguinal hernias (diagnosed with a femoral hernia), n	23 (1)	12.8 (0.5)
Recurrent hernias, n	15	8.3
Patients with recurrent hernias (diagnosed with a femoral hernia), n	0	0
Complications, n	0	0
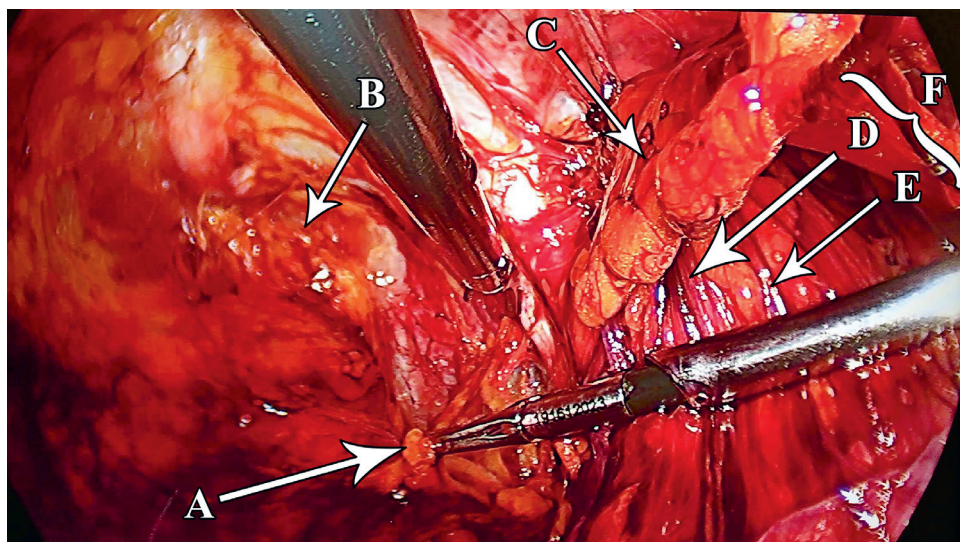
Fig. 1. Right femoral hernia

A – right femoral hernia; B – pubic bone; C – epigastric vessels; D – deferent duct; E – testicular vessels.
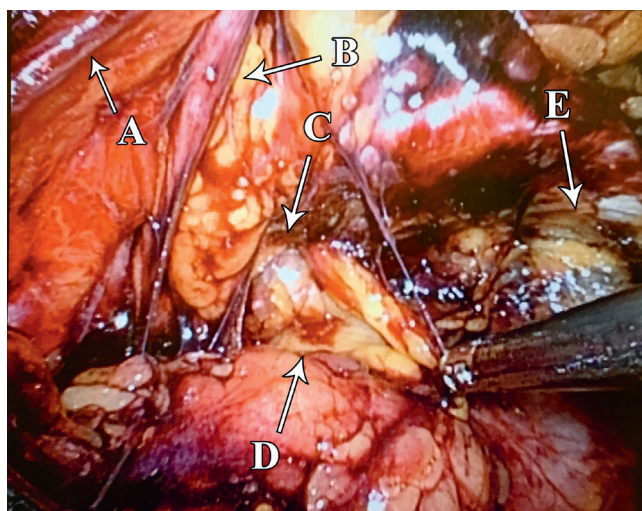
Fig. 2. Left femoral hernia

A – testicular vessels; B – deferent duct; C – femoral ring; D – left femoral hernia; E – pubic bone.
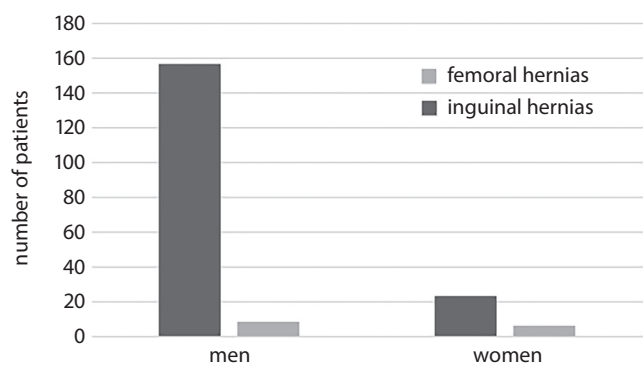
Fig. 3. Unsuspected femoral hernias in men and women

Fig. 4. The incidence of unsuspected femoral hernias and age

clinically. The incidence of femoral hernias was higher in women (6/23, 26.07%) than in men (8/157, 5.09%). The difference was statistically significant (Φ coefficient = −0.26; p = 0.003) (Fig. 3).

The incidence of femoral hernia was higher in older patients: the average age of patients with a femoral hernia was 57.86 years (median: 60 years), whereas the average age of patients without a femoral hernia was 49.92 years (median: 49 years). However, the correlation was not statistically significant (point-biserial correlation coefficient = 0.14, p = 0.064) (Fig. 4).

No correlation was found between the incidence of a femoral hernia and the type of inguinal hernia diagnosed in the patients (direct, indirect, both indirect and direct).

Discussion

The TEP procedure for inguinal hernia repair offers a unique possibility to inspect the femoral canal area for the presence of an occult femoral hernia. It is all the more

to Lichtenstein repair. Thus, 180 patients were included in the study (23 women). Detailed results are shown in Table 1.

Femoral hernias were found in 14 patients (7.77%) (Fig. 1,2). None of the hernias had previously been detected

important as the symptoms of a femoral hernia are often scarce, and thus difficult to detect (both clinically and sonographically).[4,5] Different studies give various incidence rates of a femoral hernia. The incidence reported by Putnis et al., Dulucq et al. and Old et al. was 3.7% (19 of 484 patients),[7] 5.6% (19 of 337 patients)[4] and 2.3% (32 of 1404 patients),[6] respectively. In a study by Henriksen et al., the incidence of a femoral hernia in patients with a recurrent hernia was 9.2%, whereas in patients diagnosed with a bilateral inguinal hernia it was 3.8%.[8] In turn, Waltz et al.[9] demonstrated that in a group of 250 men undergoing inguinal hernia repair, including bilateral exploration of the femoral canal area, the incidence of a femoral hernia was 13%. In our study, the incidence of a femoral hernia was significantly higher in women (26.07%) than in men (5.09%). Such a discrepancy was also observed by Putnis et al., who reported a femoral hernia in 37% of female patients and 3% of male patients.[7] This is also consistent with more general data, which indicates that a femoral hernia is much more common in women.[10,11] Therefore, one of the possible reasons for the discrepancy between the results of our study and those obtained by other authors may be the fact that the patient groups analyzed had different proportions of male and female participants (e.g., in the study by Putnis et al.,[7] 95% of the patients studied were men and 5% were women, whereas in our study, the percentage was 87% and 13%, respectively). The high incidence rate of a femoral hernia provides an additional argument for choosing the TEP method of repair over the Lichtenstein method, especially in high-risk patients, i.e., mainly women,[12] but also in elderly patients. The symptoms of an undetected femoral hernia are also worth considering. Some patients after hernia repair complain about chronic pain.[13] The symptoms are usually interpreted as being associated with the repaired inguinal hernia. Some studies indicate that patients after Lichtenstein repair are more likely to suffer from chronic pain than those undergoing TEP repair.[14,15] One might speculate that in some of these patients, the chronic pain is due to the presence of a small occult femoral hernia. The evaluation of the femoral canal is a safe and fast procedure (it does not result in a significantly longer operating time). Moreover, a femoral hernia detected during TEP inguinal hernia repair may be treated using a different arrangement of the same mesh that is utilized to repair the inguinal hernia in the patient concerned, which minimizes the costs of the procedure.

Conclusions

One additional advantage of the TEP method of repair in patients surgically treated for an inguinal hernia is that it allows for detecting and repairing an occult femoral hernia. Given the discrepancies in the incidence of unsuspected femoral hernias found intraoperatively, it would be beneficial to examine the incidence rate of femoral hernias in a larger group of patients.

ORCID iDs

Jacek Białecki https://orcid.org/0000-0002-3486-8698
Przemysław Pyda https://orcid.org/0000-0001-7988-378X
Ryszard Antkowiak https://orcid.org/0000-0003-1377-1608
Paweł Domosławski https://orcid.org/0000-0003-1903-0843

References

1. Gavriilidis P, Davies RJ, Wheeler J, de Angelis N, Di Saverio S. Total extraperitoneal endoscopic hernioplasty (TEP) versus Lichtenstein hernioplasty: A systematic review by updated traditional and cumulative meta-analysis of randomised-controlled trials. *Hernia*. 2019; 23(6):1093–1103. doi:10.1007/s10029-019-02049-w
2. Bobo Z, Nan W, Qin Q, Tao W, Jianguo L, Xianli H. Meta-analysis of randomized controlled trials comparing Lichtenstein and totally extraperitoneal laparoscopic hernioplasty in treatment of inguinal hernias. *J Surg Res*. 2014;192(2):409–420. doi:10.1016/j.jss.2014.05.082
3. Köckerling F, Bittner R, Kofler M, et al. Lichtenstein versus total extraperitoneal patch plasty versus transabdominal patch plasty technique for primary unilateral inguinal hernia repair: A registry-based, propensity score-matched comparison of 57,906 patients. *Ann Surg*. 2019;269(2):351–357. doi:10.1097/SLA.0000000000002541
4. Dulucq JL, Wintringer P, Mahajna A. Occult hernias detected by laparoscopic totally extra-peritoneal inguinal hernia repair: A prospective study. *Hernia*. 2011;15(4):399–402. doi:10.1007/s10029-011-0795-z
5. Whalen HR, Kidd GA, O'Dwyer PJ. Femoral hernias. *BMJ*. 2011;343: d7668. doi:10.1136/bmj.d7668
6. Old OJ, Kulkarni SR, Hardy TJ, et al. Incidental non-inguinals hernias in totally extra-peritoneal hernia repair. *Ann R Coll Surg Engl*. 2015;97(2):120–124. doi:10.1308/003588414X14055925058959
7. Putnis S, Wong A, Berney C. Synchronous femoral hernias diagnosed during endoscopic inguinal hernia repair. *Surg Endosc*. 2011;25(12): 3752–3754. doi:10.1007/s00464-011-1781-3
8. Henriksen NA, Thorup J, Jorgensen LN. Unsuspected femoral hernia in patients with a preoperative diagnosis of recurrent inguinal hernia. *Hernia*. 2012;16(4):381–385. doi:10.1007/s10029-012-0924-3
9. Waltz P, Luciano J, Peitzman A, Zuckerbraun BS. Femoral hernias in patients undergoing total extraperitoneal laparoscopic hernia repair: Including routine evaluation of the femoral canal in approaches to inguinal hernia repair. *JAMA Surg*. 2016;151(3):292–293. doi:10. 1001/jamasurg.2015.3402
10. Koch A, Edwards A, Haapaniemi S, Nordin P, Kald A. Prospective evaluation of 6895 groin hernia repairs in women. *Br J Surg*. 2005;92(12): 1553–1558. doi:10.1002/bjs.5156
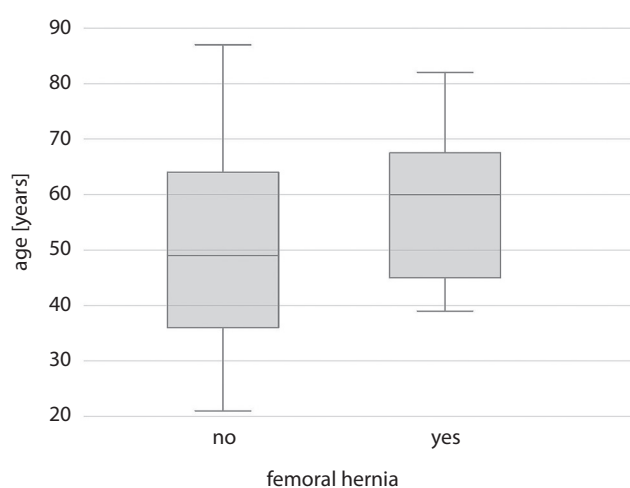11. Köckerling F, Koch A, Lorenz R. Groin hernias in women: A review of the literature. *Front Surg*. 2019;6:4. doi:10.3389/fsurg.2019.00004
12. Lundström KJ, Holmberg H, Montgomery A, Nordin P. Patient-reported rates of chronic pain and recurrence after groin hernia repair. *Br J Surg*. 2018;105(1):106–112. doi:10.1002/bjs.10652
13. Schouten N, Burgmans JP, van Dalen T, et al. Female 'groin' hernia: Totally extraperitoneal (TEP) endoscopic repair seems the most appropriate treatment modality. *Hernia*. 2012;16(4):387–392. doi:10. 1007/s10029-012-0904-7
14. Eker HH, Langeveld HR, Klitsie PJ, et al. Randomized clinical trial of total extraperitoneal inguinal hernioplasty vs Lichtenstein repair: A long-term follow-up study. *Arch Surg*. 2012;147(3):256–260. doi:10. 1001/archsurg.2011.2023
15. Eklund A, Montgomery A, Bergkvist L, Rudberg C; Swedish Multicentre Trial of Inguinal Hernia Repair by Laparoscopy (SMIL) study group. Chronic pain 5 years after randomized comparison of laparoscopic and Lichtenstein inguinal hernia repair. *Br J Surg*. 2010;97(4):600–608. doi:10.1002/bjs.6904

Stilbene glycoside upregulates SIRT3/AMPK to promotes neuronal mitochondrial autophagy and inhibit apoptosis in ischemic stroke

Yuxian Li[1,A,D,E], Ke Hu[1,A,D–F], Minghua Liang[2,A,D,F], Qing Yan[3,A,D,F],
Minjiang Huang[1,A,C], Ling Jin[1,A,F], Yuefu Chen[1,A,C], Xirong Yang[4,A–C], Xiaobo Li[5,A,D,E]

[1] School of Medicine, Hunan University of Medicine, Huaihua, China

[2] Department of Pediatrics, First People's Hospital of Huaihua, China

[3] School of Nursing, Hunan University of Medicine, Huaihua, China

[4] Department of Neurology, The First Affiliated Hospital of Hunan University of Medicine, Huaihua, China

[5] Department of Neurology, The Third Xiangya Hospital, Central South University, Changsha, China

A – research concept and design; B – collection and/or assembly of data; C – data analysis and interpretation;
D – writing the article; E – critical revision of the article; F – final approval of the article

Address for correspondence
Xiaobo Li
E-mail: lixiaoboxy3h@163.com

Conflict of interest
None declared

Abstract

Background. Ischemic stroke, also known as cerebrovascular accident or cerebral stroke, occupies the first place in the world's top 10 causes of death, with high incidence, mortality and disability rates.

Objectives. To investigate the effect of stilbene glycoside upregulated SIRT3/AMPK expression on neuronal mitochondrial autophagy and neuronal apoptosis in ischemic stroke.

Material and methods. The PC12 cells were cultured without serum to construct an ischemic neuron model. The cells were divided into 6 groups: normal group (untreated cells), model group (ischemic treated cells), TSG group (stilbene glycoside treatment), NC group (SIRT3 and AMPK negative control treatment), si-SIRT3 group (SIRT3 silencing treatment), TSG+si-SIRT3 group (joint treatment), and TSG+si-SIRT3+oe-AMPK group (joint treatment). Cell survival and the expression of related molecules were detected.

Results. Compared with normal group, the model group had significantly decreased cell survival rate, mitochondrial membrane potential, as well as the expression of Bcl-2, LC3II/I, P62, PINK1, Parkin, SIRT3, AMPK, and p-AMPK, while showing significantly increased proportion of apoptosis and the expression of caspase 3 and Bax. Compared with the model group, TSG treatment promoted cell survival rate and mitochondrial autophagy, and inhibited apoptosis, while SIRT3 silencing treatment reduced cell survival rate and mitochondrial autophagy, and increased apoptosis. The SIRT3 silencing could block the inhibitory effect of TSG on the apoptosis of ischemic PC12 cells and promote mitochondrial autophagy, and AMPK overexpression could save the apoptosis of ischemic PC12 cells caused by SIRT3 silencing, and promote mitochondrial autophagy.

Conclusions. By promoting the expression of SIRT3/AMPK, TSG promotes mitochondrial autophagy in ischemic neurons and inhibits their apoptosis.

Key words: apoptosis, PC12 cells, mitochondrial, ischemic, sirtuin 3

Background

Ischemic stroke, also known as cerebrovascular accident or cerebral stroke, occupies the first place in the world's top ten causes of death, with high incidence, mortality and disability rate.[1,2] The incidence of ischemic stroke in the elderly is very high, and there is a trend of increasing year by year, seriously threatening the life of patients in their later years.[3,4] Ischemic stroke affects the supply of oxygen, sugar and blood in some brain tissues, which leads to the destruction of corresponding brain tissues.[5,6]

Current studies mainly consider inflammation, apoptosis, oxidative stress response and mitochondrial dysfunction of neurons as the main mechanisms of occurrence of ischemic stroke.[7–9] At present, it is generally believed that apoptosis is the ultimate cause of ischemic stroke. After ischemic injury of neurons, on the one hand, caspase 3 can be activated to induce apoptosis,[10] and on the other hand, Bcl-2 protein family can promote apoptosis by binding Bax and anti-apoptosis protein Bcl-2.[11] Moreover, studies have found that autophagy occurs in neurons after ischemia and can maintain cell homeostasis through autophagy.[12] Mitochondrial autophagy is one of the ways of autophagy.[13]

Stilbene glycoside is one of the ingredients extracted from *Polygonum multiflorum*.[14] Current studies have shown that stilbene glycoside can improve ischemia-reperfusion injury by inhibiting neuronal apoptosis, and the development of ischemic stroke eventually leads to the occurrence of ischemia-reperfusion.[15,16] However, in ischemic stroke, the specific molecular mechanism of stilbene glycoside improving neuronal damage is not yet clear.

SIRT3 is a member of the NAD^+-dependent class III histone deacetylase, and as a mitochondrial histone deacetylase, has a significant inhibitory effect on tumors.[17] In addition, a study has shown that SIRT3 can activate downstream AMPK pathway after deacetylation.[18,19] AMPK is one of the typical protein kinases in eukaryotes and has a regulatory effect on mitochondrial autophagy.[20] However, the mechanism of SIRT3/AMPK on apoptosis and mitochondrial autophagy in ischemic stroke is not yet clear.

Objectives

In this study, we cultured PC12 cells of rats and treated them with hypoxia to simulate neuronal ischemic injury in vitro, and explored the mechanism of stilbene glycoside effect on ischemic neuron injury through drug treatment and transfection.

Methods

Cell culture

Rat PC12 cells were cultured and purchased from the ATTC library (Manassas, USA). PC12 cells were cultured in Dulbecco's modified Eagle's medium (DMEM), in which 10% fetal bovine serum (FBS), 100 U/mL of penicillin and 100 mg/mL of streptomycin were added. The cells were cultured at 37°C and 5% CO_2.

Grouping

The PC12 cells were divided into 6 groups: normal group (untreated cells), model group (ischemic-treated cells), NC group (SIRT3 and AMPK negative control treatment), TSG group (stilbene glycoside treatment), si-SIRT3 group (SIRT3 silencing treatment), TSG+si-SIRT3 group (joint treatment), and TSG+si-SIRT3+oe-AMPK group (SIRT3 silencing and AMPK overexpression joint treatment). The NC group, si-SIRT3 group, TSG+si-SIRT3 group, and TSG+si-SIRT3+oe-AMPK group were all transfected with Lipofectamine 2000 (Invitrogen, Carlsbad, USA) 24 h before modeling. The transfection steps were conducted according to the operation instructions of the kit. In the TSG group, TSG+si-SIRT3 group and TSG+si-SIRT3+oe-AMPK group, 10 µm/L of stilbene glycoside (6 wells and 2 mL/well) was added to the medium for culture, and the cells of other groups were added with the same amount of dimethyl sulfoxide (DMSO). The TSG was purchased from Nanjing Senberga Biotechnology Co., Ltd. (Nanjing, China), and the rest of the vectors were prepared by Wuhan Jinkairui Biological Engineering Co., Ltd (Wuhan, China). The cells were collected by centrifugation at 350 g for 6 min. Then, the cells were washed twice with phosphate-buffered saline (PBS; sterile, pH 7.4). The normal group cells were resuspended and cultured in standard DMEM. The cells in other groups were resuspended in DMEM without glucose and cultured in air at 37°C, 5% CO_2, 94% N_2, and 1% O_2 for 6 h under humid conditions. After 6 h of culture, the medium was replaced with standard DMEM to avoid the influence of secretions generated during the sugar-deficient treatment during the later experiment. The medium was then reoxygenated in a humid condition at 37°C, 5% CO_2, and 95% air for 24 h. After centrifugation at 350 g for 6 min, cells were collected for subsequent experiments.

CCK-8 experiment

Cell proliferation was measured using a cell counting kit (Art. No. GM-040101-5; Dojindo, Gaithersburg, USA) according to kit instructions. Cells with logarithmic growth after transfection were taken, digested with trypsin, washed with PBS, and then suspended. Cells were transferred into 96-well plate by adjusting the cell concentration to 5×10^3 cells/µL. Each group was set up with 6 double-hole, the cells were placed in 37°C and 5% CO_2 cell incubator, and cultured for 2 days continuously. For the last 4 h, 10 µL of CCK8 solution was added in each well. After 4 h of continuous culture, the optical density (OD) value was measured at the wavelength of 450 nm

on a spectrophotometer (model UV-1800A; Shanghai Meixi Instrument Co., Ltd., Shanghai, China). The number of living cells in different treatment groups was estimated based on the OD value, and the cell survival rate was calculated. The experiment was repeated 3 times. The OD value was experimental group cell hole OD value after the subtraction of the blank hole cell OD value; the cell survival rate was the experimental hole OD value/parallel control hole OD value multiplied by 100%.

Flow cytometry

Cell apoptosis

The cells were collected 48 h after transfection and the cell concentration was adjusted to 1×10^6 cells/mL. Pre-cooled ethanol solution with a volume fraction of 70% was added to fix the cells, and then they were stored overnight at 4°C. After washing twice with PBS, 100 μL of cell suspension (no less than 10^6 cells/mL) was taken, and the cells were centrifuged and resuspended in 200 μL of binding buffer; then, 10 μL of Annexin V-FITC and 5 μL of PI were added and lightly mixed, and the mixture was kept out of light for 15 min at room temperature. Then, 300 μL of binding buffer was added. Apoptosis was detected using flow cytometry (Attune NxT; Thermo Fisher Scientific, Waltham, USA) at the excitation wavelength of 488 nm.

Mitochondrial membrane potential detection

PC12 cells were collected and washed with PBS once, and 1 mL of PBS was added. Then, 200 μL of JC-1 staining working solution were added and mixed well. The cells was incubated at 37°C for 20 min in cell incubator. Mitochondrial membrane potential was detected with flow cytometry.

qRT-PCR

The total RNA of cells was extracted using Trizol. The primers were designed and synthesized by Shanghai Shenggong Biological Company (Shanghai, China; Table 1). The obtained RNA was reverse-transcribed into cDNA using PrimeScriPt RT kit (RR036A; TaKaRa Bio Inc., Kusatsu, Japan). The reverse transcriptional system was 10 μL with the reaction conditions as follows: 37°C for 15 min 3 times (reverse transcriptional reaction) and 85°C for 5 s. The fluorescent quantitative reverse-transcription polymerase chain reaction (qRT-PCR) was performed according to the manufacturer's instructions for SYBR® Premix Ex Taq™ II kit (RR820A; TaKaRa). The ABI7500 quantitative PCR instrument (7500; Applied Biosystems, Foster City, USA) was used for real-time quantitative PCR detection. The reaction conditions were: pre-denaturation at 95°C for 30 s, denaturation at 95°C for 5 s, annealing extension at 60°C for 30 s, and cycling 40 times. The relative

Table 1. Primer sequences

Name	Sequence (5′-3′)
Caspase 3	F: AGTTGACGCTAAGCCAGACC
	R: GCAGATCCTGCATCTTTGCG
Bax	F: TGGCGATGAACTGGACAACA
	R: CACGGAAGAAGACCTCTCGG
Bcl-2	F: CCTCCCCAAACTGCTCAAGT
	R: TCAGCTCCATGGCTAGTGCT
SIRT3	F: CCTGTCTGTACTGGCGTTGT
	R: GGACTCAGAGCAAAGGACCC
AMPK	F: ATGACAACCACCACGGAGAT
	R: AGAGAAGAGTCGGGAGACCC
GAPDH	F: TGTGAACGGATTTGGCCGTA
	R: GATGGTGATGGGTTTCCCGT

transcription levels of caspase 3, Bax, Bcl-2, SIRT3 and AMPK were calculated using the relative quantitative method ($2^{-\Delta\Delta Ct}$ method) and *GAPDH* was the internal reference primer:

$$\Delta\Delta Ct = \Delta Ct_{\text{model group}} - \Delta Ct_{\text{normal group}},$$

$$\Delta Ct = Ct_{\text{(target gene)}} - Ct_{\text{(internal reference)}},$$

and the relative transcription level = $2^{-\Delta\Delta Ct}$.

Western blot

The RIPA lysate containing phenylmethylsulfonyl fluoride (PMSF) was added to lysed cells and the total protein was obtained by centrifugation at 12,000 g for 10 min at 4°C. After protein quantitative detection, 50 μg of protein was separated with electrophoresis on a 10% SDS-PAGE gel and transferred to a polyvinylidene fluoride (PVDF) membrane. After being sealed with 5% skim milk at room temperature for 1 h, the PVDF membrane was rinsed with PBS for 2 min. The PVDF membrane was incubated with diluted primary antibody rabbit anti-caspase3 (ab133847; Abcam, Cambridge, USA), Bax (ab32503; Abcam), Bcl-2 (ab196495; Abcam), SIRT3 (ab189860; Abcam), AMPK (ab80039; Abcam), p-AMPK (ab23875; Abcam), LC3II/I (ab128025; Abcam), P62 (ab91526; Abcam), PINK1 (ab23707; Abcam), Parkin (ab233434; Abcam), and *GAPDH* (ab37168; Abcam) overnight at 4°C. After being washed with Tris-buffered saline with Tween 20 (TBST) 3 times, the PVDF membrane was incubated with 1:100 diluted horseradish peroxidase (HRP)-labeled secondary anti-goat anti-rabbit IgG antibody (ab150077; Abcam) for 1 h and washed with TBST 3 times for 10 min each. The membrane was developed using enhanced chemiluminescence (ECL) solution (ECL808-25; Biomiga, San Diego, USA). *GAPDH* was used as an internal reference, and the ratio of the gray value of the target band to the internal reference band was used as the relative expression of the protein. Each experiment was repeated 3 times.

Statistical analysis

Data analysis and processing were performed with SPSS v. 21.0 (IBM Corp., Armonk, USA) software. All measurement data was expressed as mean ± standard deviation (SD). Comparison between groups was performed with one-way analysis of variance (ANOVA) combined with post-hoc Bonferroni pairwise comparison test. The level of significant difference was set at $p < 0.05$.

Results

Cell proliferation in each group

To investigate the effects of stilbene glycoside and SIRT3/AMPK on ischemic neurons, cell viability in each group was measured using CCK-8. The results showed that compared with the normal group, the cell survival rates of model group were significantly decreased ($p < 0.05$). Compared with the model group, the cell survival rate of the TSG group was significantly higher, while that of the si-SIRT3 group was lower ($p < 0.05$), but there was no significant difference between the NC group and the TSG+si-SIRT3 group ($p > 0.05$). Compared with the TSG group, the cell survival rate of the TSG+si-SIRT3 group was lower. Compared with the TSG+si-SIRT3 group, the cell survival rate of the TSG+si-SIRT3+oe-AMPK group was significantly higher ($p < 0.05$; Fig. 1).
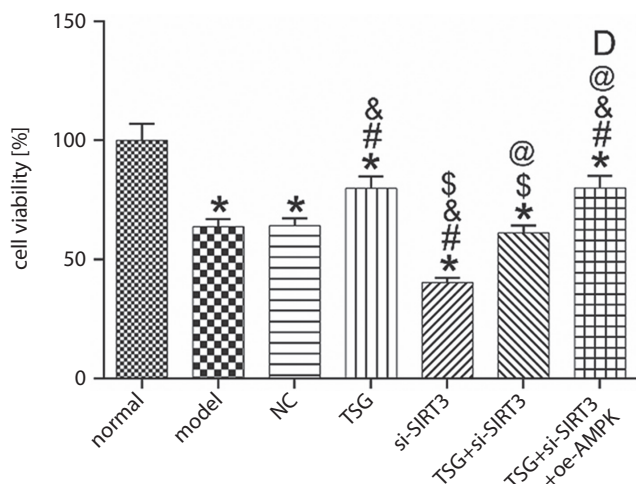
Fig. 1. Statistical results of cell viability in each group

*$p < 0.05$ – compared with the normal group; #$p < 0.05$ – compared with the model group; &$p < 0.05$ – compared with the NC group; $$p < 0.05$ – compared with the TSG group; @$p < 0.05$ – compared with the si-SIRT3 group; D$p < 0.05$ – compared with the TSG+si-SIRT3 group.

Apoptosis in each group

The apoptosis rate of each group was detected using flow cytometry (Fig. 2A,B), and the expression of apoptosis-related factors caspase 3, Bax and Bcl-2 at the molecular level were detected with qRT-PCR and western blot (Fig. 2C–E).

The results showed that compared with the normal group, the model group showed significantly increased apoptosis rate of cells, mRNA and protein expression of caspase 3 and Bax, and significantly decreased expression of Bcl-2 ($p < 0.05$). Compared with the model group, the TSG group had significantly decreased apoptosis rate and the mRNA and protein expression of caspase 3 and Bax, but significantly increased expression of Bcl-2; however, the si-SIRT3 group had opposite results in these indicators ($p < 0.05$), and there was no significant difference in these indicators between the TSG+si-SIRT3 group and si-SIRT3+oe-AMPK group ($p > 0.05$). Compared with the TSG group, the TSG+si-SIRT3 group had significantly increased apoptosis rate and expression of caspase 3 and Bax, but significantly decreased expression of Bcl-2 ($p < 0.05$). Compared with the TSG+si-SIRT3 group, the TSG+si-SIRT3+oe-AMPK group had significantly decreased apoptosis rate and the expression of caspase 3 and Bax, and significantly increased expression of Bcl-2 ($p < 0.05$).

Mitochondrial autophagy in each group

The changes of mitochondrial membrane potential in each group were detected using flow cytometry (Fig. 3A,B). The protein expression of autophagy-related genes *LC3II/I*, *P62* and mitochondrial autophagy genes *PINK1* and Parkin were detected with western blot (Fig. 3C,D). Compared with the normal group, the model group had significantly reduced mitochondrial membrane potentials and the protein expression of *LC3II/I*, *P62*, *PINK1*, and Parkin ($p < 0.05$). Compared with the model group, these indices were significantly increased in the TSG group, but significantly decreased in the si-SIRT3 group ($p < 0.05$), and there was no significant difference in each index of cells between the NC group and the TSG+si-SIRT3 group ($p > 0.05$). Compared with the TSG group, these indices were significantly reduced in the TSG+si-SIRT3 group ($p < 0.05$). Compared with TSG+si-SIRT3 group, these indices were significantly increased in the TSG+si-SIRT3+oe-AMPK group ($p < 0.05$).

Expression of SIRT3/AMPK signaling pathway

The expression of SIRT3, AMPK and p-AMPK in each group was detected with qRT-PCR and western blot (Fig. 4). The results showed that the expression of SIRT3, AMPK and p-AMPK in the model group was significantly lower than in the normal group ($p < 0.05$). Compared with the model group, the expression of SIRT3, AMPK and p-AMPK was significantly increased in the TSG group, while the si-SIRT3 group had significantly decreased expression of SIRT3 and p-AMPK ($p < 0.05$) and similar expression of AMPK ($p > 0.05$). Compared with TSG group, the TSG+si-SIRT3 group showed significantly decreased expression of SIRT3 and p-AMPK ($p < 0.05$), and

A

B

C

D

E
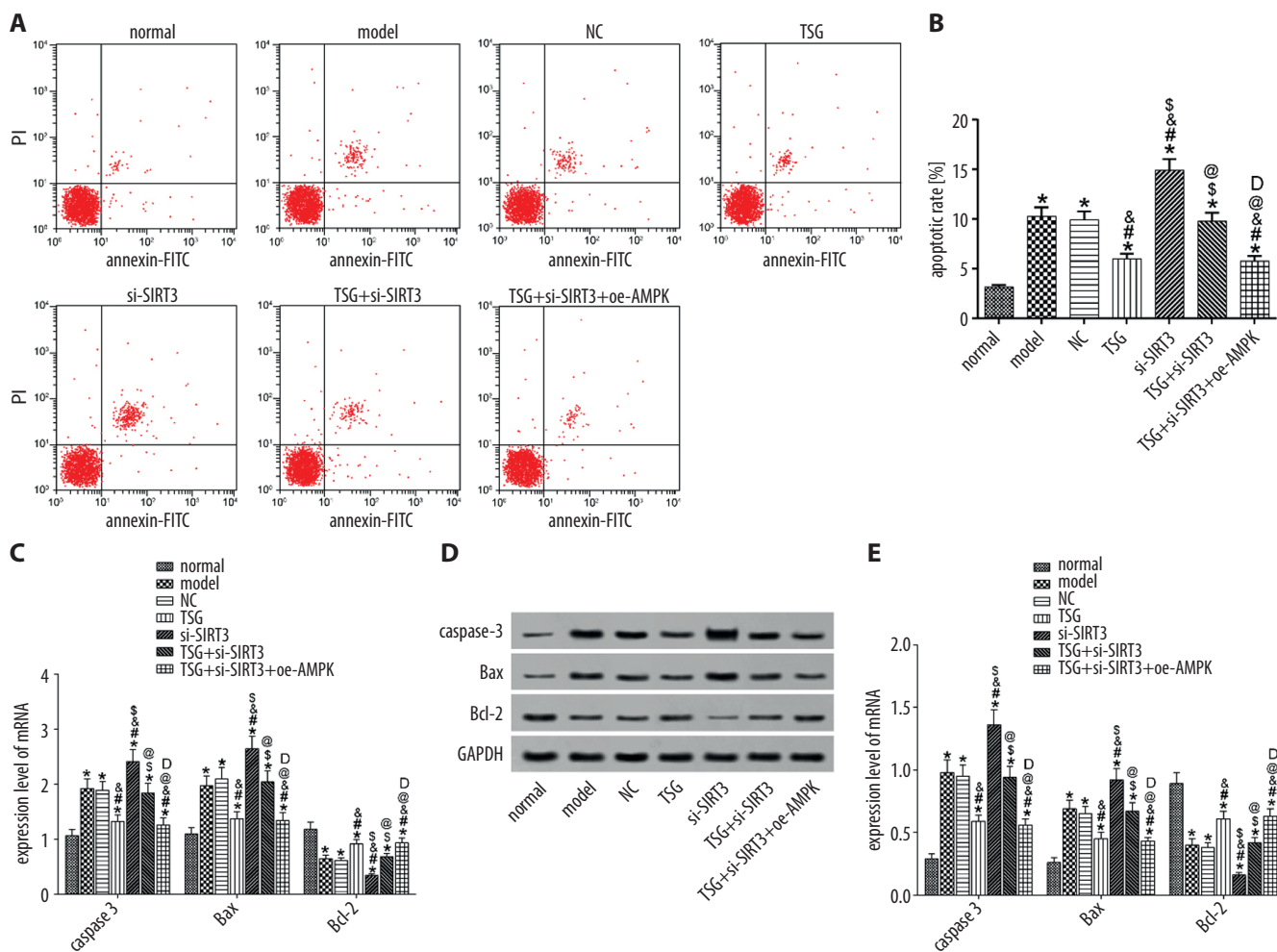
Fig. 2. Effects of stilbene glycoside and SIRT3/AMPK on ischemic neuron apoptosis. A. Flow cytometry. B. Statistical results of apoptosis rate in each group. C. qRT-PCR detetion of mRNA expression of apoptosis-related factors in each group. D. Western blot. E. Protein expression of apoptosis-related factors in each group

*p < 0.05 – compared with the normal group; #p < 0.05 – compared with the model group; &p < 0.05 – compared with the NC group; $p < 0.05 – compared with the TSG group; @p < 0.05 – compared with the si-SIRT3 group; Dp < 0.05 – compared with the TSG+si-SIRT3 group.

similar expression of AMPK (p > 0.05). Compared with TSG+si-SIRT3 group, there was no significant difference in the expression of SIRT3 in TSG+si-SIRT3+oe-AMPK group (p > 0.05), and the expression of AMPK and p-AMPK was significantly increased (p < 0.05).

Discussion

At present, studies have shown that stilbene glycoside exerts an improving effect on cerebral ischemia-reperfusion injury, and can inhibit neuronal apoptosis by affecting the expression of related proteins in the brain, thus protecting neurons in the brain.[21,22] In this study, PC12 cells were treated with stilbene glycoside after 12 h of starvation treatment in a serum-free environment. The results showed that the apoptosis of PC12 cells treated with stilbene glycoside was significantly decreased, while the mitochondrial membrane potential and mitochondrial autophagy were significantly increased. This suggests that stilbene glycoside can significantly alleviate the ischemic injury of neurons.

It is generally believed that SIRT3 is related to energy metabolism and cellular oxidation.[23] It can regulate adenosine triphosphate (ATP) production and affect mitochondrial membrane potential, and then inhibit apoptosis.[24] Other studies have shown that SIRT3 can inhibit apoptosis by inhibiting Bax translocation. After SIRT3 deacetylation, the phosphorylation level of AMPK was not affected.[25,26] The AMPK, on the one hand, can accelerate the removal of reactive oxygen species (ROS) by reducing their formation, and improve the body environment; on the other hand, it can activate the expression of Bcl-2 and inhibit apoptosis.[27] In this study, we also confirmed that in ischemic-injured PC12 cells, after SIRT3 silencing, the cell survival rate was significantly decreased, the apoptosis rate was significantly increased and the mitochondrial autophagy was significantly decreased. Moreover, after the overexpression of AMPK, ischemic injury can be partially saved by reducing apoptosis and promoting
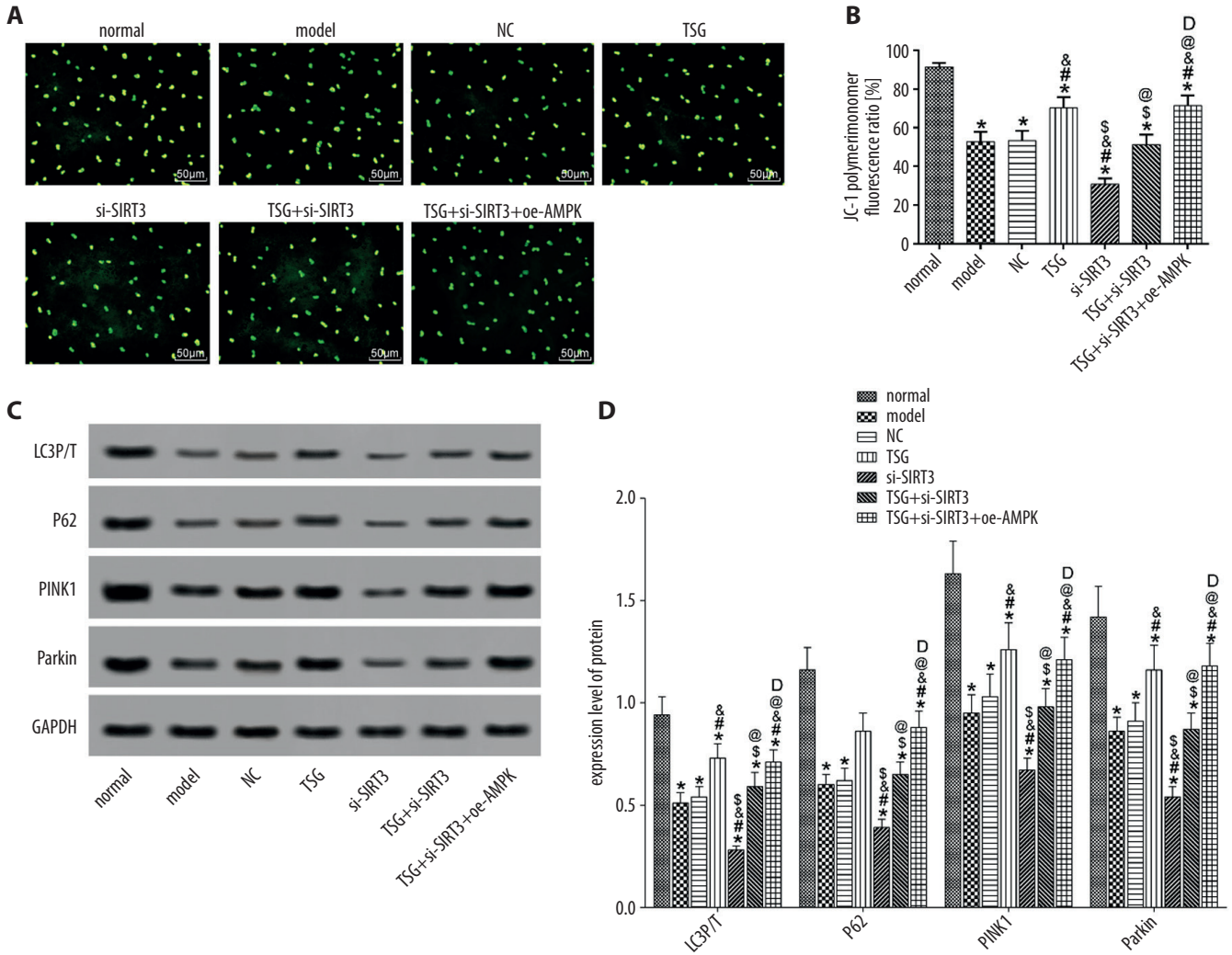
Fig. 3. Effect of stilbene glycoside and SIRT3/AMPK on ischemic neuron autophagy. A. Flow cytometry. B. Statistical results of mitochondrial membrane potential in each group. C. Western blot. D. Protein expression of autophagy marker factor and mitochondrial autophagy marker factor in each group

*p < 0.05 – compared with the normal group; #p < 0.05 – compared with the model group; &p < 0.05 – compared with the NC group; $p < 0.05 – compared with the TSG group; @p < 0.05 – compared with the si-SIRT3 group; Dp < 0.05 – compared with the TSG+si-SIRT3 group.
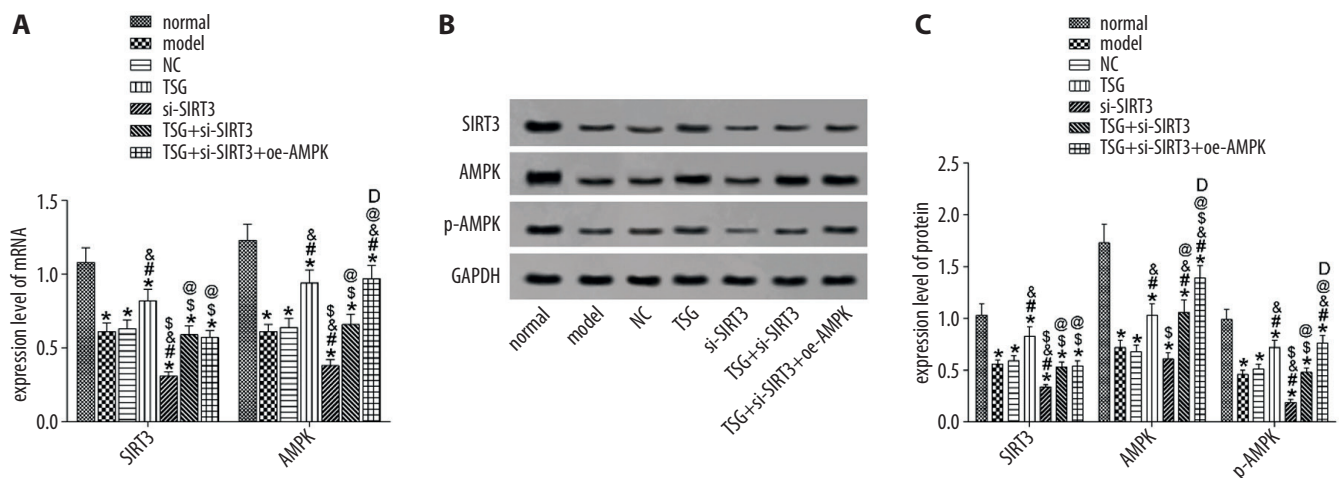
Fig. 4. SIRT3/AMPK signaling pathway expression in each group. A. qRT-PCR detection of mRNA expression of SIRT3/AMPK signaling pathway factor in each group. B. Western blot. C. Protein expression of SIRT3/AMPK signaling pathway factor in each group

*p < 0.05 – compared with the normal group; #p < 0.05 – compared with the model group; &p < 0.05 – compared with the NC group; $p < 0.05 – compared with the TSG group; @p < 0.05 – compared with the si-SIRT3 group; Dp < 0.05 – compared with the TSG+si-SIRT3 group.

mitochondrial autophagy. These results indicate that SIRT3/AMPK can promote mitochondrial autophagy and improve neuronal damage by inhibiting apoptosis.

In view of the similar effects of stilbene glycoside and SIRT3/AMPK on ischemic neurons, we speculated whether there was a regulatory relationship between stilbene glycoside and SIRT3/AMPK. We detected SIRT3/AMPK expression in model group and TSG group, and found that SIRT3 and p-AMPK expression in cells treated with stilbene glycoside were significantly increased. In order to further explore the regulatory relationship between stilbene glycoside and SIRT3/AMPK, we treated PC12 cells with both stilbene glycoside and SIRT3 silencing, and compared them with the group treated with stilbene glycoside alone. The results showed that after the joint treatment of stilbene glycoside and SIRT3 silencing, the cell survival rate was decreased, the apoptosis rate was increased and the mitochondrial autophagy was decreased. Moreover, there was no significant difference in the cell survival rate and apoptosis rate between them and the untreated ischemic PC12 cells. This suggests that SIRT3 can block the improvement effect of stilbene glycoside on ischemic neurons.

Conclusions

We found that stilbene glycoside can promote the expression of SIRT3/AMPK, thereby inhibiting the apoptosis of ischemic neurons, promoting mitochondrial autophagy and achieving the effect of improving neuron damage. On the one hand, this study shed more light on the pathogenesis of ischemic stroke and the influence mechanism of stilbene glycoside in ischemic stroke; on the other hand, it also clarified the effect of SIRT3/AMPK on mitochondrial autophagy and the effect of mitochondrial autophagy on neurons. However, we found that SIRT3 silencing did not completely block the improvement effect of stilbene glycosides on ischemic neurons, which means that stilbene glycosides can also improve ischemic neuron damage by affecting the expression of other factors. A study has shown that AMPK can regulate mitochondrial autophagy by regulating ULK1,[28] but in this research, we did not study its specific mechanism in detail. Therefore, the regulatory mechanism of SIRT3/AMPK on mitochondrial autophagy in ischemic stroke is not yet clear.

ORCID iDs

Yuxian Li https://orcid.org/0000-0002-7015-1969
Ke Hu https://orcid.org/0000-0002-7883-369X
Minghua Liang https://orcid.org/0000-0001-5216-243X
Qing Yan https://orcid.org/0000-0002-8371-8442
Minjiang Huang https://orcid.org/0000-0003-0732-3403
Ling Jin https://orcid.org/0000-0003-1639-6479
Yuefu Chen https://orcid.org/0000-0002-5380-0568
Xirong Yang https://orcid.org/0000-0002-8107-3310
Xiaobo Li https://orcid.org/0000-0003-1292-8730

References

1. Khoshnam SE, Winlow W, Farzaneh M, Farbood Y, Moghaddam HF. Pathogenic mechanisms following ischemic stroke. *Neurol Sci.* 2017; 38(7):1167–1186. doi:10.1007/s10072-017-2938-1
2. Chen J, Cui C, Yang X, et al. MiR-126 affects brain–heart interaction after cerebral ischemic stroke. *Transl Stroke Res.* 2017;8(4):374–385. doi:10.1007/s12975-017-0520-z
3. Adams RJ, Cox M, Ozark SD, et al. Coexistent sickle cell disease has no impact on the safety or outcome of lytic therapy in acute ischemic stroke. *Stroke.* 2017;48(3):686–691. doi:10.1161/STROKEAHA.116.015412
4. Liu W, Wu J, Huang J, et al. Electroacupuncture regulates hippocampal synaptic plasticity via miR-134-mediated LIMK1 function in rats with ischemic stroke. *Neural Plast.* 2017;2017:9545646. doi:10. 1155/2017/9545646
5. Tuo QZ, Lei P, Jackman KA, Li XL, Bush AI. Tau-mediated iron export prevents ferroptotic damage after ischemic stroke. *Mol Psychiatry.* 2017;22(11):1520–1530. doi:10.1038/mp.2017.171
6. Maier O, Menze BM, von der Gablentz J, et al. ISLES 2015: A public evaluation benchmark for ischemic stroke lesion segmentation from multispectral MRI. *Med Image Anal.* 2016;35:250–269. doi:10.1016/j. media.2016.07.009
7. Feng D, Wang B, Wang L, et al. Pre-ischemia melatonin treatment alleviated acute neuronal injury after ischemic stroke by inhibiting endoplasmic reticulum stress-dependent autophagy via PERK and IRE1 signaling. *J Pineal Res.* 2017;62(3):e12395. doi:10.1111/jpi.12395
8. Shireman TI, Wang K, Saver JL. Cost-effectiveness of solitaire stent retriever thrombectomy for acute ischemic stroke: Results from the SWIFT-PRIME trial (Solitaire With the Intention for Thrombectomy as Primary Endovascular Treatment for Acute Ischemic Stroke). *Stroke.* 2017;48(2):379–387. doi:10.1161/STROKEAHA.116.014735
9. Ren C, Fu J, Wang H. Effect of early rehabilitation clinical pathway on ischemic stroke patients: A randomized controlled trial. *Chin J Rehabil Med.* 2017;32(3):275–282.
10. Xue J, Huang W, Chen X, Li Q, Shao B. Neutrophil-to-lymphocyte ratio is a prognostic marker in acute ischemic stroke. *J Stroke Cerebrovasc Dis.* 2016;26(3):650–657. doi:10.1016/j.jstrokecerebrovasdis. 2016.11.010
11. Hu X, De Silva TM, Chen J, Faraci FM. Cerebral vascular disease and neurovascular injury in ischemic stroke. *Circ Res.* 2017;120(3):449–471. doi:10.1161/CIRCRESAHA.116.308427
12. Yang Y, Yang LY, Orban L, et al. Non-invasive vagus nerve stimulation reduces blood–brain barrier disruption in a rat model of ischemic stroke. *Brain Stimul.* 2018;11(4):689–698. doi:10.1016/j.brs.2018.01.034
13. Jampathong N, Laopaiboon M, Rattanakanokchai S, Pattanittum P. Prognostic models for complete recovery in ischemic stroke: A systematic review and meta-analysis. *BMC Neurol.* 2018;18(1):26. doi:10. 1186/s12883-018-1032-5
14. Chen X, Tang K, Peng Y, Xu X. 2,3,4′,5-tetrahydroxystilbene-2-O-β-d-glycoside attenuates atherosclerosis in apolipoprotein E-deficient mice: role of reverse cholesterol transport. *Can J Physiol Pharmacol.* 2018;96(1):8–17. doi:10.1139/cjpp-2017-0474
15. Yu J, Li X, Matei N, McBride D, et al. Ezetimibe, a NPC1L1 inhibitor, attenuates neuronal apoptosis through AMPK dependent autophagy activation after MCAO in rats. *Exp Neurol.* 2018;307:12–23. doi:10. 1016/j.expneurol.2018.05.022
16. Li XY, Lu SS, Wang HL. Effects of the fenugreek extracts on high-fat diet-fed and streptozotocin-induced type 2 diabetic mice. *Animal Model Exp Med.* 2018;1(1):68–73. doi:10.1002/ame2.12004
17. Chen T, Dai S, Li X, et al. Sirt1-Sirt3 axis regulates human blood–brain barrier permeability in response to ischemia. *Redox Biol.* 2018;14: 229–236. doi:10.1016/j.redox.2017.09.016
18. Liu SG, Wang YM, Zhang YJ, et al. ZL006 protects spinal cord neurons against ischemia-induced oxidative stress through AMPK-PGC-1α-Sirt3 pathway. *Neurochem Int.* 2017;108:230–237. doi:10.1016/j. neuint.2017.04.005
19. Hao Z, Luo Y, Chen L, et al. Sirt3 inhibits cerebral ischemia-reperfusion injury through normalizing Wnt/β-catenin pathway and blocking mitochondrial fission. *Cell Stress Chaperones.* 2018;23(5):1079–1092. doi:10.1007/s12192-018-0917-y
20. Zeng J, Liu W, Fan YZ, He DL, Li L. PrLZ increases prostate cancer docetaxel resistance by inhibiting LKB1/AMPK-mediated autophagy. *Theranostics.* 2018;8(1):109–123. doi:10.7150/thno.20356

21. Du H, Ma L, Chen G, Li S. The effects of oxyresveratrol abrogates inflammation and oxidative stress in rat model of spinal cord injury. *Mol Med Rep*. 2017(3):4067–4073. doi:10.3892/mmr.2017.8294

22. Duan Q, Xu Y, Marck PV, Kalisz J, Morgan EE, Pierre SV. Preconditioning and postconditioning by cardiac glycosides in the mouse heart. *J Cardiovasc Pharmacol*. 2018;71(2):95–103. doi:10.1097/FJC.0000000000000549

23. Zheng Y, Shi B, Ma M, Wu X, Lin X. The novel relationship between Sirt3 and autophagy in myocardial ischemia-reperfusion. *J Cell Physiol*. 2019;234(5):5488–5495. doi:10.1002/jcp.27329

24. Zhai M, Li B, Duan W, et al. Melatonin ameliorates myocardial ischemia reperfusion injury through SIRT3-dependent regulation of oxidative stress and apoptosis. *J Pineal Res*. 2017;63(2). doi:10.1111/jpi.12419

25. Zhao XL, Yu CZ. Vosaroxin induces mitochondrial dysfunction and apoptosis in cervical cancer HeLa cells: Involvement of AMPK/Sirt3/HIF-1 pathway. *Chem Biol Interact*. 2018;290:57–63. doi:10.1016/j.cbi.2018.05.011

26. Duan WJ, Li YF, Liu FL, et al. A SIRT3/AMPK/autophagy network orchestrates the protective effects of trans-resveratrol in stressed peritoneal macrophages and RAW 264.7 macrophages. *Free Radic Biol Med*. 2016;95:230–242. doi:10.1016/j.freeradbiomed.2016.03.022

27. Gwon DH, Hwang TW, Ro JY, et al. High endogenous accumulation of ω-3 polyunsaturated fatty acids protect against ischemia-reperfusion renal injury through AMPK-mediated autophagy in fat-1 mice. *Int J Mol Sci*. 2017;18(10):2081. doi:10.3390/ijms18102081

28. Kim J, Kundu M, Viollet B, Guan KL. AMPK and mTOR regulate autophagy through direct phosphorylation of Ulk1. *Nat Cell Biol*. 2011;13(2):132–141. doi:10.1038/ncb2152

HO-1 participate in the protection of RES in rat heart suffered from hypothermic preservation

Weiming Sun[A,B,F], Tingting Chi[B,C,F], Xiaowei Chen[B,C,F], Zeyang Li[A,D–F]

Department of Ultrasonic Imaging, First Affiliated Hospital, Wenzhou Medical University, China

A – research concept and design; B – collection and/or assembly of data; C – data analysis and interpretation;
D – writing the article; E – critical revision of the article; F – final approval of the article

Address for correspondence
Zeyang Li
E-mail: lzy0927@aliyun.com

Abstract

Background. Resveratrol (RES) is a polyphenolic compound and natural phytoalexin that plays a potential role in various human diseases. Studies have confirmed that RES has an important function in cardioprotection.

Objectives. To investigate the effect of RES on HO-1 protein expression in rat heart after different duration of hypothermic preservation.

Material and methods. The Langendorff model of isolated rat heart was used. After being stored in 4°C different Celsior solution for 9 h, Sprague–Dawley rats hearts were divided into 6 groups randomly: control group, 9 h group, 3 μM RES group, 10 μM RES group, 30 μM RES group, and 100 μM RES group. The morphological changes of cardiomyocytes were detected with the hematoxylin & eosin (H&E) staining using a light microscope. The mRNA and protein expression of HO-1 were detected using reverse-transcription polymerase chain reaction (RT-PCR) and western blotting.

Results. Compared with the control group, cardiomyocytes were obviously injured in the 9 h group and the protein and mRNA expression of HO-1 were obviously decreased. Compared with the 9 h group, the mRNA and protein expression of HO-1 were increased in dose-dependent manner in the 3 μM RES, 10 μM RES and 30 μM RES group. Compared with the 9 h group, rat myocardial injury was gradually alleviated in 3 μM RES, 10 μM RES and 30 μM RES groups. However, the rat myocardial injury in the 100 μM RES group showed no more obvious improvement than in the 30 μM RES group.

Conclusions. In the isolated rat heart, RES protects cardiomyocytes against hypothermic preservation injury through increasing HO-1 protein expression.

Key words: HO-1, RES, heart preservation

148

W. Sun et al. HO-1 in the protection of RES in rat heart

Background

Resveratrol (RES) is a polyphenolic compound and natural phytoalexin that plays a potential role in various human diseases.[1] Studies have confirmed that RES has an important role in cardioprotection.[2] Heme oxygenase-1 (*HO-1*) is a cytoprotective gene, also known as a graft survival gene, which has been used as a unique therapeutic target for organ transplantation in recent years.[3] In this study, the isolated rat heart cryopreservation model was used to observe the effect of RES on cardiomyocytes in long-term cryopreserved hearts. We found that RES plays a protective role in isolated cryopreserved hearts by upregulating the expression of HO-1, which provides a theoretical basis for the effective improvement of donor heart preservation conditions in clinical practice.

Material and methods

Animals

Healthy male Sprague–Dawley (SD) rats of SPF grade, weighing 200–250 g, were provided by the Experimental Animal Center of Wenzhou Medical University (Wenzhou, China), with the animal use license No. SYXK (Zhejiang) 2010-0150. The animal work took place in Ultrasonic Imaging Department of First Affiliated Hospital of Wenzhou Medical University and was approved by the Ethics Committee of First Affiliated Hospital of Wenzhou Medical University.

Main reagents

Primary antibodies (HO-1 antibody, β-action antibody) were purchased from Abcam (Cambridge, UK). Resveratrol was purchased from Sigma-Aldrich (St. Louis, USA). The RIPA lysate was provided by Shanghai Biyuntian Biotechnology Co., Ltd (Shanghai, China). Polyvinylidene difluoride membrane (PVDF membrane) was purchased from Millipore (Burlington, USA). Both bicinchoninic acid (BCA) protein quantification kit and chemiluminescent substrate (SuperSignal West Pico enhanced substrate, ECL) were obtained from Pierce (Dallas, USA). Resveratrol was dissolved in dimethyl sulfoxide (DMSO) before use, and the final concentration in DMSO was always less than 0.1%.

Celsior solution was used for cardiac arrest and preservation, and its composition and content were as follows (mmol/L): NaOH 100, KCl 15, MgCl$_2$ 13, CaCl$_2$ 0.25, lactobionate 80, mannitor 60, histidine 30, glutamate 20, with pH 7.4, and osmolarity 320 mOsm/L.

Main methods

The preparation of hypothermic heart preservation model

Rats were adapted to feeding for 1 week and randomized into the following 6 groups with 6 rats in each group.

1. Control group (blank group): Isolated rat hearts were taken out quickly and the samples were retained for detection;

2. 9 h group (Celsior cryopreservation group): Isolated rat hearts were preserved in Celsior solution at 4°C for 9 h;

3. 3 μM RES group: Isolated rat hearts were preserved in Celsior solution containing 3 μmol/L RES for 9 h;

4. 10 μM RES group: Isolated rat hearts were preserved in Celsior solution containing 10 μmol/L RES for 9 h;

5. 30 μM RES group: Isolated rat hearts were preserved in Celsior solution containing 30 μmol/L RES for 9 h;

6. 100 μM RES group: Isolated rat hearts were preserved in Celsior solution containing 100 μmol/L RES for 9 h.

Langendorff perfusion and cryopreservation of isolated heart was performed according to the following procedure.

Rats were fasted overnight with free access to water before surgery. The abdominal cavity of rats was fixed and incised in dorsal position after cervical dislocation. The heart and large vessels were promptly exposed by thoracotomy. We cut the pulmonary veins, and then quickly removed the heart. The blood was removed in Krebs–Henseleit (KH) solution at 4°C, and then transferred and fixed in Langendorff perfusion device rapidly. Conventional retrograde constant pressure perfusion (76 mm Hg) was performed with modified KH solution. The composition of modified KH solution was as below (mmol/L): NaCl 118.9, KCl 4.69, CaCl$_2$ 2.2, KH$_2$PO$_4$ 1.17, MgSO$_4$ 1.17, NaHCO$_3$ 17.9, EDTA 0.03, and glucose 9.99, with a pH of 7.4. The temperature was always maintained at 37°C during perfusion, and the perfusate was saturated with 95% O$_2$ and 5% CO$_2$. After a balanced perfusion with KH solution for 30 min, perfusion with Celsior solution was performed at 4°C for less than 3 min. At the same time, the heart surface was cooled. After the cardiac arrest, the hearts in each group were stored in different Celsior preservation solutions at 4°C for 9 h for indicator detection.

Light microscopic observation of H&E staining

We observed the morphological changes of myocardial cells with hematoxylin & eosin (H&E) staining under light microscope. The full thickness myocardium of left ventricular apex was cut and fixed with 4% paraformaldehyde, dehydrated, embedded with paraffin, sectioned, stained with H&E, and then observed under light microscope for the structure and morphological changes of the myocardial tissue and myocardial fibers.

Gene expression assay

Reverse transcription polymerase chain reaction (RT-PCR) was used for the gene expression assay. Total RNA was extracted using Trizol method, and cDNA was obtained with reverse transcription using Thermo Fisher reverse transcription kit (Thermo Fisher Scientific, Waltham, USA) according to the procedure. The PCR products were separated using a 2% agarose gel. Primer sequences can be seen in Table 1. The PCR reaction parameters were as follows: 1 µL of cDNA, 1 µL of each upstream and downstream primer, 12.5 µL of 2 × TaqPCR Master-Mix, and deionized water with a final volume of 25 µL. Amplification was performed under the following conditions: initial denaturation – 94°C for 3 min; PCR reaction – 94°C for 1 min; annealing for 1 min 30 s; and extension at 72°C for 5 min. Number of cycles was 33 and annealing temperature was 66°C.

Protein expression assay

We applied western blotting analysis for the protein expression assay. Specimens were lysed in RIPA lysis solution (1% phenylmethylsulfonyl fluoride (PMSF)) on ice, homogenized and centrifuged at 4°C to obtain the supernatant. Protein concentration was determined using the bicinchoninic acid assay (BCA) method. Thirty micrograms of protein were loaded, separated using 10% SDS-PAGE, transferred to PVDF membrane, blocked with 5% nonfat dry milk for 1 h, and then incubated with HO-1 primary antibody (1:500) at 4°C for 16–18 h. After washing on the next day, secondary antibody horseradish enzyme-conjugated goat anti-rabbit immunoglobulin G (IgG; 1:10,000) was added and shaken for 1 h at room temperature. Electrochemiluminescence (ECL) reaction, exposure, development, and fixation were performed in the darkroom after washing. We also employed the digital gel imaging system to take pictures, and then compared the gray values of target protein bands with internal reference β-action for the calculation of the relative gray values.

Statistical processing

All statistical analyses were performed using SPSS v. 18.0 software (SPSS Inc., Chicago, USA). All data was expressed as mean ± standard deviation (SD). Comparisons among multiple groups were conducted with one-way analysis of variance (ANOVA), and those between groups were carried out using the least significant difference (LSD) method.

Results

Myocardial cells in each group after cryopreservation detected with H&E staining

In the control group, the myocardial cells were arranged neatly, the cell morphological structure was basically normal and the nucleus was in the middle (Fig. 1A). In the 9 h group, the myocardial cells became shrunk and deformed and were disorganized, with its nucleus bordered. The intercellular space was also widened (Fig. 1B). Compared with the 9 h group, the 3 µM RES, 10 µM RES and 30 µM RES groups exhibited significantly improved myocardial cell damage with the increase of RES concentration. Among the groups, the damage improvement was more obvious in the 30 µM RES and 100 µM RES groups in comparison with the 10 µM RES group, with gradually normalized arrangement of myocardial cells, clearer boundaries, natural morphology, and abundant and uniform cytoplasm (Fig. 1C–F). Meanwhile, no more significant improvement was observed in the 100 µM RES group compared to the 30 µM RES group (Fig. 1E,F).

HO-1 gene expression in each group

HO-1 mRNA expression was remarkable in the cytoplasm of myocardial tissue in the control group and was significantly downregulated in the 9 h group ($p < 0.01$). Compared with the 9 h group, the expression of *HO-1* mRNA in the 3 µM RES, 10 µM RES, 30 µM RES, and 100 µM RES groups gradually went up with the increase of RES concentration ($p < 0.01$; Fig. 2).

HO-1 protein expression in each group

The condition of HO-1 protein expression was similar to the HO-1 mRNA expression in both control group and 9 h group ($p < 0.01$). In comparison with the 9 h group, the protein expression of HO-1 in the 4 different concentration RES groups was also gradually increasing with increasing RES concentration ($p < 0.01$; Fig. 3).

Table 1. Sequences for primers

Gene name		Primer sequence	Product
HO-1	forward	5′–GCCCTGGAAGAGGAGATAGAG–3′	164 bp
	reverse	5′–TAGTGCTGTGTGGCTGGTGT–3′	
GAPDH	forward	5′–CAGTGCCAGCCTCGTCTCAT–3′	595 bp
	reverse	5′–AGGGGCCATCCACAGTCTTC–3′	
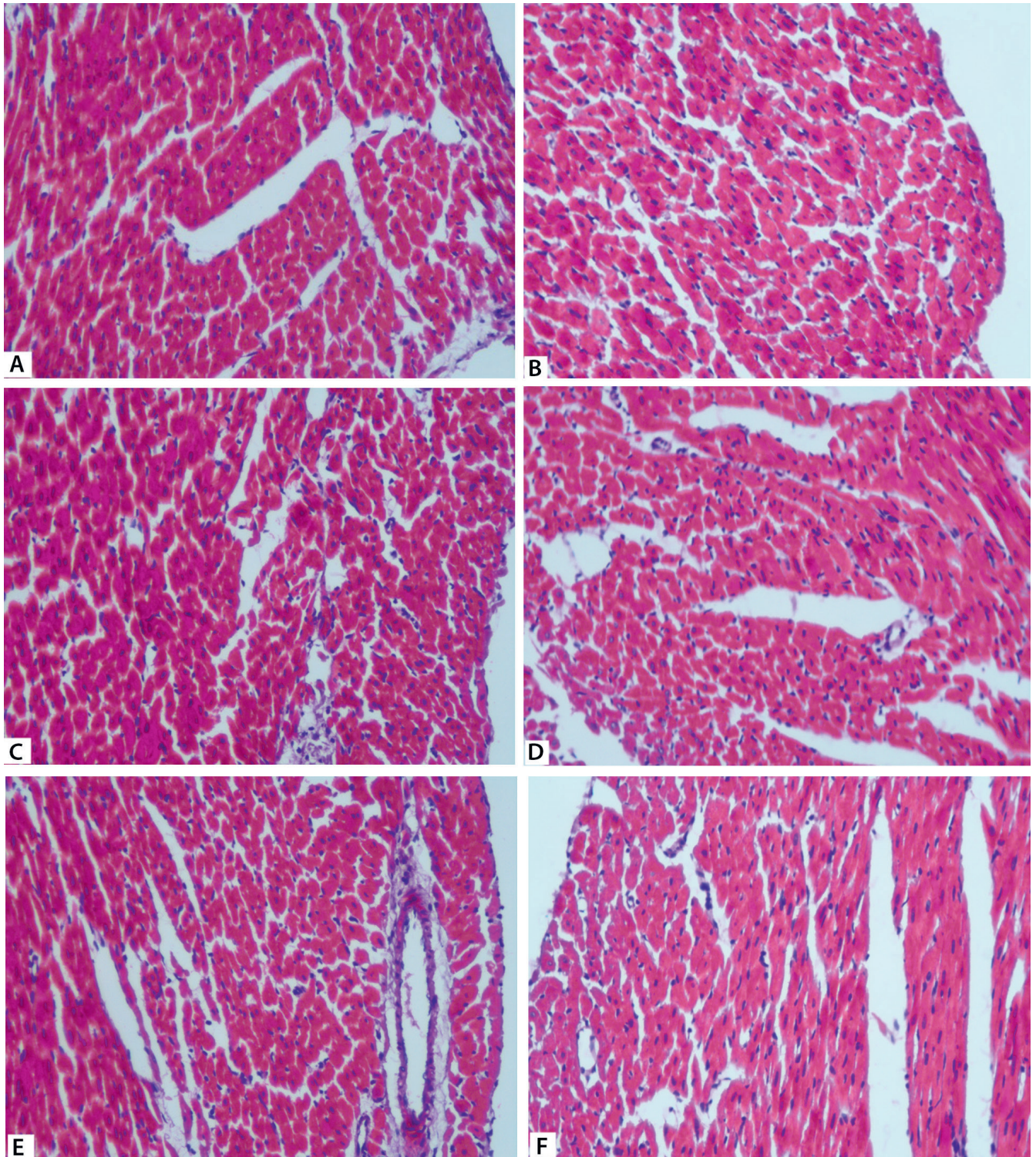
Fig. 1. The H&E staining for morphological changes of cardiomyocytes with the light microscope (H&E, ×200 magnification)

A. Control group; B. 9 h group; C. 3 μM RES group; D. 10 μM RES group; E. 30 μM RES group; F. 100 μM RES group.

Discussion

The key to a successful heart transplantation is to alleviate the hypothermic preservation injury of donor heart.[4] Researchers have continued to adjust various components of heart preservation solution, such as the addition of oxygen free radical scavengers, calcium ion antagonists, plasma active ingredients, nutrient matrix, etc., all of which improved the damage of heart during cryopreservation to varying degrees.[5,6] Cell injury during long-term cryopreservation is a critical factor affecting organ recovery after transplantation.[7] During simple hypothermic preservation,
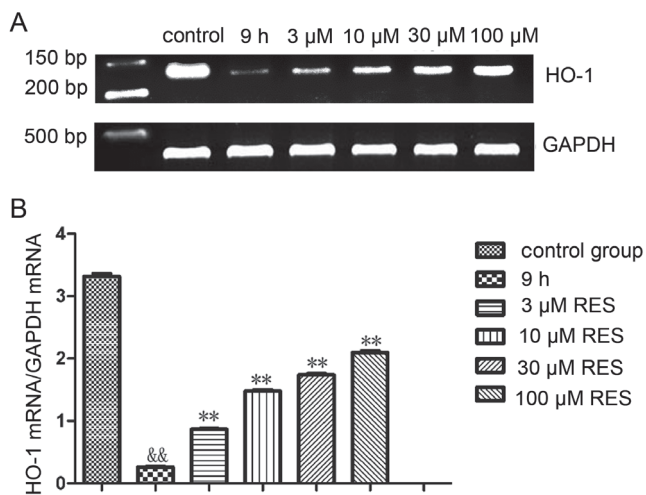
Fig. 2. Changes in *HO-1* mRNA expression in hypothermic preserved rat hearts (n = 6)

A. Representative blots of *HO-1* mRNA expression; B. Densitometric analysis shows the expression of *HO-1* mRNA.
&&p < 0.01 compared to the control group; **p < 0.01 compare to the 9 h group.
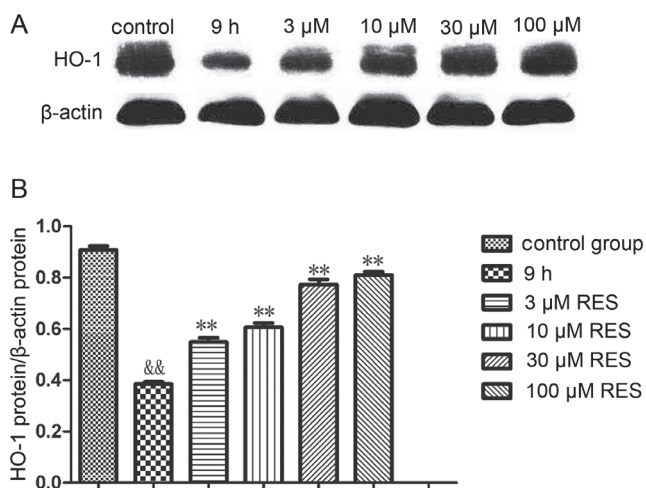
Fig. 3. Changes in HO-1 protein expression in hypothermic preserved rat hearts (n = 6)

A. Representative blots of HO-1 protein expression; B. Densitometric analysis shows the expression of HO-1 protein.
&& p < 0.01 compared to the control group; **p < 0.01 compared to the 9 h group.

the intracellular and extracellular ion imbalance due to hypoxia leads to cellular edema.[8] At the same time, intracellular anaerobic glycolysis is increased, intracellular acidosis occurs, and swelling and degeneration come up in cells due to ischemia and hypoxia. If effective drugs can be added to the preservation solution to reduce the cell damage caused by long-term cryopreservation, it may provide a new drug target for organ cryopreservation and improve the preservation effect of donor heart during heart transplantation.[9] In this study, the purpose of adding RES in the preservation solution was to improve the damage of cells in the environment of hypothermic ischemia and hypoxia, reduce

the damage caused by intracellular ion imbalance, acidosis and other changes, and try to maintain the state of cells in this condition.

Resveratrol has quite a wide range of biological activities, including anti-cancer, anti-apoptotic, anti-aging, anti-insulin resistance, anti-oxidant, anti-arteriosclerosis, anti-inflammatory, anti-platelet, and anti-estrogen bioactivities.[10] It has positive significance for the prevention and treatment of heart disease, atherosclerosis, diabetes, and neurodegenerative diseases.[11] Many studies have confirmed that RES plays an important role in cardioprotection.[2,12] The results showed that RES could protect suckling mice cardiomyocytes and human umbilical vein endothelial cells from injury.[13] However, high concentration of RES (100 mM) produce toxicity on human umbilical vein endothelial cells.[14] During cryopreservation, the morphological changes of myocardial cells can directly reflect the damage of myocardial tissue structure. The damage reflected by light microscopy results is manifested in the arrangement and boundary of myocardial cells, cell contour, cell edema, or cell shrinkage. As measured using light microscopy and H&E staining, in this experiment, myocardial cell injury was more obvious in the 9 h group compared with the control group. These results indicated that long-term hypothermic preservation could lead to severe cardiac injury in rats. The long-term hypothermic preservation model has been successfully constructed. However, in 3 µM RES, 10 µM RES, 30 µM RES, and 100 µM RES groups, myocardial cell injury was gradually alleviated compared with the 9 h group, which affirmed the protective role of RES during long-term hypothermic preservation of the heart. In the meantime, no significant improvement was observed in cardiac myocytes in the 30 µM RES and 100 µM RES groups. There are 2 possibilities for this phenomenon: 100 µM of RES exerted a protective effect on cardiac myocytes at a plateau close to 30 µM RES, or 100 µM of RES produced some toxicity to cardiac myocytes, partially counteracting its protective effect. More experiments need to be conducted to confirm whether higher concentrations are toxic to cardiomyocytes.

Heme oxygenase-1 has been found to be closely associated with many diseases.[15–17] Its upregulation reduces graft injury and can prevent chronic graft function loss after transplantation, hence it is known as a graft survival gene. The HO-1 overexpression is cytoprotective in transplantation models such as rat heart.[18] It has been found that RES can protect human hepatocytes from alcohol-induced injury to some extent, and its protective effect is associated with the induction of increased HO-1 enzyme activity.[19] Inducing the upregulation of HO-1 expression can significantly reduce the injury of the transplanted liver and decrease the level of serum transaminases in the recipients,[20] as well as dramatically prolong the duration of liver cryopreservation.[21,22] Therefore, the protective effect of HO-1 on liver transplantation was basically confirmed. However, there are only few studies on the effects of HO-1

on heart transplantation. Recombinant adeno-associated virus (rAAV)-mediated *HO-1* gene transfer has been found to be a novel therapeutic approach for chronic allograft injury in clinical heart transplantation. In this experiment, the expression of HO-1 in the 9 h group compared with the control group was remarkably decreased, and H&E staining showed that the myocardial cell injury was obvious. This result proves the protective role of HO-1 and the regulation of HO-1 by RES is involved in the protective effect of long-term hypothermic preservation of the heart.

Conclusions

We believe that RES plays a pivotal role in protecting the isolated cryopreserved hearts by upregulating HO-1.

ORCID iDs

Weiming Sun ⬤ https://orcid.org/0000-0002-1313-6439
Tingting Chi ⬤ https://orcid.org/0000-0002-3260-6387
Xiaowei Chen ⬤ https://orcid.org/0000-0002-7895-3835
Zeyang Li ⬤ https://orcid.org/0000-0001-7885-2383

References

1. Salehi B, Mishra AP, Nigam M, et al. Resveratrol: A double-edged sword in health benefits. *Biomedicines*. 2018;6(3):91. doi:10.3390/biomedicines6030091
2. Riba A, Deres L, Sumegi B, Toth K, Szabados E, Halmosi R. Cardioprotective effect of resveratrol in a postinfarction heart failure model. *Oxid Med Cell Longev*. 2017;2017:6819281. doi:10.1155/2017/6819281
3. Wu B, Song H-L, Yang Y, et al. Improvement of liver transplantation outcome by heme oxygenase-1-transduced bone marrow mesenchymal stem cells in rats. *Stem Cells Int*. 2016;2016:9235073. doi:10.1155/2016/9235073
4. Van Caenegem O, Beauloye C, Bertrand L, et al. Hypothermic continuous machine perfusion enables preservation of energy charge and functional recovery of heart grafts in an ex vivo model of donation following circulatory death. *Eur J Cardiothorac Surg*. 2016;49(5):1348–1353. doi:10.1093/ejcts/ezv409
5. Ferng AS, Schipper D, Connell AM, Marsh KM, Knapp S, Khalpey Z. Novel vs clinical organ preservation solutions: Improved cardiac mitochondrial protection. *J Cardiothorac Surg*. 2017;12(1):7. doi:10.1186/s13019-017-0564-x
6. Yang F, Chen W, Zheng M, et al. Heat shock protein 90 mediates anti-apoptotic effect of diazoxide by preventing the cleavage of Bid in hypothermic preservation rat hearts. *J Heart Lung Transplant*. 2011;30(8):928–934. doi:10.1016/j.healun.2011.04.001
7. Krezdorn N, Tasigiorgos S, Wo L, et al. Tissue conservation for transplantation. *Innov Surg Sci*. 2017;2(4):171–187. doi:10.1515/iss-2017-0010
8. Hackenhaar FS, Medeiros TM, Heemann FM, et al. Therapeutic hypothermia reduces oxidative damage and alters antioxidant defenses after cardiac arrest. *Oxid Med Cell Longev*. 2017;2017:8704352. doi:10.1155/2017/8704352
9. Chew HC, Macdonald PS, Dhital KK. The donor heart and organ perfusion technology. *J Thorac Dis*. 2019;11(Suppl 6):S938–S945. doi:10.21037/jtd.2019.02.59
10. Koushki M, Amiri-Dashatan N, Ahmadi N, Abbaszadeh HA, Rezaei-Tavirani M. Resveratrol: A miraculous natural compound for diseases treatment. *Food Sci Nutr*. 2018;6(8):2473–2490. doi:10.1002/fsn3.855
11. Petrovski G, Gurusamy N, Das DK. Resveratrol in cardiovascular health and disease. *Ann N Y Acad Sci*. 2011;1215:22–33. doi:10.1111/j.1749-6632.2010.05843.x
12. Yang Q, Wang H-C, Liu Y, Gao C, Sun L, Tao L. Resveratrol cardioprotection against myocardial ischemia/reperfusion injury involves upregulation of adiponectin levels and multimerization in type 2 diabetic mice. *J Cardiovasc Pharmacol*. 2016;68(4):304–312. doi:10.1097/FJC.0000000000000417
13. Yang J, Zhou X, Zeng X, Hu O, Yi L, Mi M. Resveratrol attenuates oxidative injury in human umbilical vein endothelial cells through regulating mitochondrial fusion via TyrRS-PARP1 pathway. *Nutr Metab (Lond)*. 2019;16:9. doi:10.1186/s12986-019-0338-7
14. Trincheri NF, Nicotra G, Follo C, Castino R, Isidoro C. Resveratrol induces cell death in colorectal cancer cells by a novel pathway involving lysosomal cathepsin D. *Carcinogenesis*. 2007;28(5):922–931. doi:10.1093/carcin/bgl223
15. Wu ML, Ho YC, Lin CY, Yet SF. Heme oxygenase-1 in inflammation and cardiovascular disease. *Am J Cardiovasc Dis*. 2011;1(2):150–158.
16. Sebastián VP, Salazar GA, Coronado-Arrázola I, et al. Heme oxygenase-1 as a modulator of intestinal inflammation development and progression. *Front Immunol*. 2018;9:1956. doi:10.3389/fimmu.2018.01956
17. Kim MK, Park HJ, Kim SR, Choi YK, Bae SK, Bae MK. Involvement of heme oxygenase-1 in orexin-A-induced angiogenesis in vascular endothelial cells. *Korean J Physiol Pharmacol*. 2015;19(4):327–334. doi:10.4196/kjpp.2015.19.4.327
18. Soares MP, Bach FH. Heme oxygenase-1 in organ transplantation. *Front Biosci*. 2007;12:4932–4945. doi:10.2741/2439
19. Faghihzadeh F, Hekmatdoost A, Adibi P. Resveratrol and liver: A systematic review. *J Res Med Sci*. 2015;20(8):797–810. doi:10.4103/1735-1995.168405
20. Miyauchi T, Uchida Y, Kadono K, et al. Up-regulation of FOXO1 and reduced inflammation by β-hydroxybutyric acid are essential diet restriction benefits against liver injury. *Proc Natl Acad Sci U S A*. 2019;116(27):13533–13542. doi:10.1073/pnas.1820282116
21. Okumura S, Uemura T, Zhao X, et al. Liver graft preservation using perfluorocarbon improves the outcomes of simulated donation after cardiac death liver transplantation in rats. *Liver Transpl*. 2017;23(9):1171–1185. doi:10.1002/lt.24806
22. Ren J, Fan C, Chen N, Huang J, Yang Q. Resveratrol pretreatment attenuates cerebral ischemic injury by upregulating expression of transcription factor Nrf2 and HO-1 in rats. *Neurochem Res*. 2011;36(12):2352–2362. doi:10.1007/s11064-011-0561-8

The clinical value of high-density lipoprotein in the evaluation of new coronavirus pneumonia

Shipeng Huang[A–C,F], Congyang Zhou[B,C,F], Zheng Yuan[B,C,F], Hui Xiao[B,C,F], Xiaoping Wu[A,D–F]

The First Affiliated Hospital of Nanchang University, China

A – research concept and design; B – collection and/or assembly of data; C – data analysis and interpretation;
D – writing the article; E – critical revision of the article; F – final approval of the article

Address for correspondence
Xiaoping Wu
E-mail: xiaopeng_wu@tom.com

Abstract

Background. The new coronavirus pneumonia (NCP, COVID-19) outbreak began in Wuhan in December 2019. The new coronavirus (2019 novel coronavirus (2019-nCoV)) can cause multiple organ damage, mainly to lung tissue, and induce inflammation in the body.

Objectives. To investigate the changes of high-density lipoprotein (HDL) level in patients with COVID-19 and assess its value in the evaluation and prognosis of this disease.

Material and methods. This paper is a cross-sectional retrospective study. Eighty-six severe COVID-19 patients, 132 non-severe COVID-19 patients and 76 healthy individuals (control group) were recruited to measure triglyceride (TG), total cholesterol (TC), high-density lipoprotein cholesterol (HDL-C), and low-density lipoprotein cholesterol (LDL-C) using enzyme-coupled colorimetry.

Results. The serum HDL-C level in COVID-19 group was 1.02 ± 0.28 mmol/L which was significantly lower than in control group (1.52 ± 0.55 mmol/L) ($p < 0.05$). In addition, the serum HDL-C level in severe COVID-19 group was 0.83 ± 1.67 mmol/L, which was significantly lower than that in non-severe COVID-19 group (1.15 ± 0.27 mmol/L) ($p < 0.05$).

Conclusions. Changes in HDL levels in patients with COVID-19 can reflect the severity of the disease and have a clinical significance in establishing the prognosis.

Key words: blood lipids, critical illness, new coronavirus pneumonia, high-density lipoprotein cholesterol

Background

The new coronavirus pneumonia (NCP, COVID-19) outbreak began in Wuhan in December 2019.[1] It can cause multiple organ damage, mainly to lung tissue, and induce inflammation in the body.[1,2] In recent years, more and more studies have shown that plasma high-density lipoprotein (HDL) not only participates in reverse transport of cholesterol, but also widely affects the inflammatory response of the body.[3]

Objectives

The purpose of this study was to analyze the changes of HDL levels in patients with COVID-19 and the clinical value of this measurement in the evaluation and prognosis of this disease.

Patients and methods

General information

Cross-sectional retrospective analysis was performed in the present study. All cases were divided into 3 groups: severe COVID-19 group, non-severe COVID-19 group and healthy control group. The severe group included 86 patients with severe/critical COVID-19, of an average age of 54.36 ±12.61 years, while the non-severe group consisted of 132 mild COVID-19 patients, of an average age of 44.02 ±17.13 years. Seventy-six healthy individuals with an average age of 47.73 ±8.68 years, receiving medical examinations, served as the healthy control group. The exclusion criteria were as follows: malignant tumors, severe head trauma and other diseases. This study was approved by the ethics committee of our hospital and all participants signed the informed consent prior to the study.

Diagnostic criteria and classification criteria

All COVID-19 patients enrolled met the diagnostic criteria of the New Coronavirus Pneumonia Diagnosis and Treatment Program (trial version 7) issued by the National Health Commission of China on March 4, 2020.[4] All cases were confirmed using the new coronavirus nucleic acid test through real-time fluorescent reverse-transcription polymerase chain reaction (RT-PCR). Patients were classified according to the new version of the diagnosis and treatment plan into the following categories: 1) light or mild clinical symptoms, no pneumonia manifestations in the imaging; 2) common type of the disease, with symptoms of fever, respiratory tract, etc. (pneumonia visible in the imaging); 3) severe disease, meeting any of the following criteria:

shortness of breath, breathing frequency ≥30 times/min; blood oxygen saturation (SO_2) ≤93%; arterial blood oxygen partial pressure (PaO_2)/oxygen absorption concentration (FiO_2) ≤300 mm Hg at rest; 4) critical form of the disease, meeting any of the following criteria: respiratory failure, mechanical ventilation required; shock (or combined with other organ failure), requiring intensive care unit (ICU) treatment.

Research methods

Cases that met the diagnostic criteria for new coronavirus pneumonia were classified according to the New Coronavirus Pneumonia Diagnosis and Treatment Program (trial version 7), and patients from categories 1 and 2 were included into the non-severe group, while patients from categories 3 and 4 were included into the severe group. Venous blood was collected from all enrolled subjects on the 1st day of admission to measure triglycerides (TG), total cholesterol (TC), high-density lipoprotein cholesterol (HDL-C), and low-density lipoprotein cholesterol (LDL-C) levels using enzyme-coupled colorimetric method.

Statistical processing

The statistical analysis was carried out using SPSS v. 20.0 software (IBM Corp., Armonk, USA). The countable data was expressed as a percentage and assessed with a χ^2 test. The measurement data was displayed as mean ± standard deviation (SD) and evaluated with the Student's t-test. A value of $p < 0.05$ indicated statistically significant difference.

Results

The serum HDL-C levels in the COVID-19 group and healthy control group were 1.02 ±0.28 mmol/L and 1.52 ±0.55 mmol/L, respectively. After data was analyzed using the Student's t-test, the serum HDL-C levels in the COVID-19 group turned out to be significantly

Table 1. Comparison of blood routine, blood glucose and blood lipid results between COVID-19 group and healthy control group

Parameters	COVID-19 group	Healthy control group
Age [years]	48.19 ±16.33	47.73 ±8.68
White blood cells [×10⁹/L]	6.77 ±3.59	6.14 ±2.05
Absolute value of lymphocytes [×10⁹/L]	1.09 ±0.81	1.92 ±0.74
Absolute value of neutrophils [×10⁹/L]	5.21 ±3.59	3.56 ±1.33
Total cholesterol [mmol/L]	3.81 ±0.82[a]	4.64 ±1.00
Triglyceride [mmol/L]	1.42 ±1.38[a]	1.64 ±1.12
High-density lipoprotein [mmol/L]	1.02 ±0.28[a]	1.52 ±0.55
Low-density lipoprotein [mmol/L]	2.46 ±0.77[a]	2.55 ±0.75

Table 2. Comparison of blood lipid results in severe group, non-severe group and healthy control group

Group	Number of patients	TC [mmol/L]	TG [mmol/L]	HDL-C [mmol/L]	LDL-C [mmol/L]
Severe	86	3.65 ±0.75	1.91 ±1.87	0.83 ±1.67	2.32 ±0.71
Non-severe	132	3.93 ±0.84	1.1 ±0.79	1.15 ±0.27*	2.56 ±0.81
Healthy control	76	4.64 ±1.01	1.64 ±1.12	1.52 ±0.55**	2.55 ±0.75

* compared with the severe group ($p < 0.05$); ** compared with the non-severe group ($p < 0.05$).

lower than those in the healthy control group ($p < 0.05$) (Table 1). The HDL-C levels in severe COVID-19 group and non-severe COVID-19 group were 0.83 ±1.67 mmol/L and 1.15 ±0.27 mmol/L, respectively. The HDL-C level in the non-severe group was significantly higher than in the severe group, and the statistical results were significantly different ($p < 0.05$) (Table 2).

Discussion

The COVID-19 is caused by a new coronavirus (2019-nCoV) infection and the disease progresses rapidly. At the same time, general population susceptibility and significant infectivity can be observed.[5] A number of studies have shown that 2019-nCoV can induce a cytokine storm after invading the body and aggravating the inflammatory response. Interleukin 2 (IL-2), granulocyte colony stimulating factor (G-SCF) and macrophage inflammatory protein (MIP-1a) as well as tumor necrosis factor α (TNF-α) and other inflammatory factors have increased to varying degree in patients' plasma.[6,7] The COVID-19 is mainly caused by lung tissue lesions and patients present abnormally increased inflammatory factors, leading to overactivation of immune cells, which accumulate and activate in the lung tissue, resulting in diffuse damage to pulmonary capillary endothelial cells and alveolar epithelial cells. Pulmonary damage produces in turn a large amount of inflammatory exudate that eventually blocks the bronchial tubes at all levels, causing continuing deterioration of lung function, leading to acute respiratory distress syndrome (ARDS) and respiratory failure.[7,8] The results of our study showed that the level of HDL-C in the COVID-19 patients was significantly lower than in the healthy control group ($p < 0.05$). At the same time, the level of HDL-C in the severe COVID-19 group was significantly lower than in the non-severe COVID-19 ($p < 0.05$). This shows that blood lipid levels, especially HDL-C levels, vary in patients with COVID-19. The severity of this disease can affect the fluctuation of HDL-C levels. Severe COVID-19 patients have significantly lower HDL-C levels than non-severe patients. Therefore, the changes of HDL-C level can be used as a predictor of the severity of COVID-19.

Among various lipoproteins in the body, HDL has the smallest volume and the highest density. It mainly reverses cholesterol from the peripheral tissues to the liver for further recycling or excretion in the form of cholic acid.[9] However, in recent years, the role of HDL in inflammatory infection has been gradually better understood. Some studies have shown that HDL can prevent the activation of peripheral blood monocytes and macrophages lipopolysaccharides (LPS) and lipid wall phosphates (LTA), thereby reducing TNF-α and interleukin 1β (IL-lβ) synthesis and secretion.[10] When the body is infected, LPS, which constitute the main component of endotoxin, are released from the outer cell membrane to form a complex with HDL, thereby achieving the effect of neutralizing toxicity and reducing inflammation; HDL levels also decrease.[11] The HDL and LPS are combined and consumed in the body. Once exhausted, the patient's inflammatory response is difficult to be effectively controlled, eventually leading to multiple organ dysfunction or even death.

Many studies have shown that HDL can inhibit the combination of various types of viruses and host cells, including enveloped and non-enveloped DNA and RNA viruses, such as Japanese encephalitis virus, rubella virus, Epstein–Barr virus, herpes simplex virus, human immunodeficiency virus (HIV), coxsackievirus, , poliovirus, and other viruses. In the early stage of viral infection, HDL exerted antiviral activity, mainly inhibiting the penetration of the virus into the cells after it was adsorbed.[12] Another study showed that the function of HDL isolated from mice infected with influenza A is impaired and its anti-inflammatory and antioxidant properties are reduced[13]; further injection of D-4F ApoAI mimic peptide into infected mice can reduce the inflammation in the lungs and inhibit the production of IL-6 and prevent macrophages from entering the arteries.[14] The D-4F ApoAI mimic peptide also has antiviral activity and can reduce influenza virus titer by 50%.[15] The above research provides new ideas for inhibiting 2019-nCoV. Perhaps exogenous HDL can be used as a kind of antiviral treatment. It also proves that the level of HDL in patients with COVID-19 can reflect the disease severity.

The HDL synthesis occurs mainly through the liver and small intestine, and most of the severe COVID-19 patients have impaired liver function and small intestinal mucosal ischemia, so HDL synthesis is also reduced; at the same time, intake of large amounts of carbonate compounds can accelerate the decomposition of proteins in HDL.[16] Therefore, treatment of severe COVID-19 patients should include maintaining liver and intestinal mucosal function, and appropriately reducing carbohydrate intake, so as to ensure the synthesis of HDL and improve the prognosis.

Conclusions

The HDL, as part of the natural immunity of the body, has antiviral and anti-inflammatory properties. The results of this study show that changes in HDL levels in patients with COVID-19 can reflect the disease severity and have clinical significance in assessing the prognosis. The lower HDL-C levels, the worse the prognosis. At the same time, HDL-C has certain application prospects in the treatment of COVID-19. This study demonstrated the change of HDL levels in patients with COVID-19, providing an important reference for the clinical diagnosis and treatment. However, other potential biomarkers need to be further investigated to enable a comprehensive understanding of COVID-19.

ORCID iDs

Shipeng Huang https://orcid.org/0000-0002-5609-3547
Congyang Zhou https://orcid.org/0000-0002-5595-1036
Zheng Yuan https://orcid.org/0000-0002-2148-9891
Hui Xiao https://orcid.org/0000-0001-8732-120X
Xiaoping Wu https://orcid.org/0000-0003-0138-8636

References

1. Lu R, Zhao X, Li J, et al. Genomic characterization and epidemiology of 2019 novel coronavirus: Implications for virus origins and receptor binding. *Lancet*. 2020;395(10224):565–574. doi:10.1016/s0140-6736 (20)30251.8
2. Huang C, Wang Y, Li X, et al. Clinical features of patients infected with 2019 novel coronavirus in Wuhan, China. *Lancet*. 2020;395(10223): 497–506. doi:10.1016/S0140-6736(20)30183-5
3. Florentin M, Liberopoulos EN, Wierzbicki AS, et al. Multiple actions of high-density lipoprotein. *Curr Opin Cardiol*. 2008;23(4):370–378.
4. National Health Commission. New Coronavirus Pneumonia Diagnosis and Treatment Program (trial 7th edition). http://www.gov.cn/zhengce/zhengceku/2020-01/28/content_5472673.htm. Accessed on May 15, 2020.
5. Zhou P, Yang X, Wang X, et al. Discovery of a novel coronavirus associated with the recent pneumonia outbreak in humans and its potential bat origin. *bioRxiv*. 2020:2020–2021. https://doi.org/10.1101/2020.01.22.914952
6. Chen N, Zhou M, Dong X, et al. Epidemiological and clinical characteristics of 99 cases of 2019 novel coronavirus pneumonia in Wuhan, China: A descriptive study. *Lancet*. 2020;395(10223):507–513. doi:10.1016/S0140-6736(20)30211-7
7. Wang DW, Hu B, Hu C, et al. Clinical characteristics of 138 hospitalized patients with 2019 novel coronavirus-infected pneumonia in Wuhan, China. *JAMA*. 2020;323(11):1061–1069. doi:10.1001/JAMA.2020.1585
8. Hui DSC, Zumla A. Severe acute respiratory syndrome: Historical, epidemiologic, and clinical features. *Infect Dis Clin North Am*. 2019;33(4): 869–889. doi:10.1016/j.idc.2019.07.001
9. Kapur NK, Ashen D, Blumenthal RS. High density lipoprotein cholesterol: An evolving target of therapy in the management of cardiovascular disease. *Vasc Health Risk Manag*. 2008;4(1):39–57. doi:10.2147/vhrm.2008.04.01.39
10. Casas AT, Hubsch AP, Rogers BC, Doran JE. Reconstituted high-density lipoprotein reduces LPS-stimulated TNF-α. *J Surg Res*. 1995;59(5): 544–552. doi:10.1006/jsre.1995.1204
11. Thompson PA, Tobias PS, Viriyakosol S, Kirkland TN, Kitchens RL. Lipopolysaccharide (LPS)-binding protein inhibits responses to cell-bound LPS. *J Biol Chem*. 2003;278(31):28367–28371. doi:10.1074/jbc. M302921200
12. Singh IP, Chopra AK, Coppenhaver DH, Ananatharamaiah GM, Baron S. Lipoproteins account for part of the broad non-specific antiviral activity of human serum. *Antiviral Res*. 1999;42(3):211–218. doi:10.1016/s0166-3542(99)00032-7
13. Van Lenten BJ, Wagner AC, Nayak DP, Hama S, Navab M, Fogelman AM. High-density lipoprotein loses its anti-inflammatory properties during acute influenza A infection. *Circulation*. 2001;103(18):2283–2288. doi:10.1161/01.CIR.103.18.2283
14. Van Lenten BJ, Wagner AC, Anantharamaiah GM, et al. Influenza infection promotes macrophage traffic into arteries of mice that is prevented by D-4F, an apolipoprotein A-I mimetic peptide. *Circulation*. 2002;106(9):1127–1132. doi:10.1161/01.CIR.0000030182.35880.3E
15. Van Lenten BJ, Wagner AC, Navab M, et al. D-4F, an apolipoprotein a-I mimetic peptide, inhibits the inflammatory response induced by influenza A infection of human type II pneumocytes. *Circulation*. 2004;110(20):3252–3258. doi:10.1161/01.CIR.0000147232.75456.B3
16. Wu A, Thiemermann CJC. High-density lipoprotein in sepsis and septic shock: Metabolism, action and therapeutic applications. *Shock*. 2004;(32):10–221. doi:10.1097/01.shk.0000111661.09279.82

Liver paraoxonase 3 expression and the effect of liraglutide treatment in a rat model of diabetes

Yuntao Liu[1,B,C], Dan Zhu[2,A,F], Guofeng Dong[1,C,D], Yuqin Zeng[3,C,D], Pan Jiang[1,D,E], Yaoling Xiao[4,F]

[1] Department of Endocrinology, Affiliated Ren He Hospital of China Three Gorges University, Second Clinical Medical College of China, Three Gorges University, Yichang, China

[2] Third Clinical Medical College of China Three Gorges University, Gezhouba Central Hospital of Sinopharm, Yichang, China

[3] Hemodialysis room, Affiliated Ren He Hospital of China Three Gorges University, Second Clinical Medical College of China Three Gorges University, Yichang, China

[4] Department of Endocrinology, Third Clinical Medical College of China Three Gorges University, Gezhouba Central Hospital of Sinopharm, Yichang, China

A – research concept and design; B – collection and/or assembly of data; C – data analysis and interpretation;
D – writing the article; E – critical revision of the article; F – final approval of the article

Address for correspondence
Dan Zhu
E-mail: danzhudr@tom.com

Abstract

Background. This study investigated liver expression of paraoxonase 3 (PON3), phosphatidylinositol 3-kinase (PI3K), protein kinase B (Akt), and nuclear factor (NF)-κB in a rat model of type-2 diabetes mellitus (T2DM), and assessed the effect of liraglutide treatment.

Objectives. To investigate liver PON3 expression in rats with T2DM assess its role in disease pathogenesis, and determine the effect of liraglutide on its expression.

Material and methods. Type 2 diabetes mellitus was induced in 3 groups of rats: positive control group (PC; no treatment), and low-dose (LL; 100 μg/kg) and high-dose (HL; 200 μg/kg) liraglutide groups. Healthy rats served as a normal control (NC) group. Protein and mRNA expression were measured with western blot and reverse-transcriptase polymerase chain reaction (RT-PCR), respectively.

Results. After liraglutide treatment, fasting plasma glucose (FPG), homeostasis model assessment-insulin resistance (HOMA-IR), fasting insulin (FINS), malondialdehyde (MDA), and interleukin 6 (IL-6) levels were lower in HL rats compared with LL ones ($p < 0.05$). Compared to NC rats, FPG, FINS, HOMA-IR, low-density lipoprotein cholesterol (LDL-C), triglyceride (TG), and IL-6 levels were the lowest in HL rats, followed by LL and PC ones ($p < 0.05$). Body weight (BW) was lower in LL and HL groups than in NC and PC ($p < 0.05$). The liver expression of PON3, PI3K and Akt were the highest in HL rats, followed by LL and PC ($p < 0.05$). The NF-κB expression was the lowest in HL rats, followed by LL and PC ($p < 0.05$). The PON3 expression was decreased in the diabetic rat liver.

Conclusions. Liraglutide can increase PI3K, Akt and PON3 expression, and decrease NF-κB expression. The effect of liraglutide on improving insulin resistance and abnormal glucolipid metabolism in T2DM rats may be associated with increased liver PON3 expression.

Key words: type 2 diabetes mellitus, liraglutide, paraoxonase 3, proprotein convertase subtilisin 9

Background

Paraoxonase 3 (PON3), a newly discovered member of the paraoxonase family, is closely related to insulin resistance, lipid metabolism and obesity.[1,2] It has an inhibitory effect on inflammatory factors and can improve insulin resistance.[3] Phosphatidylinositol 3-kinase (PI3K) and protein kinase B (Akt) play a role in regulating PON3 expression.[4]

As a long-acting analog of glucagon-like peptide-1 (GLP-1), liraglutide has the same physiological effects as natural GLP-1 through molecular modification, and these are persistent due to its long half-life low decomposition rate. Liraglutide is used as a potent hypoglycemic agent in clinical practice, and has been shown to reduce body mass index (BMI) and improve insulin resistance.[5] Moreover, it can significantly improve dysfunctional glycolipid metabolism in metabolic diseases and reduce diabetes complications. It has also been found to increase PI3K and Akt expression and inhibit inflammation.[6–8]

Objectives

The aim of this study was to investigate liver PON3 expression in rats with type 2 diabetes mellitus (T2DM), assess its role in disease pathogenesis and determine the effect of liraglutide on its expression.

Material and methods

Materials

Test materials were: streptozotocin (STZ) (Sigma-Aldrich, St. Louis, USA); peroxisome proliferator-activated receptor gamma coactivator 1-alpha (PGC-1α), irisin primers, and glyceraldehyde 3-phosphate dehydrogenase (GADPH) primers (Boster, Wuhan, China); primary antibodies (Proteintech, Rosemont, USA); and secondary antibodies (Boster). A reverse transcription polymerase chain reaction (RT-PCR) kit was purchased from Invitrogen (Carlsbad, USA).

Methods

Forty-four four-week-old, specific pathogen-free, male Sprague–Dawley rats weighing 190–210 g were purchased from the Experimental Animal Center of Wuhan University, China (animal certificate No. SCXK (E) 2017-0012). All rats were kept in specific pathogen-free rooms controlled for temperature (22–26°C) and humidity (40–70%), with 12-hour light/dark light cycle and free access to food and drinking water except during the experiments. Following 7 days of acclimatization, rats were randomly divided into a normal control (NC) group (n = 10) and experimental group (n = 34). The NC rats were fed a normal diet, and experimental rats

received a high-fat diet for 2 weeks. Subsequently, T2DM was induced in the experimental rats by ip. administration of STZ (40 mg/kg body weight (BW) Seventy-two hours after STZ administration a total of 30 out of 34 rats had glucose levels ≥16.7 mmol/L and were considered diabetic. Diabetic rats were fed a high-fat diet for another 2 weeks and randomly divided into 3 treatment groups (n = 10 each): positive control (PC; no treatment) group, and low-dose liraglutide (LL) and high-dose liraglutide (HL) groups. The LL and HL rats were given intraperitoneal injections of liraglutide 100 μg/kg/day and 200 μg/kg/day, respectively,[8] for 4 weeks. The NC and PC rats were ip. injected with the same volume of normal saline for 4 weeks.

Sample collection

Tail vein blood was collected from each of the control and diabetic rats and stored at –80°C for later use after T2DM was confirmed. At the end of week 17, tail vein blood was collected again from each of the control and diabetic rats fasted for 12 h and anesthetized with pentobarbital. Liver tissue was promptly excised from anesthetized rats and washed with normal saline (NaCl 0.9%) after blood collection. The harvested tissues were then dried using filter paper and stored at –80°C. Fasting plasma glucose (FPG) was measured using a glucometer (Johnson & Johnson, New Brunswick, USA). Plasma levels of high-density lipoprotein cholesterol (HDL-C), low-density lipoprotein cholesterol (LDL-C), total cholesterol (TC), and triglyceride (TG) were measured using an Abbott C8000 automatic analyzer (Abbott Laboratories, Chicago, USA). Interleukin 6 (IL-6) was measured with a enzyme-linked immunosorbent assay (ELISA; Boster) using a Biotek ELx800 microplate reader (BioTek, Winooski, USA). Insulin was determined using electrochemiluminescence (Cobas e411 autoanalyzer; Roche, Basel, Switzerland). Malondialdehyde (MDA) assay kits were purchased from Jiancheng (Nanjing, China). Fasting insulin (FINS) was assessed with a double antibody radioimmunoassay. Homeostasis model assessment-insulin resistance (HOMA-IR) was computed as FBG × FIN/22.5.

Liraglutide (3 mL) was purchased from Novo Nordisk (Bagsværd, Denmark). The basal diet was composed of sorghum flour, soy flour, corn flour, cod liver oil, wheat bran, multivitamins, and trace elements, with a fat content of 4% (HFK Bioscience, Beijing, China). The high-fat feed contained lard oil, cholesterol, egg yolk powder, and deoxycholate in addition to the basal diet (carbohydrate 30.01%, protein 16.24%, fat 53.75%, total calories 486 kcal/100 g; Boster).

Determination of liver PON3, PI3K, Akt, and NF-κB mRNA expression using RT-PCR

PON3, PI3K/Akt and NF-κB mRNA expression were determined using a nucleic acid/protein analyzer. For RNA extraction, 1 mL of TRIzol reagent was added to about 100 mg of fresh frozen liver tissue according

to the single-step TRIzol method. The RNA concentration and purity were determined. The cDNA was synthesized from the same amount of RNA. An appropriate amount of cDNA was then amplified using PCR.

Determination of PON3, Akt and NF-κB protein expression using western blot

A small amount of liver tissue was placed in a 1-mL or 2-mL homogenizer, minced with scissors, mixed with 400 µL of single-detergent lysis buffer (containing phenylmethylsulfonyl fluoride (PMSF)), homogenized, and placed on ice. After a few minutes, the tissue was ground and then placed on ice again. This step was repeated several times to obtain the desired fineness. After lysis for 30 min, the lysate was transferred to a 1.5-mL centrifuge tube with a pipette and centrifuged at 12,000 rpm for 5 min at 4°C. The supernatant was aliquoted into 0.5-mL centrifuge tubes and stored at –20°C. Signals generated by horseradish peroxidase (HRP)-conjugated antibodies were visualized using an enhanced chemiluminescence detection system and exposed on Kodak X-ray film (Eastman Kodak, Rocherster, USA). Protein band intensities were quantified with densitometric analysis using BandScan v. 4.3 software (Glyko, Shanghai, China) and corrected to GAPDH levels.

Statistical analysis

Statistical analysis was performed using SPSS v. 17.0 software (SPSS Inc., Chicago, USA). All data was expressed as $\bar{x} \pm s$. Differences between groups were analyzed using one-way analysis of variance (ANOVA). The least significant difference (LSD) t-test was used for comparisons between the 2 groups. For all tests, $p < 0.05$ was considered statistically significant.

Results

Figure 1 shows the relationship between FBG, HOMA-IR and FINS levels before and after liraglutide treatment. Significantly higher FBG, HOMA-IR and FINS levels were found in PC, LL and HL rats compared to NC rats
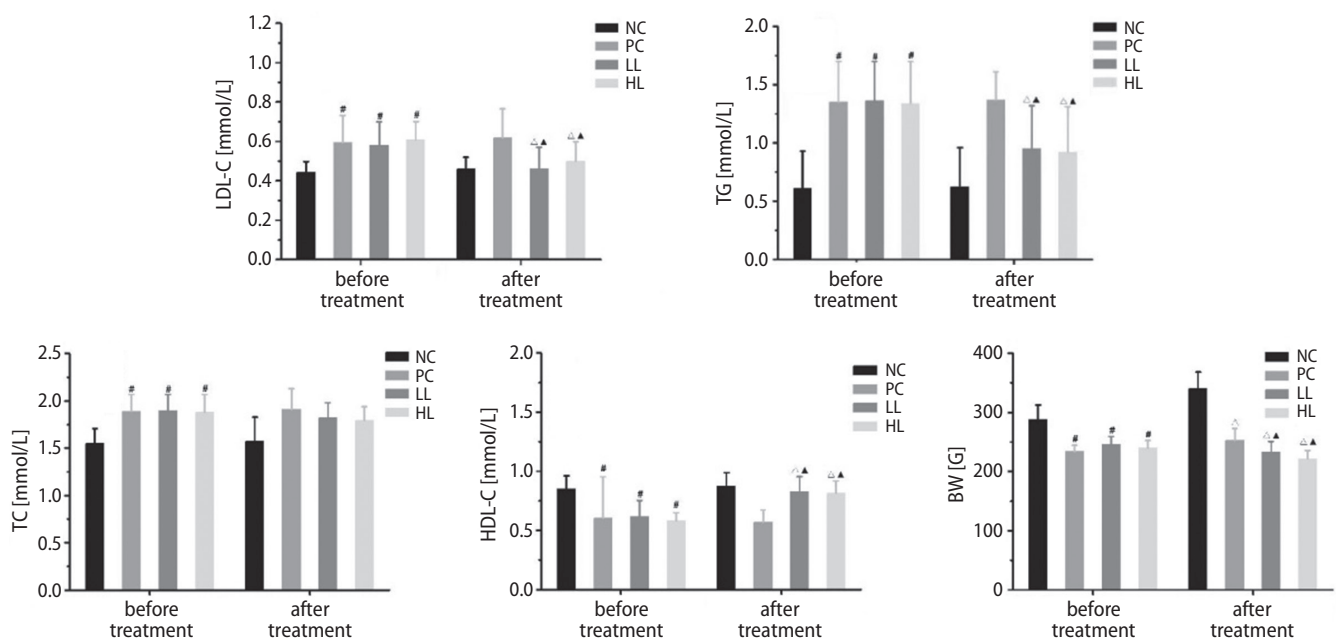
Fig. 1. FBG, HOMA-IR and FINS levels before and after liraglutide treatment

# p < 0.05 compared to NC rats before treatment; △ p < 0.05 compared to NC rats after treatment; ▲ p < 0.05 compared to PC rats after treatment; ★ p < 0.05 before and after treatment.
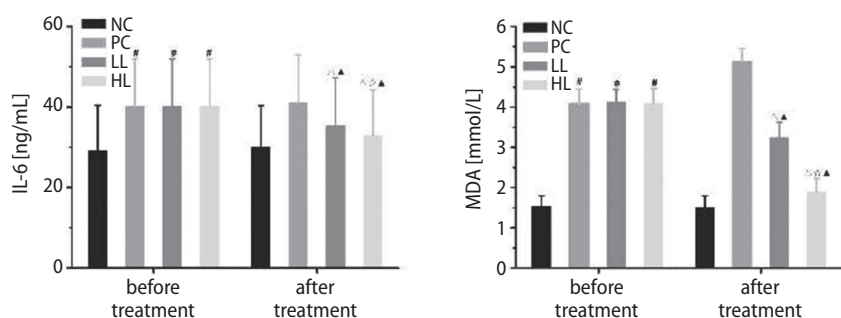
Fig. 2. LDL-C, TG, TC and HDL-C levels, and BW before and after liraglutide treatment

# p < 0.05 compared to NC rats before treatment; △ p < 0.05 compared to NC rats after treatment; ▲ p < 0.05 compared to PC rats after treatment; ★ p < 0.05 before and after treatment.
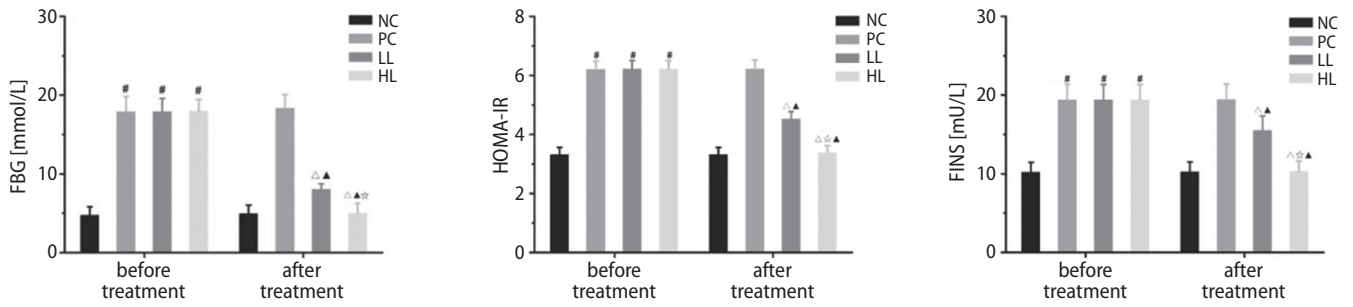
Fig. 3. IL-6 and MDA levels before and after liraglutide treatment

# $p < 0.05$ compared to NC rats before treatment; △ $p < 0.05$ compared to NC rats after treatment; ▲ $p < 0.05$ compared to PC rats after treatment; ★ $p < 0.05$ before and after treatment.
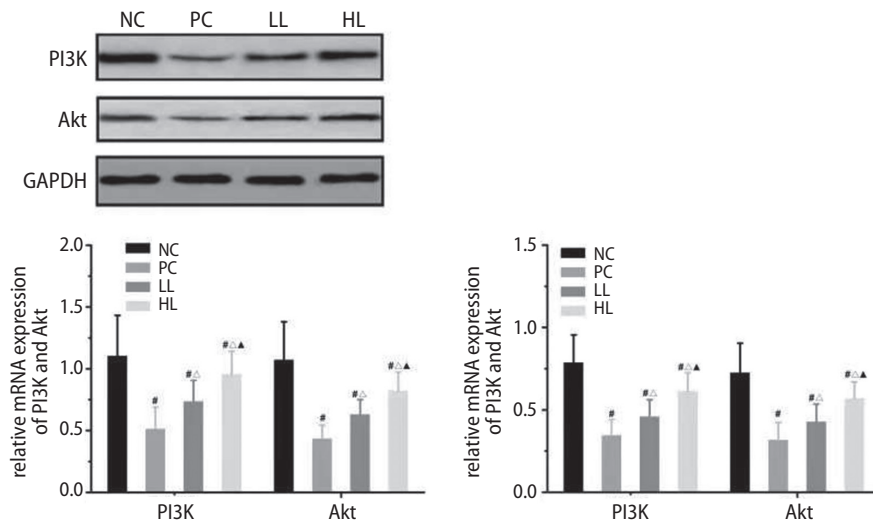
Fig. 4. Liver PI3K, Akt protein and mRNA expression in each group

# $p < 0.05$ compared to NC rats before treatment;
△ $p < 0.05$ compared to NC rats after treatment;
▲ $p < 0.05$ compared to PC rats after treatment;
★ $p < 0.05$ before and after treatment.
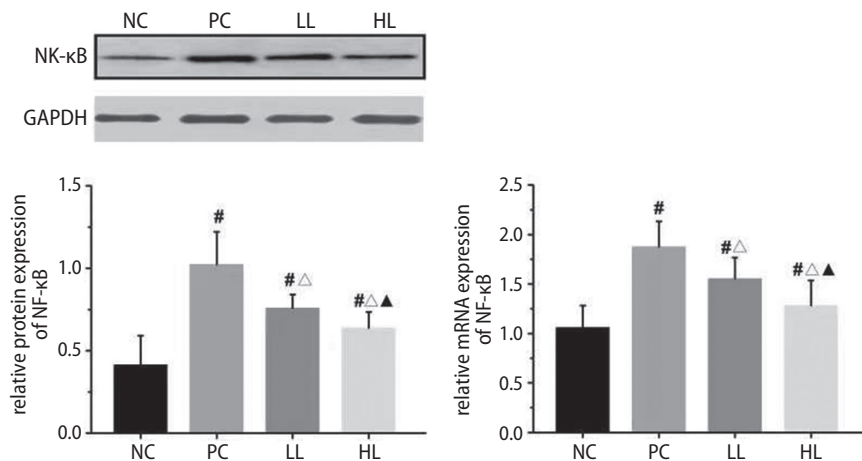
Fig. 5. Liver PON3 protein and mRNA expression in each group

# $p < 0.05$ compared to NC rats before treatment;
△ $p < 0.05$ compared to NC rats after treatment;
▲ $p < 0.05$ compared to PC rats after treatment;
★ $p < 0.05$ before and after treatment.

($p < 0.05$) before treatment. However, after treatment, these levels were significantly lower in HL rats than in LL rats ($p < 0.05$).

Figure 2 shows LDL-C, TG, TC, and HDL-C levels and BW before and after liraglutide treatment. A significantly higher TG level and BW were found in PC, LL and HL rats compared to NC rats ($p < 0.05$) before treatment. Nevertheless, BW was lower in LL and HL rats than in NC and PC rats after treatment, but no significant higher TC levels was found in HL rats than in LL rats ($p > 0.05$).

Figure 3 presents IL-6 and MDA levels before and after liraglutide treatment. Significantly higher IL-6 and MDA levels were detected in PC, LL and HL rats compared to NC rats ($p < 0.05$) before treatment, yet significantly lower in HL rats than in LL rats ($p < 0.05$) after treatment. Compared to NC rats, FPG, FINS, HOMA-IR, LDL-C, TG, and IL-6 levels were the lowest in HL rats, followed by LL and PC rats ($p < 0.05$).

Figures 4–6 depict liver PI3K, Akt protein, liver PON3 protein, liver NF-κB protein, and mRNA expression in each
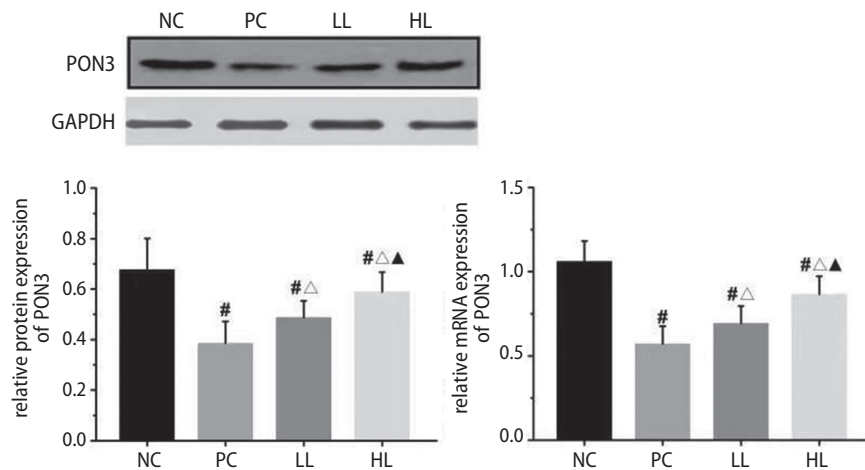
Fig. 6. Liver NF-κB protein and mRNA expression in each group

# p < 0.05 compared to NC rats before treatment;
△ p < 0.05 compared to NC rats after treatment;
▲ p < 0.05 compared to PC rats after treatment;
★ p < 0.05 before and after treatment.

group. The results showed that liraglutide increased PI3K, Akt and PON3 expression in LL and HL rats. However, it decreased FBG and HOMA-IR levels.

Discussion

The PON3 expression is closely related to insulin resistance, lipid metabolism and obesity.[1,2] In this study, liver PON3 expression was decreased in PC rats, which further suggests that low PON3 levels may be involved in the pathogenesis of T2DM. Moreover, PI3K and Akt expression in liver were increased after liraglutide treatment, accompanied by increased PON3 levels. A recent study found that PI3K and Akt enhanced PON3 expression.[4] Another study showed that liraglutide increased the expression of PI3K and Akt,[6] which is supported by our results. Therefore, it is possible that liraglutide stimulated PON3 expression by upregulating PI3K and Akt expression. In this study, PON3 expression was increased in LL and HL rats, accompanied by lowered FBG and HOMA-IR levels. Liraglutide might improve insulin resistance and glucose metabolism by upregulating PON3 expression.

Inflammation is involved in the pathogenesis and progression of T2DM. We also found higher serum IL-6 levels in PC rats compared to NC rats. Beek et al. found that patients with T2DM had higher serum IL-6 levels than normal subjects.[9] It has also been reported that high IL-6 levels inhibited insulin secretion[10] and produced cytotoxic effects that caused pancreatic β cell death.[11] Interleukin 6 can also induce T2DM by reducing cell-surface glucose transporter 4 expression.[12] This study also found higher IL-6 levels in PC rats, suggesting that increased IL-6 levels might be involved in T2DM pathogenesis. Liraglutide has been shown to inhibit inflammation,[7] which is supported by our observation of decreased IL-6 levels in both LL and HL rats. Moreover, liraglutide-treated rats showed higher PON3 expression, along with lower IL-6 levels and NF-κB expression, as compared to PC rats. The PON3 overexpression inhibits inflammatory factors in CCl$_4$-induced liver

injury. Schweikert et al.[13] suggested that PON3 reduced the activation of the NF-κB inflammatory pathway, thereby inhibiting inflammation. Thus, it can be seen that inhibition of the NF-κB inflammatory pathway is one of the anti-inflammatory mechanisms of PON3. It is possible that the effect of liraglutide on IL-6 levels is partially achieved by upregulating PON3 expression and thereby inhibiting NF-κB. The lower IL-6 levels in HL rats than in LL rats may be associated with the greater increase of PON3 expression in HL rats. The PON3 expression was decreased in PC rats. It is possible that the downregulation of PON3 may reduce the inhibition of inflammation, thereby promoting the pathogenesis of T2DM.

Furthermore, NF-κB expression was increased in PC rats, accompanied by higher MDA levels. The NF-κB can promote the production of reactive oxygen species (ROS).[14,15] The ROS-mediated oxidative stress can cause damage and dysfunction of insulin target organs and tissues, and is closely related to T2DM and obesity. Reactive oxygen species have also been shown to activate NF-κB signaling,[16,17] suggesting that the interaction between ROS and NF-κB further provokes oxidative stress. Bharathidevi et al. found that PON3 played a defensive role against oxidative stress in diabetic retina.[18] Ferreira et al. reported that PON3 was expressed in bull testis and prevented oxidative damage associated with male reproductive function.[19] The abovementioned studies demonstrate that PON3 protects against oxidative stress. It has been suggested that the antioxidative stress effect of PON3 may be related to NF-κB inhibition.[13] It is possible that reduced PON3 expression in PC rats was also involved in increased oxidative stress by reducing NF-κB inhibition. Liraglutide protects against oxidative stress.[20] In this study, PON3 expression was increased and NF-κB expression was reduced in LL and HL rats, accompanied by decreased MDA levels. It is possible that liraglutide inhibited NF-κB by upregulating PON3 expression, thereby protecting against oxidative stress. The lower MDA levels in HL rats compared to LL rats may be associated with the greater increase of PON3 expression in HL rats.

Obesity is involved in insulin resistance. Low-grade inflammation caused by obesity can impair the insulin receptor signaling pathway and is involved in the development of insulin resistance.[21] Shih et al. found that PON3 knockout mice gained more BW and had a larger average gonadal adipocyte size than wild-type mice when fed the same high-fat diet.[22] Moreover, PON3 knockout mice had significantly more subcutaneous, retroperitoneal and gonadal fat than wild-type mice. The authors suggested that PON3 can reduce obesity in mice by protecting the mitochondrial function of hepatocytes and white fat cells. These results indicate that low PON3 levels may be involved in the development of obesity. Decreased liver PON3 expression might also be involved in the development of obesity. Liraglutide enhanced PON3 expression, and BW was lower in LL and HL rats than in PC rats. The role of liraglutide in reducing BW might be related to its upregulation of PON3 expression.

In this study, PON3 expression was decreased in diabetic rats, and this was accompanied by abnormal lipid metabolism. Shih et al. found significantly increased TG levels in high-fat-fed PON3 knockout mice.[22] On the other hand, PON3 deficiency can lead to changes in lipoprotein levels, including increased LDL-C and decreased HDL-C levels, in high-fat-fed mice. The reduced PON3 expression, increased TG and LDL-C levels, and decreased HDL-C levels in diabetic rats further suggest that reduced PON3 expression is associated with abnormal lipid metabolism. Liraglutide can improve lipid metabolism.[22] In this study, PON3 expression was increased and abnormal lipid metabolism was improved after liraglutide treatment. It is possible that the effect of improved lipid metabolism was partially achieved by liraglutide increasing PON3 expression.

Limitations

Some limitations in our study should be considered. First, we have failed to investigate whether the PI3K/Akt pathway increases insulin sensitivity through PON3, although previous study showed that PI3K/Akt pathway is involved in the metabolic regulation of insulin through various mechanisms.[23,24] Second, we have also failed to investigate the role of PON3 in obesity. Further in-depth study of the role of PON3 in PC could significantly contribute to understanding the development of abnormal glycolipid metabolism and obesity.

Conclusions

Liraglutide can increase PI3K, Akt and PON3 expression, and decrease NF-κB expression. The effect of liraglutide on improving insulin resistance and abnormal glucolipid metabolism in T2DM rats may be associated with increased liver PON3 expression.

ORCID iDs

Yuntao Liu https://orcid.org/0000-0003-4033-2133
Dan Zhu https://orcid.org/0000-0003-4116-4055
Guofeng Dong https://orcid.org/0000-0001-9104-2836
Yuqin Zeng https://orcid.org/0000-0002-6021-409X
Pan Jiang https://orcid.org/0000-0001-9490-2635
Yaoling Xiao https://orcid.org/0000-0001-9368-7101

References

1. Rull A, García R, Fernández-Sender L, et al. Serum paraoxonase-3 concentration is associated with insulin sensitivity in peripheral artery disease and with inflammation in coronary artery disease. *Atherosclerosis*. 2012;22(2):545–541. doi:10.1016/j.atherosclerosis.2011.11.021
2. Shih DM, Xia YR, Yu JM, Lusis AJ. Temporal and tissue-specific patterns of PON3 expression in mouse: In situ hybridization analysis. *Adv Exp Med Biol*. 2010;660:73–87. doi:10.1007/978-1-60761-350-3_8
3. Peng W, Zhang C, Lv H, et al. Comparative evaluation of the protective potentials of human paraoxonase 1 and 3 against CCl 4-induced liver injury. *Toxicol Lett*. 2010;193(2):159–166. doi:10.1016/j.toxlet.2010.01.003
4. Zhu L, Shen Y, Sun W, et al. Paraoxonase 3 promotes cell proliferation and metastasis by PI3K/Akt in oral squamous cell carcinoma. *Biomed Pharmacother*. 2017;85:712–717. doi:10.1016/j.biopha.2016.11.084
5. Inoue K, Maeda N, Fujishima Y, et al. Long-term impact of liraglutide, a glucagon-like peptide-1 (GLP-1) analogue, on body weight and glycemic control in Japanese type 2 diabetes: An observational study. *Diabetol Metabol Syndr*. 2014;6(1):95. doi:10.1186/1758-5996-6-95
6. Shao S, Nie M, Chen C, et al. Protective action of liraglutide in beta cells under lipotoxic stress via PI3K/Akt/FoxO1 pathway. *J Cell Biochem*. 2014;115(6):1166–1175. doi:10.1002/jcb.24763
7. Gao H, Zeng Z, Zhang H, et al. The glucagon-like peptide-1 analogue liraglutide inhibits oxidative stress and inflammatory response in the liver of rats with diet-induced non-alcoholic fatty liver disease. *Biol Pharm Bull*. 2015;38(5):694–702. doi:10.1248/bpb.b14-00505
8. Guo N, Sun J, Chen H, Zhang H, Zhang Z, Cai D. Liraglutide prevents diabetes progression in prediabetic OLETF rats. *Endocrine J*. 2013;60(1):15–28. doi:10.1507/endocrj.ej12-0094
9. Beek LV, Lips MA, Visser A, et al. Increased systemic and adipose tissue inflammation differentiates obese women with T2DM from obese women with normal glucose tolerance. *Metabolism*. 2014;63(4):492–501. doi:10.1016/j.metabol.2013.12.002
10. Rabingovitch A. An update on cytokines in the pathogenesis of insulin independent diabetes mellitus. *Diabetes Metab Rev*. 1998;14(2):129–151. doi:10.1002/(sici)1099-0895(199806)14:2<129::aid-dmr208>3.0.co;2-v
11. Choi SE, Choi KM, Yoon IH, et al. IL-6 protects pancreatic islet beta cells from pro-inflammatory cytokines-induced cell death and functional impairment in vitro and in vivo. *Transpl Immunol*. 2004;13(1):43–53. doi:10.1016/j.trim.2004.04.001
12. Schweikert EM, Amort J, Wilgenbus P, et al. Paraoxonases-2 and -3 are important defense enzymes against pseudomonas aeruginosa virulence factors due to their anti-oxidative and anti-inflammatory properties. *Lipids*. 2012:352857.
13. Lagathu C, Bastard JP, Auclair M, Maachi M, Capeau J, Caron M. Chronic interleukin-6 (IL-6) treatment increased IL-6 secretion and induced insulin resistance in adipocyte: Prevention by rosiglitazone. *Biochem Biophys Res Commun*. 2003;311(2):372–379. doi:10.1016/j.bbrc.2003.10.013
14. Manea A, Manea SA, Gafencu AV, Raicu M. Regulation of NADPH oxidase subunit p22(phox) by NF-κB in human aortic smooth muscle cells. *Arch Physiol Biochem*. 2007;113(4–5):163–172.
15. Anrather J, Racchumi G, Iadecola C. NF-kappaB regulates phagocytic NADPH oxidase by inducing the expression of gp91phox. *Biol Chem*. 2006;281(9):5657–5667. doi:10.1074/jbc.M506172200
16. Wang R, Peng L, Zhao J, et al. Gardenamide A protects RGC-5 cells from H(2)O(2)-induced oxidative stress insults by activating PI3K/Akt/eNOS signaling pathway. *Int J Mol Sci*. 2015;16(9):22350–22367. doi:10.3390/ijms160922350
17. Bautista E, Vergara P, Segovia J. Iron-induced oxidative stress activates Akt and ERK1/2 and decreases Dyrk1B and PRMT1 in neuroblastoma SH-SY5Y cells. *Trace Elem Med Biol*. 2016;34:62–69. doi:10.1016/j.jtemb.2015.11.005

18. Bharathidevi SR, Babu KA, Jain N, et al. Ocular distribution of antioxidant enzyme paraoxonase & its alteration in cataractous lens & diabetic retina. *Indian J Med Res*. 2017;145(4):513–520. doi:10.4103/ijmr.IJMR_1284_14

19. Ferreira CER, Haas CS, Goularte KL, et al. Expression of paraoxonase types 1, 2 and 3 in reproductive tissues and activity of paraoxonase type 1 in the serum and seminal plasma of bulls. *Andrologia*. 2017;50(3):e12923. doi:10.1111/and.12923

20. Li PC, Liu LF, Jou MJ, Wang HK. The GLP-1 receptor agonists exendin-4 and liraglutide alleviate oxidative stress and cognitive and micturition deficits induced by middle cerebral artery occlusion in diabetic mice. *BMC Neurosci*. 2016;13(17):37. doi:10.1186/s12868-016-0272-9

21. Nandipati KC, Subramanian S, Agrawal DK. Protein kinases: Mechanisms and downstream targets in inflammation-mediated obesity and insulin resistance. *Mol Cell Biochem*. 2017;426(1–2):27–45. doi:10.1007/s11010-016-2878-8

22. Shih DM, Yu JM, Vergnes L, et al. PON3 knockout mice are susceptible to obesity, gallstone formation, and atherosclerosis. *FASEB J*. 2015;29(4):1185–1197. doi:10.1096/fj.14-260570

23. Kadowaki T, Ueki K, Yamauchi T, Kubota N. Snapshot: Insulin signaling pathways. *Cell*. 2012;148(3):624,624e1. doi:10.1016/j.cell.2012.01.034

24. Hennessy BT, Smith DL, Ram PT, Lu Y, Mills GB. Exploiting the PI3K/AKT pathway for cancer drug discovery. *Nat Rev Drug Discov*. 2005;4(12):988–1004. doi:10.1038/nrd1902

Risk factors and outcomes for acute respiratory failure in coronavirus disease 2019: An observational cohort study

Paweł Piwowarczyk[1,A–F], Marta Szczukocka[1,B–F], Paweł Kutnik[2,B–F], Michał Borys[1,B–F], Anna Mikłaszewska[3,B–F], Sławomir Kiciak[3,B–F], Mirosław Czuczwar[1,B–F]

[1] Department of Anaesthesiology and Intensive Therapy, Medical University of Lublin, Poland

[2] Student's Scientific Association at the Department of Anaesthesiology and Intensive Therapy, Medical University of Lublin, Poland

[3] Department of Infectious Diseases, Medical University of Lublin, Poland

A – research concept and design; B – collection and/or assembly of data; C – data analysis and interpretation;
D – writing the article; E – critical revision of the article; F – final approval of the article

Address for correspondence
Paweł Piwowarczyk
E-mail: piwowarczyk.pawel@gmail.com

Abstract

Background. The novel severe acute respiratory syndrome coronavirus 2 (SARS-CoV-2), has spread throughout Europe. However, there is a lack of data on the full clinical course of patients infected with SARS-CoV-2 in Europe, especially in the population that developed acute respiratory failure (ARF).

Objectives. To identify risk factors associated with developing ARF during SARS-CoV-2 infection.

Material and methods. This was an observational study of 60 adult patients with laboratory-confirmed SARS-CoV-2 infection. Data were collected from March 26, 2020 to May 26, 2020 in a tertiary academic hospital in Poland. All patients reached final outcome (discharge from the hospital or death). We divided patients into 2 groups based on whether they developed ARF, compared their clinical data, and performed multivariate logistic regression.

Results. Twenty-two patients (36%) from the observed cohort developed ARF. Logistic regression identified that a high sequential organ failure assessment score at admission (odds ratio (OR) = 6.97 (1.57–30.90, p = 0.011)), and a long time from admission until pneumonia (OR = 1.41 (1.06–1.87, p = 0.016)), correlated with ARF development. D-dimer, lactate dehydrogenase, neutrophil to lymphocyte ratio, C-reactive protein (CRP), and interleukin 6 (IL-6) differed both statistically and clinically between ARF and non-ARF groups. The mortality rate in the observed cohort of patients was 13.3%, and it was 32% in the group that developed ARF.

Conclusions. Routine vigilant examination of the above markers may identify patients at the highest risk of ARF early on during COVID-19 infection.

Key words: coronavirus, clinical characteristics, observational, SARS, respiratory failure

Background

During the past 2 decades, 2 major epidemics were caused by viruses belonging to the betacoronavirus group: severe acute respiratory syndrome coronavirus (SARS-CoV) in 2002 and the Middle East respiratory syndrome coronavirus (MERS-CoV) in 2012.[1,2] In December 2019, China reported the outbreak of pneumonia of an unknown origin in Wuhan, the capital of Hubei province.[3] The pathogen responsible for the outbreak was identified as a novel coronavirus (SARS-CoV-2) belonging to the betacoronavirus group and causing COVID-19 infection. On March 12, 2020, the World Health Organization (WHO) announced a COVID-19 pandemic, which has resulted to date in 24.48 million confirmed cases of COVID-19 worldwide and 832.378 causalities (data as of August 28, 2020). In Poland, there have been 65,480 confirmed cases, causing 2,018 deaths (data as of August 28, 2020).[4]

The clinical manifestations of COVID-19 include fever, dry cough, dyspnea, fatigue, a normal or decreased leucocyte count, and specific findings in chest imaging, including X-ray, computed tomography (CT) scan, and ultrasound examination.[5,6] A small proportion of patients presents symptoms of acute respiratory failure (ARF) or acute respiratory distress syndrome (ARDS), requiring the implementation of more advanced ventilatory support and subsequent admission to the intensive care unit (ICU). Accumulating data shows that ICU admission is associated with poor prognosis with a range of mortality from 30.9%[6] to 81.3% in the cohort of ICU patients treated in the New York City area.[7] A recent meta-analysis reports that mortality rates in patients with COVID-19 treated in ICU have fallen to 40%, which is higher than in other types of viral pneumonia.[8] Exploring the association of patients' outcomes with the clinical presentation of the disease is urgently needed, especially in the face of rapidly changing phenotype of the virus in particular populations. Moreover, the mortality rates reported in the majority of retrospective studies may present a skewed picture since a large proportion of critically ill patients are still treated in the ICU and did not reach the outcome.

Objectives

This study aimed to provide a detailed description of patients' characteristics, treatment modalities and outcomes in the Polish cohort treated due to COVID-19 at a tertiary academic hospital.

Patients and methods

This observational cohort study was approved by the Ethical Committee of the Medical University of Lublin, Poland (approval No. KE-0254/59/2020). All the study data was collected in a tertiary academic hospital in Lublin, Poland.

We included adult patients hospitalized in the Department of Anesthesiology and Intensive Care and the Department of Infectious Diseases. The study adhered to the STROBE (STrengthening the Reporting of Observational studies in Epidemiology) guidelines for collecting and interpreting observational data. All analyzed patients had a confirmed SARS-CoV-2 infection with real-time reverse transcription polymerase chain reaction (RT-PCR). Oral consent was obtained from each conscious patient. In the case of 3 patients who were transferred to our hospital from regional ICUs, guardianship court consent was obtained. All included patients were followed until the outcome (discharge from the hospital or death) was reached. Patients suspected with COVID-19 infection but unconfirmed with RT-PCR and individuals who did not give consent to participate in the study or withdrew consent were excluded from the study.

The main goal of this study was to identify the factors and outcomes associated with the development of ARF in the population of patients with confirmed COVID-19. All observed patients were divided into 2 groups (ARF and non-ARF groups) according to the results of arterial blood gas analysis and the extent of oxygenation disorders. The most recent definition of ARDS, the Berlin definition, ARDS is defined by a combination of acute hypoxemia ($PaO_2/FiO_2 \leq 300$ mm Hg), in a ventilated patient with a positive end-expiratory pressure (PEEP) of at least 5 cm H_2O, and bilateral opacities not fully explained by heart failure or volume overload. Patients included in the ARF group have fulfilled the 1st criterion of ARDS that concerns the extent of oxygenation disorders. However, not all of them have completed the 2nd and 3rd criteria concerning bilateral chest radiological changes and the presence of positive expiratory pressure of at least 5 cm of water. We did not use non-invasive ventilation due to a lack of safe interfaces for its provision and the associated threat to the staff. The secondary goal of the study was a comparison of baseline demographics, epidemiological data (history of an infected family member, history of traveling abroad in the past 2 weeks), symptoms at admission (fever, dry cough, hemoptysis, myalgia, headache, diarrhea, dyspnea), laboratory results at admission (white blood count (WBC), lymphocytes, neutrophils, neutrophil to lymphocyte ratio (NLR), immature granulocytes, platelets, hemoglobin, D-dimers, prothrombin time, activated partial thromboplastin time, aspartate transaminase (AST), alanine transaminase (ALT), as well as serum levels of creatinine, urea, bilirubin, lactate dehydrogenase (LDH), procalcitonin, C-reactive protein (CRP) and interleukin 6 (IL-6). We calculated the sequential organ failure assessment (SOFA) score at admission to the hospital and initiated monitoring of hemoglobin oxygen saturation in arterial blood (SpO_2). We obtained an arterial blood sample in patients presenting with SpO_2 below 94% or in need of oxygen supplementation; subsequently, we calculated the arterial oxygen partial pressure (PaO_2/FiO_2) ratio. We evaluated pharmacotherapy and organ support

therapies in the observed cohort, and we recorded and compared baseline chest X-rays. The data were collected from March 26, 2020 to May 26, 2020, with the latter being the day of discharge of the last included patient. All patients requiring invasive mechanical ventilation, veno-venous extracorporeal membrane oxygenation (V-V ECMO), continuous renal replacement therapy, or administration of catecholamines were treated in the ICU, whereas patients requiring pharmacotherapy or oxygen supplementation only were treated in the infectious diseases ward.

Categorical variables were presented as frequency rates and percentages. Continuous variables were tested for normal distribution using the Kolmogorov–Smirnov test; they were presented as means and 95% confidence intervals (95% CIs) for normally distributed data and as medians and interquartile range (IQR 1–3) for non-normally distributed data. Logistic regression was presented as an odds ratio (OR) with 95% CI. The sensitivity of the calculated model was presented as the area under the curve (AUC) of a receiver operating characteristic (ROC) curve. All statistical

calculations were performed using STATISTICA v. 13.3 (StatSoft Inc., Tulsa, USA). A p-value of 0.05 or below was considered statistically significant.

Results

The study population included 60 patients with a laboratory-confirmed presence of SARS-CoV-2 RNA. The demographic, clinical, and epidemiological characteristics of all included patients are presented in Table 1. The laboratory variables at the time of admission to the hospital in both groups are compared in Table 2. The median time from the first symptoms to the diagnosis of pneumonia was 7 days (4–8 days). The clinical course of 22 patients (36%) deteriorated during hospitalization because of the development of ARF. Ten patients (16.7%) were intubated and mechanically ventilated. We initiated V-V ECMO in 3 patients (2%). The number of patients who needed extracorporeal organ support and infusion

Table 1. Demographic, clinical, and epidemiological characteristics of patients. Data is presented as numbers and percentages for categorical values and as median and IQR for continuous values. Statistical analysis was performed accordingly

Parameter	ARF (n = 22)	Non-ARF (n = 38)	p-value
Demographics, n (%)			
Male sex	16 (73%)	15 (39%)	0.013*
Female sex	6 (27%)	23 (61%)	0.013
Age, [years] (IQR)	59 (50–67)	39 (25–51)	0.00006*
18–29	1 (4.5%)	12 (30.8%)	0.014
30–44	2 (9.1%)	14 (36.8%)	0.019
45–65	9 (40.9%)	10 (26.3%)	0.24
65+	9 (40.9%)	2 (5.3%)	0.0006*
Symptoms, n (%)			
Fever	21 (95.5%)	21 (55.3%)	0.001*
Cough	20 (90.9%)	22 (57.9%)	0.009*
Muscle ache	5 (22.7%)	13 (34.2%)	0.32
Productive cough	5 (22.7%)	4 (10.5%)	0.22
Headaches	5 (22.7%)	4 (10.5%)	0.22
Hemoptysis	2 (9.1%)	0 (0%)	0.135
Diarrhea	7 (31.8%)	9 (23.6%)	0.53
Comorbidities, n (%)			
COPD	1 (4.5%)	(0%)	0.37
Liver disease	2 (9.1%)	(0%)	0.13
Diabetes	2 (9.1%)	2 (5.3%)	0.56
Chronic kidney disease	(0%)	(0%)	N.A.
Hypertension	12 (54.5%)	8 (21.1%)	0.008*
Cardiovascular disease	6 (27.3%)	2 (5.3%)	0.016*
Epidemiology			
Confirmed SARS-COV-2 in family	12 (54.5%)	25 (65.8%)	0.32
Traveling abroad within 2 weeks prior to confirmation of SARS-COV-2	2 (9.1%)	4 (10.5%)	0.83

ARF – acute respiratory failure; IQR – interquartile range; SARS-CoV-2 – severe acute respiratory syndrome coronavirus 2; COPD – chronic obstructive pulmonary disease; *p values indicate differences between ARF and non-ARF patients; p < 0.05 was considered statistically significant.

Table 2. Laboratory and chest radiogram findings. Data is presented as numbers and percentages for categorical values and as median and IQR for continuous values. Statistical analysis was performed accordingly

Parameter	Norms	ARF (n = 22)	Non-ARF (n = 38)	p-value
WBC [K/uL]	4–10	6.49 [5.39–9.84]	4.99 [4.18–5.79]	0.0002
Lymphocytes [K/uL]	0.8–4.3	1.02 [0.62–1.31]	1.65 [1.22–2.18]	0.0004
Neutrophils [K/uL]	2.25–7	5.55 [4.1–8.42]	2.66 [1.94–3.28]	0.00004
NLR	1–3	8.53 [5.32–13.46]	2.96 [2.11–4.39]	0.000003*
IG [K/uL]	0–0.25	0.06 [0.03–0.12]	0.01 [0.01–0.03]	0.000002
Hemoglobin [g/dL]	12–16	13.5 [12.7–14.7]	14 [13.3–15.6]	0.08
Platelets [K/uL]	130–400	167 [140–209]	199 [163–239]	0.16
PT [s]	11–14	13.6 [12.5–15.5]	12.5 [12.2–13.3]	0.01
APTT [s]	28–38	31.8 [30.4–39.3]	34.2 [29.5–36.7]	0.26
D-dimers [ng/mL]	<500	758 [450–1900]	418 [309–773]	0.02*
Bilirubin [mg/dL]	0.2–11	0.43 [0.27–0.52]	0.39 [0.24–0.65]	0.88
ALAT [U/L]	5–34	31.3 [23.7–40.8]	19.9 [13.4–27.8]	0.004
ASPAT [IU/L]	5–35	35.0 [23.5–56]	20.7 [15.4–25]	0.0006
LDH [IU/L]	10–480	633 [526–826]	355.5 [287–412.5]	0.00003
Creatinine [mg/dL]	0.5–1.2	1.02 [0.80–1.27]	0.93 [0.71–1.02]	0.013
Urea [mg/dL]	15–40	32.5 [26.7–47.4]	28.1 [24.1–34.7]	0.018
IL-6 [pg/mL]	5–15	61 [8.87–111.5]	7.6 [2.67–18.83]	0.006
PCT [ng/mL]	<2	0.14 [0.085–0.25]	0.05 [0.04–0.07]	0.0001
CRP [mg/L]	<5	69.2 [29.2–206.7]	2.7 [1.3–8.2]	0.00000*
Chest radiogram quadrants				
0		3 (13.6%)	34 (89.5%)	0.002*
1		2 (9.1%)	4 (10.5%)	1
2		10 (45.4%)	0	0.002*
3		2 (9.1%)	0	0.15
4		5 (22.7%)	0	0.01*

IQR – interquartile range; WBC – white blood count; NLR –neutrophil to lymphocyte ratio; IG – immature granulocytes (%); PT – prothrombin time; APTT – activated partial thromboplastin time; ALAT – alanine transaminase; ASPAT – aspartate transaminase; LDH – lactate dehydrogenase; IL-6 – interleukin 6; PCT – procalcitonin; CRP – C-reactive protein; *p-values indicate statistical and clinical differences between ARF and non-ARF patients; p < 0.05 was considered statistically significant.

of vasoactive and inotropic agents is presented in Table 3. Eight patients (13.3%) died in the entire cohort. The survival rate was 68% (15/22) in the ARF group and 97% (37/38) in the non-ARF group. One patient was readmitted 16 days after the initial mild course of COVID-19. While the SARS-CoV-2 RNA test was negative during the 2nd admission, the patient died because of lung fibrosis.

We performed an additional sub-analysis in the population of COVID-19 patients who developed ARF. The baseline characteristics and treatment modalities were compared between the groups of survivors and non-survivors. Interestingly, the SOFA score at admission did not differ between the groups of ARF survivors and non-survivors (2 vs 5; p = 0.09). The extent of oxygenation disorders was similar in both groups. The need for mechanical ventilation and norepinephrine support that occurred in 45% and 45.7% of the patients from the ARF group, respectively, was associated with a negative outcome.

Our multivariate logistic regression analysis detected 2 variables associated with ARF development: OR = 6.97 (1.57–30.9, p = 0.011) and OR = 1.41 (1.06–1.87, p = 0.016), respectively.

Discussion

All patients included in this observational trial reached the outcome (death or discharge from the hospital). The data presented in our study highlighted several factors associated with the development of ARF in the patients treated in our hospital. We found that the main elements correlating with a severe course of COVID-19 are demographics, comorbidities and various laboratory findings. In our study, male gender and advanced age were found to be associated with a higher risk of developing ARF. The association between advanced age and a more severe course of SARS CoV-2 infection was previously

Table 3. Pharmacotherapy, organ support and outcome. Data is presented as numbers and percentages

Variable	ARF (n = 22)	Non-ARF (n = 38)	p-value
Pharmacotherapy			
Ritonavir – lopinavir	17 (77.3%)	13 (34.2%)	0.0017*
Antibiotics	21 (95.5%)	12 (31.6%)	<0.0001*
Chloroquine	15 (68.2%)	15 (39.5%)	0.04*
Steroids	8 (36.7%)	0 (0%)	0.0001*
Organ support and survival			
Oxygen supplementation	22 (100%)	0 (0%)	
Invasive ventilation	10 (45%)	0	N/A
ECMO	3 (13%)	0	N/A
Dobutamine infusion	4 (18.1%)	0	N/A
Norepinephrine infusion	10 (45.4%)	0	N/A
CRRT	5 (22%)	0	N/A
Survival	15 (68%)	37 (97%)	0.0013

ECMO – extracorporeal membrane oxygenation; CRRT – continuous renal replacement therapy; *p-values indicate differences between ARF and non-ARF patients; p < 0.05 was considered statistically significant.

reported.[9,10] We found cough and fever to be the dominant symptoms at admission to the hospital. This finding is in line with previously published results showing that both symptoms are observed in 88.7% and 57.6% of COVID-19 patients, respectively.[11] Moreover, we identified a significantly higher prevalence of cough and fever in the ARF group (Table 1). Muscle ache, productive cough, headaches, hemoptysis, and diarrhea were not associated with ARF occurrence, contrary to hemoptysis, which was only observed in the ARF group (Table 1).

Arterial hypertension and cardiovascular disease (CVD) were found to be risk factors for an adverse outcome in multiple retrospective COVID-19 studies.[12,13] Similarly, we found that the population of patients with hypertension or CVD was at an increased risk of developing ARF. However, it is noteworthy that we did not observe any correlation between the use of antihypertensive drugs and COVID-19 severity, which is in line with the recently published results from a large retrospective study in the USA (Table 1).[14] Moreover, the presence of other comorbidities was not associated with the development of ARF. It should be noted, however, that the number of patients suffering from these diseases in our study was relatively small. In our study, 19/22 patients (86.4%) in the ARF group and 4/38 patients (10.5%) in the non-ARF group developed radiological signs of pneumonia in the chest X-ray. We found that a long time from the first presentation of symptoms to radiological signs of pneumonia correlates with a more severe course of COVID-19, which is consistent with the findings of previously published reports.[15]

We found that many laboratory results correlate with the development of ARF. Although the majority of different variables were within the laboratory norm, we found discrepancies in the NLR, lactate dehydrogenase, D-dimers, CRP, and IL-6, which were statistically significant and potentially clinically useful. A high NLR in COVID-19 patients was previously recognized as a useful predictive marker with 88% sensitivity, 63.6% specificity, and a calculated AUC of 0.841.[16] We observed significantly higher LDH levels in the ARF group, which is consistent with previous findings showing that elevated LDH levels are associated with a more severe course of COVID-19.[6,17] We identified a significant correlation between elevated D-dimer levels and an increased risk of ARF, which is in line with the findings of previously conducted cohort studies.[18] Interestingly, a fourfold increase in D-dimer levels (>2.0 µg/mL) predicted in-hospital mortality with a sensitivity of 92.3% and a specificity of 83.3%, which makes this parameter a potentially useful tool for a negative prognosis.[19] Two analyzed pro-inflammatory markers, IL-6 and CRP, positively correlated with an increased risk of ARF. This observation is consistent with previously reported data on the potential role of both IL-6 and CRP in the early identification of patients at a high risk of a severe course of COVID-19.[20] According to the literature, CRP is suggested to have a positive correlation not only with the severity of presentation in SARS-CoV-2 infection but also with the diameter of lung lesions and negative outcome.[21,22]

In this study, most patients who developed ARF because of SARS-Cov-2 infection presented alterations in their chest X-rays. These included interstitial infiltrates or ground-glass opacities in at least 2 lung quadrants. Interestingly, none of the patients in the non-ARF group showed changes in their chest X-ray exceeding 1 quadrant of the lung. These findings could support the use of chest X-ray to facilitate diagnosis and predict the severity of the disease, especially when a chest CT scan is unavailable or not feasible. It should be noted that most authors challenge the clinical utility and validity of chest

Table 4. Pharmacotherapy, organ support and outcome in the sub-group of ARF patients. Data is presented as numbers and percentages

Variable	ARF survivors (n = 15)	ARF non-survivors (n = 7)	p-value
SOFA	2 [2–4]	5 [3–7]	0.09
PaO$_2$/FiO$_2$			
200–300	8 (53.3%)	1 (14.3%)	0.08
100–200	5 (33.3%)	3 (43.9%)	0.66
<100	2 (13.3%)	3 (43.9%)	0.12
Pharmacotherapy			
Ritonavir/lopinavir	14 (93.3%)	3(43.9%)	0.0085*
Antibiotics	14 (93.3%)	7 (100%)	1
Chloroquine	13 (86.7%)	2 (28.6%)	0.0064*
Steroids	4 (26.6%)	4 (57.1%)	0.17
Organ support			
Oxygen supplementation	15 (100%)	7 (100%)	1.0
Invasive ventilation	3 (20%)	6 (85.7%)	0.004*
ECMO	2 (13.3%)	1 (14.3%)	0.95
Dobutamine infusion	2 (13.3%)	2 (28.5%)	0.39
Norepinephrine infusion	4 (26.6%)	6 (85.7%)	0.0096*
CRRT	4 (26.6%)	1 (14.2%)	0.52

SOFA – sequential organ failure assessment; ECMO – extracorporeal membrane oxygenation; CRRT – continuous renal replacement therapy; *p-values indicate differences between ARF survivors and non-survivors; p < 0.05 was considered statistically significant.

X-ray in patients with COVID-19. The rationale is a reported high prevalence of negative chest X-ray examinations in up to 60% of cases, which was not observed in our study.[23]

We evaluated the pharmacotherapy administered in both study groups and found that steroids, ritonavir/lopinavir, antibiotics, and chloroquine were significantly more frequently used in the group that developed ARF (Table 2). Our results on the pharmacotherapy used correspond with those presented by Wang et al., which were reported from Wuhan, China, where significantly more groups of drugs were used in patients who deteriorated and were transferred to the ICU.[5] We could not evaluate the impact of pharmacotherapy on outcomes. However, recent evidence report that the use of dexamethasone in patients requiring oxygen supplementation or mechanical ventilation reduces 28-day mortality.[24] Remdesivir is another therapeutic option reported to significantly shorten the recovery time but not affect the mortality.[25]

Our sub-analysis performed in the group that developed ARF from the observed cohort showed that the need for invasive mechanical ventilation and norepinephrine infusion was associated with increased mortality (Table 4). The low survival rate in the population receiving advanced respiratory support (33%) observed in our study is identical to that reported in the British National Intensive Care Audit on the outcomes of COVID-19 treatment (33.8%).[26]

Limitations

This study has several limitations. Because of the observational nature of the study and its relatively small cohort size, the results are exposed to treatment and selection bias. The causal effect of the associations drawn cannot be determined. Furthermore, many examinations, including routine CT chest scanning at admission, could not be performed because of institutional limitations. Data regarding the pharmacotherapy used and any potential association with the outcome should be taken with caution.

Conclusions

This observational trial provides information on the demographic, clinical and epidemiological features as well as outcomes of 60 patients diagnosed with COVID-19 treated in a tertiary center in Poland. The risk factors associated with the development of ARF in 37% of the studied patients included hypertension, CVD, advanced age, male gender, high SOFA score, and a long time from the occurrence of symptoms until pneumonia. Routine D-dimer, LDH, NLR, CRP, and IL-6 examination may have the potential to identify patients at the highest risk of developing ARF during COVID-19. The mortality rate in the observed cohort of patients was 13.3%, and it was 32% in the group that developed ARF.

ORCID iDs

Paweł Piwowarczyk ⓘ https://orcid.org/0000-0002-8529-484X
Marta Szczukocka ⓘ https://orcid.org/0000-0003-1431-5495
Paweł Kutnik ⓘ https://orcid.org/0000-0002-8434-6812
Michał Borys ⓘ https://orcid.org/0000-0002-6183-811X
Anna Mikłaszewska ⓘ https://orcid.org/0000-0002-8666-2202
Sławomir Kiciak ⓘ https://orcid.org/0000-0002-4031-0076
Mirosław Czuczwar ⓘ https://orcid.org/0000-0002-9025-6717

References

1. Kuiken T, Fouchier RA, Schutten M, et al. Newly discovered coronavirus as the primary cause of severe acute respiratory syndrome. *Lancet*. 2003;362(9380):263–270.
2. Zaki AM, van Boheemen S, Bestebroer TM, Osterhaus AD, Fouchier RA. Isolation of a novel coronavirus from a man with pneumonia in Saudi Arabia [published correction appears in *N Engl J Med*. 2013;369(4):394]. *N Engl J Med*. 2012;367(19):1814–1820.
3. Phelan AL, Katz R, Gostin LO. The novel coronavirus originating in Wuhan, China: Challenges for global health governance. *JAMA*. 2020; 323(8):709–710.
4. COVID-19 Dashboard by the Center for Systems Science and Engineering (CSSE) at Johns Hopkins University (JHU). https://coronavirus.jhu.edu/map.html. Accessed August 28, 2020.
5. Wang D, Hu B, Hu C, et al. Clinical characteristics of 138 hospitalized patients with 2019 novel coronavirus-infected pneumonia in Wuhan, China. *JAMA*. 2020;323(11):1061–1069.
6. Huang C, Wang Y, Li X, et al. Clinical features of patients infected with 2019 novel coronavirus in Wuhan, China [published correction appears in *Lancet*. 2020; 15;395(10223):496]. *Lancet*. 2020;395(10223): 497–506.
7. Richardson S, Hirsch JS, Narasimhan M, et al. Presenting characteristics, comorbidities, and outcomes among 5700 patients hospitalized with COVID-19 in the New York City area. *JAMA*. 2020;323(20): 2052–2059. doi:10.1001/jama.2020.6775
8. Armstrong RA, Kane AD, Cook TM. Outcomes from intensive care in patients with COVID-19: A systematic review and meta-analysis of observational studies. *Anaesthesia*. 2020;75(10):1340–1349. doi:10.1111/anae.15201
9. Cardoso FS, Papoila AL, Machado RS, et al. Age, sex, and comorbidities predict ICU admission or mortality in cases with SARS-CoV2 infection: A population-based cohort study. *Crit Care*. 2020;24:465.
10. Wu Z, McGoogan JM. Characteristics of and important lessons from the coronavirus disease 2019 (COVID-19) outbreak in China: Summary of a report of 72 314 cases from the Chinese Center for Disease Control and Prevention. *JAMA*. 2020;323(13):1239–1242.
11. Rodriguez-Morales AJ, Cardona-Ospina JA, Gutiérrez-Ocampo E, et al; Latin American Network of Coronavirus Disease 2019-COVID-19 Research (LANCOVID-19). Clinical, laboratory and imaging features of COVID-19: A systematic review and meta-analysis. *Travel Med Infect Dis*. 2020;34:101623.
12. Nowak B, Szymański P, Pańkowski I, et al. Clinical characteristics and short-term outcomes of patients with coronavirus disease 2019: A retrospective single-center experience of a designated hospital in Poland. *Pol Arch Intern Med*. 2020;130(5):407–411.
13. Yang J, Zheng Y, Gou X, et al. Prevalence of comorbidities and its effects in patients infected with SARS-CoV-2: A systematic review and meta-analysis. *Int J Infect Dis*. 2020;94:91–95.
14. Fosbøl EL, Butt JH, Østergaard L, et al. Association of angiotensin-converting enzyme inhibitor or angiotensin receptor blocker use with COVID-19 diagnosis and mortality. *JAMA*. 2020;324(2):168–177.
15. Liu Y, Mao B, Liang S, et al. Association between age and clinical characteristics and outcomes of COVID-19. *Eur Respir J*. 2020;55(5):2001112.
16. Yang AP, Liu JP, Tao WQ, Li HM. The diagnostic and predictive role of NLR, d-NLR and PLR in COVID-19 patients. *Int Immunopharmacol*. 2020;84:106504.
17. Henry BM, Aggarwal G, Wong J, et al. Lactate dehydrogenase levels predict coronavirus disease 2019 (COVID-19) severity and mortality: A pooled analysis. *Am J Emerg Med*. 2020;38(9):1722–1726.
18. Li Y, Zhao K, Wei H, et al. Dynamic relationship between D-dimer and COVID-19 severity. *Br J Haematol*. 2020. doi:10.1111/bjh.16811
19. Zhang L, Yan X, Fan Q, et al. D-dimer levels on admission to predict in-hospital mortality in patients with COVID-19. *J Thromb Haemost*. 2020;18(6):1324–1329.
20. Aziz M, Fatima R, Assaly R. Elevated interleukin-6 and severe COVID-19: A meta-analysis. *J Med Virol*. 2020;92(11):2283–2285.
21. Wang L. C-reactive protein levels in the early stage of COVID-19. *Médecine et Maladies Infectieuses*. 2020;50:332–334.
22. Wendel Garcia PD, Fumeaux T, Guerci P, et al; RISC-19-ICU Investigators. Prognostic factors associated with mortality risk and disease progression in 639 critically ill patients with COVID-19 in Europe: Initial report of the international RISC-19-ICU prospective observational cohort. *EClinicalMedicine*. 2020;2020:100449.
23. Weinstock MB, Echenique ANA, Russell JW. Chest X-ray findings in 636 ambulatory patients with COVID-19 presenting to an urgent care center: A normal chest X-ray is no guarantee. *J Urgent Care Med*. 2020;5:13–18
24. Horby P, Lim WS, Emberson JR, et al; RECOVERY Collaborative Group. Dexamethasone in hospitalized patients with COVID-19: Preliminary report. *N Engl J Med*. 2020. doi:10.1056/NEJMoa2021436
25. Beigel JH, Tomashek KM, Dodd LE, et al; ACTT-1 Study Group Members. Remdesivir for the treatment of COVID-19: Preliminary report. *N Engl J Med*. 2020;383(19):1813–1826. doi:10.1056/NEJMoa2007764
26. Intensive Care National Audit & Research Centre (ICNARC). COVID-19 Report. https://www.icnarc.org/Our-Audit/Audits/Cmp/Reports. London, UK: ICNARC; 2020. Accessed June 16, 2020.

MiR-147a mediated by sodium new houttuyfonate could enhance radiosensitivity of non-small cell lung cancer cells via suppressing STAT3

Kejun Dai[A,C,D], Ling Chen[B,C], Jun Liu[C], Yuqiong Ding[C], Cheng Gu[E], Xujing Lu[F]

Radiotherapy Department, Changzhou Tumor Hospital Affiliated to Soochow University, China

A – research concept and design; B – collection and/or assembly of data; C – data analysis and interpretation;
D – writing the article; E – critical revision of the article; F – final approval of the article

Address for correspondence
Xujing Lu
E-mail: fgd42555@126.com

Abstract

Background. Radioresistance is a huge obstacle in radiotherapy of non-small cell lung cancer (NSCLC) and how to raise radiosensitivity is an urgent issue.

Objectives. In this study, we investigated the role and molecular mechanism of sodium new houttuyfonate (SNH) in regulation of radiosensitivity of NSCLC cells.

Material and methods. The Cell Counting Kit-8 (CCK-8) was used to measure cell viabilities of NSCLC cell lines A549 and HCC827 after a treatment with SNH (0 mM, 0.1 mM and 0.3 mM). It examined cytotoxicity induced by X-ray (0 Gy, 1 Gy, 2 Gy, 4 Gy, 6 Gy, and 8 Gy) after SNH (0.3 mM) treatment, while flow cytometry was used for apoptosis detection use. Expression of miR-147a or signal transducer and activator of transcription (STAT3) in selected cell lines was assessed through real-time quantitative polymerase chain reaction (RT-qPCR). The CCK-8 was then applied to measure cytotoxicity in cells with miR-147a upregulation or STAT3 suppression under irradiation apoptosis changes were detected with flow cytometry. Thereafter, binding conditions between miR-147a and STAT3 were checked using luciferase reporter assays. Expressions of STAT3 in A549 transfected by siNC, siSTAT3, and by siSTAT3 and miR-147a mimics were checked using RT-qPCR and the phosphorylation of STAT3 was observed using enzyme-linked immunosorbent assay (ELISA).

Results. The SNH treatment significantly suppressed cell viabilities and increased apoptosis of lung cancer cells. Cytotoxicity and apoptosis in A549 cells were both enhanced after SNH treatment and raised as the dosages of X-ray grew. MiR-147a presented lower expression in lung cancer cells and was upregulated by SNH, which further contributed to higher cell apoptosis after irradiation. STAT3 directly bound miR-147a and was more expressed in NSCLC cells. Inhibited phosphorylation of STAT3 promoted apoptosis in A549 cells after X-ray exposure. Overexpressed miR-147a inactivated STAT3 signaling, adding to cell apoptosis after irradiation.

Conclusions. SNH-induced miR-147a increased radiosensitivity of A549 cells through inactivation of STAT3 pathway.

Key words: STAT3, miR-147a, sodium new houttuyfonate

Objectives

According to data regarding occurrence rate and death rate, lung cancer is the primary cause of cancer-related mortality, and the five-year survival rate is only 13%.[1] In men, lung cancer is the most commonly diagnosed cancer and the main reason of cancer-related death; in women, lung cancer ranks the 4th most commonly diagnosed cancer and the 2nd leading cause of cancer death.[2] Non-small cell lung cancer (NSCLC) is the most frequent type of lung cancer, known to have diverse pathological features. Despite a significant progress in early diagnosis and clinical treatment, NSCLC is often diagnosed at advanced stage and has a poor prognosis. At present, radiotherapy is a key strategy in treating lung cancer for local control and recurrence reduction.[3] Through radiotherapy, survival rate and local cancer control have been improved, but resistance of cancer and radiotoxicity to normal tissues restrict its therapeutic effects.[4] Hence, it is urgently necessary to find new ways to increase sensitivity of cancer cells to radiation. Since antiquity, natural products were regarded as traditional medicines.[5] *Houttuynia cordata* Thunb is a medicinal plant having tumor suppression effect, which can induce apoptosis of colon cancer cells, leukemia and lung cancer, among others.[6–8] Sodium new houttuyfonate (SNH) is a synthetic product of Houttuyninum, an active constituent of *Houttuynia cordata* Thunb, which can inhibit tumor growth. However, whether SNH can regulate radiosensitivity of lung cancer was unknown. Therefore, functions of SNH in regulating sensitivity of radiation in lung cancer were detected to provide a new therapeutic method.

MicroRNAs belong to small noncoding RNAs (21–25 nucleotides) which can accelerate mRNA degradation through binding target mRNA.[9] The first miRNA, LIN-4, was discovered in *Caenorhabditis elegans*,[10] and more than 2500 kinds of mature miRNAs were authenticated.[11] MiRNAs expression changed after ionizing radiation in cells or tissues, suggesting that miRNAs might connect with radiation treatment.[12,13] MiR-147a acted as a tumor suppressor in progression of lung cancer by suppressing its proliferation and metastasis.[14,15] Its upregulation through irradiation resulted in increased cell apoptosis of thymus cells of mice and Chinese hamster lung fibroblasts V79 through binding PDPK1, which also obstructed PI3K/AKT signaling pathway.[16] The PI3K/AKT signaling pathway has been reported to resist radiosensitization,[17] implying that miR-147a might present the ability to promote radiosensitivity. Moreover, SNH was shown to increase RNA expression of miR-147a in lung cancer cells through repressing Linc00668 and to inhibit metastasis of NSCLC cells.[18] Therefore, we have inferred that miR-147a might be a promising facilitator to enhance effects of SNH on promoting radiosensitivity of NSCLC.

Signal transducer and activator of transcription (*STAT3*) has been detected as an oncogene in tumors that could accelerate growth of cancers cells and block apoptosis.[19,20] STAT3 was negatively regulated by miR-125a-5p and upregulation of STAT3 elevated proliferation and invasion of NSCLC cells.[21] Blocking STAT3 can impede progression of lung cancer by enhancing radiosensitivity in A549 cells.[22]

Background

Using ENCORI database (starbase.sysu.edu.cn), assumptive binding sites between miR-147a and STAT3 were shown, indicating that miR-147a might regulate STAT3 in NSCLC cells. The aim of this study was to examine the role of SNH in the radiosensitivity of NSCLC cells and unveil the potential molecular mechanism related to miR-147a and STAT3.

Material and methods

Cell culture

A549, a human NSCLC cancer cell line, is a kind of epithelial cell line established through explant culture of lung cancer from a male. HCC827 is also a human NSCLC cell line and epithelial cell line obtained from lung adenocarcinoma tissue of a female. Human normal lung epithelial cell line BEAS-2B is an epithelial cell line isolated from normal human bronchial epithelium. These 3 cell lines were all purchased from American Type Culture Collection (ATCC; Manassas, USA). A549, HCC827 and BEAS-2B cells were all incubated using RPMI-1640 medium (Gibco, Waltham, USA) replenished with 10% fetal bovine serum (FBS), 100 U/mL of penicillin and 100 µg/mL of streptomycin. Cell incubation was processed in incubator with saturated humidity at 37°C and 5%CO_2. After incubation, A549 cells were treated with SNH (0 mM, 0.1 mM and 0.3 mM) for 24 h and A549 cells were then irradiated with X-ray (0 Gy, 1 Gy, 2 Gy, 4 Gy, 6 Gy, and 8 Gy) for 30 min to prepare them for following experiments.

Transfection

To regulate the expression of miR-147a or STAT3, transfection was performed in A549 cell line. Briefly, A549 cells in log phase were selected for transfection. A549 cells were first incubated in a six-well plate at 37°C. Overexpressed miR-147a (named miR-147a mimics) and small interfering RNA of STAT3 named siSTAT3 were created by GenePharma (Shanghai, China) together with scrambled sequences, NC mimics and siNC. Later, transfection was conducted after cell confluence reached 85%.

The NC mimics, miR-147a mimics, siNC, and siSTAT3 were grouped and transfected into A549 cells using Lipofectamine 3000 Transfection Reagent (Invitrogen, Carlsbad, USA). Transfection efficiency was measured 48 h after transfection with real-time quantitative polymerase chain reaction (RT-qPCR).

RT-qPCR

The RT-qPCR was used to detect RNA expressions in selected cell lines. Strictly following manufacturer's instructions, total RNA was extracted using TRIzol reagent (Invitrogen). Thereafter, High-Capacity cDNA Reverse Transcription Kit with RNase Inhibitor (Applied Biosystems™, Foster City, USA) was performed to produce cDNA through reverse transcription of total RNA. Next, PCR was carried out using iQ™ SYBR® Green (Bio-Rad, Hercules, USA) for amplification. Sequences of primers were listed: miR-147a, forward, 5'- CGCGGTGTGTGGAAATGC-3' and reverse, 5'- AGTGCAGGGTCCGAGGTATT-3'[18]; STAT3, forward, 5'- AACTCTCACGGACGAGGAGCT-3' and reverse, 5'- AGTAGTGAACTGGACGCCGG-3'[23]; GAPDH, forward, 5'- CACCCACTCCTCCACCTTTG-3' and reverse, 5'- CCACCACCCTGTTGCTGTAG-3'[18]; and U6, forward, 5'- AGAGAAGATTAGCATGGCCCCTG-3' and reverse, 5'- ATCCAGTGCAGGGTCCGAGG-3'.[18] The first step was predenaturation at 95°C for 10 min, followed by 35 cycles with denaturation at 95°C for 30 s, annealing at 60°C for 30 s and extension at 72°C for 30 s. Relative expressions of miR-147a and STAT3 were calculated using $2^{-\Delta\Delta Ct}$ methods, with *U6* and *GAPDH* as internal references. Results were collected from 3 independent experiments.

Cell Counting Kit-8

Cell Counting Kit-8 (CCK-8) assay was used to measure cell viability after SNH treatment and irradiation. A549, HCC827 and BEAS-2B cells were seeded into 96-well plate at a density of 1×10^3 cells per well. Detections of A549 cells were grouped into NC mimics, miR-147a mimics, siNC, siSTAT3, and siSTAT3 with miR-147a mimics. For cell proliferation measurement, different concentrations of SNH (0 mM, 0.1 mM and 0.3 mM) were used to treat cells and 10 µL of CCK-8 (Beyotime, Shanghai, China) was mixed with medium at 24 h, 48 h and 72 h. Cells then were kept incubating for another 1 h and optical density (OD) values were checked with Model 680 Microplate Reader (Bio-Rad) at a wavelength of 450 nm. Cell toxicity detection aimed at A549 cells. In toxicity detection, cell survival rate by irradiation was the indicator and the 0 Gy group was the negative control. Comparing to the control group, we could detect changes in cell viability after irradiation. A549 cells were divided into 9 groups: normal group, 0.3 mM SNH group, NC mimics group, miR-147a mimics group, siNC group, siSTAT3 group, siNC+0.3 mM SNH group,

siSTAT3+0.3 mM SNH group, and siSTAT3+miR-147a mimics+0.3 mM SNH group. Then, cells in those groups were irradiated with different doses of X-ray (0 Gy, 1 Gy, 2 Gy, 4 Gy, 6 Gy, and 8 Gy) using Faxitron RX-650 (Faxitron, Tucson, USA) for 72 h. Thereafter, 10 µL CCK-8 was added and cultured for 1 h at 37°C. Model 680 Microplate Reader was used for measuring OD values of cells at 450 nm wavelength. Experiments were repeated 3 times for getting proper results.

Flow cytometry

Apoptosis rate was detected using flow cytometry. A549, HCC827 and BEAS-2B were first treated under different concentrations of SNH (0 mM, 0.1 mM and 0.3 mM). Later, A549 cells treated with 0 mM and 0.3 mM SNH were selected for apoptosis evaluation after exposure to X-ray (0 Gy, 1 Gy, 2 Gy, 4 Gy, 6 Gy, and 8 Gy) irradiation for 30 min. A549 cells transfected with NC mimics, miR-147a mimics, siNC, siSTAT3 without or with 0.3 mM SNH treatment, siNC+0.3 mM SNH, siSTAT3+0.3 mM SNH, and siSTAT+miR-147a mimics+0.3 mM SNH were selected. Then, cells were rinsed and resuspended. Thereafter, Annexin V-FITC Apoptosis Detection Kit (Beyotime) was applied for staining. After cells were dyed with 5 µL (20 mg/mL) Annexin V and 10 µL (50 mg/mL) PI, Attune Flow Cytometer (Invitrogen) was processed for checking apoptosis rate. Experiment was run in triplicate.

Dual luciferase report assay

In order to confirm whether STAT3 and miR-147a have binding site, dual luciferase reporter assay was utilized. Putative binding sites between miR-147a and STAT3 were provided by Starbase (http://starbase.sysu.edu.cn). Then, psiCHECK™-2 vector (Promega, Madison, USA) was used for inserting wild-type and mutant-type of STAT3, called STAT3-wt and STAT3-mut, respectively. Later, NC mimics and miR-147a mimics, together with STAT3-wt and STAT3-mut were co-transfected into A549 cells using Lipofectamine 3000. Cells were gathered 24 h after transfection and luciferase activity was determined using Quantus™ Fluorometer (Promega, Madison, USA).

ELISA

Enzyme-linked immunosorbent assay (ELISA) was used to detect protein expressions of phosphorylated STAT3 and total STAT3. STAT3 (pY705) + total STAT3 ELISA kit (ab126459; Abcam, Cambridge, UK) was chosen for STAT3 phosphorylation detection. After phosphor-Stat3 (Tyr705) was coated on 96-well plate, protein collected from A549 cells were pipetted and then bound to the wells. After the wells were rinsed, Detection Antibody STAT3 (Tyr705)

was used to measure phosphorylated STAT3 while Detection Antibody STAT3 was to analyze total STAT3 protein. Thereafter, horseradish peroxidase (HRP)-conjugated anti-rabbit IgG was added and incubated at 37°C for 1 h, and then wells were washed. TMB One-Step Substrate Reagent was added at 37°C for 30 min. Stop Solution was added (Thermofisher, Waltham, USA) and OD values were checked at 450 nm wavelength using Model 680 Microplate Reader. The experiment was repeated 3 times.

Statistical analysis

Each experiment was run in triplicate and all data was displayed as mean ± standard deviation (SD). GraphPad Prism v. 7 (GraphPad Software, La Jolla, USA) was used to analyze data from experiments. Data comparisons in different groups were measured with Student's t-test (for 2 groups) and one-way analysis of variance (ANOVA; for 3 groups and more). Post hoc analysis was performed adopting Bonferroni's correction. The overall alpha level is 0.05. A value of $p < 0.01$ was considered statistically significant for three-group comparisons, while $p < 0.05$ was considered significant for comparisons between 2 groups.

Results

Sodium new houttuyfonate upregulated radiosensitivity of NSCLC and miR-147a expression through promoting apoptosis

After different concentrations of SNH (0.1 mM and 0.3 mM) were added, cell viability of A549 cell line was significantly decreased compared to the control group, which was not treated with SNH (SNH 0 mM compared to SNH 0.1 mM, $p = 0.006$; SNH 0 mM compared to SNH 0.3 mM, $p = 0.002$; Fig. 1A) and cellular viability was notably increased, with a growth of the SNH concentration (SNH 0.1 mM compared to SNH 0.3 mM, $p = 0.008$; Fig. 1A). On the contrary, increasing concentrations of SNH lead to higher apoptosis rates of A549 cell line (SNH 0 mM compared to SNH 0.1 mM, $p = 0.007$; SNH 0 mM compared to SNH 0.3 mM, $p = 0.001$; SNH 0.1 mM compared to SNH 0.3 mM, $p = 0.009$; Fig. 1B). Later, different doses of X-ray (0 Gy, 1 Gy, 2 Gy, 4 Gy, 6 Gy, and 8 Gy) were used to measure functions of SNH in NSCLC cells, indicating that growing doses of irradiation significantly inhibited viability of A549 cells treated with 0.3 mM
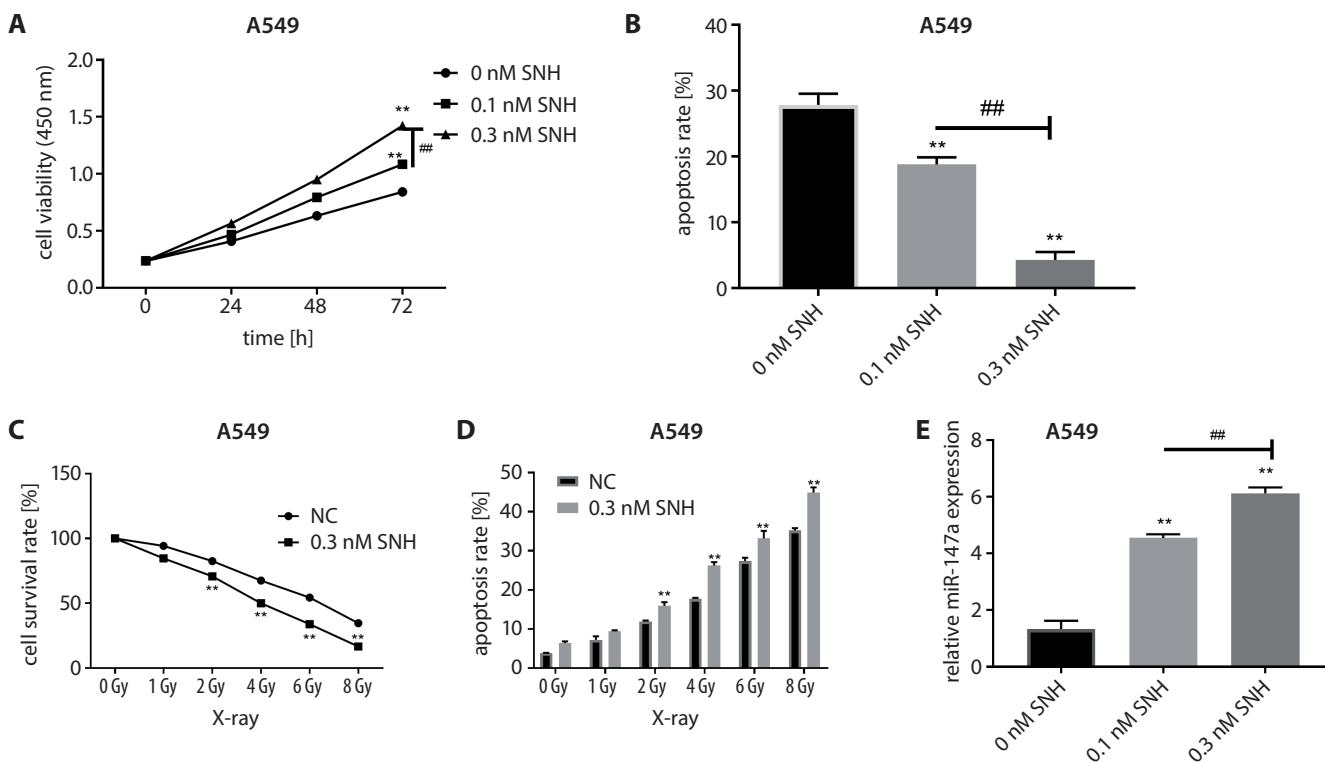
Fig. 1. Sodium new houttuyfonate upregulated radiosensitivity of NSCLC through promoting apoptosis and enhanced miR-147a expression

A. Cell viabilities of A549 cells with different concentrations of SNH (0 mM, 0.1 mM and 0.3 mM) were measured with CCK-8. ** presents the significant difference ($p < 0.01$) from the 0 mM SNH group, while ## signifies notable difference ($p < 0.01$) between 0.1 mM and 0.3 mM SNH treatment groups. B. Apoptosis rate of A549 cells was evaluated through flow cytometry. ** presents the significant difference ($p < 0.01$) from the 0 mM SNH group, while ## signifies notable difference ($p < 0.01$) between 0.1 mM and 0.3 mM SNH treatment groups. C. OD values of normal A549 cells and SNH-treated A549 cells irradiated with X-ray (0 Gy, 1 Gy, 2 Gy, 4 Gy, 6 Gy, and 8 Gy) were detected with CCK-8. ** presents the significant difference ($p < 0.05$) from the 0 mM SNH group. D. Apoptosis rates of A549 cells irradiated with X-ray (0 Gy, 1 Gy, 2 Gy, 4 Gy, 6 Gy, and 8 Gy) were checked using flow cytometry. ** presents the significant difference ($p < 0.05$) from the 0 mM SNH group. E. MiR-147a RNA expressions were measured with RT-qPCR in A549 with SNH treatment (0 mM, 0.1 mM and 0.3 mM). ** presents the significant difference ($p < 0.01$) from the 0 mM SNH group, while ## signifies notable difference ($p < 0.01$) between 0.1 mM and 0.3 mM SNH treatment groups. Each experiment was repeated 3 times.

SNH in comparison with A459 without SNH treatment. The comparisons between the NC and 0.3 mM groups are as follows: for 2 Gy p = 0.032; for 4 Gy p = 0.048; for 6 Gy p = 0.027; for 8 Gy p = 0.012 (Fig. 1C). Moreover, the apoptosis rate of SNH-treated A549 was higher than normal A549 after irradiation. The comparisons between the NC and 0.3 mM groups are as follows: for 2 Gy p = 0.044; for 4 Gy p = 0.038; for 6 Gy p = 0.035; for 8 Gy p = 0.042 (Fig. 1D). Then, miR-147a expression was evaluated after different SNH treatments, revealing that miR-147a expression was significantly raised by SNH treatment in A549 cell line, and as the SNH concentration increased, miR-147a was upregulated more significantly (SNH 0 mM compared to SNH 0.1 mM, p = 0.008 < 0.01; SNH 0 mM compared to SNH 0.3 mM, p = 0.004 < 0.01; SNH 0.1 mM compared to SNH 0.3 mM, p = 0.009 < 0.0; Fig. 1E).

Overexpressed miR-147a promoted apoptosis and enhanced radiosensitivity in NSCLC

According to RT-qPCR results, miR-147a was dramatically decreased in lung cancer cells compared to BEAS-2B cell line (A459 compared to BEAS-2B, p = 0.002; HCC827 compared to BEAS-2B, p = 0.009; Fig. 2A) and A459 cell line had the lowest expression of miR-147a (A459 compared to HCC827, p = 0.006; Fig. 2A). To better understand the role of miR-147a in A549 cells, mimics of miR-147a were transfected into A549 cells, which upregulated expression of miR-147a compared with the control group (p = 0.022; Fig. 2B). Thereafter, A549 cells were exposed to irradiation and then analyzed for cell survival and apoptosis. Results showed that cell survival rates in miR-147a mimics group were remarkably lower than in NC mimics group (for 1 Gy p = 0.023; for 2 Gy p = 0.029; for 4 Gy p = 0.021; for 6 Gy p = 0.017; for 8 Gy p = 0.039; p < 0.05; Fig. 2C) while apoptosis was higher in miR-147a mimics group (for 1 Gy p = 0.042; for 2 Gy p = 0.032; for 4 Gy p = 0.021; for 6 Gy p = 0.015; for 8 Gy p = 0.039; p < 0.05; Fig. 2D).

STAT3 directly targeted miR-147a and negatively regulated radiosensitivity of NSCLC

The RNA expression levels of STAT3 were then detected in A549, HCC827 and BEAS-2B cell lines, indicating that STAT3 was highly expressed in lung cancer cell lines, especially in A549 cell line (A459 compared to BEAS-2B, p = 0.002; HCC827 compared to BEAS-2B, p = 0.007; A459 compared to HCC827, p = 0.009; Fig. 3A). Moreover, according to Starbase, putative binding sites between STAT3 and miR-147a were provided (Fig. 3B) and binding condition between miR-147a and STAT3 was verified using luciferase report assays, showing that the co-transfected cell group of miR-147a mimics and STAT3-wt had the lowest luciferase activity compared to other groups (p = 0.008; Fig. 3C). As STAT3 was high expressed in A549 cell line, suppression of STAT3 resulted in a significantly lower level
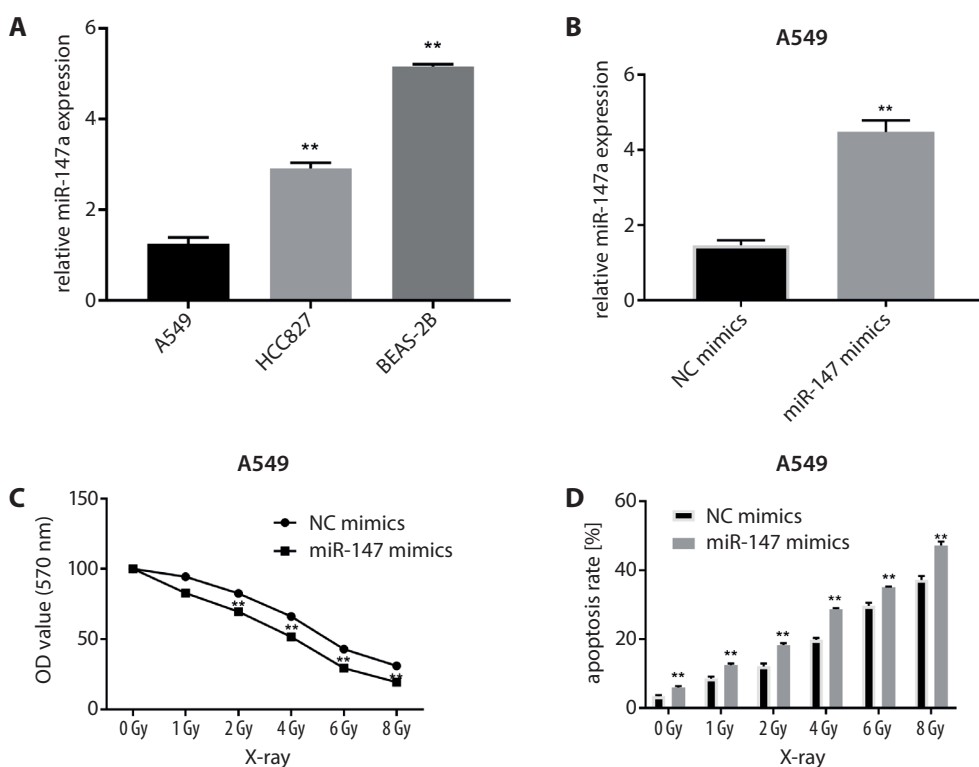
Fig. 2. Overexpressed miR-147a promoted apoptosis and enhanced radiosensitivity in NSCLC

A. RNA expressions of miR-147a were measured in A549, HCC827 and BEAS-2B using RT-qPCR. ** siginifically different (p < 0.01) from the normal cell line BEAS-2B; ## notably distinctive (p < 0.01) between the cancer cell lines.
B. Overexpressed miR-147a expressions were detected in A549 cell lines through RT-qPCR. ** statistically different (p < 0.05) in comparison with the control group and NC mimic group.
C. OD values of X-ray-irradiated (0 Gy, 1 Gy, 2 Gy, 4 Gy, 6 Gy, and 8 Gy) A549 cells with miR-147 overexpression were detected using CCK-8. ** statistically different (p < 0.05) in comparison with the control group and NC mimic group.
D. Apoptosis rates of A549 cells after irradiation (0 Gy, 1 Gy, 2 Gy, 4 Gy, 6 Gy, and 8 Gy) and miR-147a upregulation were checked with flow cytometry. ** statistically different (p < 0.05) in comparison with the control group and NC mimic group. Each experiment was repeated 3 times.
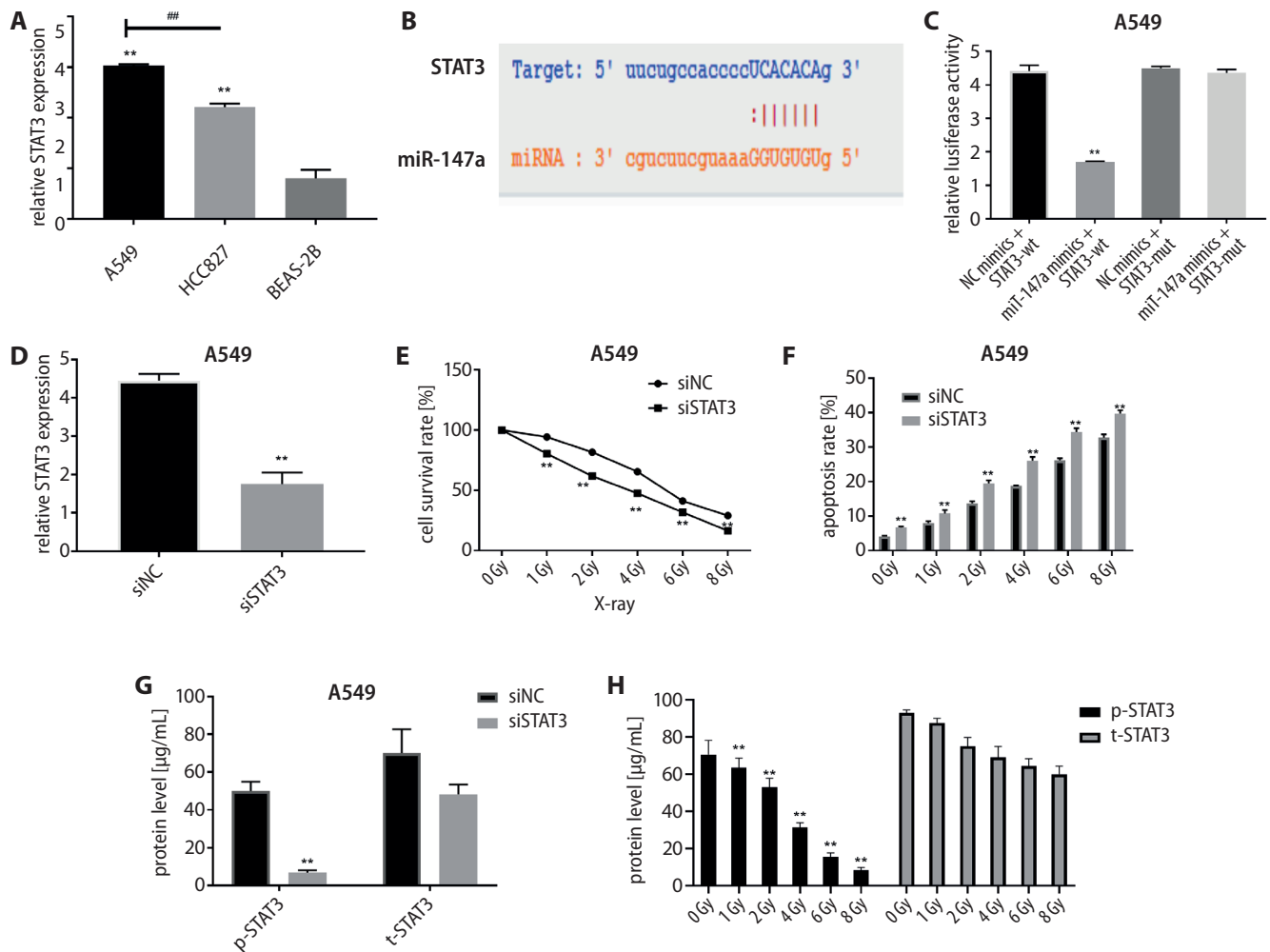
Fig. 3. STAT3 directly targeted miR-147a and negatively regulated radiosensitivity of NSCLC through suppressing apoptosis

A. STAT3 RNA expressions in A549, HCC827 and BEAS-2B cell lines were assessed with RT-qPCR. * siginificantly different (p < 0.01) from the normal cell line BEAS-2B; ## notably distinctive (p < 0.01) between the cancer cell lines. B. Binding sites between STAT3 and miR-147a were provided by StarBase (http://starbase.sysu.edu.cn). C. Binding conditions between miR-147a and STAT3 were validated using luciferase report assay. ** luciferase activity results significantly different (p < 0.01) with other groups. D. Suppressed STAT3 expression in A549 cell line was measured with RT-qPCR. ** statistically different (p < 0.05) in comparison with the control group and siSTAT3 group. E. OD values of A549 cells were examined with CCK-8 after irradiation (0 Gy, 1 Gy, 2 Gy, 4 Gy, 6 Gy, and 8 Gy). ** statistically different (p < 0.05) in comparison with the control group and siSTAT3 group. F. Flow cytometry was performed to check apoptosis rates of A549 cells with irradiation (0 Gy, 1 Gy, 2 Gy, 4 Gy, 6 Gy, and 8 Gy) and transfected using suppressed STAT3. ** statistically different (p < 0.05) in comparison with the control group and siSTAT3 group; G. The phosphorylated STAT3 conditions were examined using ELISA. ** statistically different (p < 0.05) in comparison with the control group and siSTAT3 group; H. After cells were treated with different irradiation (0 Gy, 1 Gy, 2 Gy, 4 Gy, 6 Gy, and 8 Gy), STAT3 phosphorylation was examined with ELISA. ** notably different (p < 0.01) from 0 Gy group. Each experiment was repeated 3 times.

of STAT3 (p = 0.029; Fig. 3D). Later, toxicity was detected under upregulated doses of X-ray, revealing that suppressed STAT3 significantly reduced OD values of A549 compared to control group (for 1 Gy p = 0.023; for 2 Gy p = 0.021; for 4 Gy p = 0.014; for 6 Gy p = 0.009; for 8 Gy p = 0.025; Fig. 3E). Meanwhile, apoptosis was significantly increased after STAT3 suppression (for 1 Gy p = 0.043; for 2 Gy p = 0.031; for 4 Gy p = 0.028; for 6 Gy p = 0.017; for 8 Gy p = 0.036; Fig. 3F). Then, protein concentrations of phosphorylated STAT3 and total STAT3 were detected, indicating that p-STAT3 was significantly decreased after knockdown of STAT3 (p = 0.009; Fig. 3G). Moreover, increasing doses of irradiation also resulted in decreases of p-STAT3 (for 1 Gy p = 0.009; for 2 Gy p = 0.006; for 4 Gy p = 0.004; for 6 Gy p = 0.003; for 8 Gy p = 0.002; Fig. 3H).

MiR-147a enhanced SNH-induced radiosensitivity in NSCLC through suppressing STAT3

As miR-147a and STAT3 were measured individually, correlation between STAT3 and miR-147a was investigated further. After SNH treatment, A549 cells were transfected with siNC, siSTAT3 and siSTAT3 together with miR-147a mimics. The RT-qPCR results revealed that STAT3 expression was notably decreased in siSTAT3 group and overexpression of miR-147a added to the down-regulation of STAT3 at RNA level further (siSTAT3 compared to siNC, p = 0.009; siSTAT3+miR-147a mimics compared to siSTAT3, p = 0.007; Fig. 4A). Then, cell viability of A549 cells treated with SNH was decreased
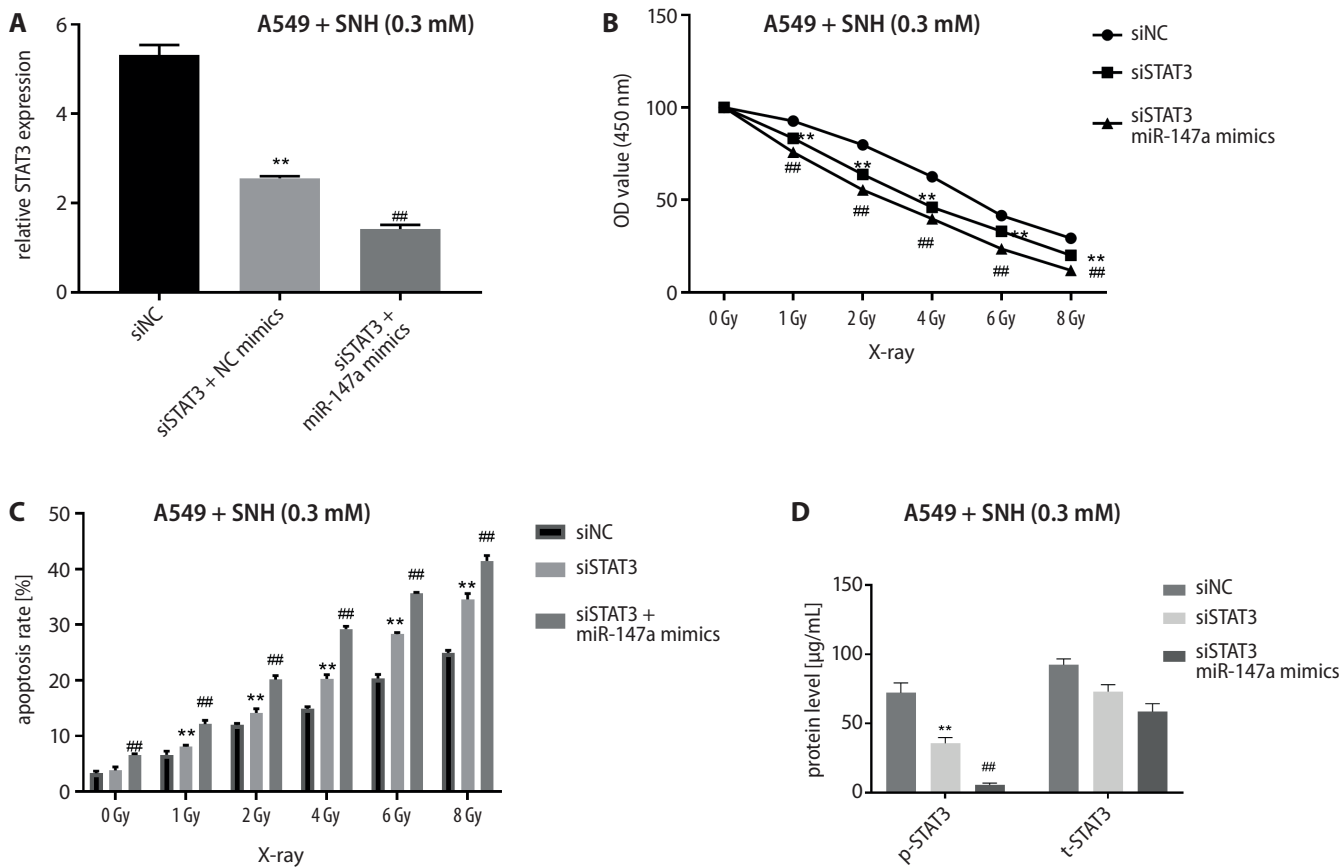
Fig. 4. MiR-147a enhanced SNH induced radiosensitivity in NSCLC through suppressing STAT3

A. RNA expression of STAT3 was examined in control siNC group, siSTAT3 group and the combined group of siSTAT3 and miR-147a mimics. ** significantly different ($p < 0.05$) from the control group; ## significantly different ($p < 0.05$) from the siSTAT3 group. B. OD values of A549 cells transfected with siNC, siSTAT3 and siSTAT3 and miR-147 mimics were evaluated with CCK-8 methods after cells were treated with SNH (0.3 mM). ** significantly different ($p < 0.05$) from the control group; ## significantly different ($p < 0.05$) from the siSTAT3 group. C. Apoptosis rates of cells in the three groups after different doses of irradiation were detected with flow cytometry. ** significantly different from the control group; ## significantly different ($p < 0.05$) from the siSTAT3 group. D. The phosphorylation of STAT3 was examined using ELISA. ** significantly different from the control group; ## significantly different ($p < 0.05$) from the siSTAT3 group. Each experiment was repeated 3 times.

after STAT3 inhibition compared with that in the control si-NC group, and miR-147a upregulation intensified cell survival decrease under irradiation in different doses. For siSTAT3 compared to siNC, the results were as follows: for 1 Gy $p = 0.008$; for 2 Gy $p = 0.006$; for 4 Gy $p = 0.003$; for 6 Gy $p = 0.009$; for 8 Gy $p = 0.003$. For the combined group compared to the siSTAT3 group, the results were as follows: for 1 Gy $p = 0.008$; for 2 Gy $p = 0.005$; for 4 Gy $p = 0.006$; for 6 Gy $p = 0.007$; for 8 Gy $p = 0.006$ (Fig. 4B). Meanwhile, apoptosis rate of cells after SNH treatment was significantly lower after STAT3 downregulation (for 1 Gy $p = 0.007$; for 2 Gy $p = 0.005$; for 4 Gy $p = 0.004$; for 6 Gy $p = 0.007$; for 8 Gy $p = 0.008$). MiR-147a overexpression added to the drop in apoptosis rates in comparison with siSTAT3 group. For the combined group compared to siSTAT3 group, the results were as follows: for 0 Gy $p = 0.005$; for 1 Gy $p = 0.007$; for 2 Gy $p = 0.004$; for 4 Gy $p = 0.008$; for 6 Gy $p = 0.007$; for 8 Gy $p = 0.009$; Fig. 4C). The changes in phosphorylation levels of STAT3 were examined using ELISA assay and results showed that p-STAT3 proteins were inhibited by STAT3 suppression and

further reduced by miR-147a upregulation ($p = 0.007$ for the siSTAT3 group compared to siNC group; $p = 0.005$ for the combined group compared to siSTAT3 group; Fig. 4D).

Discussion

Houttuyninum can suppress tumor growth through downregulating HER2/neu phosphorylation, which indicates that Houttuyninum can provide therapeutic value in tumor treatment.[24] Considering chemical instability of Houttuyninum, SNH was compounded for increasing stability, which inhibited metastasis in not only A549 and NCI-H1299 cell lines but also in lungs of mice.[18] In this study, SNH significantly decreased cell viabilities in cancer cell lines but seldom downregulated the viability of normal BEAS-2B cell line, indicating that SNH could be a useful medicine for blocking cell progression of cancer cells. Moreover, SNH also increased apoptosis of cancer cell lines. Lower cell viability and higher apoptosis of A549 cells resulted from SNH treatment. Based on those results,

SNH was proven to be a useful medicine to suppress cell viability and promote apoptosis of A459 cells. As for miR-147a, it was reported that miR-147a could suppress cell proliferation and promote apoptosis in A549 cell line by negatively regulating pRB and HOXD-AS1.[15] After irradiation, miR-147a was significantly upregulated in irradiation-induced thymus injury,[25] implying that miR-147a is a potential regulator of radiotherapy. We have measured that SNH treatment in A549 cells significantly increased expression of miR-147a, which was remarkably low in cancer cells, especially in A549 cells. Furthermore, overexpression of miR-147a downregulated cell viability but upregulated apoptosis of A549 cells after irradiation. According to these results, SNH was shown to facilitate apoptosis of A549 cells and enhanced radiosensitivity of A549 cells by increasing miR-147a RNA level.

STAT3 was proven as the target gene of miR-147a through luciferase report assay after putative binding sites were provided by Starbase. STAT3 was discovered as a component of activated acute phase response factor complex of interleukin 6 (IL-6) over 20 years ago and its activation was to form dimer by combination of mutual SH2 domain-phosphotyrosine, which was determined as the key activation mechanism of STAT3 transcriptional function stimulation.[26–28] It is constituted by 770 amino acids, containing 6 functional domains.[29] STAT3 was proven to play an important role in occurrences of tumors, and it promoted cisplatin resistance after activation by periostin in NSCLC.[30,31] Activation of STAT3 accelerated proliferation and repressed apoptosis through accumulation of the large granular lymphocyte in leukemia.[32] Suppression of STAT3 significantly declined the viability of MDA-MB-231 breast cancer cells.[33] Moreover, STAT3 inhibited radiosensitivity in VEGFR2 low expressed Calu-1 cell line and in A549 cell line, which contains high level of VEGFR2.[22] STAT3 has 1 phosphorylation site called Tyr705, which has been detected to activate STAT3 in melanoma.[34] Phosphorylated Y705 STAT3 has also been shown to be highly expressed in NSCLC cells and its suppression reduced NSCLC cell growth.[35] Therefore, STAT3 was checked in A549 and HCC827 cell lines and normal BEAS-2B cell line showing that STAT3 was highly expressed in cancer cell lines, especially A549 cell line. Suppressed STAT3 was produced to inhibit RNA level of STAT3 and apoptosis rate of A549 cells was downregulated with irradiation. Results of apoptosis with STAT3 determined that STAT3 could ihibit radiosensitivity in lung cancer through inhibiting apoptosis. As miR-147a and STAT3 were measured, correlation of those 2 genes after SNH treatment in lung cancer cells was detected, indicating that STAT3 RNA expression and phosphorylated STAT3 protein expression were notably suppressed by STAT3 inhibition, and upregulation of miR-147a further inhibited STAT3 and cell viability. Nevertheless, apoptosis rate was upregulated by siSTAT3 and became higher with miR-147a mimics. Based on these detections, *STAT3* was

the direct target gene of miR-147a and played the opposite role that downregulated radiosensitivity of A549 cells and attenuated therapeutic effect of SNH. In previous studies, BIBR1532, a selective telomerase inhibitor, increased radiosensitivity in NSCLC cells and mice models.[36] MiR-30a and miR-30b were overexpressed by low-dose radiation resulting in low cell viability and EMT in NSCLC cells and even in vivo orthotopic xenograft mouse models.[37]

Limitations

The limitation of this study lies in the lack of animal models, which might help to display the role of SNH and mir-147a/STAT3 in vivo.

Conclusions

In our study, we have shown that miR-147a, increased by SNH, could enhance cell radiosensitivity by inactivating the STAT3 signaling pathway in A549 cells. Therefore, it is possible that miR-147a might also have the ability to promote radiosensitivity in animal models and at clinical stage.

ORCID iDs

Kejun Dai   https://orcid.org/0000-0001-5648-927X
Ling Chen   https://orcid.org/0000-0002-5470-3719
Jun Liu   https://orcid.org/0000-0002-4062-0226
Yuqiong Ding   https://orcid.org/0000-0002-8588-484X
Cheng Gu   https://orcid.org/0000-0001-9125-1566
Xujing Lu   https://orcid.org/0000-0002-8118-1899

References

1. Risch A, Plass C. Lung cancer epigenetics and genetics. *Int J Cancer*. 2008;123(1):1–7. doi:10.1002/ijc.23605
2. Jemal A, Bray F, Center MM, Ferlay J, Ward E, Forman D. Global cancer statistics. *CA Cancer J Clin*. 2011;61(2):69–90. doi:10.3322/caac.20107
3. Berman AT, Rengan R. New approaches to radiotherapy as definitive treatment for inoperable lung cancer. *Semin Thorac Cardiovasc Surg*. 2008;20(3):188–197. doi:https://doi.org/10.1053/j.semtcvs.2008.09.003
4. Xue G, Ren Z, Chen Y, et al. A feedback regulation between miR-145 and DNA methyltransferase 3b in prostate cancer cell and their responses to irradiation. *Cancer Lett*. 2015;361(1):121–127. doi:10.1016/j.canlet.2015.02.046
5. Boufridi A, Quinn RJ. Harnessing the properties of natural products. *Annu Rev Pharmacol Toxicol*. 2018;58:451–470. doi:10.1146/annurev-pharmtox-010716-105029
6. Tang YJ, Yang JS, Lin CF, et al. *Houttuynia cordata* Thunb extract induces apoptosis through mitochondrial-dependent pathway in HT-29 human colon adenocarcinoma cells. *Oncol Rep*. 2009;22(5):1051–1056. https://doi.org/10.3892/or_00000535
7. Banjerdpongchai R, Kongtawelert P. Ethanolic extract of fermented Thunb induces human leukemic HL-60 and Molt-4 cell apoptosis via oxidative stress and a mitochondrial pathway. *Asian Pac J Cancer Prev*. 2011;12(11):2871–2874.
8. Chen YF, Yang JS, Chang WS, Tsai SC, Peng SF, Zhou YR. *Houttuynia cordata* Thunb extract modulates G0/G1 arrest and Fas/CD95-mediated death receptor apoptotic cell death in human lung cancer A549 cells. *J Biomed Sci*. 2013;20:18. doi:10.1186/1423-0127-20-18
9. Wu KL, Tsai YM, Lien CT, Kuo PL, Hung AJ. The roles of microRNA in lung cancer. *Int J Mol Sci*. 2019;20(7):1611. doi:10.3390/ijms20071611

10. Lee RC, Feinbaum RL, Ambros V. The *C. elegans* heterochronic gene lin-4 encodes small RNAs with antisense complementarity to lin-14. *Cell*. 1993;75(5):843–854. doi:10.1016/0092-8674(93)90529-y

11. Hashemi ZS, Khalili S, Forouzandeh Moghadam M, Sadroddiny E. Lung cancer and miRNAs: A possible remedy for anti-metastatic, therapeutic and diagnostic applications. *Expert Rev Respir Med*. 2017;11(2):147–157. doi:10.1080/17476348.2017.1279403

12. Shi Y, Zhang X, Tang X, Wang P, Wang H, Wang Y. MiR-21 is continually elevated long-term in the brain after exposure to ionizing radiation. *Radiat Res*. 2012;177(1):124–128. doi:10.1667/rr2764.1

13. Girardi C, De Pittà C, Casara S, et al. Analysis of miRNA and mRNA expression profiles highlights alterations in ionizing radiation response of human lymphocytes under modeled microgravity. *PLoS One*. 2012;7(2):e31293. doi:10.1371/journal.pone.0031293

14. Lu Y, Luan XR. miR-147a suppresses the metastasis of non-small-cell lung cancer by targeting CCL5. *J Int Med Res*. 2019;48(4):300060519883098. doi:10.1177/0300060519883098

15. Wang Q, Jiang S, Song A, et al. HOXD-AS1 functions as an oncogenic ceRNA to promote NSCLC cell progression by sequestering miR-147a. *Onco Targets Ther*. 2017;10:4753–4763. doi:10.2147/OTT.S143787

16. Wang LJ, Li NN, Xu SJ, et al. A new and important relationship between miRNA-147a and PDPK1 in radiotherapy. *J Cell Biochem*. 2018;119(4):3519–3527. doi:10.1002/jcb.2652

17. Liao J, Jin H, Li S, et al. Apatinib potentiates irradiation effect via suppressing PI3K/AKT signaling pathway in hepatocellular carcinoma. *J Exp Clin Cancer Res*. 2019;38(1):454. doi:10.1186/s13046-019-1419-1

18. Jiang R, Hu C, Li Q, et al. Sodium new houttuyfonate suppresses metastasis in NSCLC cells through the Linc00668/miR-147a/slug axis. *J Exp Clin Cancer Res*. 2019;38(1):155. doi:10.1186/s13046-019-1152-9

19. Lu S, Gao Y, Huang X, Wang X. GYY4137, a hydrogen sulfide (H_2S) donor, shows potent anti-hepatocellular carcinoma activity through blocking the STAT3 pathway. *Int J Oncol*. 2014;44(4):1259–1267. doi:10.3892/ijo.2014.2305

20. Islam M, Sharma S, Teknos TN. RhoC regulates cancer stem cells in head and neck squamous cell carcinoma by overexpressing IL-6 and phosphorylation of STAT3. *PLoS One*. 2014;9(2):e88527. doi:10.1371/journal.pone.0088527

21. Zhong L, Sun S, Shi J, Cao F, Han X, Chen Z. MicroRNA-125a-5p plays a role as a tumor suppressor in lung carcinoma cells by directly targeting STAT3. *Tumour Biol*. 2017;39(6):1010428317697579. doi:10.1177/1010428317697579

22. Hu C, Zhuang W, Qiao Y, et al. Effects of combined inhibition of STAT3 and VEGFR2 pathways on the radiosensitivity of non-small-cell lung cancer cells. *Onco Targets Ther*. 2019;12:933–944. doi:10.2147/OTT.S186559

23. Sun X, Wang J, Huang M, et al. STAT3 promotes tumour progression in glioma by inducing FOXP1 transcription. *J Cell Mol Med*. 2018;22(11):5629–5638. doi:10.1111/jcmm.1383

24. Zhou NN, Tang J, Chen WD, et al. Houttuyninum, an active constituent of Chinese herbal medicine, inhibits phosphorylation of HER2/neu receptor tyrosine kinase and the tumor growth of HER2/neu-overexpressing cancer cells. *Life Sci*. 2012;90(19–20):770–775. doi:10.1016/j.lfs.2012.03.035

25. Chen C, Lu J, Hao L, Zheng Z, Zhang N, Wang Z. Discovery and characterization of miRNAs in mouse thymus responses to ionizing radiation by deep sequencing. *Int J Radiat Biol*. 2016;92(10):548–557. doi:10.1080/09553002.2016.1207821

26. Lütticken C, Wegenka UM, Yuan J, et al. Association of transcription factor APRF and protein kinase Jak1 with the interleukin-6 signal transducer gp130. *Science*. 1994;263(5143):89–92. doi:10.1126/science.8272872

27. Zhong Z, Wen Z, Darnell JE Jr. Stat3: A STAT family member activated by tyrosine phosphorylation in response to epidermal growth factor and interleukin-6. *Science*. 1994;264(5155):95–98. doi:10.1126/science.8140422

28. Hillmer EJ, Zhang H, Li HS, Watowich SS. STAT3 signaling in immunity. *Cytokine Growth Factor Rev*. 2016;31:1–15. doi:10.1016/j.cytogfr.2016.05.001

29. Becker S, Groner B, Müller CW. Three-dimensional structure of the Stat3beta homodimer bound to DNA. *Nature*. 1998;394(6689):145–151. doi:10.1038/28101

30. Hu W, Jin P, Liu W. Periostin contributes to cisplatin resistance in human non-small cell lung cancer A549 cells via activation of Stat3 and Akt and upregulation of survivin. *Cell Physiol Biochem*. 2016;38(3):1199–1208. doi:10.1159/000443068

31. Yu H, Lee H, Herrmann A, Buettner R, Jove R. Revisiting STAT3 signaling in cancer: New and unexpected biological functions. *Nat Rev Cancer*. 2014;14(11):736–746. doi:10.1038/nrc3818

32. Epling-Burnette PK, Liu JH, Catlett-Falcone R, et al. Inhibition of STAT3 signaling leads to apoptosis of leukemic large granular lymphocytes and decreased Mcl-1 expression. *J Clin Invest*. 2001;107(3):351–362. doi:10.1172/JCI9940

33. Kim KW, Mutter RW, Cao C, et al. Inhibition of signal transducer and activator of transcription 3 activity results in down-regulation of survivin following irradiation. *Mol Cancer Ther*. 2006;5(11):2659–2665. doi:10.1158/1535-7163.MCT-06-0261

34. Sakaguchi M, Oka M, Iwasaki T, Fukami Y, Nishigori C. Role and regulation of STAT3 phosphorylation at Ser727 in melanocytes and melanoma cells. *J Invest Dermatol*. 2012;132(7):1877–1885. doi:10.1038/jid.2012.45

35. Lewis KM, Bharadwaj U, Eckols TK, et al. Small-molecule targeting of signal transducer and activator of transcription (STAT) 3 to treat non-small cell lung cancer. *Lung Cancer*. 2015;90(2):182–190. doi:10.1016/j.lungcan.2015.09.014

36. Ding X, Cheng J, Pang Q, et al. BIBR1532, a selective telomerase inhibitor, enhances radiosensitivity of non-small cell lung cancer through increasing telomere dysfunction and ATM/CHK1 inhibition. *Int J Radiat Oncol Biol Phys*. 2019;105(4):861–874. doi:10.1016/j.ijrobp.2019.08.009

37. Park G, Son B, Kang J, et al. DR-induced miR-30a and miR-30b target the PAI-1 pathway to control adverse effects of NSCLC radiotherapy. *Mol Ther*. 2019;27(2):342–354. doi:10.1016/j.ymthe.2018.10.015

Clinical significance of evaluation of collateral circulation in short-term prognosis of wake-up stroke patients

Haijing Sui[1,A,B,F], Chenggong Yan[2,B,C,F], Juan Yang[3,B,C,F], Xiaohui Zhao[3,A,D–F]

[1] Department of Radiology, Pudong New Area People's Hospital, Shanghai, China
[2] Department of Radiology, Shanghai Pudong New Area Hospital of Traditional Chinese Medicine, China
[3] Department of Neurology, Pudong New Area People's Hospital, Shanghai, China

A – research concept and design; B – collection and/or assembly of data; C – data analysis and interpretation;
D – writing the article; E – critical revision of the article; F – final approval of the article

Address for correspondence
Xiaohui Zhao
E-mail: zxh191029@sina.com

Abstract

Background. In recent years, the clinical significance of collateral circulation in vascular embolism has been gradually found.

Objectives. To investigate the relationship between collateral circulation and short-term prognosis of wake-up stroke patients.

Material and methods. The present observational study enrolled 269 cases of wake-up ischemic stroke patients. All patients presented with mismatched low perfusion volume/main infraction volume and received thrombolytic therapy after admission. The hemorrhagic transformation rate was recorded. The American Society of Interventional and Therapeutic Neuroradiology/Society of Interventional Radiology (ASITN/SIR) grading was used for evaluation of collateral circulation. The stroke condition was determined using the National Institutes of Health Stroke Scale (NIHSS). The Barthel Index (BI) score was used for measurement of quality of life. The Modified Rankin Scale (mRS) was used for measurement of prognosis.

Results. The hypertension, diabetes and current smoker rates were significantly higher. The baseline NHISS scores and NIHSS scores after 24 h were remarkably lower. The NIHSS scores were markedly lower in ASITN/SIR grade 2–3 patients compared with ASITN/SIR grade 0–1 patients at 1 week, 2 weeks, 4 weeks, and 3 months after treatment. Patients with ASITN/SIR grade 2–3 had lower mRS score and higher BI scores. The ASITN/SIR grade was an independent risk factor for bad prognosis of wake-up ischemic stroke patients in 3 months.

Conclusions. Collateral circulation condition may be associated with short-term prognosis of wake-up stroke patients. Patients with worse collateral circulation may present higher risk for bad short-term prognosis.

Key words: outcomes, coronary collateral circulation, NHISS, wake-up stroke

Background

Despite the development of treatment methods and molecular mechanisms, the incidence of stroke is still high, with almost 7 million of ischemic stroke patients and 3 million of hemorrhagic stroke patients worldwide in 2013 among 20–64 years-old adults.[1–3] It is also reported that about 1.5~2.0 million of new stroke cases are diagnosed every year in China.[4,5] Among the stroke patients, about 20–25% ischemic stroke patients are healthy before sleep and wake up with neurological deficits.[6–8] Since the accurate time of stroke onset is difficult to determine for wake-up stroke patients, the application of thrombolysis treatment for these patients is still controversial.[9,10]

In recent years, the clinical significance of collateral circulation in vascular embolism has been gradually noticed.[11] It is thought that collateral circulation is associated with intravenous thrombolysis,[12] coronary chronic total occlusion[13] and also ischemic stroke.[14] However, up to now, few studies focused on role of collateral circulation in wake-up stroke.

Objectives

In the present study, we demonstrated for the first time that collateral circulation was associated with short-term prognosis of wake-up stroke patients. The worse collateral circulation predicted higher risk for bad short-term prognosis. This research might provide more clinical evidence for collateral circulation in wake-up stroke patients.

Material and methods

Subjects

The present observational study enrolled 269 cases of wake-up ischemic stroke patients who reported to our hospital from January 2017 to June 2019. All patients were healthy before sleep and were found to show typical stroke symptoms after waking up, including a side face, arm or leg numbness or sudden onset of deviation, hemiplegia, confusion, difficulty in speaking or understanding, difficulty in single or binocular vision, difficulty in walking, dizziness, and loss of balance or coordination. The diagnosis of ischemic stroke was confirmed with computed tomography (CT) or magnetic resonance imaging (MRI) methods according to the guidelines of Chinese Medical Association.[15] All patients were consecutively enrolled. The following patients were excluded: patients with hemorrhagic stroke, patients who received anticoagulation therapy within 1 month before the study, patients who received intracranial or spinal surgeries within 3 months before the study, patients who had stroke or brain trauma within 3 months before the study, and patients with severe dysfunction of liver,

kidney or heart. Written informed consent was obtained from all study participants. The present study was approved by the Ethic Committee of Shanghai Pudong New Area Hospital of Traditional Chinese Medicine, China.

Thrombolytic therapy

All patients included in this research received thrombolytic therapy after admission. The computed tomography perfusion (CTP) was conducted using a Dual Source Imaging System (Siemens, Munich, Germany). The multimode MRI was performed using a General Electric Corporation 3.0T Magnetic Resonance Instrument (Signa Excite HD; General Electric Medical Systems, Chicago, USA). The image reconstruction was then conducted using MIStar® software (Apollo Medical Imaging Technology Ltd., Melbourne, Australia). The peak time picture of cerebral blood flow (T_{max}) was obtained and the area with $T_{max} > 6$ s was defined as low perfusion volume.[16] The diffusion-weighted imaging (DWI) high-signal volume or a volume of lesion side which reduced more than 30% of the normal side on the cerebral blood flow (CBF) picture was regarded as the main infraction volume. The thrombolytic therapy was only conducted for patients with low perfusion volume/main infraction volume ≥120% and ≥10 mL.[17–19]

The thrombolytic therapy was conducted using the recombinant tissue plasminogen activator (rt-PA) with a dose of 0.9 mg/kg. The first 10% of the drug was intravenously injected at once, and the rest of the dose was injected using a venous micropump within 60 min. The hemorrhagic transformation was evaluated using CT or MRI after 24 h of treatment.

Evaluation of collateral circulation

For evaluation of collateral circulation, the American Society of Interventional and Therapeutic Neuroradiology/ Society of Interventional Radiology (ASITN/SIR) grading was used after digital subtraction angiography (DSA).[20] The ASITN/SIR grade 0–1 was defined as bad collateral circulation compensatory, ASITN/SIR grade 2 was defined as moderate compensatory and ASITN/SIR grade 3–4 was considered as good compensatory.

The study population was then divided into 2 groups: ASITN/SIR grade 0–1 patients and ASITN/SIR grade 2–3 patients.

Data measurement

Demographic data such as age and gender, and clinical information including complications and medication condition were also recorded. The stroke condition was determined using the National Institutes of Health Stroke Scale (NIHSS). The Barthel Index (BI) score was used for measurement of quality of life after 3 months of treatment. The Modified Rankin Scale (mRS) was used for

measurement of prognosis after 3 months of treatment. The mRS score ≤2 was defined as good prognosis while mRS score >2 was a bad prognosis. The NIHSS scores were measured before treatment, 24 h after treatment, and 1 week, 2 weeks, 4 weeks and 3 months after treatment. The follow-up lasted for 3 months.

Statistical analysis

Continuous data was expressed using mean ± standard deviation (SD). The χ^2 test was used to compare the counting materials and rates. Comparison between the 2 groups was performed using the Student t-test. The Kaplan–Meier (K–M) curve was used to determine the relationship between NHISS scores and three-month mortality. Logical regression was used to analyze risk factors for three-month prognosis using a binary logistic regression model with step-back method. A value of $p < 0.05$ was considered statistically significant. All calculations were made using SPSS v. 22.0 (IBM Corp., Armonk, USA).

Results

Basic characteristics for all patients

The basic characteristics of all patients were shown in Table 1. Among the 269 patients, 142 cases had the ASITN/SIR grade 0–1 and 127 cases had the ASITN/SIR grade 2–3. The hypertension, diabetes and current smoker rates were found significantly higher in ASITN/SIR grade 0–1 patients ($p < 0.05$). Besides, the baseline NHISS scores were remarkably lower in ASITN/SIR grade 2–3 patients

($p < 0.05$). Moreover, NIHSS scores after 24 h were also lower in ASITN/SIR grade 2–3 patients ($p < 0.05$). No significant differences were found in other indices.

Dynamic changes of NIHSS scores and its relationship with ASITN/SIR grading

To further investigate the relationship between ASITN/SIR grading and clinical outcomes of wake-up stroke, NIHSS scores were evaluated before treatment, 24 h after treatment, and 1 week, 2 weeks, 4 weeks and 3 months after treatment. As shown in Fig. 1, at all timepoints, the NIHSS scores were remarkably lower in ASITN/SIR grade 2–3 patients compared with ASITN/SIR grade 0–1 patients ($p < 0.05$), indicating that the ASITN/SIR grade at admission might be associated with the treatment outcomes.
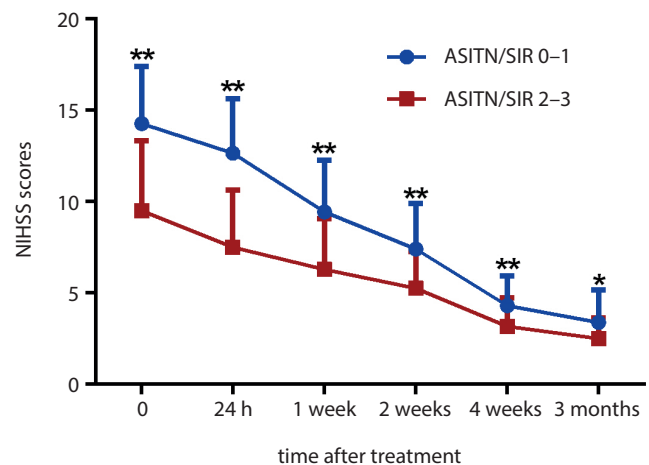
Fig. 1. Dynamic changes of NIHSS and their relationship with ASITN/SIR grading

Table 1. Basic characteristics for all patients

Variables	All patients (n = 269)	ASITN/SIR 0–1 (n = 142)	ASITN/SIR 2–3 (n = 127)	p-value*
Age [years]	56.64 ±10.09	56.44 ±10.07	56.85 ±10.15	0.742
Gender (male:female)	153 (56.9): 116 (43.1)	78 (54.9): 64 (45.1)	75 (59.1): 52 (40.9)	0.668
Complications, n (%)				
Hypertension	126 (46.8)	78 (54.9)	48 (37.8)	0.023
Diabetes	74 (27.5)	49 (34.5)	25 (19.7)	0.026
Current smoker	139 (51.7)	85 (59.9)	54 (42.5)	0.016
Atrial fibrillation	21 (7.8)	11 (7.7)	10 (7.9)	0.602
Stroke family history	54 (20.1)	29 (20.4)	25 (19.7)	0.570

TOAST type, n (%)
  cardiogenic embolism
  large-artery atherosclerosis
  small-artery occlusion
  others
	81 (30.1)
	76 (28.3)
	79 (29.4)
	33 (12.3)
		45 (31.7)
		37 (26.1)
		33 (23.2)
		20 (14.1)
			36 (28.3)
			39 (30.7)
			36 (28.3)
			13 (10.2)
				0.644

Baseline NIHSS	12.02 ±4.20	14.28 ±3.12	9.50 ±3.82	<0.001
NIHSS after 24 h	10.22 ±4.00	12.66 ±2.98	7.50 ±3.15	<0.001
Hemorrhagic transformation, n (%)	71 (26.4)	39 (27.5)	32 (25.2)	0.749

* ASITN/SIR 0–1 compared with ASITN/SIR 2–3. The χ^2 test was used to compare the counting materials and rates. Comparison between the 2 groups was performed using the Student's t-test. ASITN/SIR – the American Society of Interventional and Therapeutic Neuroradiology/Society of Interventional Radiology; NIHSS – the National Institutes of Health Stroke Scale; N/A – not applicable.

186

H. Sui et al. Collateral circulation in wake-up stroke

Prediction value of ASITN/SIR grading for three-month prognosis of wake-up ischemic stroke patients

Finally, we analyzed the relationship between ASITN/SIR grading and three-month prognosis of wake-up ischemic stroke patients. Both mRS and BI scores were measured 3 months after treatment. Results showed that patients with ASITN/SIR grade 2–3 had lower mRS score and higher BI scores than patients with ASITN/SIR grade 0–1 (Table 2). However, the three-month mortality rate did not show significant difference. Then, we defined mRS score >2 as bad prognosis and analyzed risk factors for three-month prognosis. Results showed that the ASITN/SIR grade was the independent risk factor for bad prognosis of wake-up ischemic stroke patients in 3 months (Table 3). The K–M curve showed patients with ASITN/SIR grade 2–3 might have longer survival in 3 months; however, the difference was not statistically significant (Fig. 2, p = 0.116).

Fig. 2. Kaplan–Meier curve for three-month mortality

Discussion

Despite numerous studies on ischemic stroke, the wake-up stroke is still a clinical problem, especially due to the difficulty to determine the accurate time of onset. In recent years, the importance of collateral circulation has been noticed in embolism diseases. In a clinical trial, it was found that the coronary collateral circulation could be increased by intensive exercise for coronary artery disease patients.[21] In patients with celiac artery compression syndrome, the authors also found that different types of collateral circulation were also observed in patients with celiac artery compression syndrome.[22] However, up to now, no research reported the relationship between collateral circulation and wake-up stroke. In the present research, we demonstrated that collateral circulation condition was associated with short-term clinical outcomes of wake-up stroke patients after thrombolytic therapy. Better collateral circulation condition predicted better clinical outcomes, and collateral circulation was also an independent risk factor for bad short-term prognosis of wake-up stroke patients.

The treatment of wake-up stroke is still a clinical challenge and the application of thrombolytic therapy shows different outcomes in different studies. Kurz et al. considered that stroke onset occurred close to wake-up and not during earlier sleep phases in the wake-up stroke patients, and thus the proper use of MRI could select patients who would benefit from thrombolysis.[23] Another clinical research also demonstrated that the wake-up stroke and normal stroke within therapeutic window had similar clinical severity, imaging characteristics and clinical outcome.[24] Odland et al. also stated that current diffusion-weighted imaging-fluid-attenuated inversion recovery (DWI-FLAIR) mismatch concept might exclude lager amount of wake-up stroke patients who might benefit from thrombolysis.[25] In our research, we also used thrombolytic therapy only in patients with mismatched low perfusion volume and main infraction volume. Results showed the application of thrombolytic therapy could achieve good clinical outcomes. Meanwhile, the treatment outcomes were associated with collateral circulation.

Table 2. The mRS and BI scores after 3 months of treatment

Variables	ASITN/SIR 0–1 (n = 142)	ASITN/SIR 2–3 (n = 127)	p-value*
mRS	2.19 ±1.41	1.49 ±1.14	<0.001
BI	71.81 ±7.61	79.41 ±8.67	<0.001
Mortality, n (%)	15 (10.6)	7 (5.5)	0.216

mRS – Modified Rankin Scale; BI – Barthel Index; ASITN/SIR – the American Society of Interventional and Therapeutic Neuroradiology/Society of Interventional Radiology.

Table 3. Relationship between ASITN/SIR grade and mRS score >2 as bad prognosis

Variable	Wald	OR	95% CI	p-value
ASITN/SIR grade 0–1	15.750	0.313	0.731 (0.627~0.853)	<0.001

OR – odds ratio; 95% CI – 95% confidence interval; ASITN/SIR – the American Society of Interventional and Therapeutic Neuroradiology/Society of Interventional Radiology; mRS – Modified Rankin Scale.

Studies on collateral circulation in stroke have also been reported. It was considered that the premature rarefaction of the collateral circulation might be associated with ischemic tissue injury, and cardiovascular risk factors might enhance the risk.[26] In a review, Iwasawa et al. demonstrated the development of collateral circulation in ischemic stroke and pointed that good collateral circulation was associated with better neurological outcomes and smaller infarct volume in stroke patients.[27] Seyman et al. demonstrated in a clinical research that collateral circulation determined cortical infarct volume in anterior circulation ischemic stroke.[28] A meta-analysis also showed that good collateral circulation predicted favorable outcomes in intravenous thrombolysis in stroke patients.[12] In this study, we demonstrated for the first time that better collateral circulation condition was associated with better clinical outcomes of wake-up stroke patients.

Limitations

The present study has also some limitations. Firstly, the study only included a small sample size. Secondly, we mainly showed the relationship between ASITN/SIR grading, NIHSS score and prognosis. The relationship between ASITN/SIR grading and other laboratory indices requires further studies to confirm.

Conclusions

We conducted a prospective observational study and found that collateral circulation condition was associated with short-term prognosis of wake-up stroke patients. Patients with worse collateral circulation might present a higher risk for bad short-term prognosis. This study might give more clinical evidence for the use of collateral circulation measurement in prediction of prognosis of stroke patients.

ORCID iDs

Haijing Sui https://orcid.org/0000-0002-5594-2201
Chenggong Yan https://orcid.org/0000-0002-1792-7625
Juan Yang https://orcid.org/0000-0002-6269-8534
Xiaohui Zhao https://orcid.org/0000-0001-5378-0934

References

1. Wen LT, Abdin E, Vaingankar JA, et al. Prevalence of stroke, risk factors, disability and care needs in older adults in Singapore: Results from the WiSE study. *BMJ Open*. 2018;8(3):e020285. doi:10.1136/bmjopen-2017-020285
2. Rofes L, Muriana D, Palomeras E, et al. Prevalence, risk factors and complications of oropharyngeal dysphagia in stroke patients: A cohort study. *Neurogastroenterol Motil*. 2018;30(8):e13338. doi:10.1111/nmo.13338
3. Krishnamurthi RV, Moran AE, Feigin VL, et al. Stroke prevalence, mortality and disability-adjusted life years in adults aged 20–64 years in 1990–2013: Data from the global burden of disease 2013 study. *Neuroepidemiology*. 2015;45(3):190–202. doi:10.1159/000441098
4. Wang W, Jiang B, Sun H, et al. Prevalence, incidence and mortality of stroke in China: Results from a nationwide population-based survey of 480,687 adults. *Circulation*. 2017;135(8):759. doi:10.1161/CIRCULATIONAHA.116.025250
5. Gelin X, Minmin M, Xinfeng L, Hankey GJ. Is there a stroke belt in China and why? *Stroke*. 2013;44(7):1775–1783. doi:10.1161/STROKEAHA.113.001238
6. Thomalla G, Gerloff G. Treatment concepts for wake-up stroke and stroke with unknown time of symptom onset. *Stroke*. 2015;46(9):2707–2713. doi:10.1161/STROKEAHA.115.009701
7. Silva GS, Lima FO, Camargo ECS, et al. Wake-up stroke: Clinical and neuroimaging characteristics. *Cerebrovasc Dis*. 2010;29(4):336–342. doi:10.1159/000278929
8. Peter-Derex L, Derex L. Wake-up stroke: From pathophysiology to management. *Sleep Med Rev*. 2019;48:101212. doi:10.1016/j.smrv.2019.101212
9. Dankbaar JW, Bienfait HP, Van Den Berg C, et al. Wake-up stroke versus stroke with known onset time: Clinical and multimodality CT imaging characteristics. *Cerebrovasc Dis*. 2018;45(5–6):236–244. doi:10.1159/000489566
10. Bücke P, Pérez MA, Hellstern V, AlMatter M, Bäzner H, Henkes H. Endovascular thrombectomy in wake-up stroke and stroke with unknown symptom onset. *Am J Neuroradiol*. 2018;39(3):494–499. doi:10.3174/ajnr.A5540
11. Moutinho M, Silvestre L, Silva E, Pedro LM. Coarctation of the aorta and the nature of collateral circulation. *J Vasc Surg Cases Innov Tech*. 2018;4(4):339–340. doi:10.1016/j.jvscit.2018.08.006
12. Leng X, Lan L, Liu L, Leung TW, Wong KS. Good collateral circulation predicts favorable outcomes in intravenous thrombolysis: A systematic review and meta-analysis. *Eur J Neurol*. 2016;23(12):1738–1749. doi:10.1111/ene.13111
13. Ying S, Feng HD, Yang D, et al. Reduced coronary collateralization in type 2 diabetic patients with chronic total occlusion. *Cardiovasc Diabetol*. 2018;17(1):26. doi:10.1186/s12933-018-0671-6
14. Iwasawa E, Ichijo M, Ishibashi S, Yokota T. Acute development of collateral circulation and therapeutic prospects in ischemic stroke. *Neural Regen Res*. 2016;11(3):368–371. doi:10.4103/1673-5374.179033
15. W. L. The fourth cerebrovascular diseases academic meeting of the Chinese Medical Association: Diagnostic points of various cerebrovascular diseases. *Chinese J Neurol*. 1996;29:379–380.
16. Lou M, Chen Z, Wan J, et al. Susceptibility-diffusion mismatch predicts thrombolytic outcomes: A retrospective cohort study. *AJNR*. 2015;35(11):2061–2067. doi:10.3174/ajnr.A4017
17. Yue-Han L, Min L, Ren-Yang Z, Yu-Qing Y, Zhi-Cai Z, Mei-Ping D. Multimode MRI-based intravenous thrombolysis with recombinant tissue plasminogen activator (rtPA) reduces hemorrhagic transformation in ischemic stroke patients [in Chinese]. *Zhejiang Da Xue Xue Bao Yi Xue Ban*. 2012;41(6):665–671.
18. Shih LC, Saver JL, Alger JR, et al. Perfusion-weighted magnetic resonance imaging thresholds identifying core, irreversibly infarcted tissue. *Stroke*. 2003;34(6):1425–1430. doi:10.1161/01.STR.0000072998.70087.E9
19. Carrera E, Simon Jones P, Iglesias S, et al. The vascular mean transit time: A surrogate for the penumbra flow threshold? *J Cereb Blood Flow Metab*. 2011;31(4):1027–1035. doi:10.1038/jcbfm.2010.197
20. Wufuer A, Mijiti P, Abudusalamu R, et al. Blood pressure and collateral circulation in acute ischemic stroke. *Herz*. 2019;44(5):455–459. doi:10.1007/s00059-018-4691-5
21. Möbiuswinkler S, Uhlemann M, Adams V, et al. Coronary collateral growth induced by physical exercise: Results of the impact of intensive exercise training on coronary collateral circulation in Patients With Stable Coronary Artery Disease (EXCITE) Trial. *Circulation*. 2016;133(15):1438–1448; discussion 1448. doi:10.1161/CIRCULATIONAHA.115.016442
22. van Petersen AS, Kolkman JJ, Gerrits DG, Van dPJ, Zeebregts CJ, Geelkerken RH. Clinical significance of mesenteric arterial collateral circulation in patients with celiac artery compression syndrome. *J Vasc Surg*. 2017;65(5):1366–1374. doi:10.1016/j.jvs.2016.11.052
23. Kurz MW, Advani R, Behzadi GN, Eldøen G, Farbu E, Kurz KD. Wake-up stroke: Amendable for thrombolysis-like stroke with known onset time? *Acta Neurol Scand*. 2017;136(1):4–10. doi:10.1111/ane.12686

24. Costa R, Pinho J, Alves JN, Amorim JM, Ribeiro M, Ferreira C. Wake-up stroke and stroke within the therapeutic window for thrombolysis have similar clinical severity, imaging characteristics and outcome. *J Stroke Cerebrovasc Dis*. 2016;25(3):511–514. doi:10.1016/j.jstrokecerebrovasdis.2015.10.032

25. Odland A, Særvoll P, Advani R, Kurz MW, Kurz KD. Are the current MRI criteria using the DWI-FLAIR mismatch concept for selection of patients with wake-up stroke to thrombolysis excluding too many patients? *Scand J Trauma Resusc Emerg Med*. 2015;23(1):22. doi:10.1186/s13049-015-0101-7

26. Moore SM, Zhang H, Maeda N, Doerschuk CM, Faber JE. Cardiovascular risk factors cause premature rarefaction of the collateral circulation and greater ischemic tissue injury. *Angiogenesis*. 2015;18(3):265–281. doi:10.1007/s10456-015-9465-6

27. Iwasawa E, Ichijo M, Ishibashi S, Yokota T. Acute development of collateral circulation and therapeutic prospects in ischemic stroke. *Neural Regen Res*. 2016;11(3):368–371. doi:10.4103/1673-5374.179033

28. Seyman E, Shaim H, Shenhar-Tsarfaty S, Jonash-Kimchi T, Bornstein NM, Hallevi H. The collateral circulation determines cortical infarct volume in anterior circulation ischemic stroke. *BMC Neurol*. 2016;16(1):206. doi:10.1186/s12883-016-0722-0

Pack-year cigarette smoking affects the course of palmoplantar pustulosis

Magdalena Putra-Szczepaniak[1,B–D], Adam Reich[2,B,E], Alina Jankowska-Konsur[1,D,E], Anna Czarnecka[3,4,E], Marta Bagłaj-Oleszczuk[1,B], Anita Hryncewicz-Gwóźdź[1,A,D,F]

[1] Department of Dermatology, Venereology and Allergology, Wroclaw Medical University, Poland

[2] Department of Dermatology, University of Rzeszow, Poland

[3] Regional Specialist Hospital, Research and Development Centre, Wrocław, Poland

[4] University School of Physical Education, Faculty of Physiotherapy, Wrocław, Poland

A – research concept and design; B – collection and/or assembly of data; C – data analysis and interpretation;
D – writing the article; E – critical revision of the article; F – final approval of the article

Address for correspondence
Alina Jankowska-Konsur
E-mail: alina.jankowska-konsur@umed.wroc.pl

Abstract

Background. Palmoplantar pustulosis (PPP) is a chronic inflammatory disease with poorly understood pathogenesis. The disease has a chronic course with improvements and exacerbations. Due to palmoplantar location, PPP has a severely negative impact on patients' quality of life.

Objectives. To identify demographic and environmental factors, concomitant diseases, medications, and bacterial factors which may affect the course of PPP.

Material and methods. A total of 51 patients suffering from PPP took part in the study. They were classified according to the Palmoplantar Pustulosis Psoriasis Area and Severity Index (ppPASI) into 3 groups due to the severity of the disease. Pack-year of smoking score was established as a quotient of packets smoked every 24 h and the years of being addicted. Diagnosis of metabolic syndrome was based on the IDF criteria from 2009. *Chlamydia trachomatis* was detected using enzyme-linked immunosorbent assay (ELISA) technique, *Staphylococcus aureus* by the culture swabs. Contact hypersensitivity was examined with the T.R.U.E. test.

Results. Significantly high severity of PPP was observed in patients addicted to smoking with a high pack-year score (p = 0.03). Significantly lower intensity of PPP lesions was observed in patients treated with ibuprofen (p < 0.01). There was no correlation between severity of PPP skin lesions and comorbidities.

Conclusions. Addiction to cigarette smoking and a high pack-year score aggravates the course of PPP. Treatment with ibuprofen can improve the course of the disease.

Key words: smoking addiction, pack-year score, comorbidities, ibuprofen, palmoplantar pustulosis

Background

Palmoplantar pustulosis (PPP) is a chronic inflammatory disease with poorly understood pathogenesis. The lesions are localized on the palms and soles, usually symmetrically.[1,2] Sterile pustules on the erythematous skin, with superficial scaling and fissures are observed. The disease has a chronic course with improvements and exacerbations. Middle-aged women are more common affected than men. Palmoplantar pustulosis has a severely negative impact on quality of life. Clinical observations and research data indicate that genetic, immunological and environmental factors play a role in the development of PPP.[2] The disease is classified by some authors as a variant of psoriasis, and by others treated as a separate condition.[2–5] Some lesions are common for psoriasis and PPP. The co-occurrence of cutaneous psoriatic lesions and psoriatic nail changes is observed in patients with PPP. Some patients with PPP report arthralgia as well as a positive family history of psoriasis. Moreover, focal bacterial infections seem to play a role in the pathogenesis of both diseases.[1,6,7] On the other hand, there are differences between psoriasis and PPP. Palmoplantar pustulosis occurs more often in middle-aged women and it does not occur in children. Many publications confirm the relationship between PPP and cigarette smoking, as well as the co-occurrence of contact allergies[8–11] and other comorbidities.[8–15] Thyroid dysfunction in PPP patients is observed more frequently than in the case of psoriasis.[16,17]

Objectives

The objective of this study was to identify demographic and environmental factors, concomitant diseases, medications, and bacterial factors that may affect the course of PPP.

Material and methods

A total of 51 people suffering from PPP, who had been hospitalized in the Dermatology Department of Wroclaw Medical University, Poland, took part in the study. The severity of PPP was assessed according to the Palmoplantar Pustulosis Psoriasis Area and Severity Index (ppPASI). The ppPASI is a modification of the PASI index with evaluation of erythema, vesicles/pustules and scaling/desquamation. Patients were classified into 3 groups due to the severity of the disease: mild (ppPASI: 0–9), moderate (ppPASI: 10–19) and severe (ppPASI: 29–72) disease. Pack-year of smoking score was established as a quotient of packets smoked every 24 h and the years of being addicted. The diagnosis of metabolic syndrome was based on the International Diabetes Federation (IDF) criteria from 2009.[18] *Chlamydia trachomatis* was detected in urethral specimens with enzyme-linked immunosorbent assay (ELISA) technique. *Staphylococcus aureus* (*S. aureus*) colonization of the nasal vestibule was established using culture swabs. Contact hypersensitivity was examined with the thin-layer rapid-use epicutaneous (T.R.U.E.) test with 35 allergens.

The influence of age, sex, co-occurrence of psoriatic lesions and metabolic syndrome, environmental factors such as: cigarette smoking, contact allergies, medications taken for other diseases, and infectious factors on the severity of PPP skin lesions were assessed.

The results obtained during the research were statistically analyzed using STATISTICA v. 12.0 (StatSoft Polska Sp. z o.o.; Kraków, Poland). Student's t-test, χ^2, Kolmogorov–Smirnov test, Pearson correlation, the Yates's correction, and the analysis of variance (ANOVA) were used. The analysis was performed at the significance level of p = 0.05.

The study was approved by the Ethics Committee of Wroclaw Medical University. All study participants signed informed consent forms.

Results

The results of the study are presented in Table 1. A total of 51 patients with PPP, 11 (22%) men and 40 (78%) women, aged 20–77 years (mean age: 54.2 years), were included in the study. The predominance of women among the patients was statistically significant (p = 0.03). Skin lesions were most often located on: hands and feet in 36 (70.6%) patients, in 5 (9.8%) patients only on the hands, and in 10 (19.6%) only on the feet. The values of ppPASI ranged from 2.4 to 72 with the average value of 21.64. Nine (17.65%) patients were classified into the group with mild disease (ppPASI < 10), 18 (35.29%) with moderate (ppPASI 10–19) and 24 (47.06%) with severe disease (ppPASI ≥ 20). There was no correlation between the severity of skin lesions and the age or sex of patients (p = 0.66; p = 0.81, respectively). The disease onset was between 45 and 65 years of age (mean: 47.1 years). The duration of the disease ranged from 1 year to 45 years. The age of onset and duration of the disease did no influence the severity of PPP skin lesions (p = 0.63; p = 0.91, respectively).

Concomitant psoriasis

In 14 (27.45%) patients with PPP, pustular lesions were accompanied by plaque psoriasis. The majority of these patients (8, 57.1%) suffered from severe PPP (ppPASI > 20), and only 1 patient (7.4%) had mild disease (ppPASI < 10); however, no significant correlation was established.

Cigarettes smoking

In the study group, 47 (92.2%) patients were active cigarette smokers. Four non-smoking patients had

Table 1. Severity of PPP symptoms depending on concomitant treatment

| Medicines | Use of medications | Number of patients with different intensity of skin lesions in the course of PPP (n = 51) | | | p-value |
		mild (ppPASI < 10) n (%)	moderate (ppPASI 10–19) n (%)	severe (ppPASI ≥ 20) n (%)	
β-blockers	no	8 (19.5%)	17 (41.5%)	16 (39%)	0.06
	yes	1 (10%)	1 (10%)	8 (80%)	
Angiotensin converting enzyme (ACE) inhibitors	no	8 (18.2%)	18 (40.9%)	18 (40.9%)	0.06
	yes	1 (14.3%)	0 (0%)	6 (85.7%)	
Statins	no	8 (20%)	14 (35%)	18 (45%)	0.69
	yes	1 (9.1%)	4 (36.4%)	6 (54.5%)	
Ibuprofen	no	6 (12.8%)	18 (38.3%)	23 (48.9%)	<0.01
	yes	3 (75%)	0 (0%)	1 (25%)	
Indapamide	no	8 (17.4%)	18 (39.1%)	20 (43.5%)	0.2
	yes	1 (20%)	0 (0%)	4 (80%)	
Hydrochlorothiazide	no	9 (18.8%)	17 (35.4%)	22 (45.8%)	0.66
	yes	0 (0%)	1 (33.3%)	2 (66.7%)	
Acetylsalicylic acid (ASA)	no	9 (19.6%)	17 (37%)	20 (43.5%)	0.27
	yes	0 (0%)	1 (20%)	4 (80%)	
Levothyroxine	no	6 (15.4%)	15 (38.5%)	18 (46.1%)	0.61
	yes	3 (25%)	3 (25%)	6 (50%)	

mild-to-moderate lesions. Severe course of the disease with ppPASI > 20 was observed only in smokers. The mean pack-year score among patients with PPP was 21.36. Significantly higher severity of PPP was observed in patients with a higher pack-year score (p = 0.03).

Concomitant contact hypersensitivity

Contact hypersensitivity was found in 14 (27.5%) patients. The most common allergen was nickel. An allergy to this metal was present in 7 (14.73%) patients. Four (7.84%) patients were allergic to preservatives used in cosmetics and topical medications. Two patients reacted to KATHON™ CG, 2 to thiomersal and 3 to: sterol alcohols from lanolin, cobalt hydrochloride, p-tert-butylphenol-formaldehyde resins, a mixture of parabens, a mixture of carbon derivatives, potassium dichromate, and a thiuram mix. There was no correlation between the severity of PPP skin lesions and the presence of contact allergy (p = 0.89).

Co-infections

Chlamydia trachomatis urethritis was found in only 2 (3.92%) patients, and *S. aureus* colonization of the nasal vestibule was found in 10 (19.61%) patients. There was no statistically significant correlation between the severity of PPP and the coexistence of chlamydia infection or *S. aureus* colonization.

Treatment of comorbidities

Due to comorbidities, 33 (64.71%) of the studied patients were taking medications. Severe PPP with ppPASI ≥ 20 was observed in 8 of 10 patients treated with β-blockers and in 6 of 7 patients treated with angiotensin-converting-enzyme (ACE) inhibitors. However, there was no correlation between the severity of PPP and treatment with these medications, although the p-value was low (0.06). On the other hand, significantly lower intensity of PPP lesions was observed in patients treated with ibuprofen (p < 0.01). Only 4 patients were treated with ibuprofen, but 3 of them had mild disease (Table 2).

BMI and metabolic syndrome

Patients' BMI ranged from 17.18 to 48.33, with mean value of 26.82. Twenty-one (41.18%) patients had normal weight, 19 (37.25%) were overweight and 11 (21.57%) were obese. Despite the fact that over half of obese patients had severe disease (ppPASI ≥ 20), no correlation was found between the severity of skin lesions and their BMI (p = 0.3). A total of 24 patients had metabolic syndrome that did not correlate with the PPP severity.

Thyroid disease and arthralgia

Of all 51 of the studied patients, 14 (27.45%) had thyroid disease or had a history of thyroid disease. Twenty-six patients (50.98%) complained of arthralgia. However, these conditions did not correlate with the severity of PPP.

Table 2. Severity of PPP symptoms depending on lesions location, demographic factors, duration of the disease, smoking, concomitant diseases, bacterial factors, and coexistence of metabolic syndrome

Factors potentially influencing the severity of PPP	Number of patients with different intensity of skin lesions in the course of PPP PPP (n = 51)			p-value
	mild (ppPASI < 10) n (%)	moderate (ppPASI 10–19) n (%)	severe (ppPASI ≥ 20) n (%)	
Localization of skin lesions hands feet hands and feet	2 (40%) 2 (20%) 5 (13.88%)	3 (60%) 4 (40%) 11 (30.56%)	0 4 (40%) 20 (55.56%)	0.21
Age <30 years 30–54 years ≥55 years	1 (33.3%) 2 (10%) 6 (21.4%)	1 (33.3%) 9 (45%) 8 (28.6%)	1 (33.3%) 9 (45%) 14 (50%)	0.66
Sex women men	7 (17.5%) 2 (18.2%)	15 (37.5%) 3 (27.3%)	18 (45%) 6 (54.5%)	0.81
The onset of the disease <30 years 30–55 years ≥55 years	3 (33.3%) 3 (12%) 3 (17.6%)	2 (22.2%) 11 (44%) 7 (41.2%)	4 (44.4%) 11 (44%) 7 (41.2%)	0.63
Duration of the disease <10 years 10–19 years ≥20 years	7 (17.9%) 1 (14.3%) 1 (20%)	15 (38.5%) 2 (28.6%) 1 (20%)	17 (43.6%) 4 (57.1%) 3 (60%)	0.91
Coexistence of cutaneous psoriasis PPP without psoriasis PPP with psoriasis	8 (21.6%) 1 (7.4%)	13 (35.1%) 5 (35.7%)	16 (43.2%) 8 (57.1%)	0.44
Smoking smoker non-smoker	7 (14.9%) 2 (50%)	16 (34%) 2 (50%)	24 (51.1%) 0 (0%)	0.09
Pack-year score <10 10–19 ≥20	4 (50%) 0 (0%) 3 (11.1%)	2 (25%) 5 (41.7%) 9 (33.3%)	2 (25%) 7 (58.3%) 15 (55.6%)	0.03
Patch test negative positive	6 (16.2%) 3 (21.4%)	13 (35.1%) 5 (35.7%)	18 (48.7%) 6 (42.9%)	0.89
C. trachomatis infection yes no	0 (0%) 9 (18.37%)	1 (50%) 17 (34.69%)	1 (50%) 23 (46.94%)	0.75
S. aureus colonization yes no	1 (10%) 8 (19.51%)	3 (30%) 15 (36.59%)	6 (60%) 18 (43.9%)	0.62
BMI normal overweight obese	4 (19%) 2 (10.5%) 3 (27.3%)	9 (42.9%) 8 (42.1%) 1 (9.1%)	8 (38.1%) 9 (47.4%) 7 (63.6%)	0.3
Metabolic syndrome present absent	7 (29.2%) 2 (7.4%)	9 (37.5%) 9 (33.3%)	8 (33.3%) 16 (59.3%)	0.07
Thyroid disease yes no	4 (28.6%) 5 (13.5%)	3 (21.4%) 15 (40.5%)	7 (50%) 17 (46%)	0.3
Arthralgia yes no	6 (23.08%) 2 (8.33%)	10 (38.46%) 8 (33.33%)	10 (38.46%) 14 (58.33%)	0.17

Discussion

Palmoplantar pustulosis is a rare disease. In Western Europe, the incidence of this disease ranges from 0.01% to 0.05%,[1] and in the Japanese population it is 0.12%.[6] Palmoplantar pustulosis accounts for 20% of hand and foot skin diseases.[19] The etiopathogenesis of the disease is not fully understood. In the literature, PPP is classified as a subtype of psoriasis or a separate disease entity. In our study, about 1/3 of patients with PPP had comorbid psoriasis, which is slightly more than data from other studies (about 20%).[1] Typically, PPP occurs in adults. The age of PPP patients varies from 21 to 50 years[1]; however some authors pointed a higher mean age (56.7 years).[6]

Most of our patients, as in other publications,[20] suffered from skin lesions located both on hands and feet. Among our patients, the disease onset was between 18 and 74 years of age (mean: 47.1 years). The duration of the disease was 1–45 years (mean: 7.14 years).

Clinical studies and case reports indicate that certain genetic, environmental and infectious factors affect the onset and/or the exacerbation of PPP. Recently, the pathogenic relationship between PPP and cigarette smoking was analyzed in the literature.[10] Cigarette smoke contains over 4000 chemicals, 300 of which are carcinogens or have pro-inflammatory activities.[21] Hagforsen et al. documented the relationship between smoking and the occurrence of PPPs, and found that this addiction increases the risk of developing PPP seventy-fold.[22] In our study, we found a statistically significant correlation between the severity of skin lesions and pack-year score. The relationship between the severity of PPP skin lesions and cigarette smoking has not been published before. The mechanism of smoking impact on the PPP symptoms has not been precisely established. Characteristic locations of the lesions on the palmar and plantar region support the theory that sweat glands and acetylcholine receptors (AChR) play the role in the PPP pathogenesis. There are 2 main types of acetylcholine receptor receptors: nicotinic (nAChR) and muscarinic (mAChR), which are found on keratinocytes and on sweat gland cells. The increased expression of alpha7 nAChR which controls homeostasis and terminal differentiation of epidermal cells was observed on the sweat glands and in the epidermis of patients with PPP compared to healthy individuals.[22–24] These receptors show greater affinity for nicotine than for acetylcholine. New theory explains that nicotine-stimulated nAChR play a role in the PPP pathogenesis by leading to the accumulation of neutrophils and eosinophils in the epidermis.[25,26] Additionally, peripheral arterial disease caused by smoking may probably trigger PPP. This idea is supported by the case report of a patient with Leriche syndrome. Symptoms of PPP improved after smoking cessation and authors observed complete cure of skin lesions after vascular surgery and improved arterial circulation.[27]

Contact hypersensitivity may coexist with PPP, or may have an impact on the course of the disease.[28] In our study, 27.5% of patients had positive result of patch tests. Nickel was the most common allergen. In the literature, even higher percentage of PPP patients with coexisting contact hypersensitivity (39–60%) has been reported.[8,11] The most common contact allergens in these patients were: nickel, balsam of Peru and a mixture of fragrances. More frequent use of jewellery and cosmetics may promote the PPP occurrence in women. Furthermore, patients with PPP, due to the chronic disease, use topical medications and cosmetics for a long time and contact allergy to creams and ointments ingredients can exacerbate skin symptoms. Therefore, patch tests should be performed in patients with no reaction to topical therapy or if disease worsening during topical treatment is observed.

The relationship between focal bacterial infections and the severity of skin lesions in PPP has recently been discussed in the literature. Tonsillectomy or treatment of any bacterial infections led to significant improvement or cure of PPP in some patients.[29,30] The etiopathogenetic relationship of PPP and *Helicobacter pylori* infection has been observed as well.[31,32] No relationship between the appearance or exacerbation of PPP skin lesions with bacterial infections or symptoms of gastric ulcer was observed in our study. However, 26 (51%) of study participants suffered from tooth caries. According to the literature, odontogenic and other infections may exacerbate skin lesions in the course of PPP.[29,30,33,34]

Pustular skin lesions are also observed in the course of reactive arthritis caused by chlamydia infection. Isolated PPP caused by *C. trachomatis* was considered recently and higher level of chlamydial antibodies in PPP patients in comparison to healthy people was documented.[35] Nevertheless, only 2 (3.92%) of our patients had chlamydia infection. In recent years, the colonization of skin and mucous membranes by *S. aureus* in patients with psoriasis has been carefully examined. Immunological processes triggered by bacterial antigens probably play a role in the course of this disease. Keratinocytes stimulated by bacterial antigens produce antimicrobial proteins (e.g., protein S-100) that contribute to local inflammation. Elevated levels of these proteins have been shown in psoriatic lesions. Studies on the colonization of the skin and nasal vestibule in people with psoriasis were performed, but their results are ambiguous. A higher and similar percentage of psoriatic patients with *S. aureus* colonization in the atrium of the nasal vestibule in comparison to control was documented.[36] So far, colonization of the nasal vestibule by *S. aureus* in PPP patients has not been studied. In our study, bacteria were found in 10 (19.61%) patients. In 6 patients, we observed severe PPP (ppPASI ≥ 20); however, there was no correlation between staphylococcal colonization and PPP severity.

The correlation between PPP and treatment of comorbidities should be also taken under consideration. A significant percentage of patients with PPP described in the literature

were simultaneously treated for concomitant diseases.[14] However, the influence of drugs on the course of the disease has not been observed. In our study, most of the studied patients receiving medications for high blood pressure suffered from severe PPP. In the group of 10 patients treated with β-blockers, 8 (80%) had severe PPP. Similarly, 7 patients treated with ACE inhibitors presented severe skin lesions with ppPASI ≥ 20. No relationship was observed between the occurrence or exacerbation of PPP lesions and starting treatment for hypertension. Only 1 person claimed that the PPP lesions began after introducing a new drug (amlodipine) and improved a few weeks after discontinuation of this calcium channel blocker. Stanford et al. described the occurrence of PPP following the initiation of β-blockers.[37] On the other hand, statistically significant lower severity of skin lesions was observed in patients taking ibuprofen (p < 0.01). Anti-inflammatory activity of this medication could have a beneficial effect on the severity of PPP symptoms. This positive impact of ibuprofen in PPP requires further verification due to a small group of patients taking this drug in our study.

A numerous publications of increased prevalence of the metabolic syndrome in patients with psoriasis, as well as more severe course of psoriasis in patients with this condition[38] encouraged us to study the coexistence of PPP and the metabolic syndrome. Among our patients, 47.1% had the metabolic syndrome and the PPP course was more severe in these patients (p = 0.07).

Inflammatory and pustular lesions located on the hands and feet are very characteristic for PPP, but these lesions are also observed in chronic inflammatory disorders such as SAPHO (synovitis, acne, hands and feet pustulosis, periosteal hyperplasia and osteitis) syndrome, pustular osteomyelitis (PAO), and Sonozaki syndrome.[39] None of our patients had SAPHO, PAO or Sonozaki syndrome. However, 26 participants (50.98%) reported arthralgia, but no correlation was observed between the severity of PPP skin lesions of and joint pain.

Conclusions

Cigarette smoking has been shown to affect the PPP course. As this is a modifiable factor, patients with PPP should be advised to quit smoking. As the research results show, a positive effect of ibuprofen on skin lesions in the course of PPP and the use of ibuprofen in the therapy should be considered, but it requires further studies on a larger number of patients.

ORCID iDs

Magdalena Putra-Szczepaniak https://orcid.org/0000-0001-6340-7164
Adam Reich https://orcid.org/0000-0002-5573-1754
Alina Jankowska-Konsur https://orcid.org/0000-0003-4944-5388
Anna Czarnecka https://orcid.org/0000-0002-6621-9537
Marta Bagłaj-Oleszczuk https://orcid.org/0000-0002-4554-7603
Anita Hryncewicz-Gwóźdź https://orcid.org/0000-0002-1601-471X

References

1. Khandpur S, Singhal V, Sharma V. Palmoplantar involvement in psoriasis: A clinical study. *Indian J Dermatol Venereol Leprol*. 2011;77(5):625. doi:10.4103/0378-6323.84071
2. Yamamoto T. Extra-palmoplantar lesions associated with palmoplantar pustulosis. *J Eur Acad Dermatol Venereol*. 2009;23(11):1227–1232. doi:10.1111/j.1468-3083.2009.03296.x
3. Ammoury A, El Sayed F, Dhaybi R, Bazex J. Palmoplantar pustulosis should not be considered as a variant of psoriasis. *J Eur Acad Dermatol Venereol*. 2008;22(3):392–393. doi:10.1111/j.1468-3083.2007.02344.x
4. Misiak-Galazka M, Wolska H, Rudnicka L. Is palmoplantar pustulosis simply a variant of psoriasis or a distinct entity? *J Eur Acad Dermatol Venereol*. 2017;31(7):e342–e343. doi:10.1111/jdv.14136
5. Misiak-Galazka M, Wolska H, Rudnicka L. What do we know about palmoplantar pustulosis? *J Eur Acad Dermatol Venereol*. 2017;31(1): 38–44. doi:10.1111/jdv.13846
6. Kubota K, Kamijima Y, Sato T, et al. Epidemiology of psoriasis and palmoplantar pustulosis: A nationwide study using the Japanese national claims database. *BMJ Open*. 2015;5(1):1–9. doi:10.1136/bmjopen-2014-006450
7. Kumar B, Saraswat A, Kaur I. Palmoplantar lesions in psoriasis: A study of 3065 patients. *Acta Derm Venereol*. 2002;82(3):192–195. doi:10.1080/00015550260132488
8. Caca-Biljanovska N, V'lckova-Laskoska M, Balabanova-Stefanova M, Grivceva-Panovska V. Frequency of delayed-type hypersensitivity to contact allergens in palmo-plantar psoriasis. *Prilozi*. 2005;26(2): 131–141. https://pubmed.ncbi.nlm.nih.gov/16400235/
9. De Waal AC, Van de Kerkhof PCM. Pustulosis palmoplantaris is a disease distinct from psoriasis. *J Dermatolog Treat*. 2011;22(2):102–105. doi:10.3109/09546631003636817
10. Hagforsen E, Awder M, Lefvert AK, Nordlind K, Michaëlsson G. Palmoplantar pustulosis: An autoimmune disease precipitated by smoking? *Acta Derm Venereol*. 2002;82(5):341–346. doi:10.1080/000155502320624069
11. Yiannias JA, Winkelmann RK, Connolly SM. Contact sensitivities in palmar plantar pustulosis (acropustulosis). *Contact Dermatitis*. 1998; 39(3):108–111. doi:10.1111/j.1600-0536.1998.tb05857.x
12. Hayashi S, Shimaoka Y, Hamasaki Y, Hatamochi A. Palmoplantar pustulosis and pustulotic arthro-osteitis treatment with potassium iodide and tetracycline, a novel remedy with an old drug: A review of 25 patients. *Int J Dermatol*. 2017;56(8):889–893. doi:10.1111/ijd.13608
13. Becher G, Jamieson L, Leman J. Palmoplantar pustulosis: A retrospective review of comorbid conditions. *J Eur Acad Dermatol Venereol*. 2015;29(9):1854–1856. doi:10.1111/jdv.12545
14. Hiraiwa T, Yamamoto T. Comorbidities of Japanese patients with palmoplantar pustulosis: A report from a single center. *Int J Dermatol*. 2018;57(7):e40–e41. doi:10.1111/ijd.14023
15. Misiak-Galazka M, Zozula J, Rudnicka L. Palmoplantar pustulosis: Recent advances in etiopathogenesis and emerging treatments. *Am J Clin Dermatol*. 2020;21(3):355–370. doi:10.1007/s40257-020-00503-5.
16. Pontikides N, Krassas GE. Influence of cigarette smoking on thyroid function, goiter formation and autoimmune thyroid disorders. *Hormones*. 2002;1(2):91–98. doi:10.14310/horm.2002.1156
17. Rosen K, Lindstedt G, Mobacken H, Nystrom E. Thyroid function in patients with pustulosis palmplantaris. *J Am Acad Dermatol*. 1988; 19(6):1009–1016. doi:10.1016/s0190-9622(88)70265-0
18. Alberti KG, Eckel RH, Grundy SM, et al. Harmonizing the metabolic syndrome: A joint interim statement of the International Diabetes Federation Task Force on Epidemiology and Prevention; National Heart, Lung, and Blood Institute; American Heart Association; World Heart Federation; International Atherosclerosis Society; and International Association for the Study of Obesity. *Circulation*. 2009;120(16): 1640–1645. doi:10.1161/CIRCULATIONAHA.109.192644
19. Hongal AA, Rajashekhar N, Gejje S. Palmoplantar dermatoses: – A clinical study of 300 cases. *J Clin Diagn Res*. 2016;10(8):4–7. doi:10.7860/JCDR/2016/20818.8364
20. Pettey AA, Balkrishnan R, Rapp SR, Fleischer AB, Feldman SR. Patients with palmoplantar psoriasis have more physical disability and discomfort than patients with other forms of psoriasis: Implications for clinical practice. *J Am Acad Dermatol*. 2003;49(2):271–275. doi:10.1067/s0190-9622(03)01479-8

21. Miot HA, Miot LD, Lopes PS, Haddad GR, Marques SA. Association between palmoplantar pustulosis and cigarette smoking in Brazil: A case-control study. *J Eur Acad Dermatol Venereol.* 2009;23(10): 1173–1177. doi:10.1111/j.1468-3083.2009.03282.x

22. Hagforsen E, Michaëlsson K, Lundgren E, et al. Women with palmoplantar pustulosis have disturbed calcium homeostasis and a high prevalence of diabetes mellitus and psychiatric disorders: A case-control study. *Acta Derm Venereol.* 2005;85(3):225–232. doi:10.1080/00015550510026587

23. Hagforsen E, Hedstrand H, Nyberg F, Michaëlsson G. Novel findings of Langerhans cells and interleukin-17 expression in relation to the acrosyringium and pustule in palmoplantar pustulosis. *Br J Dermatol.* 2010;163(3):572–579. doi:10.1111/j.1365-2133.2010.09819.x

24. Hagforsen E, Michaëlsson G, Stridsberg M. Normal and PPP-affected palmoplantar sweat gland express neuroendocrine markers chromogranins and synaptophysin differently. *Arch Dermatol Res.* 2010; 302(9):685–693. doi:10.1007/s00403-010-1070-3

25. Hagforsen E, Awder M, Lefvert AK, Nordlind K, Michaëlsson G. Palmoplantar pustulosis: An autoimmune disease precipitated by smoking? *Act Derm Venereol.* 2002;82(5):341–346. doi:10.1080/000155502320 624069

26. Hagforsen E. Palmoplantar pustulosis. Pathogenetic studies with special reference to the role of nicotine. Acta Universitatis Upsaliensis. Comprehensive Summaries of Uppsala Dissertations from the Faculty of Medicine 2001. https://www.diva-portal.org/smash/record.jsf? pid=diva2%3A167253&dswid=mainwindow. Acceesed May 29, 2017.

27. Murao K, Minato M, Kubo Y. Improvement of palmoplantar pustulosis lesions after angioplasty for Leriche syndrome. *Australas J Dermatol.* 2013;54(3):e80–81. doi:10.1111/j.1440-0960.2012.00940.x

28. Ito T, Mori T, Fujiyama T, Tokura Y. Dramatic exacerbation of palmoplantar pustulosis following strongly positive nickel patch testing. *Int J Dermatol.* 2014;53(5):327–329. doi:10.1111/ijd.12242

29. Takahara M, Hirata Y, Nagato T, et al. Treatment outcome and prognostic factors of tonsillectomy for palmoplantar pustulosis and pustulotic arthro-osteitis: A retrospective subjective and objective quantitative analysis of 138 patients. *J Dermatol.* 2018;45(7):812–823. doi:10.1111/1346-8138.14348

30. Yamamoto T. Triggering role of focal infection in the induction of extra-palmoplantar lesions and pustulotic arthro-osteitis associated with palmoplantar pustulosis. *Adv Otorhinolaryngol.* 2011;72: 89–92. doi:10.1159/000324620

31. Martin Hübner A, Tenbaum SP. Complete remission of palmoplantar psoriasis through *Helicobacter pylori* eradication: A case report. *Clin Exp Dermatol.* 2008;33(3):339–240. doi:10.1111/j.1365-2230.2007. 02634.x

32. Sáez-Rodríguez M, Noda-Cabrera A, García-Bustínduy M, et al. Palmoplantar pustulosis associated with gastric *Helicobacter pylori* infection. *Clin Exp Dermatol.* 2002;27(8):720. doi:10.1046/j.1365-2230. 2002.01102_6.x

33. Kouno M, Nishiyama A, Minabe M, et al. Retrospective analysis of the clinical response of palmoplantar pustulosis after dental infection control and dental metal removal. *J Dermatol.* 2017;44(6):695–698. doi:10.1111/1346-8138.13751

34. Kikuchi N, Yamamoto T. Dental infection as a triggering factor in palmoplantar pustulosis. *Acta Derm Venereol.* 2013;93(6):721–722. doi:10. 2340/00015555-1552

35. Jansen CT, Hollmén, Pajarre R, Terho P. Antichlamydial antibodies in chronic palmoplantar pustulosis. *Acta Derm Venereol.* 1980;60(3): 263–266.

36. Ng CY, Huang YH, Chu CF, Wu TC, Liu SH. Risks for *Staphylococcus aureus* colonization in psoriasis patients: A systematic review and meta-analysis. *Br J Dermatol.* 2017;177(4):967–977. doi:10.1111/bjd. 15366

37. Stanford CW, Kollipara R, Melookaran AM, Hall JC. Palmoplantar pustular psoriasis following initiation of a beta-blocker: Disease control with low-dose methotrexate. *Cutis.* 2014;94:153–155.

38. Armstrong AW, Harskamp CT, Armstrong EJ. Psoriasis and metabolic syndrome: A systematic review and meta-analysis of observational studies. *J Am Acad Dermatol.* 2013;68(4):654–662. doi:10.1016/j.jaad. 2012.08.015

39. Brzezińska-Wcisło L, Bergler-Czop B, Lis-Święty A. Sonozaki syndrome: Case report and review of literature. *Rheumatol Int.* 2012;32(2): 473–477. doi:10.1007/s00296-009-1335-3

Eotaxin-2 as a potential marker of preterm premature rupture of membranes: A prospective, cohort, multicenter study

Grzegorz Raba[1,A–F], Marian Kacerovsky[2,3,A,C,E,F], Piotr Laudański[4,A,C,E,F]

[1] Department of Gynecology end Obstetrics, University of Rzeszow, Poland

[2] Department of Obstetrics and Gynecology, University Hospital Hradec Kralove, Charles University, Czech Republic

[3] Biomedical Research Center, University Hospital Hradec Kralove, Czech Republic

[4] 1st Department of Obstetrics and Gynecology, Medical University of Warsaw, Poland

A – research concept and design; B – collection and/or assembly of data; C – data analysis and interpretation;
D – writing the article; E – critical revision of the article; F – final approval of the article

Address for correspondence
Grzegorz Raba
E-mail: rabagrzegorz@gmail.com

Abstract

Background. Despite advances in medicine, there is currently no effective procedure for predicting and the early diagnosis of preterm premature rupture of membranes (pPROM).

Objectives. To apply measurements of selected biochemical markers of inflammation for diagnosing cases of pPROM without clinical signs of infection.

Material and methods. This is a prospective cohort study. Three groups were compared, a study group: 82 women between 22 and 37 weeks of pregnancy hospitalized due to pPROM, a control group: 64 women between 22 and 37 weeks of pregnancy in the 1st stage of preterm labor with intact fetal membranes, and a reference group: 99 women between 37 and 42 weeks of pregnancy in the 1st stage of physiological term labor and intact fetal membranes. To assess the concentration of cytokines, a multiplex method was used for measurement of: IGFBP-1, IGFBP-2, BDNF, L-selectin, E-selectin, PECAM-1, ICAM-1, and VCAM-1, MIP-1d, MIP-3b, BLC, eotaxin-1, and eotaxin-2.

Results. Out of the studied molecules, we found that eotaxin-2 concentrations in the study group were significantly lower than in the control group and the reference group: 9.22 pg/mL compared to 13.76 pg/mL and 14.14 pg/mL (p = 0.014), respectively. We also showed that serum concentration of eotaxin-2 below 8.24 pg/mL could be used as a cut-off level of pPROM (sensitivity: 0.58; specificity: 0.57).

Conclusions. Findings of significant differences in eotaxin-2 can be the basis for further studies on the use of this molecule as a biochemical marker of pPROM.

Key words: preterm rupture of membranes, cytokine, preterm labor, molecular biology

Background

Premature rupture of membranes (PROM) is one of the major complications of physiological pregnancy resulting in the leakage of amniotic fluid. It occurs in around 3% of singleton pregnancies and around 7–20% of multiple ones.[1–3] Despite application of advanced immunohistochemical tests, including detecting vaginal fetal fibronectin, insulin-like growth factor binding protein-1 and placental alpha-microglobulin-1, in some clinical cases diagnosis of PROM still remains difficult. An extremely important event in the context of obstetric complications is preterm PROM (pPROM), defined as the rupture of fetal membranes before the 37th week of pregnancy, or more than 24 h before the onset of labor.[4] Preterm PROM is the cause of about 1/3 of premature births.[5] The diagnosis of pPROM mainly depends on a medical interview carried out with the patient. Up to 90% of cases can be diagnosed on this basis.[6,7] The diagnosis of pPROM is usually confirmed based on accessory examinations, which include: nitrazine test and/or immunochromatographic tests, based on the detection of placental alpha-microglobulin-1 (PAMG-1) or insulin-like growth factor binding protein-1 (IGFBP-1), present in vaginal secretion.[13,14] In contrast to the rupture of membranes during term labor, in the etiology of pPROM inflammatory, mechanisms linked to infection are far more common. Cytokines, including chemokines produced by activated immune cells, are the largest group of biochemical factors involved in the pathogenesis of pPROM and can potentially be used as valuable biomarkers of preterm labor.[15]

In the fetal membranes, cytokines may exhibit direct autocrine or paracrine activity. Endocrine cytokines might also be released by cells located within other sites of the pregnant woman's body.[8,9] Despite advances in medicine, there is as yet no effective test to predict pPROM. Endothelial cells express endothelial-specific adhesion molecules (integrins): L-selectin, E-selectin, ICAM-1, VCAM-1, and PECAM.[8,9] They are involved in the regulation of migration as well as permeability of blood cells through the endothelium. This process may play an important role in the pathogenesis of pPROM by participating in the formation of inflammation in the placenta and fetal membranes.

Chemokines: MIP-1d, MIP-3b, eotaxin-1, eotaxin-2, and B lymphocyte chemoattractant (BLC), as factors associated with inflammatory processes, may also play a role in the pathogenesis of pPROM through chemotactic effects on inflammatory cells. In the reproductive system, MIP-1d, MIP-3b, eotaxin-1, eotaxin-2, and BLC interact with numerous peptides that induce smooth muscle contractions. They are biologically active by interacting with G-protein binding membrane receptors (chemokine receptors) that are selectively located on the surfaces of target cells.

The 3rd group of potential biochemical markers that were the subject of research in this work are circulating proteins with variable expression during the inflammatory phase: IGFBP-1, IGFBP-2 and BDNF. They can be associated with the formation of inflammatory infiltrates within the fetal membranes, placenta and/or umbilical cord, and thus are involved in the pPROM pathogenesis.

The development of research methods, including multiplexed technologies,[10] may be the basis for implementation of new diagnostic methods for early diagnosis of this complication or even identification of high-risk groups, which could contribute to improvement in antenatal monitoring.

Objectives

This paper attempts to apply paralleled measurements of selected biochemical markers of inflammation for diagnosing pPROM in pregnant women without clinical signs of infection.

Material and methods

This is a prospective cohort study reviewed and approved by an institutional review board of a Local Bioethics Committee before it began. The study group consisted of 82 women between 22 and 37 weeks of pregnancy hospitalized due to pPROM. The control group consisted of 64 women between 22 and 37 weeks of pregnancy in the 1st stage of preterm labor with cervical dilatation of up to 3 cm, and intact fetal membranes. We used the reference group consisting of 99 women between 37 and 42 weeks of pregnancy in the 1st stage of physiological term labor, with cervical dilatation of up to 3 cm, and intact fetal membranes. As exclusion criteria we considered antibiotic treatment up to 3 weeks prior to the study, placenta previa, multiple pregnancy, and clinical symptoms of infection: temperature above 37°C, cough, chills, and fetal tachycardia. The diagnosis of pPROM was based on ACOG recommendations,[11] that is: 1) gynecological examination – visualization of amniotic fluid passing from the external cervical os; 2) nitrazine test (change in the color of paper impregnated with nitrazine from yellow to blue); 3) immunochromatographic tests.

The diagnosis of pPROM was confirmed by the presence of at least 2 of the 3 criteria. The average time between fetal membrane rupture and the patient's inclusion was 3 h 46 min (min. 30 min, max. 26 h). A total of 79 women were in early pPROM (up to 18 h) and 3 women were in late pPROM (more than 18 h passed between the rupture and the onset of labor).

Samples collection

Whole blood samples of 15 mL were collected from the ulnar vein of each pregnant woman using 2 tubes: 5 mL for serum into a test tube with a serum separating

tube (SST) and 10 mL for plasma into an EDTA tube. In the study group, blood was collected immediately after pPROM diagnosis. In the control and reference groups, blood was collected at the onset of labor with cervix dilatation below 3 cm. In all 3 groups, samples were taken before pregnant women were given any medication. From the EDTA tube, 2×2.5 mL were pipetted and the rest was centrifuged together with the serum (taken to the separator tube), at 3000 rpm for 5 min at 4°C. Serum and EDTA treated plasma were titrated 10×250 μL, each separately. Samples were preserved immediately at −80°C. The concentrations of the following biochemical markers were determined in the patients' blood serum: 1) Circulating proteins expressed during inflammation: IGFBP-1, IGFBP-2, and BDNF; 2) Adhesion molecules involved in leukocyte-endothelial transduction: L-selectin, E-selectin, PECAM-1, ICAM-1, and VCAM-1; 3) Chemokines: MIP-1d, MIP-3b, BLC, eotaxin-1, and eotaxin-2.

Determination of the level of biochemical markers was made using protein macroarrays in accordance with the detailed specifications of the manufacturer (RayBiotech, Norcross, USA).

Statistical analysis

We used the Shapiro–Wilk test for analysis of normality. We compared study group with the control group, and study group with the reference group. When comparing 2 groups for quantitative data that did not come from a normal distribution, the U Mann–Whitney test was used. For data with a normal distribution, Student's t-test was used to evaluate eotaxin-2 threshold value; receiver operating characteristic (ROC) curve was performed. Statistical significance level was assumed at $p < 0.05$.

Results

Characteristics of the groups

The mean age of women with pPROM was 26.4 years (ranging from 18 to 41 years), and was not statistically significantly different ($p > 0.05$) from the age of women in the control and reference groups. There were no statistically significant differences ($p > 0.05$) between the groups in the number of pregnancies, urine pH, hemoglobin, and white blood cells levels. There were important differences in smokers in the study group compared to reference group and vaginal pH between study group compared to control and reference groups due to pPROM (Table 1).

Analysis of the concentration levels of selected biochemical markers

Serum concentrations of IGFBP-1, IGFBP-2; L-selectin, MIP-1d, BDNF, BLC, eotaxin-1, E-selectin, ICAM-1, MIP-3b, PECAM-1, and VCAM-1 were not significantly different ($p > 0.05$) between the study group, control group and reference group (Table 2,3). Women with pPROM showed lower mean eotaxin-2 concentrations compared

Table 1. Characteristic of the groups

Factor	Study group	Control group	Reference group	p_1	p_2
Age [years]	26.4 (18–41)	25.1 (18–39)	24.4 (19–40)	0.241	0.182
Smokers	11	7	5	0.072	0.034
Alcohol abuse	0	0	0	NA	NA
Drug abuse	0	0	0	NA	NA
Number of pregnancies	2 (1–6)	1.8 (1–4)	1.6 (1–3)	0.112	0.075
Pregnancy age [weeks]	31.1 (22–36)	28.3 (23–36)	39.6 (38–41)	0.068	0.003
Fetal weight USG [g]	1761 (507–2482)	1642 (612–2412)	3620 (3238–4216)	0.136	<0.001
BMI	27.3 (24.4–28.3)	25.8 (23.6–29.12)	32.1 (29.8–35.2)	0.061	0.042
Vaginal pH	6.4 (5.9–7.2)	4.3 (4.0–5.2)	4.8 (4.4–5.5)	0.026	0.044
Hemoglobin [g%]	11.6 (10.3–14.3)	11.2 (10.6–13.9)	11.5 (11.2–12.3)	0.072	0.103
WBC [/1 mm³]	1071 (7358–13235)	9836 (8532–14533)	12300 (9275–13288)	0.211	0.178
Urine pH	6.3 (5.7–6.7)	5.9 (5.3–7.2)	6.0 (5.5–7.6)	0.06	0.078

p_1 – study group compared to control group; p_2 – study group compared to reference group; NA – not applicable.

Table 2. Analysis of concentration levels of selected biochemical markers

Concentration of markers [pg/mL]	Mean			Student's t-test p_1	Student's t-test p_2
	study group	control group	reference group		
iGFBP-1	177.97	144.57	158.93	0.056	0.096
IGFBP-2	429.72	424.00	422.36	0.695	0.753
L-selectin	2369.2	2379.9	2456.4	0.888	0.687
MIP-1d	25.01	27.79	24.78	0.092	0.132

p_1 – study group compared to control group; p_2 – study group compared to reference group.

Table 3. Analysis of concentration levels of selected biochemical markers – cont.

Concentration of markers [pg/mL]	Median			Mann–Whitney U test (p_1)	Mann–Whitney U test (p_2)
	study group	control group	reference group		
BDNF	42.22	38.82	40.93	0.062	0.112
BLC	32.25	34.66	31.78	0.491	0.621
Eotaxin-1	1.42	1.78	1.66	0.178	0.225
E-selectin	380.24	398.18	376.15	0.953	0.871
ICAM-1	435.66	420.22	341.61	0.699	0.575
MIP-3b	22.50	17.02	19.50	0.093	0.182
PECAM-1	26.34	29.15	31.91	0.248	0.154
VCAM-1	37.42	36.85	33.89	0.158	0.344

p_1 – study group compared to control group; p_2 – study group compared to reference group.

Table 4. Comparison of eotaxin-2 concentrations in the study group vs the control and reference groups (pg/mL)

Concentration of markers [pg/mL]	Mean	Median	Lower quartile	Upper quartile	Standard deviation	Standard error	p_1	p_2	p_3
Study group	9.22	7.45	5.03	11.0	5.64	0.66			0.075
Control group	13.76	10.22	7.34	17.46	8.31	2.29	0.037	0.014	
Reference group	14.14	11.90	9.78	16.88	7.26	1.94			

p_1 – study group compared to control group = 0.037 (Mann–Whitney U test); p_2 – study group compared to reference group = 0.014 (Mann–Whitney U test); p_3 – control group compared to reference group = 0.075 (Mann–Whitney U test).

Table 5. Analysis of sensitivity and specificity of pPROM dignosis based on Eotaxin-2 concentrations

Eotaxin-2 threshold value [pg/mL]	Sensitivity	95% CI	Specificity	95% CI
8.24	0.58	0.496 to 0.821	0.57	0.433 to 0872

with women with preterm labor and intact membranes and to women with physiological term labor (Table 4). Serum concentrations of eotaxin-2 below 8.24 pg/mL show significance as a potential pPROM biomarker with sensitivity of 0.58 and specificity of 0.57 (Fig. 1, Table 5).

Discussion

This study has shown that eotaxin-2 exhibits statistically lower concentrations in women with pPROM than in women in preterm labor and intact membranes or women in physiological term labor. This may be an important factor in the pathogenesis of pPROM, because eotaxin-2, like eotaxin-1, is responsible for the activation and chemotaxis of eosinophils,[12] as well as neutrophils, macrophages and T lymphocytes.[13] Its activity was observed in decidual fibroblasts. By modifying the apoptosis of decidual cells, eotaxin-2 may contribute to premature membrane weakening and rupture. It is worth noting that the concentration of eotaxin-2 receptors is dependent on estrogen, progesterone and placental gonadotropin.[14]

The obtained results indicate that eotaxin-2 may be a potential marker of pPROM, and may also play a role in the pathogenesis of premature rupture of membranes, which could increase the predictive value of this molecule. The biomarker potential of eotaxin-2 is to confirm rupture but not to predict latency between rupture and
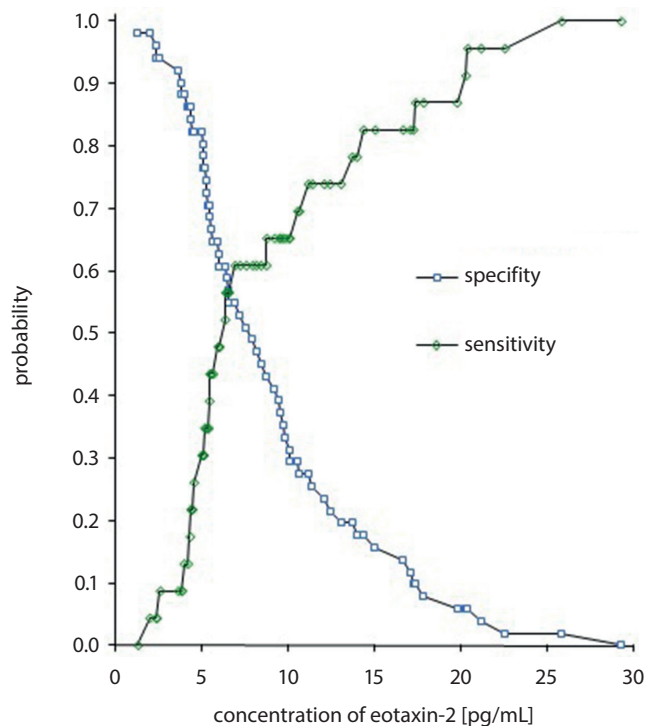
Fig. 1. ROC analysis of sensitivity and specificity of pPROM diagnosis based on eotaxin-2 concentrations

delivery. Despite excluding patients with clinical and laboratory symptoms of infection from the study, the existence of asymptomatic inflammation of the fetal membranes in women with pPROM cannot be ruled out, which might have affected the concentrations of biochemical markers. It remains unknown whether the reduction in eotaxin-2 concentrations in women with pPROM resulted from latent infection or the onset of labor.

When interpreting the results of concentrations of eotaxin-2 in women with pPROM, one should take into account physiological changes in the concentration of some proteins during pregnancy. However, regardless of gestational age, there are other mechanisms that affect the concentration of individual biochemical markers in the blood serum. Liu Y et al.[15] showed a change in calgranulin B concentrations (a protein whose expression appears on the surface of macrophages and epithelial cells of tissues in the acute phase of inflammation) synthesized in the fetal membranes and decidua in the course of intrauterine infections. These changes occur before the onset of clinical symptoms of infection, which gives grounds for searching for biochemical markers of pPROM among cytokines. In contrast, not all cytokine concentrations undergo modulation in the course of intrauterine inflammatory processes.[16]

Likewise, in this study no significant changes have been found in the concentrations of IGFBP-1, IGFBP-2, BDNF, L-selectin, E-selectin, ICAM-1, PECAM-1, VCAM-1, as well as MIP-1d, MIP-3b, eotaxin-1, and BLC. However, the role of expression of some cytokines in the diagnosis of early stages of intrauterine inflammations is indisputable and

some have already been studied in preterm labor.[17] Despite no women exhibiting symptoms of chorioamnionitis in the examined group (patients with clinical signs of infection were excluded from the study), the presence of such infections cannot be ruled out. Asymptomatic inflammatory changes in afterbirth can affect the immune system. So far, no pathomechanisms are known to occur with the reduction of eotaxin-2 concentration, directly corresponding to pPROM. There are only suggestions that alterations of immune reactivity, such as decreased cervical cytokines, may predispose to urinary tract infections, pPROM and preterm labor.[18] Physiological body mass index (BMI) alteration is evidenced during pregnancy. Although BMI, as a chronic stress state, is a strong pro-inflammatory nature disorder, little is known about how body composition interferes with inflammatory markers during pregnancy. Therefore, in this study, we evaluated the biomarkers in the reference group, which exclusively include obese subjects. This work demonstrates how the amount of fat mass interferes with the balance of cytokines. Changes in the concentration of pro-inflammatory cytokines may result in a reduced immune response, thus contributing to a symptomatic infection.[19–21] Chronic immune response may lead to a decrease in reactivity, manifested by a decrease in the concentration of some cytokines.[22,23] This study has shown eotaxin-2 to be such a phenomenon. In women with pPROM, eotaxin-2 concentrations were significantly lower compared with the values in the group of women with physiological labor. This interpretation of the reduced level of eotaxin-2 in women with pPROM is not the only one. Simhan et al. found that a reduced level of some cytokines may be a primary phenomenon resulting from genetic conditions, which causes decreased intrinsic resistance to intrauterine inflammations and promotes the occurrence of pPROM.[24] This is consistent with the studies of Dizon-Townson et al., according to which premature labor, at least in part, is genetically determined,[25] which allows a hypothesis that genetically determined decreased levels of eotaxin-2 may lead to pPROM. In view of encouraging results, the role of cytokines in the course of pPROM should be the aim of further research, as well as the use of eotaxin-2 as a pPROM marker.

Limitations

The weakness of the study is a poor sensitivity and specificity of this test and its small sample size, which is why the presented results should be considered as pilot ones. Further studies are necessary on larger groups, which would help define the exact role particular cytokines play in premature rupture of membranes.

Conclusions

We concluded that eotaxin-2 could be the basis for further studies on the use of this molecule as a biochemical

marker of pPROM. Defining the potential for eotaxin-2 as a biochemical marker of pPROM requires further investigation on a larger group of patients.

ORCID iDs

Grzegorz Raba   https://orcid.org/0000-0002-9196-8548
Marian Kacerovsky   https://orcid.org/0000-0001-9858-7900
Piotr Laudański   https://orcid.org/0000-0001-8955-8198

References

1. Caughey AB, Robinson JN, Norwitz ER. Contemporary diagnosis and management of preterm premature rupture of membranes. *Rev Obstet Gynecol*. 2008;1(1):11–22.
2. Raba G, Kotarski J. Evaluation of risk factors can help to predict preterm delivery within 7 days in women hospitalized for threatened preterm labour. *J Matern Fetal Neonatal Med*. 2016;29(19):3142–3146. doi:10.3109/14767058.2015.1115477
3. Lee T, Carpenter MW, Heber WW, Silver HM. Preterm premature rupture of membranes: Risks of recurrent complications in the next pregnancy among a population-based sample of gravid women. *Am J Obstet Gynecol*. 2003;188(1):209–213. doi:10.1067/mob.2003.115
4. Müller H, Storbeck T, Katzer D, et al. Neurological outcome at 24 months corrected age of prematurely born infants after preterm premature rupture of membranes (PPROM) of at least 7 days: A two-center experience in Germany. *J Matern Fetal Neonatal Med*. 33(8):1315–1320. doi:10.1080/14767058.2018.1517327
5. Pasquier JC, Picaud JC, Rabilloud M, et al. Neonatal outcomes after elective delivery management of preterm premature rupture of the membranes before 34 weeks' gestation. *Eur J Obstet Gynecol Reprod Biol*. 2009;143(1):18–23. doi:10.1016/j.ejogrb.2008.10.017
6. Friedman ML, McElin TW. Diagnosis of ruptured fetal membranes. Clinical study and review of the literature. *Am J Obstet Gynecol*. 1969;104(4):544–550. doi:10.1016/s0002-9378(16)34244-2.
7. Abdelazim IA, Abdelrazak KM, Al-Kadi M, Yehia AH, Abdulkareem AF. Fetal fibronectin (Quick Check fFN test) versus placental alpha microglobulin-1 (AmniSure test) for detection of premature rupture of fetal membranes. *Arch Gynecol Obstet*. 2014;290(3):457–464. doi:10.1007/s00404-014-3225-5
8. Zhang JM, An J. Cytokines, inflammation and pain. *Int Anesthesiol Clin*. 2007;45(2):27–37. doi:10.1097/AIA.0b013e318034194e
9. Yang L, Froio RM, Sciuto TE, Dvorak AM, Alon R, Luscinskas FW. ICAM-1 regulates neutrophil adhesion and transcellular migration of TNF-alpha-activated vascular endothelium under flow. *Blood*. 2005;106(2):584–592. doi:10.1182/blood-2004-12-4942
10. Polettini J, Cobo T, Kacerovsky M, et al. Biomarkers of spontaneous preterm birth: A systematic review of studies using multiplex analysis. *J Perinat Med*. 2017;45(1):71–84. doi:10.1515/jpm-2016-0097
11. Di Renzo GC, Roura LC, Facchinetti F, et al. Guidelines for the management of spontaneous preterm labor: Identification of spontaneous preterm labor, diagnosis of preterm premature rupture of membranes, and preventive tools for preterm birth. *J Matern Fetal Neonatal Med*. 2011;24(5):659–667. doi:10.3109/14767058.2011.553694
12. Gravett MG, Novy MJ, Rosenfeld RG, et al. Diagnosis of intra-amniotic infection by proteomic profiling and identification of novel biomarkers. *JAMA*. 2004;292(4):462–469. doi:10.1001/jama.292.4.462
13. Rüetschi U, Rosén A, Karlsson G, et al. Proteomic analysis using protein chips to detect biomarkers in cervical and amniotic fluid in women with intra-amniotic inflammation. *J Proteome Res*. 2005;4(6):2236–2242. doi:10.1021/pr050139e
14. Raba G, Baran P. Hemodynamic parameters following bilateral internal iliac arteries ligation as a treatment of intrapartum hemorrhage. *Ginekol Pol*. 2009;80(3):179–183. https://pubmed.ncbi.nlm.nih.gov/19382608/
15. Liu Y, Du C, Zhang R, Feng Z, Zhang J. Diagnostic value of amniotic fluid inflammator biomarkers for subclinical chorioamnionitis. *Int J Gynaecol Obstet*. 2016;134(2):160–164. doi:10.1016/j.ijgo.2016.01.007
16. Buhimschi CS, Weiner CP, Buhimschi IA. Proteomics, Part II: The emerging role of proteomics over genomics in spontaneous preterm labor/birth. *Obstet Gynecol Surv* 2006;61(8):543–553. doi:10.1097/01.ogx.0000228779.39568.59
17. Laudanski P, Lemancewicz A, Kuc P, et al. Chemokines profiling of patients with preterm birth. *Mediators Inflamm*. 2014;2014:185758. doi:10.1155/2014/185758
18. Laudanski P, Charkiewicz K, Kisielewski R, et al. Plasma C16-Cer levels are increased in patients with preterm labor. *Prostaglandins Other Lipid Mediat*. 2016;123:40–45. doi:10.1016/j.prostaglandins.2016.04.005
19. Soni S, Moldenhauer JS, Spinner SS, et al. Chorioamniotic membrane separation and preterm premature rupture of membranes complicating in utero myelomeningocele repair. *Am J Obstet Gynecol*. 2016;214(5):647.e1–7. doi:10.1016/j.ajog.2015.12.003
20. Gomez-Lopez N, Romero R, Xu Y, et al. Are amniotic fluid neutrophils in women with intraamniotic infection and/or inflammation of fetal or maternal origin? *Am J Obstet Gynecol*. 2017;217(6):693. doi:10.1016/j.ajog.2017.09.013
21. Kmiecik G, Niklińska W, Kuć P, et al. Fetal membranes as a source of stem cells. *Adv Med Sci*. 2013;58(2):185–195. doi:10.2478/ams-2013-0007
22. Lee SM, Park KH, Jung EY, Kook SY, Park H, Jeon SJ. Inflammatory proteins in maternal plasma, cervicovaginal and amniotic fluids as predictors of intra-amniotic infection in preterm premature rupture of membranes. *PLoS One*. 2018;13(7):e0200311. doi:10.1371/journal.pone.0200311
23. Marvin KW, Keelan JA, Eykholt RL, Sato TA, Mitchell MD. Use of cDNA arrays to generate differential expression profiles for inflammatory genes in human gestational membranes delivered at term and preterm. *Mol Hum Reprod*. 2002;8(4):399–408. doi:10.1093/molehr/8.4.399
24. Simhan HN, Caritis SN, Krohn MA, Martinez de Tejada B, Landers DV, Hillier SL. Decreased cervical proinflammatory cytokines permit subsequent upper genital tract infection during pregnancy. *Am J Obstet Gynecol*. 2003;189(2):560–567. doi:10.1067/s0002-9378(03)00518-0
25. Dizon-Townson DS. Preterm labour and delivery: A genetic predisposition. *Paediatr Perinat Epidemiol*. 2001;15(2):57–62. doi:10.1046/j.1365-3016.2001.00008.x

Radionuclide-guided sentinel lymph node mapping in urachal cancer

Wojciech Połom[1,A–D], Wojciech Cytawa[2,B], Anna Połom[3,B,C], Edyta Szurowska[3,C], Piotr Lass[2,C], Marcin Matuszewski[1,F]

[1] Department of Urology, Medical University of Gdańsk, Poland

[2] Department of Nuclear Medicine, Medical University of Gdańsk, Poland

[3] Department of Radiology, Medical University of Gdańsk, Poland

A – research concept and design; B – collection and/or assembly of data; C – data analysis and interpretation;
D – writing the article; E – critical revision of the article; F – final approval of the article

Address for correspondence
Wojciech Połom
E-mail: wojtek.polom@gmail.com

Abstract

Background. Urachal cancer gives metastases through the lymph nodes (LNs). No lymphadenectomy scheme in the case of this cancer exist, yet it is proposed as a staging procedure. An assessment of lymphatic outflow from the tumor site with the use of single-photon emission computed tomography/computed tomography (SPECT/CT) lymphangiography is possible for staging purposes.

Objectives. To perform the mapping of the LNs draining the lymph from urachal cancer with the use of radioisotope-based technique and to propose the lymphadenectomy template in case of urachal cancer.

Material and methods. A prospective study was conducted in 5 patients with urachal cancer. The 99m-technetium (Tc-99m)-nanocolloid was injected during a cystoscopy prior to the surgery. Lymphangiography was performed using SPECT/CT. A radioactive LNs analysis with the use of a hand-held gamma-ray detection probe was conducted during the surgery and the sentinel lymph node (SLN) biopsy procedure was performed. An additional lymphadenectomy containing the lymphatic basin of identified radioactive LNs was performed.

Results. In all cases lymphatic outflow from the urachal tumor to the LNs was present. Preoperative SPECT/CT allowed detecting the activity of the radiotracer in the common iliac region in all the studied patients. In 3 cases, bilateral lymphatic outflow, and in 2 cases, unilateral lymphatic outflow was observed. All preoperatively visualized LNs were found and excised with the use of a gamma-ray detection probe during a lymphadenectomy. In all cases, SLNs did not contain metastases.

Conclusions. Mapping of the LNs draining the lymph from urachal cancer with the use of radiotracer is possible. Lymphatic outflow in the case of this cancer can be both unilateral and bilateral. No recommendations about the extension of lymphadenectomy are proposed. We recommend individual assessment and treatment based on additional knowledge about lymphatic outflow. This allows for minimally invasive yet targeted treatment as an SLN basin lymphadenectomy.

Key words: lymphadenectomy, urachal cancer, lymphangiography, single-photon emission computed tomography/computed tomography, dynamic sentinel lymph node biopsy

Background

The urachus is a structure measuring from 5 cm up to 10 cm that connects allantois and the bladder of the fetus. It consists of 3 layers: the luminal layer composed of cuboidal or transitional epithelium, the intermediate connective tissue, and the outer layer of smooth muscle. In the 4th to 5th month of fetus development, the bladder descends caudally, urachal lumen is stretched and then obliterated until median umbilical ligament is formed, which joins the bladder dome with the umbilicus.[1,2] Urachal cancer is a rare non-urothelial carcinoma. Its incidence rate varies from 0.35% to 0.7% out of all bladder cancers and from 22% up to 35% of adenocarcinomas of the bladder.[3,4] It is formed from the malignant transformation of enteric epithelium located in the urachus, between the bladders dome and the umbilicus. The first description of this malignancy was published in 1930 by Begg.[5] There are only few case series about this neoplasm in the literature and therefore the management of each patient should be performed with an individual approach.[1,6,7] This cancer is most common in men and most of the cases are in patients who are over the age of 50 years.[1]

There are 5 histological subtypes of urachal carcinoma described by Grignon et al.[8] The first symptom of the disease is usually hematuria, which usually occurs when the disease is already advanced. Mucosuria is another, very unusual symptom, found in 9% of patients, which indicates the possibility of urachal pathology.[4] If urachal cancer is suspected, a diagnostic evaluation, physical examination and urinalysis with cytology should be performed and medical history should be taken. Cystoscopy must be performed to evaluate if the tumor penetrates the bladder urothelium and to determine the decision for a transurethral biopsy. Further diagnosis – the evaluation of the local extent, lymph node (LN) involvement and possible metastases – should consist of magnetic resonance imaging (MRI) or computed tomography (CT) of the abdomen and pelvis.

The most common metastatic sites are diagnosed in LNs, peritoneum and lungs. There are some characteristic features of the urachal tumor in imaging findings that help differentiate it from other bladder tumors. Solid urachal masses and calcification in the tumor mass as well as elevated carcinoembryonic antigen indicate urachal adenocarcinoma.[9] Moreover, an elevated level of carbohydrate antigen 19-9 has been described as a tumor marker for some urachal carcinomas.[10]

There are few clinicopathological criteria that can be helpful in diagnosing urachal cancer. The criteria include: tumor localized in the bladders dome, absence of cystitis cystica as well as cystica glandularis, invasion of the bladder's muscle layer and deeper layers with a sharp margin between the healthy bladder epithelium and the tumor, its extension into the bladder wall and space of Retzius, abdominal wall or the umbilicus, the presence of urachal remnants in the tumor, and no evidence of primary neoplasm elsewhere.[1,4] Not every urachal cancer is associated with the urachal remnants. Some of them develop in the presence of cystitis cystica or cystica gladularis.[11] All cases diagnosed as adenocarcinoma of the bladder dome should be treated as urachal cancer until proven otherwise.[11] Sheldon et al. proposed a staging system that is commonly used.[4] However, several other staging systems have also been proposed.[12,13]

The treatment of the urachal cancer is rather ineffective. Surgical management consisting of partial and radical cystectomy and en bloc removal of the median umbilical ligament with the umbilicus[14] is the main therapeutic option. A retrospective study was performed including 40 patients with urachal adenocarcinoma where surgical treatment was associated with higher survival rates.[13] When authors compared partial to total cystectomy, they observed no difference in survival between those 2 groups of patients,[15] but recurrence rate after partial cystectomy was higher compared to radical cystectomy.[1] Extensive tumor resection in non-metastatic patients can be curative in most cases.[14] As for today, there is no evidence of the curative effect of lymphadenectomy, chemotherapy or radiotherapy.[4,16] Even if the urachal cancer spreads through the LNs, no lymphadenectomy template, which should be performed during the operation, is proposed. There is also no data about the lymphatic regions where metastases are found during a lymphadenectomy. Several cases of chemotherapy treatment based on irinotecan or oxaliplatin with or without bevacizumab have been reported, as it is the first-line chemotherapy for metastatic colon cancer. This regiment was used because urachal adenocarcinomas are often histologically similar to adenocarcinomas of the gastrointestinal tract,[17] but the final result of the chemotherapeutic treatment does not bring expected results.

Objectives

The goal of the present study was to assess the lymphatic outflow from the urachal cancer with the use of a radioactive tracer and mapping of first LNs draining the tumor site with the use of SPECT/CT lymphangiography. Moreover, we wanted to determine the possibility of sentinel lymph nodes (SLNs) mapping in case of urachal cancer with the use of a 99m-technetium (Tc-99m) radioisotope and compare the results of preoperative hybrid single-photon emission computed tomography/computed tomography (SPECT/CT) lymphangiography with intraoperative detection of LNs containing radioisotope with the use of a handheld gamma ray detection probe. An additional aim was to propose a scheme of individually tailored lymphadenectomy containing the SLN and its basin in case of this cancer. To our knowledge, this is the first study describing this issue.

Material and methods

Five patients with diagnosed urachal tumor were prospectively included in our study. The diagnosis of urachal cancer was based on tumor localization in cystoscopy, transurethral tumor biopsy with histopathology of adenocarcinoma, and CT scan of the pelvis and abdomen. The exclusion criteria were previous chemotherapy, pelvic radiotherapy, and previous abdominal operations. The study was approved by the local ethics committee (Independent Bioethics Committee for Scientific Research at Medical University of Gdańsk, approval No. NKBBN/522/2017-2018).

An injection of the radiocolloid was performed 1 day before the scheduled operation. The 99m-technetium-nanocolloid (Nano-Albumon; Medi-Radiopharma Kft. Érd, Hungary) was injected during the cystoscopy procedure under local anesthesia. Radiocolloid particles of 10–100 nm and the total activity of 1 mCi dissolved in 1 mL were used. The injection was performed with the use of Williams cystoscopy needle 3.7 F (Cook Urological, Spencer, USA) around the location of the tumor submucosally divided into 4 portions of 0.25 mCi per injection.

Twelve hours after the radiotracer injection, hybrid SPECT/CT lymphangiography was performed in each case with the use of the Symbia™ T6 SPECT/CT (Siemens, Erlangen, Germany) dual-head γ-camera equipped with a six-row spiral CT scanner.

The SPECT/CT acquisition parameters used during the procedure were as follows: 128 × 128 matrix, 64 frames at 30 s each, low-dose CT without an intravenous injection of contrast media. The imaging time was 30 miN. Syngo software (Copyright© Siemens AG, Berlin and Munich, 2008) was used for the reconstruction and fusion of the images. Additionally, a three-dimensional (3D) reconstruction of superimposed images was performed for better visualization of the structures before the operation. Any focal activity of the radiotracer detected in the region of interest excluding the site of injection was considered to be an SLN. In each case, a partial cystectomy with en block resection of the median umbilical ligament including the umbilicus was performed. Furthermore, during the surgery radioactive LNs analysis with the use of hand-held gamma ray detection probe (Neoprobe 2000; Neoprobe Corporation) was conducted

for radiotracer detection. Afterwards, dynamic sentinel lymph node biopsy (DSLNB) procedure was performed with additional lymphadenectomy containing the lymphatic basin of identified radioactive LNs. Criteria for the SLN was radioactivity at least 10 times higher than the background tissue.

Results

Clinicopathological features of the described group of patients are presented in Table 1. The mean age of patients was 64.4 years (range: 56–73 years). The study included 4 men and 1 woman. All the patients reported gross hematuria during the diagnosis; in 3 patients, irritative voiding symptoms such as urgency were present. Mucinuria was present in 3 patients. Moreover, 1 patient reported suprapubic and lumbar pain. In the course of further radiological studies, distant metastasis to the spinal cord (lumbar part) was diagnosed. In all cases, an ultrasound examination of the abdomen with a special focus on the bladder was performed (Fig. 1).

All the patients underwent a cystoscopy for the assessment of the presence of the local extension to the bladder according to the Sheldon scale (4) with tumor biopsy (Fig. 2).

Fig. 1. Urachal cancer seen at the dome of the bladder with the use of ultrasound examination

Table 1. Clinicopathological features of the described group of patients

Case	Sex	Symptoms	Tumor localization	Tumor histology	Sheldon stage
1	M	gross hematuria; mucinuria, suprapubic pain; lumbar pain	dome	mucinous adenocarcinoma	IVB
2	M	gross hematuria; urgency	dome	adenocarcinoma; NOS	IIIA
3	M	gross hematuria	dome	mucinous adenocarcinoma	IIIA
4	F	gross hematuria; mucinuria; urgency	dome	mucinous adenocarcinoma	IIIA
5	M	gross hematuria; mucinuria; urgency	dome	adenocarcinoma; NOS	IIIC

M – male; F – female; NOS – not otherwise specified.

206

W. Połom et al. Lymph node mapping in urachal cancer
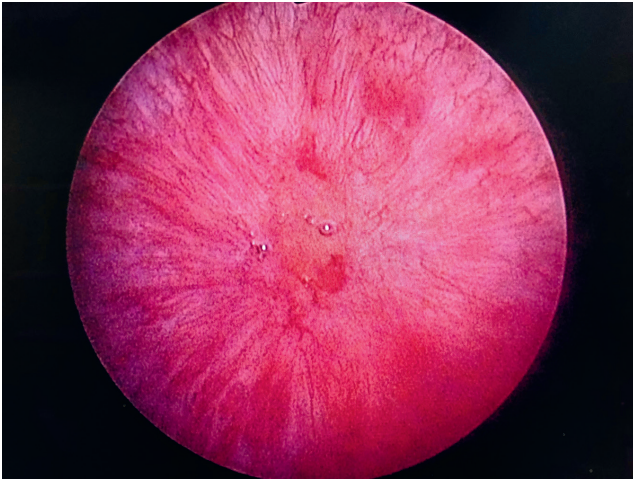
Fig. 2. Urachal cancer seen during cystoscopy examination at the bladder dome

Fig. 4. Urachal cancer with extension to the bladder wall (stage IIIA) seen during partial cystectomy
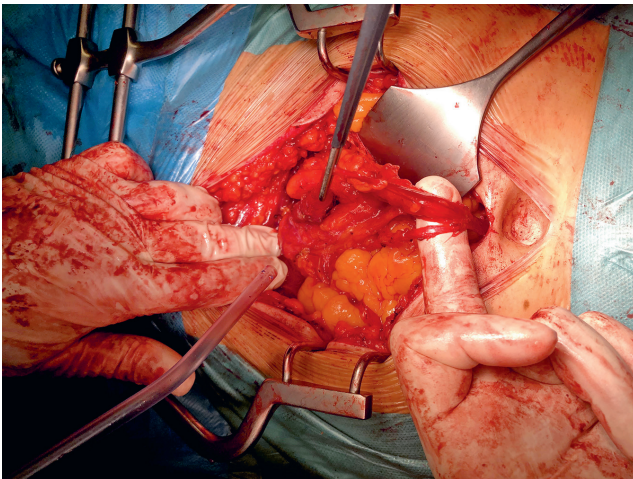
Fig. 3. Excision of the remnants of the urachus connecting umbilicus with the doom of the bladder
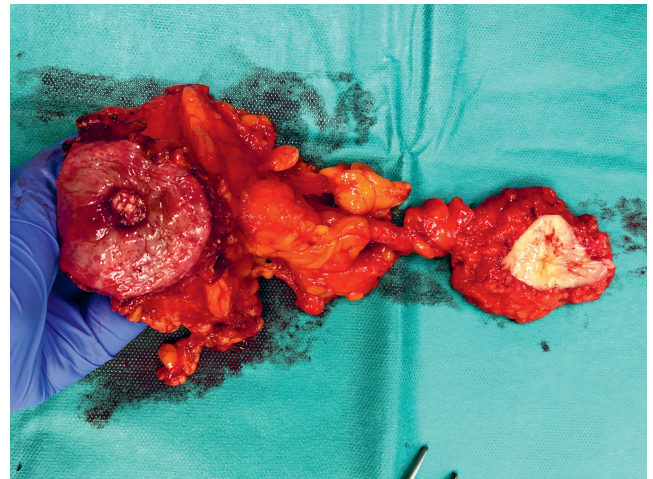
Fig. 5. Specimen after excision containing the umbilicus, remnants of the urachus and urachal cancer with the fragment of bladder wall after partial cystectomy

For a potential distant metastases evaluation, a contrast-enhanced CT examination of the chest, abdomen and pelvis was conducted. In 3 cases, partial cystectomy, and in 2 cases total cystectomy with umbilectomy were performed (Fig. 3–5).

In each case, the DSLNB procedure was performed with bilateral pelvic lymph node dissection (PLND) containing the basin of the SLNs. In all cases, we diagnosed the lymphatic outflow with the use of Tc-99m-nanocolloid from the urachal tumor site to the external iliac lymphatic region during preoperative SPECT/CT lymphoscintigraphy. In 3 cases – bilateral, and in 2 cases – unilateral lymphatic outflow was observed. In both cases with unilateral outflow, SLNs were located in the right iliac region. A 3D reconstruction of the images allowed for a better visualization of the position of the radioactive LNs according to the surrounding structures, which enabled a better surgeon's preparation before the scheduled operation (Fig. 6).

All LNs preoperatively identified as SLNs on SPECT/CT were found intraoperatively with the use of hand-held gamma ray detection probe and separately excised during a lymphadenectomy for histopathologic examination. In all cases neither SLNs nor the rest of excised LNs contained metastases. The total number of excised SLNs was 8 and the total number of other removed LNs was 41 (mean: 8.2). The analysis of lymphatic outflow and excised LNs analysis is presented in Table 2.

Discussion

Urachus is an embryological remnant of the urogenital sinus and allantois. Its spontaneous closure is usually observed after forming the medium umbilical ligament as its remnant in the third trimester. In about 1/3 of adults, urachal remnants persist as a tubular or cystic structure from which cancer can develop.[18] Morphologically, urachal

Fig. 6. SPECT/CT lymphangiography illustrating the lymphatic outflow from the urachal cancer to the common iliac lymphatic region on the right

Table 2. Lymphatic outflow and lymph nodes analysis

Case	Lymphatic outflow	SLNs localization in SPECT/CT	SLNs localization gamma probe intraoperatively	Surgery	Number of SNLs	Number of other nodes	SLN metastases	Lymph nodes metastases
1	unilateral	external iliac right	external iliac right	PC + DSLNB + PLND	1	10	no	no
2	bilateral	common iliac right and left	common iliac right and left	TC + DSLNB + PLND	2	8	no	no
3	bilateral	common iliac right and left	common iliac right and left	PC+ DSLNB + PLND	2	8	no	no
4	bilateral	external iliac right and left	external iliac right and left	TC + DSLNB + PLND	2	6	no	no
5	unilateral	external iliac right	external iliac right	PC+ DSLNB + PLND	1	9	no	no

PC – partial cystectomy; TC – total cystectomy; DSLNB – dynamic sentinel lymph node biopsy; PLND – pelvic lymph node dissection; SLNs – sentinel lymph nodes.

cancers are all adenocarcinomas but not all adenocarcinomas of the bladder are urachal cancers. Roughly, 10–40% of bladder adenocarcinomas are reported to be of urachal origin.[1,12,19] Urachal cancer is aggressive, yet its biologic behavior presents a long and silent course. Due to its rare incidence, there is not enough literature about its treatment

and biology. There are several factors affecting the prognosis of urachal cancer. The most important ones include margin status, LN metastases, stage of the disease, distant metastases, and pathologic type.[20–22] Signet ring cell adenocarcinoma as well as small cell carcinoma are the most aggressive types and cause a local invasion and dissemination even when they appear to be localized.[23] On the other hand, mucinous adenocarcinoma has a strong tendency for a local invasion, which can result in peritoneal dissemination with a low frequency of distant metastasis.[24] Urachal cancer is reported to have male predilection.[1,2,12] Our study confirms this tendency, as male to female ratio was 4:1.

The prognosis for the patients with urachal cancer is poor, with five-year survival rates reported to be less than 50%. The reason for that are: late occurrence of symptoms, extravesical growth of the tumor and the risk of early metastases.[25] A metastatic disease can be often diagnosed in case of the tumor not invading the bladder wall, diagnosed because of metastatic symptoms.[26] Typical symptoms, such as gross hematuria and mucinuria, do not occur until the tumor invades the bladder wall.[27] Other symptoms include dysuria, abdominal pain, suprapubic mass, and discharge of blood, pus and mucus from the umbilicus.[1,12,22] In our study, all patients reported gross hematuria. Mucinuria as well as urgency were present in 3 cases. One patient reported lumbar pain which in further studies corresponded to the metastatic site. The most commonly described sites of distant metastases are lungs, bone with the prevalence to spine, peritoneum, LNs, and brain.[2] In our study group, only 1 patient was diagnosed with distant metastases to the lumbar part of the spine. We have not found any metastases to the LNs. The median survival rate for patients with a metastatic disease is less than 24 months.[26] Patients with early stage disease have a better prognosis.[12,16]

Primary surgical resection in case of non-metastatic patients is recommended. It consists of a partial cystectomy and en bloc excision of the urachal tumor, urachal tract and umbilicus. In some cases, adjacent removal of organs involved with the cancer is required.[28] Both partial and radical cystectomy provide comparable outcomes.[15] In our group of patients, 3 underwent partial cystectomy and 2 total cystectomies because of conditions unrelated to the tumor. Survival rate is lower for patients who did not undergo umbilectomy.[2] What is more, authors agree that negative surgical margin status is one of the most significant predictors of prognosis.[2,14]

Urachal cancer gives metastases through LNs, yet it is not clear which of them are involved in lymphatic outflow from the tumor site, how many LNs should be excised and which lymphatic regions should be excised during the lymphadenectomy procedure. What is more, lymphatic outflow from the bladder in case of bladder tumor is complicated. Both unilateral and bilateral lymphatic outflow schemes were proven. Authors also describe the position of SLNs in non-standard localizations.[29] Other urological cancers like penile cancer often have the same tendency in lymphatic outflow.[30] There is no data available about lateralization of the lymphatic outflow in case of urachal cancer. Moreover, distant metastases to the parotid LNs are described without pelvic LNs involvement,[31] which can support the hypothesis about unpredictable metastatic spread.

Some authors suggest that there is no benefit in survival for patients who underwent pelvic lymphadenectomy when compared with the patients who did not undergo this procedure.[15] Chen et al. suggested that this procedure should be performed in case of patients with LNs involvement confirmed with preoperative imaging studies. In their series, 5 out of 17 patients underwent lymphadenectomy. In 2 cases, LNs metastases were confirmed, while, in 3 cases, LNs were negative in pathological examinations.[6] It is not clear why the authors decided to perform PLND in 5 patients while LNs metastases were present only in 2 cases in preoperative CT scans, and what radiological criteria were applied to distinguish between metastatic and non-metastatic LNs involvement. In early stages of the disease, micro-metastatic disease has to be considered. Micro-metastases are defined as measuring between 0.2 mm and 2 mm, and as for now, there is no radiological method to distinguish them from the non-metastatic LNs. When performing DSLNB for the staging purposes, we can expect to find the LNs with the most chance to acquire metastatic tumor cells from the tumor site. With the use of this technique, we can also avoid vast pelvic lymphadenectomy, which can cause side effects and may not bring additional benefits. Lymph nodes after DSLNB are also examined by a pathologist according to the SLN paragraph which differs from the standard one and which can detect a micro-metastatic disease. In our group of patients, preoperative radiological examinations did not suggest metastases to LNs. The performed SPECT/CT revealed unilateral lymphatic outflow in 2 cases and bilateral in 3 cases. No metastases to SLNs nor metastatic cells were found in the rest of the excised LNs.

It is still debatable whether to routinely perform a bilateral lymphadenectomy in patients qualified for surgical treatment because of urachal cancer. The procedure may be challenging and cause postsurgical complications, but on the other hand, omitting lymphadenectomy results in the lack of information about the stage of the disease. This can have a significant effect on the course of the adjuvant treatment.

Patients with a metastatic disease can be treated effectively with systemic chemotherapy, but as for now, no standard chemotherapeutic regiment is proposed. Various chemotherapeutics have been used with different treatment results.[32] Chemotherapeutics used for bladder cancer based on cisplatin were used in patients with urachal cancer, with limited clinical effect.[33] Other regiments including 5-fluorouracil (5-FU) were expected to be efficient because of the histological and clinical similarities of urachal to colonic adenocarcinoma.[34] While comparing

studies with the use of cisplatin-based, 5-FU-based and combined cisplatin + 5-FU-based regiments, the highest response rate and lowest progression was observed in case of the use of combined regiment.[25] Other authors suggest the usage of neoadjuvant gemcitabine + cisplatin (GC) and subsequently l-leucovorin + 5-FU + irinotecan (FOLFIRI) regiment for mucinous adenocarcinoma, aiming at tumor shrinkage allowing the curative surgery.[24]

Our primary results can be used as a recommendation to perform an individual assessment of patients with urachal cancer and perform targeted lymphadenectomy containing the SLN and its basin, depending on the results of preoperative SPECT/CT lymphoscintigraphy. In case of a metastatic disease to the LNs and distant metastases, adjuvant chemotherapy should be implemented. In our group of patients, we did not find a micro-metastatic disease while performing pathological examination on SLNs, so no recommendations in that case can be presented.

Conclusions

Urachal cancer gives metastases through the LNs. In case of this cancer, no lymphadenectomy scheme is proposed, and no range of the lymphatic tissue excision is accepted as a standard. In case of urachal cancer, lymphadenectomy is performed as a staging procedure, but it does not bring any benefit for the patient's survival. Its performance can lead to adverse events and complications during and after the surgery, like lymphoedema and lymphocele.

An assessment of the lymphatic outflow from the urachal cancer with the use of radioactive tracer and mapping of first LNs draining the tumor site is possible. An assessment of lymphatic outflow from the tumor site with the use of SPECT/CT lymphangiography is feasible and gives additional information to the surgeon, allowing for a better planning of the operation.

Lymphatic outflow from the injection site around the urachal cancer can be unilateral and bilateral. The DSLNB in case of urachal cancer with the use of an intraoperative gamma ray detection probe is possible. A combination of both techniques – preoperative SPECT/CT lymphangiography with 3D images reconstruction and an intraoperative gamma ray detection probe – allows the surgeon for an excellent estimation of the localization of radioactive LNs.

Since no recommendations about the extension of lymphadenectomy are proposed, we recommend an individual assessment of each patient and treatment based on additional knowledge about the lymphatic outflow. This allows for a minimally invasive yet targeted treatment as an SLN basin lymphadenectomy. This technique can spare the performance of a bilateral pelvic lymphadenectomy in case of unilateral lymphatic outflow.

Further studies on a larger group of patients are needed for a better lymphatic outflow assessment in case of this cancer.

ORCID iDs

Wojciech Połom ● https://orcid.org/0000-0002-2234-1151
Wojciech Cytawa ● https://orcid.org/0000-0002-9583-7721
Anna Połom ● https://orcid.org/0000-0002-5644-1134
Edyta Szurowska ● https://orcid.org/0000-0002-7042-4381
Piotr Lass ● https://orcid.org/0000-0001-7144-1370
Marcin Matuszewski ● https://orcid.org/0000-0002-7799-685X

References

1. Gopalan A, Sharp DS, Fine SW, et al. Urachal carcinoma: A clinicopathologic analysis of 24 cases with outcome correlation. *Am J Surg Pathol.* 2009;33(5):659–68. doi:10.1097/PAS.0b013e31819aa4ae
2. Ashley RA, Inman BA, Sebo TJ, et al. Urachal carcinoma: Clinicopathologic features and long-term outcomes of an aggressive malignancy. *Cancer.* 2006;107(4):712–720. doi:10.1002/cncr.22060
3. Reuter VE, Al-Ahmadie H. Urothelial tract: Renal pelvis, ureter, urinary bladder, and urethra. *Eur Urol.* 2015;68(6): 970–977. doi:10.1016/j.eururo.2015.07.039
4. Sheldon CA, Clayman R V, Gonzalez R, Williams RD, Fraley EE. Malignant urachal lesions. *J Urol.* 1984;131(1):1–8. doi:10.1016/s0022-5347(17)50167-6
5. Begg RC. The urachus: Its anatomy, histology and development. *J Anat.* 1930;64(Pt 2):170–183.
6. Chen D, Li Y, Yu Z, et al. Investigating urachal carcinoma for more than 15 years. *Oncol Lett.* 2014;8(5):2279–2283. doi:10.3892/ol.2014.2502
7. Quan J, Pan X, Jin LU, et al. Urachal carcinoma: Report of two cases and review of the literature. *Mol Clin Oncol.* 2017;6(1):101–104. doi:10.3892/mco.2016.1082
8. Grignon DJ, Ro JY, Ayala AG, Johnson DE, Ordonez NG. Primary adenocarcinoma of the urinary bladder: A clinicopathologic analysis of 72 cases. *Cancer.* 1991;67(8):2165–2172. doi:10.1002/1097-0142(19910415)67:8<2165::aid-cncr2820670827>3.0.co;2-m
9. Carr NJ, McLean AD. A mucinous tumour of the urachus: Adenoma or low grade mucinous cystic tumour of uncertain malignant potential? *Adv Clin Path.* 2001;5(3):93–97.
10. Shinohara T, Misawa K, Sano H, Okawa Y, Takada A. Pseudomyxoma peritonei due to mucinous cystadenocarcinoma in situ of the urachus presenting as an inguinal hernia. *Int J Clin Oncol.* 2006;11(5): 416–419. doi:10.1007/s10147-006-0594-1
11. Henly DR, Farrow GM, Zincke H. Urachal cancer: Role of conservative surgery. *Urology.* 1993;42(6):635–659. doi:10.1016/0090-4295(93)90526-g
12. Molina JR, Quevedo JF, Furth AF, Richardson RL, Zincke H, Burch PA. Predictors of survival from urachal cancer: A Mayo Clinic study of 49 cases. *Cancer.* 2007;110(11):2434–2440. doi:10.1002/cncr.23070
13. Pinthus JH, Haddad R, Trachtenberg J, et al. Population based survival data on urachal tumors. *J Urol.* 2006;175(6):2042–2047; discussion 2047. doi:10.1016/S0022-5347(06)00263-1
14. Herr HW, Bochner BH, Sharp D, Dalbagni G, Reuter VE. Urachal carcinoma: Contemporary surgical outcomes. *J Urol.* 2007;178(1): 74–88; discussion 78. doi:10.1016/j.juro.2007.03.022
15. Bruins HM, Visser O, Ploeg M, Hulsbergen-van de Kaa CA, Kiemeney LALM, Witjes JA. The clinical epidemiology of urachal carcinoma: Results of a large, population based study. *J Urol.* 2012;188(4):1102–1107. doi:10.1016/j.juro.2012.06.020
16. Siefker-Radtke AO, Gee J, Shen Y, et al. Multimodality management of urachal carcinoma: The M.D. Anderson Cancer Center experience. *J Urol.* 2003;169(4):1295–1298. doi:10.1097/01.ju.0000054646.49381.01
17. Tran B, McKendrick J. Metastatic urachal cancer responding to FOLFOX chemotherapy. *Can J Urol.* 2010;17(2):5120–5123.
18. Schubert GE, Pavkovic MB, Bethke-Bedürftig BA. Tubular urachal remnants in adult bladders. *J Urol.* 1982;127(1):40–42. doi:10.1016/s0022-5347(17)53595-8
19. Wright JL, Porter MP, Li CI, Lange PH, Lin DW. Differences in survival among patients with urachal and nonurachal adenocarcinomas of the bladder. *Cancer.* 2006;107(4):721–728. doi:10.1002/cncr.22059
20. Martinez-Cornelio A, Flores-Lopez D, Ojeda RF, Quintero-Becerra J, Hernandez-Toriz N. Surgical experience with urachal carcinoma [in Spanish]. *Cir Cir.* 2009;77(1):33–38.
21. Egevad L, Hakansson U, Grabe M, Ehrnstrom R. Urachal signet-cell adenocarcinoma. *Scand J Urol Nephrol.* 2009;43(1):88–91. doi:10.1080/00365590802361914

22. Zhang J, Wu J. Options for diagnosis and treatment of urachal carcinoma. *Asia Pac J Clin Oncol.* 2013;9(2):117–122. doi:10.1111/j.1743-7563.2012.01592.x

23. Loggie BW, Fleming RA, Hosseinian AA. Peritoneal carcinomatosis with urachal signet-cell adenocarcinoma. *Urology.* 1997;50(3):446–448. doi:10.1016/S0090-4295(97)00247-1

24. Yasui M, Jikuya R, Tatenuma T, et al. Urachal carcinoma with peritoneal dissemination treated with chemotherapy and surgical resection leading to prolonged survival with no recurrence. *Case Rep Urol.* 2018;2018:9836154. doi:10.1155/2018/9836154

25. Szarvas T, Modos O, Niedworok C, et al. Clinical, prognostic, and therapeutic aspects of urachal carcinoma: A comprehensive review with meta-analysis of 1,010 cases. *Urol Oncol.* 2016;34(9):388–398. doi:10.1016/j.urolonc.2016.04.012

26. Hayashi T, Yuasa T, Uehara S, et al. Clinical outcome of urachal cancer in Japanese patients. *Int J Clin Oncol.* 2016;21(1):133–138. doi:10.1007/s10147-015-0866-8

27. Siefker-Radtke A. Urachal adenocarcinoma: A clinician's guide for treatment. *Semin Oncol.* 2012;39(5):619–624. doi:10.1053/j.seminoncol.2012.08.011

28. Paras FAJ, Maclennan GT. Urachal adenocarcinoma. *J Urol.* 2008;180(2):720. doi:10.1016/j.juro.2008.05.039

29. Polom W, Markuszewski M, Cytawa W, Lass P, Matuszewski M. Radioguided lymph node mapping in bladder cancer using SPECT/CT and intraoperative gamma-probe methods. *Clin Nucl Med.* 2016;41(8):362–367. doi:10.1097/RLU.0000000000001224

30. Markuszewski M, Polom W, Cytawa W, Czapiewski P, Lass P, Matuszewski M. Comparison of real-time fluorescent indocyanine green and (99m)Tc-nanocolloid radiotracer navigation in sentinel lymph node biopsy of penile cancer. *Clin Genitourin Cancer.* 2015;13(6):574–580. doi:10.1016/j.clgc.2015.06.005

31. Shimoyama T, Horie N, Yamada T, Ide F. Parotid lymph node metastasis from adenocarcinoma of the urachus. *Dentomaxillofac Radiol.* 2000;29(3):185–188. doi:10.1038/sj/dmfr/4600525

32. Yazawa S, Kikuchi E, Takeda T, et al. Surgical and chemotherapeutic options for urachal carcinoma: Report of ten cases and literature review. *Urol Int.* 2012;88(2):209–214. doi:10.1159/000334414

33. Miyata Y, Sagara Y, Matsuo T, et al. Response of recurrent urachal cancer to gemcitabine and cisplatin therapy: A case report and literature review. *Anticancer Res.* 2011;31(6):2335–2338.

34. Kanamaru T, Iguchi T, Yukimatsu N, et al. A case of metastatic urachal carcinoma treated with FOLFIRI (irinotecan and 5-fluorouracil/leucovorin) plus bevacizumab. *Urol Case Rep.* 2014;3(2):9–11. doi:10.1016/j.eucr.2014.11.004

Wharton's jelly-derived mesenchymal stem cells in the treatment of four patients with alopecia areata

Anna Czarnecka[1,2,A–D,F], Agnieszka Odziomek[1,B–D], Magdalena Murzyn[3,B,E],
Joanna Dubis[1,C,E], Marta Bagłaj-Oleszczuk[4,B,C], Anita Hyncewicz-Gwóźdź[4,A,D,F]

[1] Regional Specialist Hospital, Research and Development Centre, Wrocław, Poland

[2] Faculty of Physiotherapy, University School of Physical Education, Wrocław, Poland

[3] The Polish Stem Cells Bank, Warszawa, Poland

[4] Department of Dermatology, Venereology and Allergology, Wroclaw Medical University, Poland

A – research concept and design; B – collection and/or assembly of data; C – data analysis and interpretation;
D – writing the article; E – critical revision of the article; F – final approval of the article

Address for correspondence
Anita Hyncewicz-Gwóźdź
E-mail: anhryn@gmail.com

Abstract

Background. Alopecia areata (AA) is the second most common cause of non-scarring alopecia. Little is known on the etiopathogenesis of AA. It is considered an autoimmune disease, with T lymphocytes and antibodies directed against hair follicle structures. Topical and systemic therapies are used for the treatment of AA, but none of the therapies used to date have a permanent therapeutic effect.

Objectives. To evaluate the efficacy and safety of AA treatment through a single intradermal injection of a suspension of allogeneic MSCs extracted from Wharton's jelly (WJ-MSCs) into the alopecia foci.

Material and methods. The study involved 4 AA patients who underwent experimental therapy with a suspension of WJ-MSCs. The AA intensity was measured using the SALT score. This measure was performed 3 times during treatment: 1st measure ($SALT_0$) prior to treatment; 2nd measure ($SALT_{12}$) 12 weeks after the treatment; and 3rd measure ($SALT_{24}$) 24 weeks after the treatment. Furthermore, during each follow-up visit (6, 12, 18, and 24 weeks after the administration of WJ-MSCs) the patient's general condition (physical examination) and local condition were assessed, their mood was evaluated, and a photo of the scalp was taken.

Results. Hair regrowth was observed in all patients by an average of 67% at the sites where the cell suspension was administered. In all cases, we observed greater dynamics of hair regrowth in the first 3 months after the treatment, with an average increase of 52.2%, compared to the following 3 months, with an average of 32%.

Conclusions. The results of the applied intradermal injections of an allogeneic WJ-MSC suspension were positive with hair growth observed in all participants and the therapy was found to be safe, with no side effects.

Key words: alopecia areata, Wharton's jelly, mesenchymal stem cells, MSC, WJ-MSC

Background

Alopecia areata (AA) is the 2nd most common cause of non-scarring alopecia after androgenic alopecia (AGA).[1] The prevalence is estimated at 2% and has increased tenfold since the 1970s when it affected 0.1–0.2% of the population.[2] It equally affects both genders.[1] The severity of the disease varies widely, from a single focus of a few centimeters in diameter to extensive hair loss in all or some regions of the body, including the scalp, eyebrows and eyelashes, and the rest of the body. In some patients, nail dystrophy has also been observed. The disease leads to a significant deterioration of patients' quality of life.[3] There are several clinical forms of the disease: focal hair loss (the most common), diffuse alopecia, ophiasis, total alopecia (total loss of scalp hair), and alopecia universalis (loss of all body hair).[4] Alopecia focal lesions are not usually accompanied by subjective complaints, although 14% of patients report itching or burning. The course of the disease is unpredictable, with 90% of patients experiencing recurrences after the 1st episode in the first 5 years, and some showing spontaneous remissions.[5]

Little is known on the AA etiopathogenesis. It is considered an autoimmune disease, with T lymphocytes and antibodies directed against hair follicle structures.[6] Indeed, histopathological examination of the skin reveals abundant perifollicular lymphocytic infiltrates,[7,8] and this infiltration mainly affects follicles in the anagen phase.[6]

The autoantigenic epitopes are thought to include melanin and melanin-related proteins, and keratinocyte antigens. In the pathogenesis of the disease, the loss of immune privilege is also important. Healthy hair follicles are classified as tissues with immune privilege, i.e., they do not induce an aggressive immune response when transplanted using an allogeneic regimen. The immunological privilege in healthy hair follicles is attributed to the reduced expression of class I major histocompatibility complex (MHC I) antigens on the keratinocytes, a lack of expression of these antigens on melanocytes and a lack of antigen-presenting cells in the lower part of the hair follicle, together with a small number of immunocompetent cells and the presence of immunosuppressive factors.[9,10]

Genome-wide association studies (GWAS) have identified various genes associated with the pathogenesis of AA (e.g., *IL2/IL21*, *IL2RA*, *CTLA4*, *ULBP3*, and *STX17*).[11] Genetic factors are also involved in the pathogenesis of AA, as the disease is also seen in first-degree relatives and monozygotic twins.[12,13] In 16% of patients, other autoimmune diseases are also present, most often vitiligo and autoimmune thyroid diseases.[1,2,12]

Topical and systemic therapies are used for the treatment of AA. In topical therapy, the following medications are used: glucocorticoids in the form of external preparations and injections into the affected skin, minoxidil, contact immunotherapy (e.g., diphenylcyclopropenone and cygnolin), and drugs administered systematically (e.g.,

glucocorticoids, methotrexate, cyclosporine, azathioprine, and sulfasalazine).[1,6,14] Moreover, treatment also includes UV phototherapy in the form of excimer laser and psoralen and ultraviolet A (PUVA) therapy,[1] as well as superficial cryotherapy.[15,16] However, none of the therapies used to date have a permanent therapeutic effect.

The risk of side effects of the commonly used therapies significantly reduces their use. New therapeutic alternatives are therefore constantly being sought. Recently, the efficacy of Janus kinase inhibitors (applied topically and systematically), prostaglandin analogues, statins, platelet-rich plasma, and stem cells has been reported. The medical literature contains limited descriptions of experimental therapies using autologous mesenchymal stem cells (MSCs) extracted from the patient's adipose tissue for the treatment of AA.[9,17]

Stem cells can be divided into 3 different types: embryonic stem cells (ESCs), adult stem cells (ASCs) and induced pluripotent stem cells (IPSCs). The use of ESCs raises ethical controversies that do not apply to tissue-derived stem cells, e.g., MSCs.[17] In cell therapies, MSCs are used most commonly. The MSCs can be extracted from various tissues: bone marrow, adipose tissue, umbilical cord blood, Wharton's jelly (allogeneic MSCs extracted from Wharton's jelly – WJ-MSCs), and the amniotic membrane.[18] Cells extracted from bone marrow, adipose tissue and Wharton's jelly (WJ) are of most practical importance.[17,19,20] It is worth noting that the extraction of MSCs from WJ is noninvasive.[21] In 2006, the International Society for Cellular Therapy (ISCT) defined the minimum criteria required for a cell to qualify as an MSC: (1) adhesion to plastic; (2) expression of CD73, CD90 and CD105 surface antigens in the absence of hematopoietic antigens CD34, CD45, CD14 or CD11b, CD79α or CD19, and human leukocyte antigen – DR isotype (HLA DR) surface antigens; and (3) the ability to differentiate into osteoblasts, adipocytes or chondrocytes in vitro.[22]

Mesenchymal stem cells possess immunomodulatory properties.[18] It has been demonstrated that MSCs reduce the proliferative properties of T and B lymphocytes and NK cells, secrete numerous paracrine factors including anti-inflammatory cytokines, and have the ability to migrate toward the site of damage. The MSCs change the secretion profile of immune cells towards anti-inflammatory cytokines and contribute to an increase in the regulatory T lymphocyte population.[9,22] The most important cytokine secreted by MSCs that modulate T lymphocytes is interleukin 6 (IL-6).[18]

Due to the immunological properties of MSCs harnessed from adult and fetal tissues they can be administered through an allogeneic regimen without the need to test the recipient and donor's HLA systems and initiate immunosuppressive therapy in the recipient. Unlike embryonic cells, MSCs have no tumorigenic potential.[23]

In the European Union, cell therapy products that include MSCs have been considered medications since

2003.[24] They are used to treat shin ulcers[25] and hematological, orthopedic, urological, and gastroenterological disorders.[26]

Previous attempts to use autologous MSCs for the treatment of alopecia have demonstrated the effectiveness and safety of this form of treatment.[9] So far, allogeneic transplantation of WJ-MSCs has not been used in AA treatment. Due to the limited efficacy of the currently applied methods for the treatment of AA, it is important to search for new forms of therapy.

Objectives

The aim of this study was to evaluate the efficacy and safety of AA treatment through a single intradermal injection of a WJ-MSC suspension into the alopecia foci. The primary endpoint was the percentage change in the Severity of Alopecia Tool (SALT) score during treatment.

Material and methods

This experimental study was conducted with patients undergoing treatment at the Regional Specialist Hospital in Wrocław, Poland, and was performed in collaboration with the Polish Stem Cell Bank (Polski Bank Komórek Macierzystych – PBKM). The study protocol was approved by the local bioethics committee of the Research and Development Centre of the Regional Specialist Hospital in Wroclaw (approval No. KB 01/2019) and all procedures performed in the study were carried out in accordance with the ethical standards of the Helsinki Declaration. All patients were informed in detail about the purpose and methods of the study, as well as the potential benefits and risks of therapy. All participants provided written informed consent to participate in the study.

Patients

The study involved 4 AA patients who underwent experimental therapy with a suspension of WJ-MSCs. The patient population included 3 men aged 36, 43 and 49 years and 1 woman aged 57 years. The duration of the disease ranged from 2 to 9 years (mean of 5 years). Three or more AA foci were observed in each patient (Table 1). In the past,

all of the patients had undergone the following therapies: systemic and topical glucocorticoids, topical minoxidil, cryotherapy, and phototherapy (UVB 311 nm). One patient was treated with contact immunotherapy (diphenylcyclopropenone). None of these methods resulted in complete hair regrowth.

The patients did not suffer from any skin diseases or systemic diseases other than alopecia. For 6 weeks prior to the study, the patients did not take any medications. In all patients with AA, additional tests were performed prior to the initiation of therapy, which revealed C-reactive protein (CRP) values ≤5 mg/L, negative antinuclear antibodies (ANA) panel results, and no hepatitis C virus (HCV), hepatitis B virus (HBV) and human immunodeficiency virus (HIV) infections. On the day of administration of the WJ-MSC suspension, no clinical signs of other active infections were found.

Preparation of the Wharton's jelly mesenchymal stem cell suspension

All umbilical cord (UC) collections were performed after obtaining informed consent of the parents. The UCs samples were collected after natural delivery or caesarean sections. The fragment of the UC as long as 20–30 cm was placed in a sterile container into with 0.9% natrium chloratum solution (Fresenius Kabi, Bad Homburg vor der Höhe, Germany) and transported in protective boxes to the laboratory. The transport conditions were monitored and UC tissue was processed within 72 h after delivery. Qualification of UC tissue requires providing complete responses to a medical questionnaire and submitting by donor-mother a peripheral blood sample for infectious agents testing for HBV, HCV, HIV, cytomegalovirus (CMV), and syphilis. All steps of manufacturing were performed in accordance the principles of Good Manufacturing Practice (GMP) and Good Laboratory Practice (GLP). Umbilical cord fragment was removed from transportation container and placed into a new container with 0.9% natrium chloridum solution (Fresenius Kabi) supplemented with 1% Antibiotic Antimycotic (Thermo Fisher Scientific/Gibco, Waltham, USA). After washing, the fragment was dissected into 2 cm fragments, put on 90 mm Petri dish (Medlab Products Sp. z o.o., Raszyn, Poland) and cut along with surgical blade; then, the arteries and the vein were removed with tweezers. After all blood vessels were removed, WJ

Table 1. Characteristics of the patients

Patient/patients' initials	Gender	Age [years]	Duration of the disease [years]	Number of foci of alopecia
1/BR	female	57	9	3
2/PT	male	43	6	4
3/DH	male	36	2	4
4/PI	male	49	3	9

214

A. Czarnecka et al. Stem cells in treatment of alopecia areata

tissue was minced into 1–2 mm^3 scraps and placed in xeno-free, serum-free media into culture flasks for primary explants cultures development. Flasks were incubated in optimal conditions. After 14 days in culture, the tissues were removed from culture and the adherent cells were trypsinized using TrypLE™ Select 1× (Life Technologies, Carlsbad, USA) and passed into new flasks for further expansion. The criteria for defining multipotent MSCs were established in 2006 by ISCT.[27] They are based on cells adherence to plastic, presence of specific antigens like CD90, CD73 and CD105, together with the absence of hematopoietic and immune system markers (CD45, CD34, CD14 or CD11b, CD79a, CD19) and HLA-DR surface antigens, as well as conferring stem cell identity to differentiate into osteoblasts, chondrocytes and adipocytes. The pharmaceutical form of the product is a frozen preparation of cells in a cryoprotective liquid. The administration and dosage form of the treatment is a thawed suspension of WJ-MSCs with the phenotype CD73(+), CD90(+), CD105(+).

Procedure

For each patient, a single WJ-MSC suspension was administered to several alopecia foci with a total area of about 15 cm^2 in the form of intradermal injections. For 1 treatment, 2 mL of the suspension was used, which contained 5×10^6 WJ-MSCs of phenotype CD73(+), CD90(+), CD105(+) suspended in a saline solution. Injections were performed into every 0.5 cm of skin surface. For each injection site, 0.01 mL of the suspension was administered. A needle (32 G, 0.23 × 6 mm) was used to administer the treatment. The scalp was anesthetized locally with EMLA cream (5% lidocaine) (Aspen Pharmacare, Durban, South Africa) 1 h before the treatment.

On the day of WJ-MSCs administration, patients were hospitalized for 1 day. Before the procedure, the severity of alopecia was assessed using the SALT score (SALT$_0$), the patient's general condition (physical examination) and well-being were assessed, and photographs of scalp skin were taken. Patients' general and local condition and well-being were reassessed 24 h after the procedure.

Evaluation of disease severity and effect of therapy

The AA intensity was measured with the SALT score.[28] For this purpose, the scalp was divided into 4 areas where hair loss was assessed (40% vertex, 18% right side, 18% left side, 24% posterior); then, the percentage of hair loss over the entire scalp was calculated.[28] This measure was performed 3 times during treatment: SALT$_0$ prior to treatment; SALT$_{12}$ 12 weeks after the treatment; and SALT$_{24}$ 24 weeks after the treatment; then, the observations concluded.

To evaluate the effects of therapy, we calculated the difference in alopecia surface area before and after application of the WJ-MSC suspension in the 12th and 24th weeks, assuming that the condition before treatment commencement was 100%,[28] according to the following formula:

$$(A - B/A) \times 100\% = I \text{ or } D,$$

where A indicates the percentage of baldness before treatment, B is the percentage of baldness after treatment and I (improvement) indicates the amount of hair regrowth. If increased hair loss was observed after treatment, the condition was indicated by D (deterioration). Regrowth observed 12 weeks following treatment was marked as I$_{12}$ and regrowth after 24 weeks was marked as I$_{24}$ (in both cases taking the pretreatment condition as baseline). Additionally, in order to examine the dynamics of hair regrowth in relation to the time that had passed since treatment, the I$_{24:12}$ regrowth was determined 24 weeks after the treatment, taking the 12-week condition as baseline.

The efficacy of therapy was assessed for the whole surface of the scalp and for the following individual areas: vertex, right side, left side, and posterior (Table 2). Hair regrowth or loss in individual areas was determined according to the formula:

$$(I \text{ or } D)_{12vertex}.$$

Follow-up visits

Follow-up visits took place on an outpatient basis 6, 12, 18, and 24 weeks after the WJ-MSCs administration. During each follow-up visit, the patient's general condition (physical examination), mental wellbeing and topical conditions were assessed, and a photo of the scalp was taken. When assessing the condition of the topical local site, particular attention was paid to symptoms that could indicate adverse effects of intradermal cell administration, such as redness or swelling. The SALT assessments were performed 12 weeks (SALT$_{12}$) and 24 weeks SALT$_{24}$) following treatment. Hair regrowth or loss were calculated and expressed as (I or D)$_{12}$, (I or D)$_{24}$ and (I or D)$_{24:12}$.

Results

On the day of the administration of the WJ-MSC suspension, the SALT$_0$ score for the 4 patients (Table 2) was 26.4% for patient 1 (BR), 23.4% for patient 2 (PT), 19.4% for patient 3 (DH), and 40% for patient 4 (PI). The average SALT$_0$ score for all patients was 27.3% of hair loss.

In all patients, hair regrowth was observed at the sites of cell suspension administration 12 weeks after the procedure, together with a decrease in the SALT$_{12}$ value. The SALT$_{12}$ values for patients 1, 2, 3, and 4 were 17.6%, 7.2%, 12.2%, and 22.5%, respectively, with an average SALT$_{12}$ score of 14.9%.

Further improvement was observed in the 24th week. Hair loss after 24 weeks, measured using the SALT$_{24}$ score, was lower than that observed after 12 weeks (SALT$_{12}$), and

Table 2. The AA intensity measured using the SALT score in the 4 regions (vertex, right side, left side, posterior) and in the total scalp. Improvement or deterioration in the 4 regions (vertex, right side, left side, posterior) and in the total scalp

Parameter	Patient 1 (BR)			Patient 2 (PT)			Patient 3 (DH)			Patient 4 (PI)		
Injected sites of the scalp	posterior, left side, right side			posterior, right side			vertex, posterior, right side			vertex, posterior, left side, right side		
Follow-up visit	week 0	week 12	week 24	week 0	week 12	week 24	week 0	week 12	week 24	week 0	week 12	week 24
Vertex SALT	**0%**	**8%**	**12%**	**0%**	**0%**	**0%**	**12%**	**8%**	**6%**	**28%**	**16%**	**14%**
Vertex improvement I_{12}, I_{24}	–	0	0	–	–	–	–	33%	50%	–	42.8%	50%
Vertex deterioration D_{12}, D_{24}	–	8%	12%	–	–	–	–	0	0	–	0	0
Vertex improvement $D_{24:12}$	–	–	–	–	–	–	–	–	25%	–	–	12.5%
Vertex deterioration $D_{24:12}$	–	–	33%	–	–	–	–	–	0	–	–	0
Left side SALT	1.8%	0%	0%	0%	0%	0%	0%	0%	0%	1.8%	0.9%	0.9%
Left side improvement I_{12}, I_{24}	–	100%	100%	–	–	–	–	–	–	–	50%	50%
Left side improvement $I_{24:12}$	–	–	–	–	–	–	–	–	–	–	–	0
Right side SALT	1.8%	0%	0%	0.4%	0%	0%	3.6%	1.8%	1.8%	1.8%	0.9%	0.9%
Right side improvement I_{12}, I_{24}	–	100%	100%	–	100%	100%	–	50%	50%	–	50%	50%
Right side improvement $I_{24:12}$	–	–	0	–	–	0	–	–	0	–	–	0
Posterior SALT	22.8%	9.6%	4.8%	18%	7.2%	4.8%	4.8%	2.4%	1.2%	8.4%	3.6%	2.4%
Posterior improvement I_{12}, I_{24}	–	57%	79%	–	60%	73%	–	50%	75%	–	57%	71%
Posterior improvement $I_{24:12}$	–	–	50%	–	–	33%	–	–	50%	–	–	33%
Total scalp SALT	24.6%	17.6%	16.8%	23.4%	7.2%	4.8%	19.4%	12.2%	9%	40%	22.5%	18.2%
Improvement in injection site I_{12}, I_{24}	–	60%	80%	–	69%	79%	–	37%	53%	–	43%	54%
Improvement in injection site $I_{24:12}$	–	–	50%	–	–	33%	–	–	26%	–	–	19%

SALT – Patients' Severity of Alopecia Tool; Improvement I_{12}, I_{24}/Deterioration D_{12}, D_{24} – difference between the alopecia surface area before the treatment and after the treatment in the 12th and 24th week, assuming that the condition before treatment was 100%; Improvement $I_{24:12}$/Deterioration $D_{24:12}$ – difference between the alopecia surface area after the 12th week and after the 24th week, assuming that the condition in the 12th week was 100%.

was 16.8% for patient 1, 4.8% for patient 2, 9% for patient 3, and 18.2% for patient 4. The average $SALT_{24}$ score was 12.2% (Table 2).

Regrowth (I_{24}) of the scalp where the procedure was carried out was between 53% and 80%, with values of 80%, 79%, 53%, and 54% for patients 1, 2, 3, and 4, respectively (Table 2). None of the observed cases achieved 100% hair regrowth. The mean hair regrowth in the injected sites (I_{24}) was 67%.

All the patients were found to present with more hair regrowth after the first 12 weeks (I_{12}) than in the following 12 weeks ($I_{24:12}$) at the site where the intradermal WJ-MSC suspension was administered (Table 2). For patient 1, the I_{12} was 60% for the first 12 weeks and the $I_{24:12}$ was 50% for the following 12 weeks; patient 2 had an I_{12} of 69% and $I_{24:12}$ of 33%; patient 3 had values of 37% and 26%, respectively; and patient 4 had an I_{12} of 43% and $I_{24:12}$ of 19% (Table 2). The mean I_{12} and $I_{24:12}$ were 52.2% and 32%, respectively.

A noteworthy case was patient 1 (BR), who received posterior, left- and right-side injections, and by the 12th week was found to have hair loss in the vertex area which was not treated with injections of the WJ-MSC suspension. This deterioration was expressed by the symbol (D_{vertex}), and in the 12th week of therapy, the deterioration ($D_{12vertex}$) was 8% and increased to 12% after the following 12 weeks

of observation ($D_{24vertex}$). The rate of hair loss increased and the $D_{24:12vertex}$ score was 33% (Table 2). No hair loss was found in the remaining area of the scalp, while hair regrowth was observed in the injected sites (Table 2).

In patients 2, 3 and 4, no new foci of alopecia were found during the 24-week observation period. Improvement was observed in all treated areas: vertex, posterior, left side, and right side. Detailed results are presented in Table 2.

During the 24-week observation period, patients did not present any abnormalities in the physical examination. No local side effects (rash or swelling) at the site of intradermal injection of the WJ-MSC suspension were found in any patients. All patients reported good general health state and did not report any subjective symptoms.

Figures 1,2,3 present the condition before the treatment and results of the therapy in patient 1.

Discussion

The introduction of stem cell-based therapies to repair and regenerate various tissues and organs offers innovative therapeutic solutions. Mesenchymal stem cells play an important role in the production of active agents for tissue regeneration, affecting the proliferation and migration

Fig. 1. Patient No. 1, posterior region of the scalp, before treatment

Fig. 2. Patient No. 1, posterior region of the scalp, 12 weeks after treatment

Fig. 3. Patient No. 1, posterior region of the scalp, 24 weeks after treatment

of endothelial cells, fibroblasts and skin cells.[29,30] Studies also show that, in addition to proangiogenic, chemoattractive and anti-inflammatory potential, MSCs may modulate the activity of the immune system.[31] Attempts have recently been made to use MSCs to reactivate hair follicle stem cells and thus prevent hair loss.[32]

There are only a few reports in the medical literature on the use of MSCs in the treatment of alopecia. The most commonly used MSCs in AA therapy are those derived from bone marrow or adipose tissue.[33–35] In a therapeutic experiment, autologous MSCs derived from bone marrow were used on a group of 40 people with hair loss, including 20 people with AA and 20 people with AGA. Six months after a single injection of stem cells into the scalp, the authors observed a significant improvement, confirmed with digital dermoscopy. There was no significant difference in the effectiveness of treatment between the 2 types of alopecia. No serious adverse events were reported.[36]

Another interesting study reported the use of human autologous adipose-derived adult cells of stromal vascular fraction (ADSVC) for the treatment of 20 AA patients. Patients were given a single injection of autologous ADSVC cells extracted by lipoaspiration from adipose tissue into the alopecia foci at concentrations of $4{-}4.7 \times 10^6$ cells. The growth and thickness of the hair improved significantly within the first 6 months after treatment. A decrease in the intensity of the hair pull test was also observed. No side effects of ADSVC treatment were observed, and patients assessed the therapy as satisfactory.[34]

Mesenchymal stem cells can also be extracted from WJ in the umbilical cord. It is an ideal source of stem cells due to its availability, noninvasive and painless extraction, weak immunogenic potential, no risk of adverse effects for the donor or recipient, and no ethical restrictions.[22,32,35] Medical literature suggests the potential effectiveness of WJ-MSCs in hair follicle regeneration and hair regrowth.[33,34] An additional advantage of using material extracted from WJ is the possibility of obtaining its decellularized fraction (DWJM), which is considered an excellent natural biocompatible 3D scaffold. The DWJM, as a 3D scaffold, can be used as a regenerative drug to promote stem cell adhesion, penetration, growth, and multiplication both in vitro and in vivo.[37]

In our study, a single suspension of allogeneic WJ-MSCs was injected into the selected AA foci at a concentration of 5×10^6 cells, followed by a six-month observation of the treatment effects. All patients who participated in this experimental study had previously been treated with standard procedures, but without significant long-term clinical improvements. All patients showed a reduction in the area of baldness by an average of 67%. None of the patients experienced complete hair regrowth. Notably, we observed improved hair regrowth dynamics in all cases in the first 3 months after the procedure, with an increase of 52.2% on average compared to the following 3 months, when the increase was 32% on average.

The case of patient 1 (BR) is particularly interesting, because in the 12th week of observation, the subject was diagnosed with hair loss in the frontal area where no intradermal injection of WJ-MSC suspension was applied. No hair loss was detected in the remaining area of the scalp, while in the injected sites (i.e., the parietal area, right and left side of the scalp), hair regrowth did occur. This case indicates that the applied therapy is effective only at the site of cell administration itself.

There are very few reports of allogeneic therapies with WJ-MSCs in the medical literature to date. The authors of these papers stress the safety of this type of therapy, including the lack of tumorigenic potential.[22,32,38]

Our experiment also evaluated the safety of the procedures used. No side effects were observed during the procedure or after application of the WJ-MSC suspension in the allogeneic system.

Limitations

The limitation of the study was the small number of patients enrolled.

Conclusions

The presented report supports the effectiveness and safety of the applied therapy – intradermal injections of an allogeneic WJ-MSC suspension. To our knowledge, this is the first clinical study to describe the application of an allogeneic MSC transplant in patients with AA. The results of treatment were positive, with hair growth observed in all participants, and the therapy was found to be safe, with no side effects. The question remains as to how many cells should be given to the patient to achieve full hair regrowth and how often the treatments should be repeated to achieve 100% therapy efficacy with no relapse. We emphasize the need to conduct further studies with a randomized control group.

ORCID iDs

Anna Czarnecka https://orcid.org/0000-0002-6621-9537
Agnieszka Odziomek https://orcid.org/0000-0002-3574-171X
Magdalena Murzyn https://orcid.org/0000-0001-8115-4287
Joanna Dubis https://orcid.org/0000-0002-6814-580X
Marta Bagłaj-Oleszczuk https://orcid.org/0000-0002-4554-7603
Anita Hyncewicz-Gwóźdź https://orcid.org/0000-0002-1601-471X

References

1. Pratt CH, King LE Jr, Messenger AG, Christiano AM, Sundberg JP. Alopecia areata. *Nat Rev Dis Primers*. 2017;3:17011. doi:10.1038/nrdp. 2017.11
2. Safavi K. Prevalence of alopecia areata in the First National Health and Nutrition Examination Survey. *Arch Dermatol*. 1992;128(5):702. doi:10.1001/archderm.1992.01680150136027
3. Abedini R, Hallaji Z, Lajevardi V, et al. Quality of life in mild and severe alopecia areata patients. *Int J Womens Dermatol*. 2017;4(2):91–94. doi:10.1016/j.ijwd.2017.07.001
4. Burgdorf WHC, Plewing G, Wolff HH, Landthaler M. *Dermatologia*. Vol. 1. Lublin, Poland: Czelej; 2017.
5. Strazzulla LC, Wang EHC, Avila L, et al. Alopecia areata: An appraisal of new treatment approaches and overview of current therapies. *J Am Acad Dermatol*. 2018;78(1):15–24. doi:10.1016/j.jaad.2017.04.1142
6. Simakou T, Butcher JP, Reid S, Henriquez FL. Alopecia areata: A multifactorial autoimmune condition. *J Autoimmun*. 2019;98:74–85.
7. Gilhar A, Etzioni A, Paus R. Alopecia areata. *N Engl J Med*. 2012;366(16): 1515–1525. doi:10.1056/NEJMra1103442
8. Guo H, Cheng Y, Shapiro J, McElwee K. The role of lymphocytes in the development and treatment of alopecia areata. *Expert Rev Clin Immunol*. 2015;11(12):1335–1351. doi:10.1586/1744666X.2015.1085306
9. Li Y, Yan B, Wang H, et al. Hair regrowth in alopecia areata patients following Stem Cell Educator therapy. *BMC Med*. 2015;13:87. doi:10.1186/s12916-015-0331-6
10. Sudnik W. *Rola selektyn E, L, P w patomechanizmie łysienia plackowatego* [PhD thesis]. Poznań, Poland: Poznan University of Medical Sciences; 2012.
11. Hordinsky MK. Treatment of alopecia areata: What is new on the horizon? *Dermatol Ther*. 2011;24(3):364–368. doi:10.1111/j.1529-8019.2011. 01421.x
12. Biran R, Zlotogorski A, Ramot Y. The genetics of alopecia areata: New approaches, new findings, new treatments. *J Dermatol Sci*. 2015;78(1): 11–20. doi:10.1016/j.jdermsci.2015.01.004
13. Hordinsky MK. Overview of alopecia areata. *J Investig Dermatol Symp Proc*. 2013;16(1):S13–S15. doi:10.1038/jidsymp.2013.4
14. Łuczak M, Łuczak T, Ciesińska C, Czajkowski R. Leczenie ogólne łysienia plackowatego. *Przegl Dermatol*. 2013;100:53–58.
15. Nowicka D, Maj J, Jankowska-Konsur A, Hryncewicz-Gwóźdź A. Efficacy of diphenylcyclopropenone in alopecia areata: A comparison of two treatment regimens. *Postepy Dermatol Allergol*. 2018;35(6): 577–581. doi:10.5114/ada.2018.77608
16. Dainichi T, Kabashima K. Alopecia areata: What's new in epidemiology, pathogenesis, diagnosis, and therapeutic options? *J Dermatol Sci*. 2017;86(1):3–12. doi:10.1016/j.jdermsci.2016.10.004
17. Szabłowska-Gadomska I, Bużańska L, Małecki M. Właściwości komórek macierzystych, regulacje prawne oraz zastosowanie w medycynie. *Postepy Hig Med Dosw (Online)*. 2017;71:1216–1230.
18. Marino L, Castaldi MA, Rosamilio R, et al. Mesenchymal stem cells from the Wharton's jelly of the human umbilical cord: Biological properties and therapeutic potential. *Int J Stem Cells*. 2019;12(2):218–226. doi:10.15283/ijsc18034
19. Bajek A, Olkowska J, Drewa T. Mezenchymalne komórki macierzyste narzędziem terapeutycznym w regeneracji tkanek i narządów. *Postepy Hig Med Dosw*. 2011;65:124–132.
20. Wang HS, Hung SC, Peng ST, et al. Mesenchymal stem cells in the Wharton's jelly of the human umbilical cord. *Stem Cells*. 2004;22(7): 1330–1337. doi:10.1634/stemcells.2004-0013
21. Davies JE, Walker JT, Keating A. Concise review: Wharton's jelly: The rich, but enigmatic, source of mesenchymal stromal cells. *Stem Cells Transl Med*. 2017;6(7):1620–1630. doi:10.1002/sctm.16-0492
22. Dominici M, Le Blanc K, Mueller I, et al. Minimal criteria for defining multipotent mesenchymal stromal cells: The International Society for Cellular Therapy position statement. *Cytotherapy*. 2006;8(4): 315–317. doi:10.1080/14653240600855905
23. Pojda Z, Machaj E, Kurzyk E, et al. Mezenchymalne komórki macierzyste. *Adv Biochem*. 2013;59(2):187–197.
24. Martín PG, Martinez AR, Lara VG, Naveros BC. Regulatory considerations in production of a cell therapy medicinal product in Europe to clinical research. *Clin Exp Med*. 2014;14(1):25–33. doi:10.1007/s10238-012-0213-6
25. Masłowski L, Paprocka M, Czyżewska-Buczyńska A, et al. Autotransplantation of the adipose tissue-derived mesenchymal stromal cells in therapy of venous stasis ulcers. *Arch Immunol Ther Exp (Warsz)*. 2020;68(1):5. doi:10.1007/s00005-020-00571-9
26. Szydlak R. Produkty lecznicze zaawansowanej terapii medycznej oparte na mezenchymalnych komórkach macierzystych. *Farm Pol*. 2018;74(3):178–183.
27. Dominici M, Le Blanc K, Mueller I, et al. Minimal criteria for defining multipotent mesenchymal stromal cells: The International Society for Cellular Therapy position statement. *Cytotherapy*. 2006;8(4):315–317. doi:10.1080/14653240600855905

28. Olsen EA, Hordinsky MK, Price VH, et al; National Alopecia Areata Foundation. Alopecia areata investigational assessment guidelines. Part II. National Alopecia Areata Foundation. *J Am Acad Dermatol*. 2004;51(3):440–447.

29. Maxson S, Lopez EA, Yoo D, Danilkovitch-Miagkova A, Leroux MA. Concise review: Role of mesenchymal stem cells in wound repair. *Stem Cells Transl Med*. 2012;1(2):142–149. doi:10.1016/j.jaad.2003.09.032

30. López JF, Sarkanen JR, Huttala O, Kaartinen IS, Kuokkanen HO, Ylikomi T. Adipose tissue extract shows potential for wound healing: In vitro proliferation and migration of cell types contributing to wound healing in the presence of adipose tissue preparation and platelet rich plasma. *Cytotechnology*. 2018;70(4):1193–1204. doi:10.1007/s10616-018-0211-y

31. Otero-Viñas M, Falanga V. Mesenchymal stem cells in chronic wounds: The spectrum from basic to advanced therapy. *Adv Wound Care (New Rochelle)*. 2016;5(4):149–163. doi:10.1089/wound.2015.0627

32. Owczarczyk-Saczonek A, Krajewska-Włodarczyk M, Kruszewska, A, et al. Therapeutic potential of stem cells in follicle regeneration. *Stem Cells Int*. 2018;2018:1049641. doi:10.1155/2018/1049641

33. Egger A, Tomic-Canic M, Tosti A. Advances in stem cell-based therapy for hair loss. *CellR4 Repair Replace Regen Reprogram*. 2020;8:e2894.

34. Anderi R, Makdissy N, Azar A, Rizk F, Hamade A. Cellular therapy with human autologous adipose-derived adult cells of stromal vascular fraction for alopecia areata. *Stem Cell Res Ther*. 2018;9(1):141. doi:10.1186/s13287-018-0889-y

35. Sabapathy B, Sundaram SVM, Mankuzhy P, Kumar S. Human Wharton's jelly mesenchymal stem cells plasticity augments scar-free skin wound healing with hair growth. *PLoS One*. 2014;9 (4):e93726. doi:10.1371/journal.pone.0093726

36. Ibrahim ZA, Elmaadawi IH, Mohamed BM, et al. Stem cell therapy as a novel therapeutic intervention for resistant cases of alopecia areata and androgenetic alopecia. *J Dermatol Treat*. 2018;29(5):431–440. doi:10.1080/09546634.2016.1227419

37. Jadalannagari S, Converse G, McFall C, et al. Decellularized Wharton's jelly from human umbilical cord as a novel 3D scaffolding material for tissue engineering applications. *PLoS One*. 2017;12(2):e0172098. doi:10.1371/journal.pone.0172098

38. Gentile P, Garcovich S. Advances in regenerative stem cell therapy in androgenic alopecia and hair loss: Wnt pathway, growth-factor, and mesenchymal stem cell signaling impact analysis on cell growth and hair follicle development. *Cells*. 2019;8(5):466. doi:10.3390/cells8050466

Overhydration: A cause or an effect of kidney damage and how to treat it

Anna Szymczak[A–D], Mariusz Kusztal[C–F], Magdalena Krajewska[C–F]

Department of Nephrology and Transplantation Medicine, Wroclaw Medical University, Poland

A – research concept and design; B – collection and/or assembly of data; C – data analysis and interpretation;
D – writing the article; E – critical revision of the article; F – final approval of the article

Address for correspondence
Mariusz Kusztal
E-mail: mariusz.kusztal@umed.wroc.pl

Abstract

Volume overload can be both the cause and effect of chronic kidney disease (CKD). Overhydration often accompanies renal insufficiency. In cardiovascular disease (CVD), fluid overload can also be the cause of renal function impairment. Beside salt restriction, loop diuretics are the first-line therapy. Frequently developed resistance can be overcome by switching to intravenous administration, adding albumin alone or in combination with other diuretics. Transient factors like infection or contrast media can impair diuretic response and contribute to congestion. Apart from conservative management, ultrafiltration (UF) and peritoneal dialysis (PD) are used. In huge congestion with inadequate diuretic effect, hemodialysis with UF plays an important role as a temporary or permanent remedy. An increasing amount of data indicates that sodium–glucose cotransporter-2 inhibitors (SGLT2i) have allowed for a breakthrough in controlling fluid volume in diabetic and non-diabetic patients with CKD. Sodium-glucose cotransporter 2 inhibitors show cardio- and renoprotective effects and have a positive impact on hard cardiovascular and renal endpoints.

Key words: chronic kidney disease, diuretics, dialysis, cardiorenal syndrome, SGLT2 inhibitors

Introduction

A patient exhibiting legs swelling, orthopnea and shortening of breath with known heart failure (HF) or diabetes mellitus (DM) can develop deterioration of kidney function. If correcting the redundant amount of fluid, regardless of the intervention, restores kidney function, we can assume that overhydration was the cause of renal injury. Progressively declining glomerular filtration rate (GFR) in the course of renal disease results in hypertension, sodium retention and fluid overload. In anuric patients, overhydration, as the effect of kidney damage, can be life threatening. The most frequent clinical situation is the mixture of the 2 examples mentioned, best described as cardiorenal syndrome (CRS) with overhydration as a net effect. In the last few years, new data about how overhydration correction is beneficial has been published.

Do we have enough good quality data in CKD?

Circulatory system abnormalities occur frequently in patients with chronic kidney disease (CKD). Overhydration is one of the symptoms resulting predominantly from cardiovascular disease (CVD) cardiac insufficiency. Unfortunately, there is still not enough data of sufficient quality to fully understand the cardiorenal interactions. The problem should not be downplayed, because CKD in various stages affects over 850 million people worldwide, which doubles diabetes and exceeds twentyfold cancer occurrence. Because of the often insidious course of the disease, many patients are unaware not only of the existence of CKD itself, but also of the potential complications, including CVD. It should be emphasized that almost half of CKD patients die because of major cardiac events.[1]

Cardiorenal syndromes

Overhydration can be perceived in the context of cardiorenal crosstalk, which is bidirectional. The systematic classification of the organ interactions was proposed at the consensus conference of the Acute Dialysis Quality Initiative in 2008.[2] An interdisciplinary group of experts and opinion leaders categorized CRS into 5 classes on the basis of the primarily underlying pathology and its acute or chronic character: acute cardiorenal syndrome (type 1), chronic cardiorenal syndrome (type 2), acute reno-cardiac syndrome (type 3), chronic reno-cardiac syndrome (type 4), and secondary cardiorenal syndromes (type 5). Vicious cycle of sodium and water retention is a hallmark of most frequent CRS type 2 (Fig. 1).

Although the cardiovascular mortality among hemodialysis patients is intuitively more understandable, it has been proven that even patients in earlier stages of CKD are at higher CVD risk.[3] Among CVDs, there is the lethal triad: congestive HF, acute myocardial infarction (MI) and sudden cardiac death that take the largest toll.[4] Already microalbuminuria, even with preserved GFR, speaks for cardiovascular mortality,[3] and the influence of estimated glomerular filtration rate (eGFR) on the major adverse cardiovascular events risk is direct.[5] Furthermore, CKD patient is less likely to progress to end-stage renal disease (ESRD) than to pass away because of CVD.[6] On the basis of numerous analyses including large database examination consisting of over million patients,[7] it should be concluded that CKD is one of the most significant risk factors for cardiovascular events.[3] The up-to-date World Health Organization (WHO) charts to evaluate ten-year cardiovascular mortality ratio do not include CKD as a risk factor, while CKD is not less meaningful in this regard than encompassed DM.[3,8] This may lead to underestimation of its meaning.

Overhydration: An effect

Chronic kidney disease inevitably causes volume overload in more advanced stages. It leads to hypertension, arterial stiffness, the shift of the fluids to the third space, left ventricular hypertrophy, and the development of HF.[9,10] Volume overload is believed to be the most common mortality risk factor in CKD.[10,11] Hypervolemia is an adverse
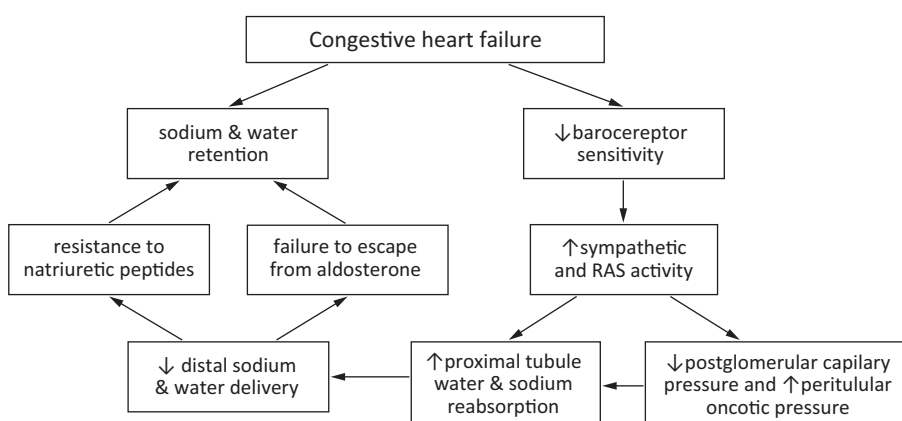

Fig. 1. Vicious cycle of sodium and water retention is a hallmark of most frequent CRS type 2

prognostic factor not only for patients undergoing renal replacement therapy, but also for those in pre-dialysis stadium. It is an independent risk factor for the development of cardiac dysfunction.[12]

Overhydration: A cause

It is agreed that good delivery of blood to the kidneys is vital to preserve their function, but the proper outflow is not less important. "Congestive kidney failure"[13] could be a good description of a pathology that takes place in patients with diastolic HF and CKD. It is believed that sodium retention is always connected to water expansion, a primary therapeutic target, and it increases central venous pressure (CVP). The association of CVP and kidney function impairment and higher all-cause mortality was described in a study where cardiovascular patients underwent the catheterization of the right heart.[14] Although some doubts in blocking activated both renin–angiotensin–aldosterone system (RAAS) and sympathetic system exist, the need to lower CVP to treat congestion appears to be unquestionable.[14] In chronic HF, diastolic dysfunction, which coexists with increased filling pressure, is often accompanied by kidney failure (Fig. 1); the diastolic dysfunction progression worsens the mortality outcomes.[15] The exact pathomechanism is yet not well understood, but the interstitial overpressure and venous congestion, described together as increased renal afterload, seems to play an important role.[13] One must remember that transient exposition to inflammatory mediators, endotoxins or changed bowel wall permeability can be additional pro-congestive factors (Fig. 2). Sometimes, a proper antibiotic course can break diuretic resistance by lowering inflammatory response.
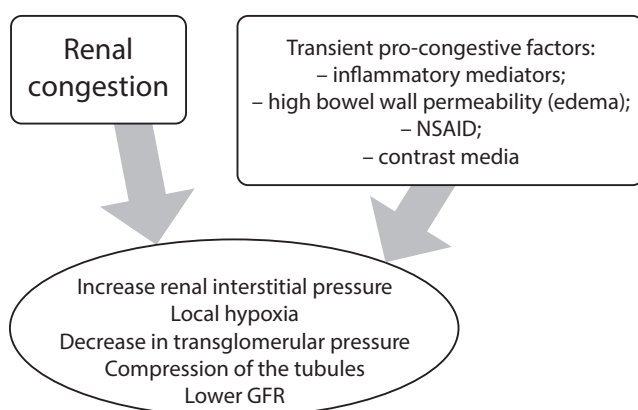

Fig. 2. Pro-congestive factors and renal congestion consequences

Treatment

Regardless of the direction of interactions between overhydration and the kidneys, effective dehydration is crucial. The therapeutic strategy should be subtly tailored, because the window for fluid balance in cardiorenal patients is narrow. The universal recommendation for the majority of patients with CKD – low dietary sodium delivery – should be the first step.[16] In more advanced CKD or HF exacerbation, such management is insufficient and pharmacological treatment should be introduced.

Loop diuretics

The most frequently used class of diuretics in HF are loop diuretics, which work in the loop of Henle; furosemide and torsemide are the most common among them. The inevitable, but also undeniable side effect of loop diuretics is the increased activity of sympathetic nervous system (SNS) and RAAS.

Loop diuretics relieve congestion but do not change mortality and rehospitalization rate in the short and long term.[17] The decrease in its effect in the course of time is a common phenomenon, resulting in the reduction of sodium and chloride elimination; the causes are multiple. Pharmacodynamics and pharmacokinetics play an important role. Loop diuretics are highly bound to serum proteins and require secretion into the proximal tubule to be active. This Na/K/2Cl pump is located on the luminal side of the nephron. Therefore, loop diuretics must reach the tubular fluid to be active. Hence, in patients with severe renal insufficiency (e.g., GFR < 15 mL/min), larger doses of loop diuretics are required to achieve effective concentrations.[18] The various loop diuretics differ in intestinal absorption, especially with an edematous bowel wall present in decompensated HF. Reduced drug excretion to the lumen of the tubule, reduced filtered load of sodium and increased RAAS and SNS activation due to HF-related underfilling and extracellular fluid volume (ECFV) depletion, which attenuates the peak effect of the diuretic, also contribute to the resistance.[19,20] The vasopressin release, enhanced by angiotensin II and baroreceptor-mediated mechanism in more advanced HF, increases nephron water reabsorption.[21] The braking phenomenon, which impairs sodium loss in the course of time, distal tubular hypertrophy and hypochloremia, which plays a role in the activation of neurohormonal activity, can also contribute to diuretic resistance.[22] The attempts to break the resistance encompass more frequent dosing, sometimes multiple times per day,[22] as well as adjusting the dose to the renal function, intravenous administration of the drug and switching from furosemide to torsemide or bumetanide.[16]

The combination of different diuretics is another step to break the resistance. Blocking sodium reabsorption in different sections of nephron seems to be the key target.

Loop diuretic act from the lumen and are responsible for inhibition of Na/K/Cl2 cotransporter in thick ascending loop of Henle and macula densa. They inhibit the transporter by binding within the translocation pocket through the chloride-binding site. The use of loop diuretics leads to the increase of sodium concentration in distal parts

of nephron and stimulates sodium reabsorption through the intensification of Na/Cl cotransporter activation, which is one of the resistance mechanisms.[23]

Thiazides and thiazide-like drugs also act from the lumen through the inhibition of Na/Cl cotransporter in distal convoluted tubule, and, as a result, decrease sodium reuptake. Although their effectiveness finishes with the drop in eGFR below 30 mL/min/1.73 m^2, the combination of loop diuretics with thiazides to the certain point is justified.

Mineralocorticoid receptor antagonists (MRAs) – spironolactone and eplerenone – have been shown to improve morbidity and mortality in HF patients, for example in RALES study. They inhibit the aldosterone receptors in distal nephron and collecting tube, reducing Na channel and Na/K ATPase. One must remember that all the diuretics that target collecting tubule can cause hyperkalemia; therefore, they are not often used in HF patients. This, however, can be controlled by giving concomitant loop diuretic, oral bicarbonate (if acidosis is confirmed) or potassium binders in gut. Natriuretic doses need to be greater than 25 mg/day of spironolactone or 50 mg/day of eplerenone.

Tolvaptan

Tolvaptan, a selective antagonist for the vasopressin receptor V2, was investigated in the EVEREST trial to assess its usefulness for inpatient HF individuals. It diminished dyspnea, edema, body weight, and serum sodium level, but did not affect overall survival, mortality connected with CVD and hospitalizations for HF.[24]

Ultrafiltration

When diuretic response is poor or the resistance to diuretic therapy develops and the heart or kidney insufficiency deteriorates, ultrafiltration (UF) is a solution worth considering.[25] In comparison to loop diuretics, it warrants decongestion with more efficient sodium loss and lower RAAS stimulation.[19] Several randomized trials were conducted to investigate the potential benefits of UF strategy.

RAPID-CHF (Relief for Acutely Fluid-Overloaded Patients with Decompensated Congestive Heart Failure) and UNLOAD (Ultrafiltration vs Intravenous Diuretics for Patients Hospitalized for Acute Decompensated Congestive Heart Failure) trials showed superiority of UF in the loss of fluid over diuretic therapy.[26,27] In CUORE (Continuous Ultrafiltration for Congestive Heart Failure) trial, weight loss effect was similar in both UF and diuretic groups, but the increase in serum creatinine in the group treated with diuretics and a minor incidence of HF rehospitalizations in HF group were observed.[28] CARRESS-HF (Cardiorenal Rescue Study in Acute Decompensated Heart Failure) study revealed similar weight loss effect in UF and diuretic patients, but also the worsening of serum

creatinine results and greater adverse effects ratio in patients undergoing UF.[29] Also, in AVOID-HF (Aquapheresis vs Intravenous Diuretics Hospitalizations for Heart Failure) study, greater adverse events ratio in UF patients were underlined, while no significant difference in three-month rehospitalization between the diuretic and the UF group was observed. The trial was terminated prematurely due to slow enrollment.[30]

Sustained low-efficiency dialysis (SLED) is carried out in patients with NYHA (New York Heart Association) class IV with good clinical effect. Although this solution requires central vascular access, it offers better hemodynamic stability in critically ill patients. The single SLED session, in comparison to conventional hemodialysis, lasts longer (6–12 h) and uses lower blood (50–200 mL/min) and dialysate (200–400 mL/min) flow. Fluid volume is removed slowly over a longer time, ensuring hemodynamic stability.[31,32]

Peritoneal dialysis

The usefulness of peritoneal dialysis (PD) in the management of volume excess in patients with refractory HF and renal failure is justified by greater sodium removal compared with traditional diuretic strategies. Recently, both nephrologist and cardiologist appreciate this modality in CRS.[33,34]

For CRS type 1, tidal PD was found to be a safe and effective mean of removing toxins and large quantities of excess fluid. In a small randomized study, it was superior to UF therapy when the preservation of renal function, improvement of cardiac function and net fluid loss was considered.[35] Moreover, a higher rate of adverse events was noticed in the UF arm. A prospective Brazilian study also confirmed the high-volume PD (prescribed Kt/V = 0.50/ session) as effective in CRS type 1 patients, allowing adequate metabolic and fluid control.

In chronic HF with CKD, when eGFR falls below 25 mL/min/1.73 m^2, peritoneal UF may improve daily functioning and reduce hospitalizations. A systematic review prepared by Ronco group assessed the efficacy of PD in patients with refractory CHF.[34] Twenty-one studies encompassed 673 patients; the authors suggested that in patients with refractory CHF, PD can be an effective and safe treatment option, leading to heart function improvement and better weight control.

Wojtaszek et al. showed the efficacy of peritoneal UF with nightly, 12-hour, 7.5% icodextrin exchange in the long-term treatment of refractory HF in the majority of NYHA class IV patients.[36] One overnight icodextrin exchange appeared to be a promising therapeutic option as an adjunct to pharmacological management. The authors emphasized that the treatment can have a great impact on the quality of life and the total treatment costs.

In recent years, even more studies confirmed PD as a safe and feasible palliative treatment for refractory

CHF in type 2 CRS.[37] Pavo et al. analyzed multiple factors to identify patients with refractory HF and congestive right ventricular dysfunction who would benefit most from PD.[38] Patients with more pronounced backward failure, less marked residual renal functional impairment and those not dependent upon others for assistance are likely to profit most from PD.

In summary, PD should be taken under consideration when refractoriness to conservative therapy appears. Typical clinical situations, such as persistent right heart congestion, ascites with intensified diuretic treatment, ≥2 hospitalizations within 6 months because of cardiac decompensation despite optimal medical treatment, or acute renal failure during intensified conservative treatment of cardiac decompensations are those in which PD should be considered.

The special group of patients: Diabetics

Diabetes mellitus is the most frequent cause of CKD in the world and is an independent death risk factor in the course of CVD.[39] According to post hoc ACCORD trial analysis, in diabetic patients, CKD and/or CVD worsens the all-cause mortality and cardiovascular events prognosis.[40] Therefore, modern anti-diabetic drugs are expected to be not only a good hypoglycemic effect, but also nephro- and cardioprotective result are expected.

Because of its beneficial characteristics, such as low price, safety of use and possible benefits on cardiovascular system, metformin is the first-line drug.[41] It does not have to be ceased in CKD patients, even if the eGFR falls below 45 mL/min/1.73 m^2, and, under appropriate surveillance, can be used up to 30 mL/min/1.73 m^2.[39] However, for the vast amount of patients, monotherapy is not sufficient. Taking into account the immense cardiovascular risk, the studies went in the direction of seeking more pleiotropic solutions. Two groups of medicines should be distinguished here: sodium-glucose cotransporter 2 (SGLT2) inhibitors and incretin agent – glucagon-like peptide-1 (GLP-1) receptor agonist.[42] These novel antidiabetic drug groups reduce cardiovascular death risk, with SGLT2 inhibitors (SGLT-2i) influencing HF risk, and GLP-1RAs reducing MI risk.[42]

Sodium-glucose co-transporter-2 inhibitors

The EMPA-REG OUTCOME trial was a study focused on assessing cardiovascular endpoints. The researchers randomized over 7020 type 2 DM (T2DM) patients with high cardiovascular risk and examined the influence of empagliflozin. During the study, the primary outcomes, such as death from cardiovascular causes, non-fatal MI or non-fatal stroke, and all-cause mortality among patients receiving different doses of empagliflozin (an SGLT2 inhibitor) and placebo, were assessed. It was concluded that the administration of the SGLT2i, which acts in the proximal tubule by increasing glucosuria, in 2 doses, 10 mg and 25 mg, significantly reduced hard endpoints (by 14% and 32%, respectively) compared to placebo. The exact mechanism of action is not well understood, but the protective effect of the drug lies probably in changes in lipid levels and a reduction in the following: sympathetic activity, blood pressure, albuminuria, uric acid retention, oxidative stress, and insulin resistance.[43,44]

Slowing down the progression of CKD was the additional hypothesized result of empagliflozin. The CKD patients in stages G1-3b were assessed for the eGFR during the trial and it was observed that after the initial transient drop in eGFR in the first 4 weeks of observation, the progression of the disease was stabilized in patients receiving empagliflozin, while eGFR declined over time in the group receiving placebo.[45] The eGFR slope analysis from the EMPA-REG OUTCOME trial evaluated GFR variability in 3 different periods, that is, shortly after initiation of the therapy, during chronic maintenance period and after drug cessation. Their observations – eGFR relative decline in the 1st stage, inhibition of the eGFR loss in the 2nd period, and eventually eGFR increase in the last phase after drug cessation – support the hypothesis that there is a renoprotective effect of empagliflozin, reduction in intraglomerular pressure caused by the drug and the SGLT2i effect on hemodynamic changes and its reversibility.[46]

EMEROR Reduced [ejection fraction] trial assessed the effect of empagliflozin on HF, regardless of the diabetic status, on patients with ejection fraction of 40% and less. In this trial, 3730 patients with NYHA class II–IV HF were randomized into 2 groups – placebo and 10 mg empagliflozin once daily. It turned out that the patients receiving empagliflozin had lower risk of meeting primary outcomes, such as cardiovascular death or hospitalization for HF, than the patients receiving placebo (19.4% compared to 24.7%). The study showed not only a positive cardiovascular, but also renal effect of empagliflozin. The secondary outcome, the rate of the decline in the eGFR over the duration of treatment period, was slower in the empagliflozin group than in the placebo group (–0.55 mL/min/1.73 m^2 compared to –2.28 mL/min/1.73 m^2). Also, a composite renal outcome, that is, the beginning of renal replacement therapy (chronic dialysis or renal transplantation) or a profound, sustained reduction in the eGFR occurred in less patients in the empagliflozin than in the placebo group (1.6% compared to 3.1%). It is worth mentioning that 48% of enrolled patients had eGFR of less than 60 mL/min/1.73 m^2.[47]

The effect of empagliflozin on patients with HF with preserved ejection fraction is still being studied in similarly designed EMPEROR Preserved [ejection fraction] trial.

Empagliflozin is beneficial for CKD patients because of the influence on fluid management. This is important, as CRS frequently coexists with overhydration. Positive

impact of empagliflozin on HF with both preserved and reduced ejection fraction (HFpEF and HFrEF) and hypertension is explained by natriuresis enhancement.[48] The resistance to physiological natriuretic peptide and administered diuretics in HF is common; the sodium-hydrogen antiporter 3 or, in other words, sodium-hydrogen exchanger (NHE 3), in the proximal renal tubule, whose activation increases in HF, is hypothesized to be the culprit.[49] The NHE3 protein, which co-localizes with SGLT2,[50] is responsible for the majority of sodium reuptake in the tubules. The SGLT2i interacts with NHE3 by its inhibition and causes natriuresis. The simultaneous administration of loop diuretics can prevent the compensatory increase in sodium reuptake in different parts of the nephron.[51]

Another proposed mechanism for empagliflozin efficacy is the hypothesis of renal congestion and SGLT2i grip point focused on intracellular water. Because of local SGLT2i-induced hypovolemia in the kidney, the interstitial fluid passes easily to the vascular space to compensate for the fluid loss. Due to this assumption, the circulating volume, and thus, the organ perfusion and arterial filling, would not be affected. In addition, the interstitial renal volume overload reduction decreases and protects renal function.[52]

The other gliflozin worth mentioning is dapagliflozin. DECLARE-TIMI 58 (Effect of Dapagliflozin on the Incidence of Cardiovascular Events – Thrombolysis in Myocardial Infarction 58) trial was established to define the dapagliflozin cardiovascular safety profile. In this trial, 17,160 T2DM patients were randomized into groups receiving the drug or placebo. Dapagliflozin treatment lowered the rate of HF hospitalizations and cardiovascular deaths, but did not influence major adverse cardiovascular events (MACE), defined as cardiovascular death, MI or ischemic stroke, in the group of patients with primary atherosclerotic CVD or at risk of one.[53] Promising results were observed in Dapagliflozin and Prevention of Adverse outcomes in Chronic Kidney Disease (DAPA-CKD) phase III trial, focused on primary renal outcomes. In DAPA-CKD trial, the composite endpoint (≥50% sustained decline in eGFR, onset of ESKD, or cardiovascular or renal death) in a comprehensive group of CKD patients with eGRF of 25–75 mL/min/1.73 m² with and without DM had been assessed.[54] At the end of March 2020, the trial was terminated prematurely due to the overwhelming efficacy in renal insufficiency patients. Similarly designed EMPA-Kidney trial is being conducted, but the results we will be available in 2022.

Other SGLT2i were also assessed in the trials. Focused on cardiovascular outcomes, CANVAS (Canagliflozin Cardiovascular Assessment Study) program encompassed 2 trials of 10,142 T2DM patients with high CVD risk. It was designed to assess the canagliflozin benefit–risk balance. The program showed the superiority of SGLT2i over the placebo group in cardiovascular events reduction, but the adverse effects – amputations at the level

of toe or metatarsal – was more frequent in the canagliflozin group.[55] CREDENCE (Canagliflozin and Renal Endpoints in Diabetes with Established Nephropathy Clinical Evaluation) study was focused on canagliflozin primary renal outcomes. Included patients had eGFR of 30–90 mL/min/1.73 m² and an estimated daily proteinuria at the level of 0.3–5 g. The study showed that both kidney failure and the risk of cardiovascular events were lower in the group receiving canagliflozin compared to the placebo group. The study was ceased after planned interim analysis, as the demonstration of efficacy was obtained already after randomizing 4401 patients.[56]

The summary analysis of the SGLT2i mentioned above is as follows: empagliflozin, canagliflozin and dapagliflozin were recently collected in a meta-analysis. It was concluded that SGLT2i reduce HF hospitalizations, for which the evidence is the strongest, MACE and all-cause mortality. The evidence is weaker in the group of patients with eGFR < 60 mL/min/1.73 m²; yet, the impact on lowering adverse renal effects is observable even in this group of patients.[57]

Among the desirable features of SGLT2i, weight loss, blood pressure lowering, uricosuric effect, and lack of the hypoglycemia risk are worth mentioning. Gliflozins reduce hyperfiltration in the early stages of diabetic nephropathy, as they restore tubuloglomerular feedback (TGF).[58]

CVD-REAL3 was an observational study to assess the SGLT-2i effects on kidney function in comparison to other glucose-lowering drugs in real-world clinical practice. It was concluded that initiation of the therapy with SGLT2i, that is: dapagliflozin, empagliflozin, canagliflozin, ipragliflozin, tofogliflozin, and luseogliflozin, was associated with a lower risk of major kidney events and a slower decline in kidney function than the initiation of other anti-diabetic medications.[59]

The recommendations of American Diabetes Association suggest that second-line DM therapy should be chosen on the basis of the existence of atherosclerotic CVD (ASCVD), HF or CKD comorbidity. Heart failure or CKD predominance implies SGLT2i usage to reduce CKD progression and/or HF, while ASCVD predominance suggests SGLT2i or GLP-1 receptor agonist usage with suspected cardiovascular benefits.[60,61]

Incretin drugs

Glucagon-like peptide-1 (GLP-1) receptor agonists are the other anti-hyperglycemic agents that reveal nephroprotective properties, as they prevent macroglobinuria occurrence and the impairment in renal function.[62] The putative renoprotective effect of the GLP-1 receptor agonists is direct and indirect (dichotomic). Indirect actions consist, among others, of better glycemic and blood pressure control, weight loss, and improvement in coronary flow and left ventricular wall motion. Direct effects encompass the decrease in renal and systemic inflammation,

reduction of oxidative stress, decrease of renal hypoxia, and sodium and water modulation.[63] Natriuresis seem to be the main mechanism of decreasing overhydration. It was hypothesized that natriuretic effect of GLP-1 primarily involves inhibition of NHE3 activity in the brush border of the renal proximal tubule.[64] Other authors, who studied the impact of GLP-1 agonists on healthy saline loaded men, suggest that the natriuretic effect is rather induced through a tubular mechanism in distal nephron segments. This mechanism is believed to be secondary to suppression of angiotensin II (ANG II) and independent of renal hemodynamics. Such hypothesized mechanism of action supports the existence of a GLP-1–renal axis.[65] Improving tubuloglomerular feedback and ameliorating glomerular hyperfiltration in patients with T2DM would also be anticipated.[64]

In LEADER (Liraglutide Effect and Action in Diabetes: Evaluation of Cardiovascular Outcome Results) trial, 9340 diabetic patients were randomized. The time-to-event of death from cardiovascular causes, nonfatal MI or nonfatal stroke was assessed. The results showed that the time to the first occurrence of the event was shorter in liraglutide than in the placebo group.[66] There were also other trials evaluating GLP-1 agonists, like ELIXA[67] with lixisenatide, SUSTAIN-6[68] with semaglutide, AWARD-7[69] with dulaglutide, EXCEL[70] with exenatide, and LIRA-RE-NAL[71] again with liraglutide. Although there is evidence for GLT-1 agonists to reduce albuminuria, the evidence for hard renal endpoints are still to be found.[62] Surprisingly, in contrast to SGLT2, there are no GLP-1 receptors in the renal tubuli or other kidney compartments.

Summary

Cardiovascular disease resulting in HF is a common CKD complication, but cardiac insufficiency can also cause renal function deterioration. Cardiorenal syndromes present a common symptom: overhydration. Because the therapeutic target is not always met by means of classical loop diuretics because of resistance, alternative management of fluid overload is required. Ultrafiltration reduces symptoms effectively, but there is no evidence that it improves long-term survival. Peritoneal dialysis seems an attractive solution in refractory CRS type 2 and in selected patients in CRS type 1 treatment. Tolvaptan turned out to diminish the symptoms, but did not prove to influence hard endpoints. The interesting therapeutic option emerges for diabetic and non-diabetic patients with CRS. The SGLT2i are particularly noteworthy, showing reno- and cardioprotective effects, for instance, by reducing overhydration (mainly by NHE3 inhibition). Liraglutide, a GLP-1 receptor agonist, probably shares the NHE3 inhibition effect with SGLT2i and also has cardio- and renoprotective properties.

Although the new agents seem promising in overhydrated patients with CRS, further studies are required to thoroughly assess their potential. To date, the management of CKD patients with HF and fluid overload remains challenging.

ORCID iDs

Anna Szymczak https://orcid.org/0000-0000-0000-0001
Mariusz Kusztal https://orcid.org/0000-0002-6502-0374
Magdalena Krajewska https://orcid.org/0000-0002-2632-2409

References

1. Heywood JT, Fonarow GC, Costanzo MR, et al. High prevalence of renal dysfunction and its impact on outcome in 118,465 patients hospitalized with acute decompensated heart failure: A report from the ADHERE database. *J Card Fail*. 2007;13(6):422–430. doi:10.1016/j.cardfail.2007.03.011
2. Ronco C, McCullough P, Anker SD, et al. Cardio-renal syndromes: Report from the consensus conference of the acute dialysis quality initiative. *Eur Heart J*. 2010;31(6):703–711. doi:10.1093/eurheartj/ehp507
3. Hajhosseiny R, Khavandi K, Goldsmith DJ. Cardiovascular disease in chronic kidney disease: Untying the Gordian knot. *Int J Clin Pract*. 2013;67(1):14–31. doi:10.1111/j.1742-1241.2012.02954.x
4. Granata A, Clementi A, Virzì GM, et al. Cardiorenal syndrome type 4: From chronic kidney disease to cardiovascular impairment. *Eur J Intern Med*. 2016;30:1–6. doi:10.1016/j.ejim.2016.02.019
5. Currie CJ, Berni ER, Berni TR, et al. Major adverse cardiovascular events in people with chronic kidney disease in relation to disease severity and diabetes status. *PLoS One*. 2019;14(8):1–17. doi:10.1371/journal.pone.0221044
6. Gargiulo R, Suhail F, Lerma EV. Cardiovascular disease and chronic kidney disease. *Dis Mon*. 2015;61(9):403–413. doi:10.1016/j.disamonth.2015.07.005
7. Foley RN, Murray AM, Li S, et al. Chronic kidney disease and the risk for cardiovascular disease, renal replacement, and death in the United States Medicare population, 1998 to 1999. *J Am Soc Nephrol*. 2005;16(2):489–495. doi:10.1681/ASN.2004030203
8. WHO. World Health organization/International Society of Hypertension (WHO/ISH) risk prediction charts. Geneva, Switzerland: World Health Organization; 2014:1–40. https://www.who.int/ncds/management/WHO_ISH_Risk_Prediction_Charts.pdf?ua=1.
9. Ortiz A, Covic A, Fliser D, et al. Epidemiology, contributors to, and clinical trials of mortality risk in chronic kidney failure. *Lancet*. 2014;383(9931):1831–1843. doi:10.1016/S0140-6736(14)60384-6
10. Ekinci C, Karabork M, Siriopol DI, Incer N, Covic A, Kanbay M. Effects of volume overload and current techniques for the assessment of fluid status in patients with renal disease. *Blood Purif*. 2018;46(1):34–47. doi:10.1159/000487702
11. Vega A, Abad S, Macías N, et al. Any grade of relative overhydration is associated with long-term mortality in patients with stages 4 and 5 non-dialysis chronic kidney disease. *Clin Kidney J*. 2018;11(3):372–376. doi:10.1093/ckj/sfy018
12. Yilmaz A, Yilmaz B, Küçükseymen S, Özpelit E, Pekel N. Association of overhydration and cardiac dysfunction in patients have chronic kidney disease but not yet dialysis. *Nephrol Ther*. 2016;12(2):94–97. doi:10.1016/j.nephro.2015.08.003
13. Ronco C, Bellomo R, Kellum JA, Ricci Z. *Critical Care Nephrology E-Book*. Philadelphia, PA: Elsevier Health Sciences; 2017.
14. Damman K, van Deursen VM, Navis G, Voors AA, van Veldhuisen DJ, Hillege HL. Increased central venous pressure is associated with impaired renal function and mortality in a broad spectrum of patients with cardiovascular disease. *J Am Coll Cardiol*. 2009;53(7):582–588. doi:10.1016/j.jacc.2008.08.080
15. Bruch C, Rothenburger M, Gotzmann M, et al. Chronic kidney disease in patients with chronic heart failure: Impact on intracardiac conduction, diastolic function and prognosis. *Int J Cardiol*. 2007;118(3):375–380. doi:10.1016/j.ijcard.2006.06.066
16. Hadjiphilippou S. Cardiorenal syndrome: Review of our current understanding. *J R Soc Med*. 2016;109(1):12–17. doi:10.1177/0141076815616091
17. Faris RF, Flather M, Purcell H, Poole-Wilson PA, Coats AJS. Diuretics for heart failure. *Cochrane Database Syst Rev*. 2012;(2):CD003838. doi:10.1002/14651858.CD003838.pub3

18. Khatir DS, Pedersen M, Jespersen B, Buus NH. Evaluation of renal blood flow and oxygenation in CKD using magnetic resonance imaging. *Am J Kidney Dis*. 2015;66(3):402–411. doi:10.1053/j.ajkd.2014.11.022

19. Rangaswami J, Bhalla V, Blair JEA, et al; American Heart Association Council on the Kidney in Cardiovascular Disease and Council on Clinical Cardiology. Cardiorenal syndrome: Classification, pathophysiology, diagnosis, and treatment strategies. A scientific statement from the American Heart Association. *Circulation*. 2019;139(16):e840–e878. doi:10.1161/CIR.0000000000000664

20. Ellison DH. Diuretic resistance: Physiology and therapeutics. *Semin Nephrol*. 1999;19(6):581–597.

21. Schrier RW, Abraham WT. Hormones and hemodynamics in heart failure. *N Engl J Med*. 1999;341(8):577–585. doi:10.1056/NEJM199908193410806

22. Hanberg JS, Rao V, Ter Maaten JM, et al. Hypochloremia and diuretic resistance in heart failure. *Circ Heart Fail*. 2016;9(8):1–12. doi:10.1161/CIRCHEARTFAILURE.116.003180

23. Ellison DH. Clinical pharmacology in diuretic use. *Clin J Am Soc Nephrol*. 2019;14(8):1248–1257. doi:10.2215/CJN.09630818

24. Konstam MA, Gheorghiade M, Burnett JC, et al. Effects of oral tolvaptan in patients hospitalized for worsening heart failure: The EVEREST Outcome Trial. *JAMA*. 2007;297(12):1319–1331. doi:10.1001/jama.297.12.1319

25. Jessup M, Bozkurt B, Butler J, et al; American College of Cardiology Foundation/American Heart Association Task Force on Practice Guidelines. 2013 ACCF/AHA Guideline for the Management of Heart Failure: A report of the American College of Cardiology Foundation/American Heart Association Task Force on Practice Guidelines. *Circulation*. 2013;128(16):240–327. doi:10.1161/CIR.0b013e31829e8776

26. Bart BA, Boyle A, Bank AJ, et al. Ultrafiltration versus usual care for hospitalized patients with heart failure: The Relief for Acutely Fluid-Overloaded Patients with Decompensated Congestive Heart Failure (RAPID-CHF) trial. *J Am Coll Cardiol*. 2005;46(11):2043–2046. doi:10.1016/j.jacc.2005.05.098

27. Costanzo MR, Guglin ME, Saltzberg MT, et al. Ultrafiltration versus intravenous diuretics for patients hospitalized for acute decompensated heart failure. *J Am Coll Cardiol*. 2007;49(6):675–683. doi:10.1016/j.jacc.2006.07.073

28. Marenzi G, Muratori M, Cosentino ER, et al. Continuous ultrafiltration for congestive heart failure: The CUORE trial. *J Card Fail*. 2014;20(1):9–17. doi:10.1016/j.cardfail.2013.11.004

29. Bart BA, Goldsmith SR, Lee KL, et al. Ultrafiltration in decompensated heart failure with cardiorenal syndrome. *N Engl J Med*. 2012;367(24):2296–2304. doi:10.1056/NEJMoa1210357

30. Costanzo MR, Negoianu D, Jaski BE, et al. Aquapheresis versus intravenous diuretics and hospitalizations for heart failure. *JACC Heart Fail*. 2016;4(2):95–105. doi:10.1016/j.jchf.2015.08.005

31. Kron J, Kron S, Wenkel R, et al. Extended daily on-line high-volume haemodiafiltration in septic multiple organ failure: A well-tolerated and feasible procedure. *Nephrol Dial Transplant*. 2012;27(1):146–152. doi:10.1093/ndt/gfr269

32. Kościelska M, Żebrowski P, Małyszko J. The role of slow low efficiency dialysis (sled) in renal replacement therapy [in Polish]. *Wiad Lek*. 2019;72(11 cz. 2):2250–2253.

33. Grossekettler L, Schmack B, Meyer K, et al. Peritoneal dialysis as therapeutic option in heart failure patients. *ESC Heart Fail*. 2019;6(2):271–279. doi:10.1002/ehf2.12411

34. Pernias V, González M, Miñana G, et al. Refractory congestive heart failure: When the solution is outside the heart. *ESC Hear Fail*. 2020;7(1):311–314. doi:10.1002/ehf2.12554

35. Al-Hwiesh AK, Abdul-Rahman IS, Al-Audah N, et al. Tidal peritoneal dialysis versus ultrafiltration in type 1 cardiorenal syndrome: A prospective randomized study. *Int J Artif Organs*. 2019;42(12):684–694. doi:10.1177/0391398819860529

36. Wojtaszek E, Grzejszczak A, Niemczyk S, Malyszko J, Matuszkiewicz-Rowińska J. Peritoneal ultrafiltration in the long-term treatment of chronic heart failure refractory to pharmacological therapy. *Front Physiol*. 2019;10:310. doi:10.3389/fphys.2019.00310

37. Shao Q, Xia Y, Zhao M, et al. Effectiveness and safety of peritoneal dialysis treatment in patients with refractory congestive heart failure due to chronic cardiorenal syndrome. *Biomed Res Int*. 2018;2018:6529283. doi:10.1155/2018/6529283

38. Pavo N, Yarragudi R, Puttinger H, et al. Parameters associated with therapeutic response using peritoneal dialysis for therapy refractory heart failure and congestive right ventricular dysfunction. *PLoS One*. 2018;13(11):e0206830. doi:10.1371/journal.pone.0206830

39. Kidney Disease: Improving Global Outcomes (KDIGO) CKD Work Group. KDIGO 2012 Clinical Practice Guideline for the Evaluation and Management of Chronic Kidney Disease. *Kidney Int Suppl (2011)*. 2013;3(1):4–4. doi:10.1038/kisup.2012.76

40. Branch M, German C, Bertoni A, Yeboah J. Incremental risk of cardiovascular disease and/or chronic kidney disease for future ASCVD and mortality in patients with type 2 diabetes mellitus: ACCORD trial. *J Diabetes Complications*. 2019;33(7):468–472. doi:10.1016/j.jdiacomp.2019.04.004

41. Inzucchi SE, Bergenstal RM, Buse JB, et al. Management of hyperglycaemia in type 2 diabetes, 2015: A patient-centred approach. Update to a Position Statement of the American Diabetes Association and the European Association for the Study of Diabetes. *Diabetologia*. 2015;58(3):429–442. doi:10.1007/s00125-014-3460-0

42. Rocha NA, McCullough PA. Cardiovascular outcomes in diabetic kidney disease: Insights from recent clinical trials. *Kidney Int Suppl (2011)*. 2018;8(1):8–17. doi:10.1016/j.kisu.2017.10.004

43. Zinman B, Wanner C, Lachin JM, et al. Empagliflozin, cardiovascular outcomes, and mortality in type 2 diabetes. *N Engl J Med*. 2015;373(22):2117–2128. doi:10.1056/NEJMoa1504720

44. Strojek K, Rokicka D, Szymborska-Kajanek A, Wróbel M. Empagliflozin. Results of the EMPA-REG OUTCOME trial. A breakthrough in treatment of type 2 diabetes? *Clin Diabet*. 2016;5(3):107–110. doi:10.5603/DK.2016.0018

45. Wanner C, Inzucchi SE, Lachin JM, et al. Empagliflozin and progression of kidney disease in type 2 diabetes. *N Engl J Med*. 2016;375(4):323–334. doi:10.1056/NEJMoa1515920

46. Wanner C, Heerspink HJL, Zinman B, et al. Empagliflozin and kidney function decline in patients with type 2 diabetes: A slope analysis from the EMPA-REG OUTCOME trial. *J Am Soc Nephrol*. 2018;29(11):2755–2769. doi:10.1681/ASN.2018010103

47. Packer M, Anker SD, Butler J, et al. Cardiovascular and renal outcomes with empagliflozin in heart failure. *N Engl J Med*. 2020;383(15):1413–1424. doi:10.1056/nejmoa2022190

48. Perkins BA, Udell JA, Cherney DZI. No need to sugarcoat the message: Is cardiovascular risk reduction from SGLT2 inhibition related to natriuresis? *Am J Kidney Dis*. 2016;68(3):349–352. doi:10.1053/j.ajkd.2016.03.410

49. Inoue BH, dos Santos L, Pessoa TD, et al. Increased NHE3 abundance and transport activity in renal proximal tubule of rats with heart failure. *Am J Physiol*. 2012;302(1):166–174. doi:10.1152/ajpregu.00127.2011

50. Pessoa TD, Campos LCG, Carraro-Lacroix L, Girardi ACC, Malnic G. Functional role of glucose metabolism, osmotic stress, and sodium-glucose cotransporter isoform-mediated transport on Na+/H+ exchanger isoform 3 activity in the renal proximal tubule. *J Am Soc Nephrol*. 2014;25(9):2028–2039. doi:10.1681/ASN.2013060588

51. Packer M, Anker SD, Butler J, Filippatos G, Zannad F. Effects of sodium-glucose cotransporter 2 inhibitors for the treatment of patients with heart failure: Proposal of a novel mechanism of action. *JAMA Cardiol*. 2017;2(9):1025–1029. doi:10.1001/jamacardio.2017.2275

52. Kuriyama S. A potential mechanism of cardio-renal protection with sodium-glucose cotransporter 2 inhibitors: Amelioration of renal congestion. *Kidney Blood Press Res*. 2019;44(4):449–456. doi:10.1159/000501081

53. Wiviott SD, Raz I, Bonaca MP, et al. Dapagliflozin and cardiovascular outcomes in type 2 diabetes. *N Engl J Med*. 2019;380(4):347–357. doi:10.1056/NEJMoa1812389

54. Heerspink HJL, Stefansson BV, Chertow GM, et al. Rationale and protocol of the Dapagliflozin And Prevention of Adverse outcomes in Chronic Kidney Disease (DAPA-CKD) randomized controlled trial. *Nephrol Dial Transplant*. 2020;35(2):274–282. doi:10.1093/ndt/gfz290

55. Neal B, Perkovic V, Mahaffey KW, et al. Canagliflozin and cardiovascular and renal events in type 2 diabetes. *N Engl J Med*. 2017;377(7):644–657. doi:10.1056/NEJMoa1611925

56. Perkovic V, Jardine MJ, Neal B, et al. Canagliflozin and renal outcomes in type 2 diabetes and nephropathy. *N Engl J Med*. 2019;380(24):2295–2306. doi:10.1056/NEJMoa1811744

57. Lo KB, Gul F, Ram P, et al. The effects of SGLT2 inhibitors on cardiovascular and renal outcomes in diabetic patients: A systematic review and meta-analysis. *Cardiorenal Med*. 2020;10(1):1–10. doi:10.1159/000503919

58. Thomson SC, Vallon V. Renal effects of sodium-glucose co-transporter inhibitors. *Am J Cardiol*. 2019;124(Suppl 1):S28–S35. doi:10.1016/j.amjcard.2019.10.027

59. Heerspink HJL, Karasik A, Thuresson M, et al. Kidney outcomes associated with use of SGLT2 inhibitors in real-world clinical practice (CVD-REAL 3): A multinational observational cohort study. *Lancet Diabetes Endocrinol*. 2020;8(1):27–35. doi:10.1016/S2213-8587(19)30384-5

60. Davies MJ, D'Alessio DA, Fradkin J, et al. Management of hyperglycemia in type 2 diabetes, 2018: A consensus report by the American Diabetes Association (ADA) and the European Association for the Study of Diabetes (EASD). *Diabetes Care*. 2018;41(12):2669–2701. doi:10.2337/dci18-0033

61. American Diabetes Association. 9. Pharmacologic approaches to glycemic treatment: Standards of medical care in diabetes – 2019. *Diabetes Care*. 2019;42(Suppl 1):S90–S102. doi:10.2337/dc19-S009

62. Greco EV, Russo G, Giandalia A, Viazzi F, Pontremoli R, De Cosmo S. GLP-1 receptor agonists and kidney protection. *Medicina (Kaunas)*. 2019;55(6):233. doi:10.3390/medicina55060233

63. Górriz JL, Soler MJ, Navarro-González JF, et al. GLP-1 Receptor agonists and diabetic kidney disease: A call of attention to nephrologists. *J Clin Med*. 2020;9(4):947. doi:10.3390/jcm9040947

64. Muskiet MHA, Tonneijck L, Smits MM, et al. GLP-1 and the kidney: From physiology to pharmacology and outcomes in diabetes. *Nat Rev Nephrol*. 2017;13(10):605–628. doi:10.1038/nrneph.2017.123

65. Asmar A, Cramon PK, Simonsen L, et al. Extracellular fluid volume expansion uncovers a natriuretic action of GLP-1: A functional GLP-1–renal axis in man. *J Clin Endocrinol Metab*. 2019;104(7):2509–2519. doi:10.1210/jc.2019-00004

66. Marso SP, Daniels G, Brown-Frandsen K, et al. Liraglutide and cardiovascular outcomes in type 2 diabetes. *N Engl J Med*. 2016;375(4):311–322. doi:10.1056/NEJMoa1603827

67. Pfeffer MA, Claggett B, Diaz R, et al. Lixisenatide in patients with type 2 diabetes and acute coronary syndrome. *N Engl J Med*. 2015;373(23):2247–2257. doi:10.1056/NEJMoa1509225

68. Marso SP, Bain SC, Consoli A, et al. Semaglutide and cardiovascular outcomes in patients with type 2 diabetes. *N Engl J Med*. 2016;375(19):1834–1844. doi:10.1056/NEJMoa1607141

69. Tuttle KR, Lakshmanan MC, Rayner B, et al. Dulaglutide versus insulin glargine in patients with type 2 diabetes and moderate-to-severe chronic kidney disease (AWARD-7): A multicentre, open-label, randomised trial. *Lancet Diabetes Endocrinol*. 2018;6(8):605–617. doi:10.1016/S2213-8587(18)30104-9

70. Whelton A, MacDonald PA, Chefo S, Gunawardhana L. Preservation of renal function during gout treatment with febuxostat: A quantitative study. *Postgrad Med*. 2013;125(1):106–114. doi:10.3810/pgm.2013.01.2626

71. Davies MJ, Bain SC, Atkin SL, et al. Efficacy and safety of liraglutide versus placebo as add-on to glucose-lowering therapy in patients with type 2 diabetes and moderate renal impairment (LIRA-RENAL): A randomized clinical trial. *Diabetes Care*. 2016;39(2):222–230. doi:10.2337/dc14-2883